CRANFIELD UNIVERSITY

Hameed Al-Awadi

Multiphase Characteristics of High Viscosity Oil

School of Engineering
Department of Offshore, Process, and Energy Engineering

PhD Thesis
Academic Year: 2008 - 2011

Supervisor: Prof. Hoi Yeung
November, 2011

CRANFIELD UNIVERSITY

School of Engineering
Department of Offshore, Process, and Energy Engineering

Ph.D. Thesis

Academic Year 2008 - 2011

Hameed Al-Awadi

Multiphase Characteristics of High Viscosity Oil

Supervisor: Prof. Hoi Yeung

November 2011

This thesis is submitted in partial fulfilment of the requirements for the degree of Doctor of Philosophy

ABSTRACT

Heavy oil production has drawn more and more attention in petroleum industry. The amount of heavy oil in the world is twice more than the conventional oil (low viscosity), which has been consumed rapidly from the past. The understanding of flow patterns and pressure losses in multiphase flow with high viscosity oil are vital to assist the design of transportation pipeline.

This thesis involves experimental investigation of two phase and three phase flows under high oil viscosity conditions (up to 17000cP) in horizontal pipelines. The multiphase (oil/water/solid/gas) facility was designed and constructed at Cranfield University and consists of 6m long horizontal pipeline of 0.026m diameter along with instrumentations.

The principal objectives of the work were to study the effect of viscosity, water cut, temperature variance, and flow conditions on flow patterns and pressure drops for (oil/gas and oil/water) two phase flows; to compare the measured flow parameters and phase distribution with those predicted from models found in the literature for two phase flows; and to conduct an experimental study of gas injection effect on pressure gradient in (oil/water/gas) three phase flow. Due to the nature of heavy oil reservoirs, sand is associated with oil/water mixture when extracted; therefore sand concentration effect on pressure drop in (oil/water/sand) three phase flow is also examined.

For oil-air flow, a smooth oil coating was observed in the film region of slug flow, while a ripple structure of oil coating film was found at higher superficial air velocity for slug flow regime and annular flow regime. The ripple structure was believed to increase the effective roughness of the pipe wall, which resulted in higher pressure gradients.

The pressure drop correlations from Beggs and Brill (1973) and Dukler et al. (1964) were used to compare with experimental pressure gradients for oil/air flow. It was found that these correlations failed to predict the pressure gradients for heavy oil/air flows in this work.

Several new heavy oil/water flow patterns were named and categorized based on observations. Though the heavy oil viscosity is an essential parameter for oil continuous phase flow on pressure drop, it had no significant effect beyond Water Assist Flow (WAF) condition, as a threshold was found for water cut with fixed superficial oil velocity. The transition criterion by McKibben et al. (2000b) for WAF was found to be able to predict this threshold reasonably well.

Core Annular Flow (CAF) models were found to greatly under predict the pressure gradients mainly due to the coating (oil fouling) effect associated with this study. A new coating coefficient was introduced to models presented by Bannwart (2001) and Rodriguez et al (2009).

The addition of solid in the mixed flow led to minor increase in the pressure gradient when the particles were moving with the flow. However, higher sand concentration in the system led to higher pressure gradient values.

The addition of gaseous phase to the oil/water flow was more complex. The gaseous injection was beneficial toward reducing the pressure gradient when introduced in oil continuous phase only at very low water cuts.

Keywords: Heavy oil, high viscosity, flow assurance, water cut, flow patterns, pressure gradient, modelling, two phase, three phase, sand.

ACKNOWLEDGEMENTS

First and foremost, I thank the almighty himself “Allah” for giving me the will, knowledge, and strength to overcome the obstacles that were associated with this work in particular and life in general.

I wish to express my sincere thanks and gratitude to my supervisor Prof. Hoi Yeung for his advice and support throughout my research. His continuous enthusiasm, inspiration, and great efforts to explain things clearly helped me to understand the true values of research and set me on the right path to a smooth and easy journey to graduation. I would like to thank him for being such a great advisor, without him this work would not have been a success.

I greatly appreciate and wish to thank all the technical and library staff at Cranfield University for their great assistance during this project. I would further like to thank my friends and colleagues in the Group with whom it has been very enjoyable to work.

Furthermore, I must thank for the Public Authority for Applied Education and Training (PAEET, State of Kuwait) for their academic and financial support of the present thesis. Thanks to British Petroleum (BP) for partial support of the project.

This would be incomplete without sincere thanks to my parents for their continuous believe and prayers. To my wife Rania and daughters Masah and Kady for their love, support, and patience during our stay in Cranfield.

TABLE OF CONTENTS

LIST OF FIGURES

LIST OF TABLES

NOMENCLATURE

A_g	gas layer cross sectional area	m^2
b,n	best curve fitting constants	-
c	constant determined by flow pattern	-
C	fouling/coating parameter	Pa/m
$C_{a,c}$, $n_{a,c}$	constants associated with flow regime	-
C_v	sand volume fraction, v/v	%
C_w	Water fraction	-
$\widetilde{D}_c^2$	core fluid in-situ holdup	-
D	pipe diameter	m
f_a	wall friction factor	-
f_{Arney}	Arney's friction factor	-
f_i	interfacial friction factor	-
f_{NS}	no-slip friction factor	-
Fr_m	mixture Froude number	-
f_{TP}	two-phase friction factor	-
g	gravitational acceleration	m/s^2
g_c	conversion factor = 32.2	$lb_m \cdot ft/(lb_f \cdot s^2)$
$H_{L\beta}$	actual liquid holdup in inclined pipe	-
H_{LO}	actual liquid holdup in horizontal pipe	-
J_o	superficial oil velocity	cm/s
J_w	superficial water velocity	cm/s
L1, L2, L3, L4	parameters used in Beggs and Brill correlations	-

P	pressure	Pa
$\tilde{Q}$	ratio between core to annulus volumetric flowrate	-
Q	volumetric flowrate	l/s
Re_{Arney}	modified Reynolds number by Arney	-
Re_{as}	superficial Reynolds numbers of the annular	-
Re_{cs}	superficial Reynolds numbers of the core	-
Re_{NS}	no-slip Reynolds number	-
S	liquid holdup parameter	-
$s_{i,o}$	experimental determined slip value between fluids	-
U_o	superficial oil velocity	ft/s
U_w	superficial water velocity	ft/s
V_a	annular fluid average velocity	m/s
V_c	core fluid average velocity	m/s
V_g	gas averaged velocity	m/s
V_i	interfacial velocity	m/s
V_m	mixture velocity	m/s
V_o	oil averaged velocity	m/s
V_{sg}	superficial gas velocity	m/s
V_{sl}	superficial liquid velocity	m/s
V_{so}	superficial oil velocity	m/s
V_w	water averaged velocity	m/s
x	distance	m
X^2	Martinelli parameter	-

Greek Symbols

β	actual angle of the pipe from horizontal	°
$\tilde{\rho}$	ratio between core to annulus densities	-
ρ	density	kg/m^3
ρ_a	annular fluid density	kg/m^3
ρ_c	core fluid density	kg/m^3
ρ_g	gas density	kg/m^3
ρ_l	liquid density	kg/m^3
ρ_m	average density	kg/m^3
ρ_o	oil density	kg/m^3
ρ_{TP}	two-phase density	kg/m^4
ρ_w	water density	kg/m^5
ε	core volume fraction (oil)	-
λ_L	no-slip liquid hold up	-
μ	dynamic viscosity	cP
μ_o	oil dynamic viscosity	cP
μ_w	water dynamic viscosity	cP
σ	interfacial tension	dyne/cm
τ_a	wall shear stress	Pa
τ_i	interfacial shear stress	Pa
ν_o	kinematic viscosity	m^2/s
Φ_i^2	two-phase multiplier	-

LIST OF ABBREVIATIONS

3L	Three Layer
AAPE	Absolute Average Percent Error
ACR	Alberta Chamber of Resources
AO	Annular Oil
APE	Average Percent Error
API	American Petroleum Institute
ASVAHL	Association for the Valorization of Heavy Oils
BP	British Petroleum
BPRI	British Petroleum Research International
BTEX	Benzene, Toluene, Ethylbenze, and Xylene
CAF	Core Annular Flow
CCDS	Cyclic Carbon Dioxide Stimulation
CEAA	Canadian Environmental Assessment Agency
CHOPS	Cold Heavy Oil Production with Sand
CSS	Cyclic Steam Stimulation
DO/W	Dispersion of water in oil
DO/W	Dispersion of oil in water
DO/W&W	Dispersion of Oil in Water over a Water layer
ECT	Electrical Capacitance Tomography
HIPR	High Internal Phase Ratio
ID	Inner Diameter
LHS	Left Hand Side
M	Mixed
MEOR	Microbial Enhanced Oil Recovery

MI	Mixing Interface
MSE	Mean Square Error
O/W	Oil in Water
OD	Oil-Dispersed
ODST	Oil-Droplet Stratified
ODW	Oil Dispersion in Water
OLW	Oil Lumps in Water
OOIP	Original Oil In Place
P.E.	Percentage Error
PC	Personal Computer
PCAF	Perfect Core Annular Flow
PCP	Progressing Cavity Pump
PGRF	Pressure Gradient Reduction Factor
ppm	part per million
PPT	Pressure Pulse Flow Enhancement Technology
PVC	Polyvinyl Chloride
RHS	Right Hand Side
RTA	Resource Technology Associates
RTS	Ratio of Two phase to Single phase
SAGD	Steam Assisted Gravity Drainage
SD	Standard Deviation
SG	Specific Gravity
SHIP	Single Heated electrically Insulated Pipeline
SM	Stratified Mixed flow pattern
SR	Stratified roll wave

SSE	Sum of Square of Error
ST	Stratified
SW	Stratified Wavy
SW&OI	Stratified Wavy with Oil Droplets at Interface
SWO	Swirl of Water and Oil
THAI	Toe to Heel Air Injection
VAPEX	Vapour Assisted Petroleum Extraction
W/O	Water in Oil
WAG	Water Alternating Gas
WPO	Water Plug in Oil
WCAF	Wavy Core Annular Flow
SRC	Saskatchewan Research Council

1 Introduction

1.1 Reasons behind this Thesis

Heavy oil production has shown increasing attention in petroleum industry. The amount of heavy oil in the world is double that of the conventional oil (low viscosity), which has been consumed rapidly in the past.

An effective and economical recovery method is required to produce and deliver the multiphase hydrocarbon stream from the wellhead to the delivery point. Cold Heavy Oil Production with Sand (CHOPS) is considered one of the most effective production methods; however, it presents a major challenge involving the flow mechanics of high viscosity oil, water, gas and sand together.

To date, not only research on sand transportation has been limited in this viscous hydraulic transport, but also the studies on flow patterns and mechanism of oil/ gas and oil/water flows are still limited for heavy oils. Therefore, more investigations are required, along with oil/water/gas and oil/water/sand flows in order to design pipeline effectively; as the pressure drop and stability characteristics of the flow in these transfer lines are very crucial toward pipelines design.

The present work was inspired with the desire to explore the multiphase flow patterns and pressure loss information which contributes toward Flow Assurance-hydraulic analysis to assist the design of transportation pipeline.

1.2 Background

The key component of sustainable advancement of human society has been the availability and continuous supply of energy. Fossil fuels have been able to meet the world's energy demand to date, however the increasing population and the growing economies are putting more strain on the already diminishing hydrocarbon resources of the world. Although renewable resources are

available, the technology is years away from sufficiently meeting the energy demand.

In oil and gas production from light oil reservoirs, it is normal to suppress sand production in order to reduce operational problems in wells, flowlines, risers and production facilities. For heavy oil reservoirs, primary recovery factors are generally low due to high fluid viscosity (1000 – 20,000 cP). It appears that any conventional non-thermal method is not possible for this type of oil. Meanwhile, the applications of various thermal recovery schemes are also restricted due to their high cost. Therefore, an effective and economical recovery method is required for those types of heavy oil reservoirs.

The demand for more energy and the decline in production rate from conventional oil reserves shows a trend that supply would be inadequate to meet demand; therefore unconventional oil sources will play a vital role in supplementing current supply. Heavy oil, Extra heavy oil, Bitumen, Oil sands etc are categorized as heavy oils and as the name suggests is any type of oil that does not flow easily owing to higher density and viscosity when compared to conventional crude oil. Heavy oil forms a major part of the world's known hydrocarbon resources up to more than two times that of conventional crude oil. Heavy oil has been overlooked as a viable petroleum source due to higher costs and difficulties in production and transportation. The current technologies adopted involve higher energy input for extraction and transport, in addition, the extracted heavy oil has to be upgraded to be made suitable for refinery feed stock. The overall procedure leads to nominal profit margins when compared to conventional crude oil.

In the current scenario, high demand and increased prices offer scope for heavy oil to be exploited adequately. There is a tremendous need for an improved recovery and transportation techniques for optimization and energy efficiency, which would in turn provide more profit margins.

1.3 Thesis Overview

Transport using pipelines has the capacity to provide more economical solutions for transport rather than using trucks to supply the process plants. Furthermore, current research has shown that numerous techniques can be applied for flow enhancement; tests have shown that a high reduction in frictional energy losses can be achieved using these techniques, the best method or a combination of these methods has to be adopted for these applications. The key issue is to understand the different flow patterns produced under the different conditions and predict the possible effect on changing the variables of each method to study the extent of the enhancement produced and where the safe operating conditions would lie.

The work presented in this thesis focuses on heavy oil transport behaviour in two phase (with water or air), three phase (with air-water and sand-water) flows. The effects of fluid properties, oil viscosity, water-cuts, sand concentration, and pipe diameter were studied. The conditions of the laboratory experimental work were done to address and cover the conditions associated with the complex flow in petroleum pipelines.

The different flow patterns were obtained by visual observations. Moreover, the pressure drops and flowing conditions were acquired and linked to the related flow patterns.

1.4 Thesis Objectives

The main objectives of this thesis are to improve the understanding of heavy oil transport characteristics and the prediction of pressure drop associated with different flow conditions. The impact is directed toward Flow Assurance-hydraulic analysis to assist the design of transportation pipeline from the well-head to the separator.

To accommodate with the above statement, the following tasks are carried out:

- Carry out background study to existing heavy oil production and transportation technologies.
- Perform literature review of light and heavy viscous oil in multiphase flow systems and associated prediction models for pressure drop for each system.
- Design and build multi-phase facility and its instrumentations to assess the study of heavy viscous oil in pipelines under different multi-phase flow conditions.
- Investigate the oil viscosity effect (using heater/chillers) on pressure drop and flow patterns in two-phase liquid/liquid and liquid/gas flow, three-phase air-liquid-liquid and liquid-liquid-sand flow.
- Investigate the water-cut effect on pressure drop and flow patterns in two-phase liquid/liquid flow, three-phase air-liquid-liquid and liquid-liquid-sand flow.
- Study the possibility of using Electrical Capacitance Tomography (ECT) for multiphase to determine the flow patterns and phase distribution under dynamic conditions.
- Develop flow pattern map charts for the different phase flows for the selected flowing conditions.
- Analyse the measured pressure drops and evaluate published prediction models against experimental data.

Based on the outcome from the last objectives, a set of proposal for future study will be provided.

1.5 Thesis Structure

The rest of this thesis is divided into 7 chapters, the contents of which are described below.

Chapter 2 reviews previous research activities and pressure drop prediction models on oil related multiphase flows (oil/air, oil/water, oil/water/air, and oil/water/sand). The general background of heavy oil, production technologies, and transportation are also presented in this chapter.

Chapter 3 describes the experimental setup for the 1 inch rig in PSE Lab in Cranfield University. The viscometer and ECT setup are covered as well.

Chapter 4 presents the results of the experimental finding from oil/air, oil/water, oil/water/air, and oil/water/sand flows; covering the pressure drop and flow pattern classifications for two and three phase flows.

Chapter 5 discusses and analyzes the experimental results from this work and compare them to the findings from previous investigation available in the literature.

Chapter 6 evaluates other published pressure drop prediction models in Core Annular Flow (CAF) against experimental data and develops new correlation to account for oil coating effect. The validation of Water Assist Flow (WAF) is also covered in this chapter.

Chapter 7 gives the conclusions and recommendations for future work.

2 Literature review

2.1 Heavy oil origin, composition, definition, and reserves

2.1.1 Origin of heavy oil

Heavy oil begins as conventional oil which migrates to the surface as result of inadequate closure of the crude formation. It migrates from the deep reservoirs to near the surface and accumulates in shallow depths (Clark, 2007).

At the depths where the light oil is found, the temperature is high and the bacteria does not survive. As the light oil is moved up through the faults to the much cooler shallow reservoirs, the bacteria degrades the oil to produce the viscous heavy oil (BP, 2009) as shown in Figure 2-1. Microbial degradation is initiated at temperatures less than 80^{o}C and therefore restricted to reservoirs down to about 4 km (Alboudwarej et al., 2006).

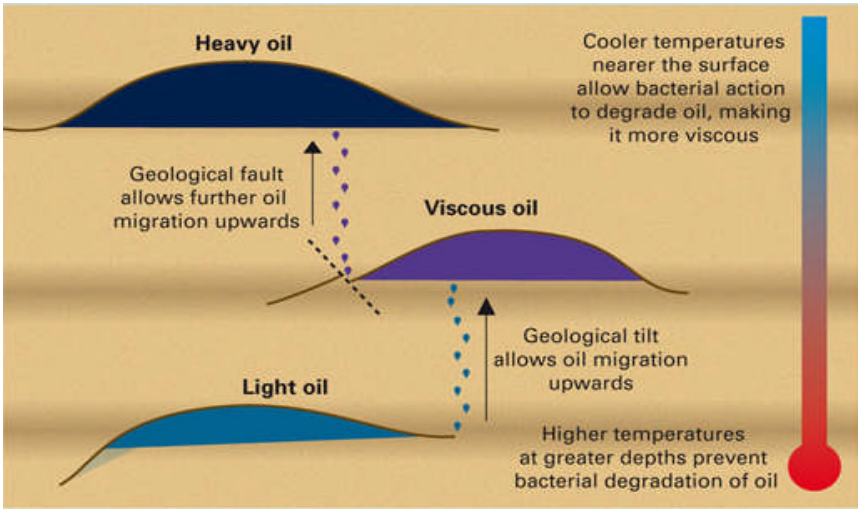

Figure 2-1: Origin of Heavy Oil (BP, 2009)

Microorganisms degrade light and medium oil producing methane and enriched heavy hydrocarbons. Biodegradation causes oxidation of the oil, decreasing gas oil ratio, increasing the density, acidity, viscosity, sulphur and other metal content. The biodegradation of the oil causes significant reduction to its original mass. The bacterial action removes the hydrogen to produce denser, more

viscous heavy oil and bitumen (Clark, 2007). Water washing and phase fractionation facilitate the formation of heavy oil by physically separating the lighter components from the heavy crude oil.

2.1.2 Composition of heavy oil

Heavy oil is characterized by a dense and viscous nature and defined as asphaltic, dense (low API gravity), and viscous oil that are typically composed of relatively low proportions of volatile compounds with low molecular weight such as Benzene, Toluene, Ethylbenzene, and Xylene (BTEX).

Large amounts of asphaltenes contain up to 90 percent of the sulphur and metals in the oil. It contains impurities such as waxes and carbon residue which have to be removed before being processed to refinery feed stock. Asphaltenes are responsible for the high viscosity of heavy oil (Pierre et al., 2004).The presence of asphaltenes, chemically altered fragments of organic chemical compounds, in oil can greatly complicate the production process. Subsequently, certain asphaltene elements require that the heavy oil also undergo a special refining process called deasphalting. The chemical composition of asphaltenes can consist of various amounts of sulphur, oxygen, hydrogen, nitrogen, carbon, and the heavy metals nickel and vanadium and are also present (Halliburton, 2011a).

They also typically contain some two ring napthalenes and high proportions of high molecular weight compounds (Cooper, 2006). The high molecular weight compounds can be paraffins (straight chain alkanes), asphaltenes (aromatic-type hydrocarbon), resins and other compounds with high melting points and high pour points. Paraffins tend to act as solvent molecules for a mix of high molecular weight compounds and actually help improve the overall flow characteristics of the oil (viscosity). Some, but not all, heavy oils contain moderate to high levels of asphaltenes. These asphaltenes can become problematic if they precipitate out and build up in equipment.

The density of the oil is the result of a large proportion of a mixture of complex, high molecular weight, non-paraffinic compounds and a low proportion of low molecular weight, volatile compounds. Heavy oils typically contain very little paraffin and the quantity of asphaltenes can vary greatly.

2.1.3 Definition of heavy oil

When referring to “heavy” or “light” oil, the term “API gravity” is commonly used in the oil industry around the world. The American Petroleum Institute gravity, or API gravity, is a measure of how heavy or light petroleum liquid is compared to water. If its API gravity is greater than 10, it floats on water; if less than 10, it sinks underneath water. API gravity is thus a measure of the relative density of a petroleum liquid and the density of water, but it is used to compare the relative densities of petroleum liquids. Although mathematically API gravity has no units, it is nevertheless referred to as being in “degrees”. The formula used to obtain the API gravity of petroleum liquids (API) is:

$$\mathrm{API} = \frac{141.5}{\mathrm{SG}} - 131.5 \qquad [1]$$

where SG is the specific gravity at 60°F (15.56°C). The definition of specific gravity is the following:

$$\mathrm{SG} = \frac{\rho_o}{\rho_w} \qquad [2]$$

The higher the density of the oil the lower is its API gravity. As shown in Figure 2-2, heavy oil falls within the range from 10^0 API to 21.5^0 API.

Figure 2-2: API gravity, Canadian Centre for Energy Information/Petroleum Communication Foundation (Rigzone, 2011)

Heavy oil has a gas free viscosity of 100cP to 10000cP at reservoir temperature. As seen from Figure 2-3, its viscosity is comparable to that of maple syrup all the way to tomato ketchup.

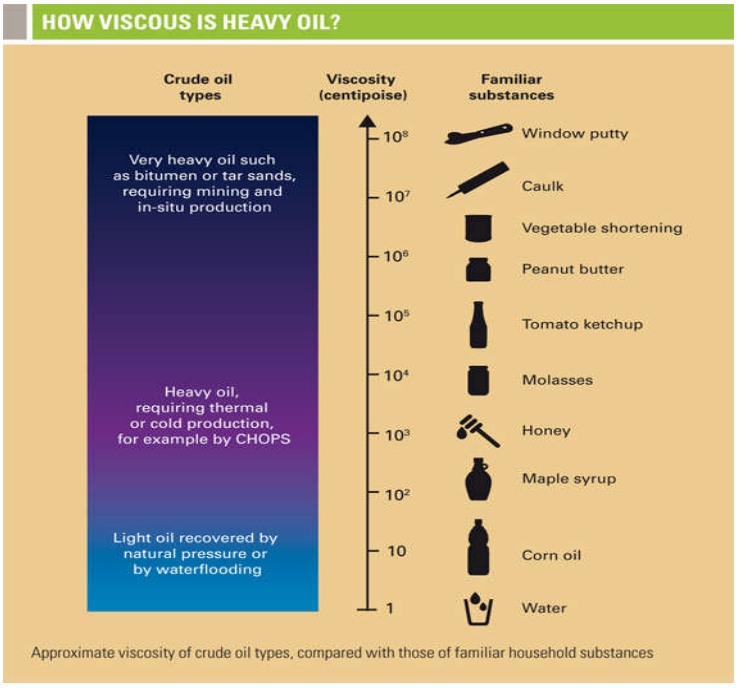

Figure 2-3: Viscosity variation chart (BP, 2009)

Although specific API value varies for heavy oil from different researchers, the general agreement on that is ranging from 10^0 to 20^0 API (Dusseault, 2001; Sainere et al., 2004). Sainere et al. (2004) clearly defined heavy crudes into two

categories (Figure 2-4): heavy oils, of which having the API between 10^0 and 20^0; and extra heavy oil or bitumen, of which having API of less than 10^0.

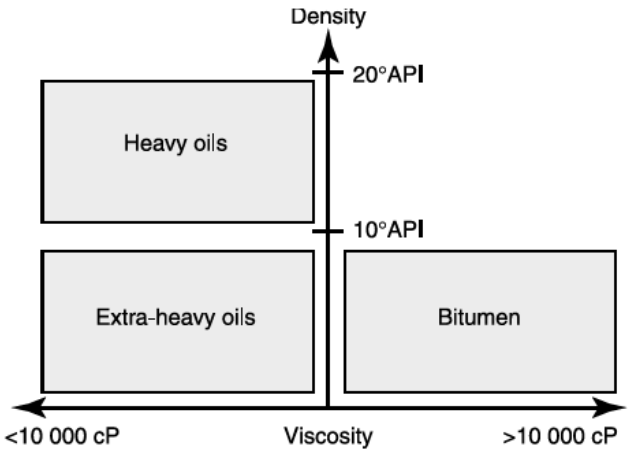

Figure 2-4: Difference of heavy/extra heavy oils and bitumen in regards to their densities and viscosities (Saniere et al., 2004)

Meanwhile, the heavy oils are also known as having high viscosity. Dusseault (2002) suggested that, heavy oil could be defined as oil having a natural flowing viscosity in the reservoir between 100cP to 10000cP at reservoir condition.

A definition for “heavy oil” could also be expressed in terms of “produceability” (Dusseault, 2002). One may assume that the oil in “oil sands” (or “super-heavy crude oil or “bituminous sands”…) is essentially an immobile fluid under existing reservoir conditions. This means that the oil is so viscous that it cannot be made to flow by non-thermal oil production methods (or other special methods), and this in turn means that there is no possibility to produce enough oil by conventional methods to be profitable. On the other hand, “heavy oils” have some mobility under naturally existing conditions and can flow to wells and be produced economically, with or without sand, although the production rate in each well may be modest. Such a definition is also empirical, as some low-cost operators may consider a certain production rate economical, whereas an integrated oil company would not.

2.1.4 Heavy oil world reserves

Heavy oil resources are widely discovered in the world. As of today, more than 7 trillion barrels of oil, consisting of 70% of total world oil resources, have been attributed to the heavy hydrocarbons by the International Energy Agency (IEA, 2005). This is more than twice the amount of world reserves of conventional oil. The large heavy oil deposits of Canada, Iraq, Kuwait, Former USSR, and Venezuela account for about 55-65% of the known <20 degree API oil deposits in the world as shown in Figure 2-5. Other countries with appreciable heavy oil resources include Russia, Nigeria, Indonesia and China, as well as several of the Middle East nations (well-endowed with conventional) where more shallow heavy oil has been ignored because of the large production capacity of their conventional oil reservoirs.

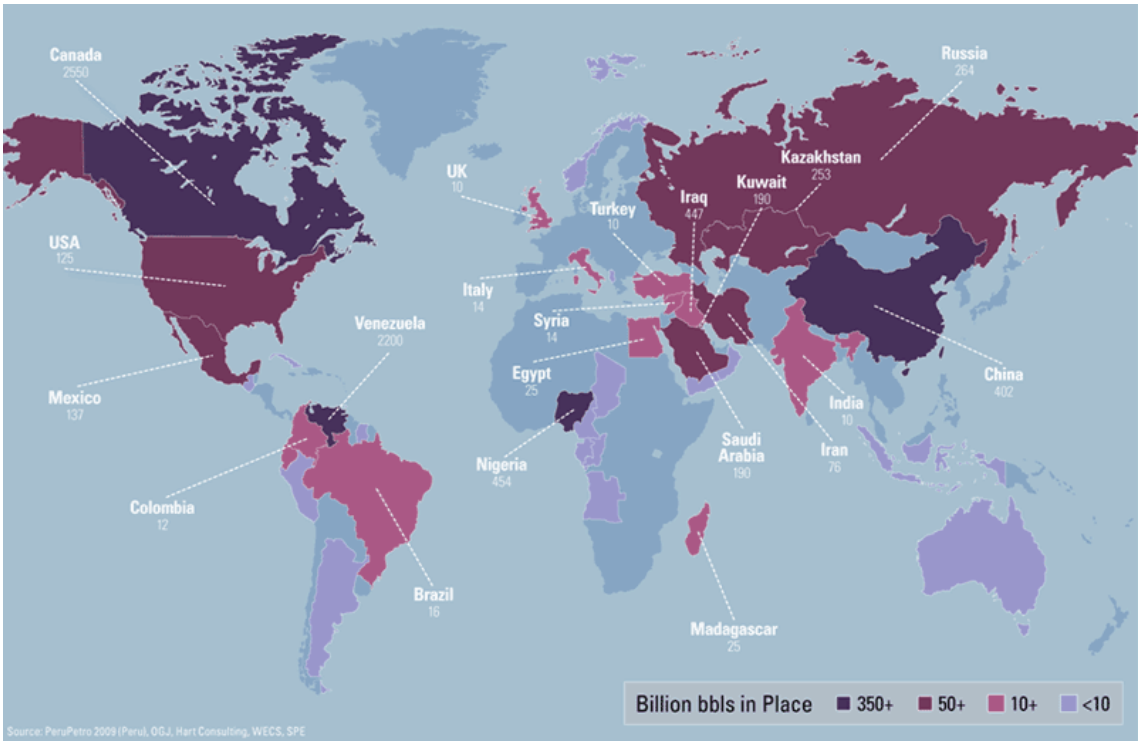

Figure 2-5: World Heavy Oil Reserves (Schlumberger, 2011)

Western Canada is estimated to hold 2.5 trillion barrels, Venezuela is estimated to hold 1.5 trillion barrels, Russia is estimated to contain in excess of 1 trillion barrels and the United States is estimated to hold 100 to 180 billion barrels

Heavy oil is also found and produced in Indonesia, China, Mexico, Brazil, Trinidad, Argentina, Ecuador, Colombia, Oman, Kuwait, Egypt, Saudi Arabia, Turkey, Australia, India, Nigeria, Angola, Eastern Europe, the North Sea, Romania, Iran, and Italy (Clark, 2007).The location of the very large resources is already known and hence further exploration is not required although exploration techniques have been further developed for locating smaller resources. The main challenge however remains the technology for optimizing production and transport.

2.2 Heavy oil production

Based on the reservoir characteristics, heavy oil, extra-heavy oil and bitumen are differentiated, thereby requiring unique production technologies tailor made for the specific resource and its fluid properties. A selected production method may only be suitable to a particular situation and would be insufficient for another; therefore adequate knowledge of the resource is the key to the selection of the production technology. The selection of any of these methods will depend on many factors, including the stage of reservoir production, formation and fluid properties, reservoir geology, available production and transportation facilities, and the underlying heavy oil economics in a particular region.

Production of heavy oil proceeds with surface mining or well production. Well production which is a subsurface production method is further classified as thermal production methods and cold production process (non–thermal production). The production of heavy oil can be summarized in Figure 2-6 providing the different techniques including most of the techniques that are being used today.

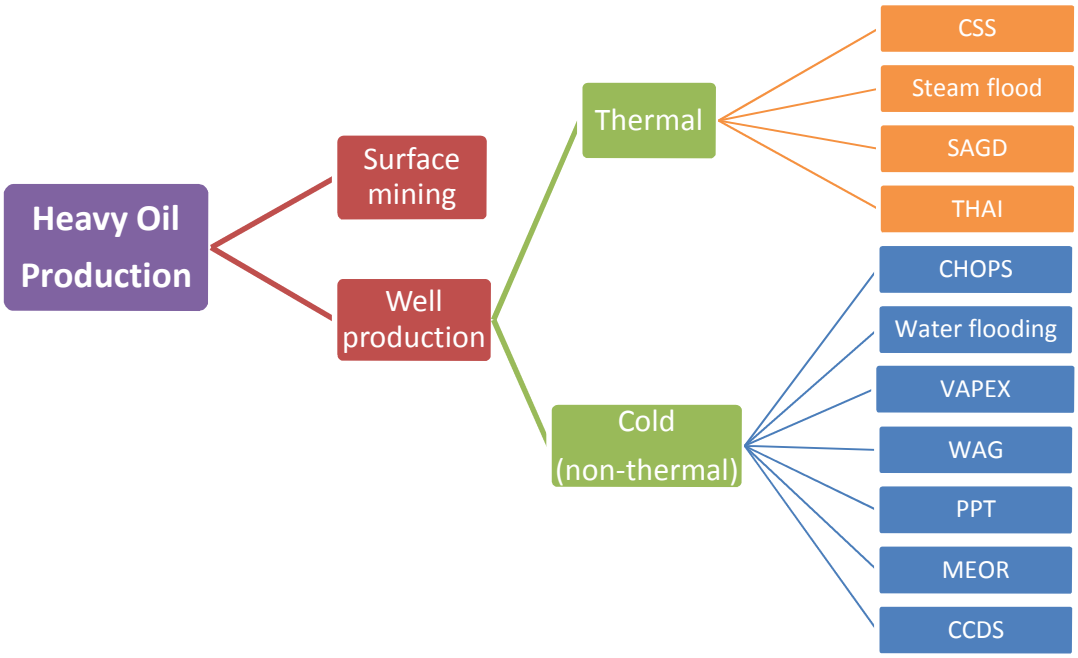

Figure 2-6: Heavy oil production structure

All methods for well production are founded to be based on pressure driven flow to wells, a process dominated by the permeability of the sand and the viscosity of the oil, thermal process to reduce viscosity, and high differential pressures to promote flow were the obvious choices. Billions of dollars have been spent on exploring the different schemes of generating and extracting the heavy oil from wells. However to this date, no specific method was determined to be dominant and significant successes are rare to be achieved (Dusseault, 2002; Clark, 2007).

As mentioned above, the selection of the most appropriate recovery method for heavy oil can be very challenging since many factors have to be considered. These include viscosity, reservoir complexity, environment, economics and refining. The viscosity will be studied thoroughly and intensively in this research.

- Surface (open-pit) mining

For over forty years surface mining has been the technique deployed to recover bitumen, it is now, a tried and tested technology with adequate knowhow and hence is a safe bet for commercial application. Fort McMurray, Alberta, Canada

holds large oil sands reservoirs which are essentially bitumen that has to be processed to obtain the heavy oil. Up to 10 percent of the heavy oil and bitumen in Western Canada is recovered using this method (Clark, 2007).

When the resource lies at a depth of 50 to 75m depth, open-pit mining is proved to be the only commercial method for extraction (Clark, 2007). As shown in Figure 2-7, surface mining begins primarily by clearing the vegetation over the resource. The overburden, usually rocks and soil, is removed from the work site and either stock pilled for later refilling the exhausted mine pit or used for construction purposes. Large excavators are used to load the ore on to trucks and then transported from the mine face to an ore crusher where it is crushed into smaller chunks and then water slurry is generated. The slurry is then transported through pipes. The transported slurry is separated to sand, bitumen and water in a primary separation vessel and then the bitumen is further treated with solvents to water and fine solids. The clean sand from the primary separation vessel is removed and stored. A mixture of the bitumen, water and fine tailings (fine particles and clay) is transported to a holding pond where it is held for long periods to ensure complete separation.

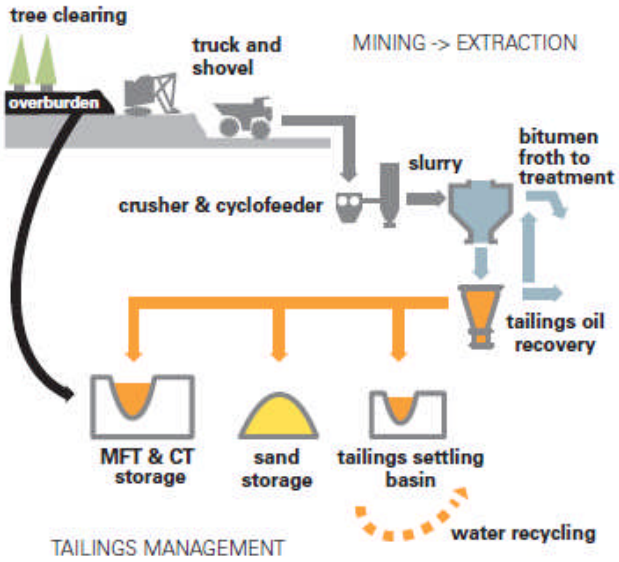

Figure 2-7: Mining Process (ACR, 2004)

The current technology improvement possibilities are limited but the main focus has been on optimization and reducing the environmental impact. Optimizing process control and monitoring, increasing bitumen recovery, reducing water usage and transport of slurry from the mine face are essentially some of the methods of improving overall efficiency.

- Well production

When the resource is too deep for surface mining, in situ production techniques have to be employed to recover the heavy oil. The correct technique has to be adapted to the particular characteristics of the resource. The primary recovery technique uses natural reservoir energy, such as gravity drainage, displaces hydrocarbons from the reservoir into the wellbore and up to surface. As the reservoir pressure declines, it is necessary to implement an artificial lift using progressive cavity pumps or electrical submersible pump. Most of the cases the high viscosity of the resource hinders it from being pumped and therefore enhanced oil recovery techniques employed, and as mentioned above, these are categorized as Thermal and Cold (non-thermal) production processes.

2.2.1 Thermal production processes

Thermal methods assure some of the highest recovery factors. They also promise the largest potential capital expenditure and operating costs—and therefore risk. Four techniques tested for new thermal production methods currently stand out above the rest:

2.2.1.1 Cyclic steam stimulation (CSS)

It is considered to be the oldest commercial method among all the techniques. A single well is used to inject steam into the reservoir for the purpose of heating the oil and reducing its viscosity. After the reservoir has been through a soak phase, the operation of the injector well is reversed to produce the oil. The “huff and puff” process is divided into three stages as shown in Figure 2-8.

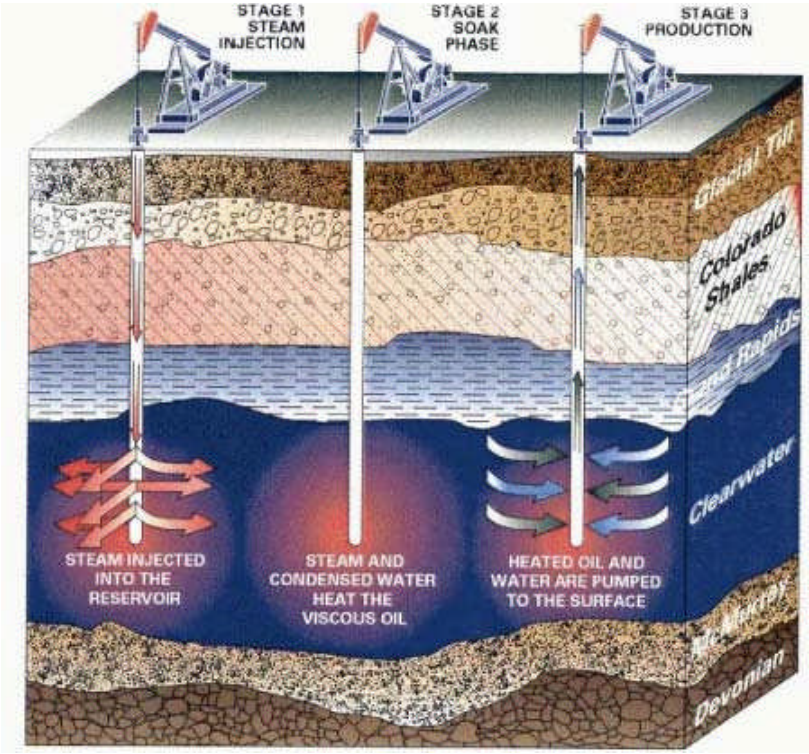

Figure 2-8: Stages of CSS for a single well (CEAA, 2011)

In order to soften the oil sand before pumping, for several weeks high-pressure steam is injected into the oil sand formation, since the steam helps recover the resource in several ways. The heat softens the oil sand and the water vapour helps to break up the bitumen and heavy oil from the sand. The pressure created in the underground environment causes cracks to be formed that adds drive to move the bitumen to producing wells. After a portion of the reservoir has been satisfactorily saturated, the steam is turned off and the reservoir allowed to sit for several weeks. After it has been allowed to sit and soak up the steam and moisture, the production phase brings the bitumen to the surface. It either flows on its own, or is pumped up the well to the surface. When the rates of production start to decline, the reservoir is pumped with steam once again.

CSS is the preferred method for production when the heavy oil reservoirs can contain the high-pressure steam without fracturing the overburden, therefore a minimum depth of 300 m but have been successfully deployed at depths

between 200 and 300 m. Resource recoveries using this technique are in the range of 20-35 percent (Clark, 2007).

However many problems arises from using this method. The very high cost of injecting the generated heat is one, trying to maintain it in the reservoir without escaping to the surface due to being lighter than rocks or fluids is another, also drawdown to low pressures during production cycles leads to water coming into the production region, giving excessive water production and high heat losses.

2.2.1.2 Steam flooding

In a steam flood, sometimes known as a steam drive, some wells are used as steam injection wells and other wells are used for oil production. Two mechanisms are at work to improve the amount of oil recovered. The first is to heat the oil to higher temperatures and to thereby decrease its viscosity so that it more easily flows through the formation toward the producing wells. A second mechanism is the physical displacement employing in a manner similar to water flooding, in which oil is meant to be pushed to the production wells as shown in Figure 2-9. While more steam is needed for this method than for the cyclic method, it is typically more effective at recovering a larger portion of the oil.

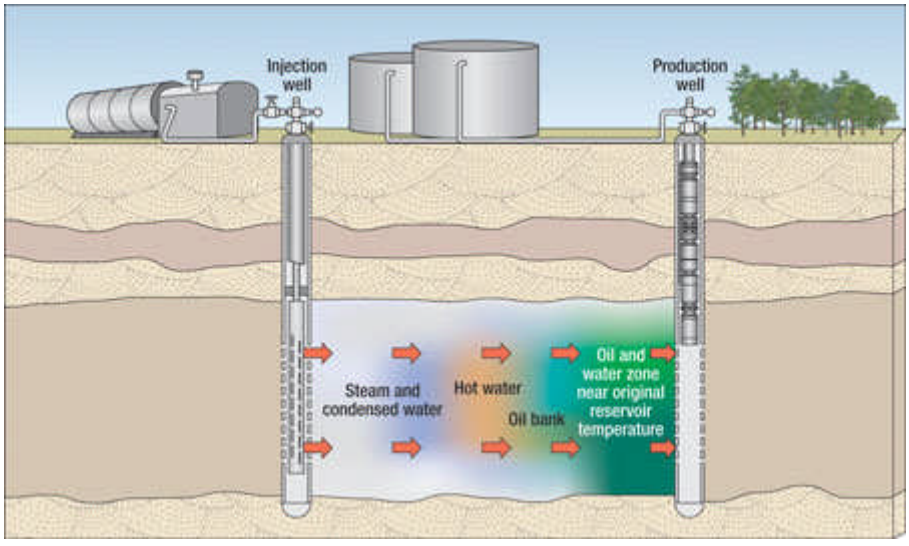

Figure 2-9: Steam flood technique (James and Wing, 2011)

This method posses all of the same problems listed above for CSS method, except for the premature water breakthrough that happen in the low-pressure production phase of CSS depending on the specific geometry of the drive process. Casing shear can be much more serious than in CSS because of the high shear stresses generated in a “2-D” in line drive (In CSS, which is a process that develops radically around a well, the shear stresses drop off with distance from the heated zone leading edge).

2.2.1.3 Steam Assisted Gravity Drainage (SAGD)

SAGD is a more recent development when compared to other thermal methods. It is becoming a very popular option because of its ability to produce from reservoirs too shallow for other thermal methods. As the SAGD process operates at lower steam pressures than CSS or Steam flooding, less overburden is required for steam containment in the reservoir (Clark, 2007).The SAGD production involves the use of two horizontal wells. The horizontal injector well, located above a horizontal producer, is used to raise and form a suitable environment “steam chamber” to encourage increasing the temperature of the oil. The heated oil then drains downward to the horizontal producer well located parallel and beneath the injector well, as shown in Figure 2-10.

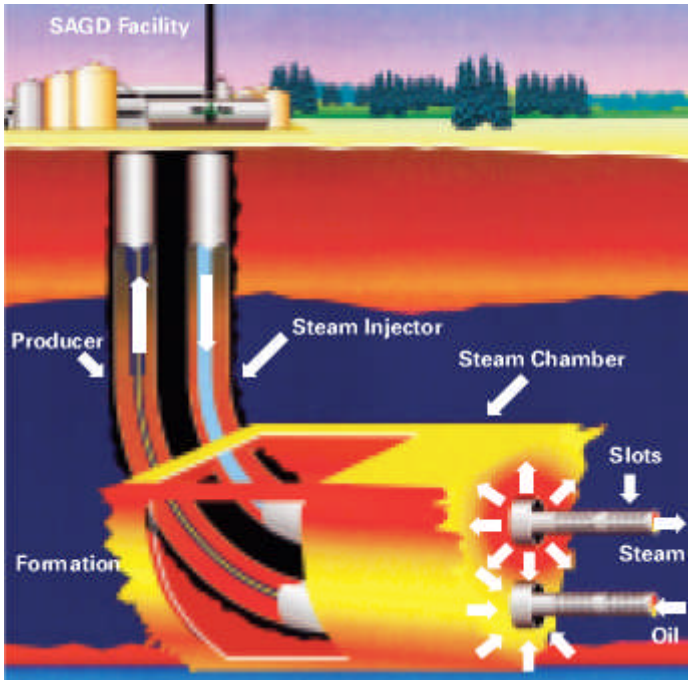

Figure 2-10: SAGD principle (ACR, 2004)

The SAGD is not exempt from challenges and difficulties. Building a well reservoir knowledge and fluid characterization is one factor to help a more productive and informed decision making in using the SAGD, because the viscosity can change significantly within the same reservoir; however accurate evaluation is difficult to be achieved. The quantity of steam injected and fluid produced depend on reservoir characteristics such as permeability, porosity, water saturation, and on the length of the well. Some of the factors that determine the length of a well include geology and the pressure drop between the heel and the toe in the horizontal section. The pressure drop in an injector is a function of steam volume, pressure and pipe size. Using a larger casing will reduce this pressure drop. The selection of the size of the liner and the intermediate casing is also influenced by the size of tubing and other instrumentation strings inside the casings (Knoll and Yeung, 2000). Another issue is sand production control; where the sand has to be monitored for most optimized rate of oil production, as it always the case for all production methods.

2.2.1.4 Toe to Heel Air Injection (THAI)

The THAI process was invented in 1993; it combines vertical air injection with a horizontal production well. In this approach, the heat, which generated by burning part of the oil in place in the formation, expands outward in the formation.

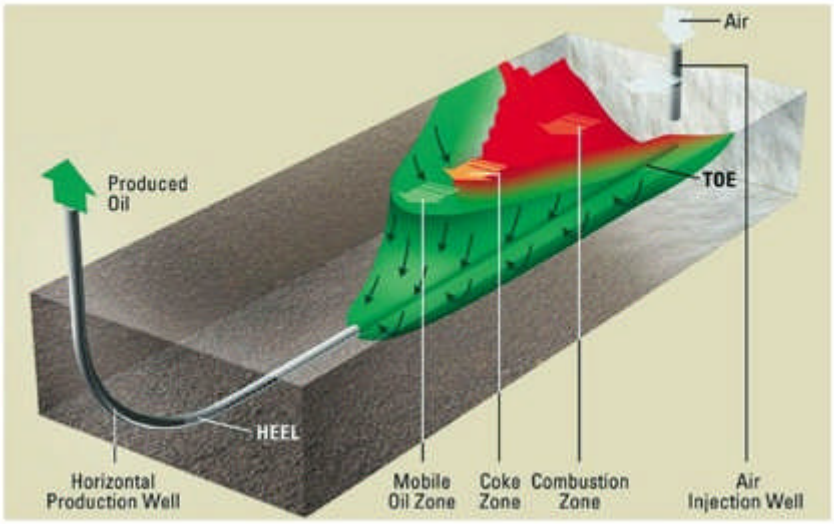

Figure 2-11: THAI diagram (The oil drum, 2009)

For the first three months, steam is injected in the vertical well to heat the horizontal well and condition the reservoir around the vertical well. After the first three months, compressed air is injected in the vertical well and combustion is initiated, as shown in Figure 2-11. The well geometry enforces a short flow path so that the instabilities associated with conventional combustion methods are avoided or reduced. Estimates from experimental tests indicate that the process can recover 80% of original oil-in-place while partially upgrading the crude oil in situ (The oil drum, 2007)

2.2.2 Cold (non-thermal) production processes.

Several cold production methods offer recovery options for heavy oil:

2.2.2.1 Cold Heavy Oil Production with Sand (CHOPS)

CHOPS is widely used as production approach in unconsolidated sandstones. CHOPS involves "the deliberate initiation of sand influx during the completion procedure, maintenance of sand influx during the productive life of the well, and implementation of methods to separate the sand from the oil for disposal. No sand exclusion devices (screens, liners, gravel packs, etc.) are used. The sand is produced along with oil, water, and gas and separated from the oil before upgrading to a synthetic crude" (Dusseault, 2007).

The first discoveries in the Canadian heavy-oil belt were made in the Lloydminster area in the late 1920s. High asphaltene-content heavy crude, an ideal feedstock for asphalt products, has been produced since that time. Pump jacks were limited by slow rod-fall velocity in the viscous oil to a maximum of 8 to 10 m^3/day of production, usually less. Small local operators found that wells which continued to produce sand tended to be better producers, and efforts to exclude sand with screens usually led to total loss of production.

The sharp oil price increases in the 1970s and 1980s led to great interest in heavy-oil-belt resources. Many international companies arrived and introduced the latest screen and gravel-pack technology. However, in most of cases, the productivity was reduced remarkably or total stopped. The development of progressing cavity pumps (PCPs) since the 1980s changed the non-thermal heavy oil industry in Canada. The production rate limits of beam pumps were no longer a barrier. Sand became an asset because more sand meant more oil. More highly integrated sand separation, transportation, and disposal methods were developed (Dusseault, 2002). To date, deliberate massive sand influx has been used only in unconsolidated sandstones ($C_v \approx 30\%$) containing viscous oil ($\mu > 500$ cP). It has been used almost exclusively in the Canadian heavy-oil belt and in shallow (< 800 m), low-production-rate wells (up to 100 to 125 m^3/day).Also, from 12~20% original oil in place (OOIP) can be developed. However, wider acceptance of this technology is still expected. The reasons for the lack of acceptance include the non-traditional nature of the production

mechanisms, difficulty in production predictions, complexity in implementation, and the need for high level of sand management and disposal strategies.

CHOPS technology is used as recovery heavy oil's reservoirs to increase porosity and permeability of the formation significantly and improve flowability of heavy oil by inducing sand production to form wormhole net. Where Vertical wells are drilled into the zone of interest, and sand production is encouraged using special screens and slotted liners shown in Figure 2-12 and Figure 2-13. As production continues, substantial quantities of sand, 1% to 8% of the total volume, are produced along with the oil. High-porosity, high-permeability channels, known as wormholes, penetrate into the formation and become preferential production paths (Drebit and Tesciuba, 2008). These wormholes tend to develop and grow in the weakest sand and propagate toward the highest pressure gradient. The recovery mechanism of CHOPS includes: wormhole net formed due to a great deal of sand production, steady foamy oil flow, elastic expansion of reservoir, compressive derive of overlying formation, and edge/bottom water providing drive energy, etc (Wang *et al.*, 2005).

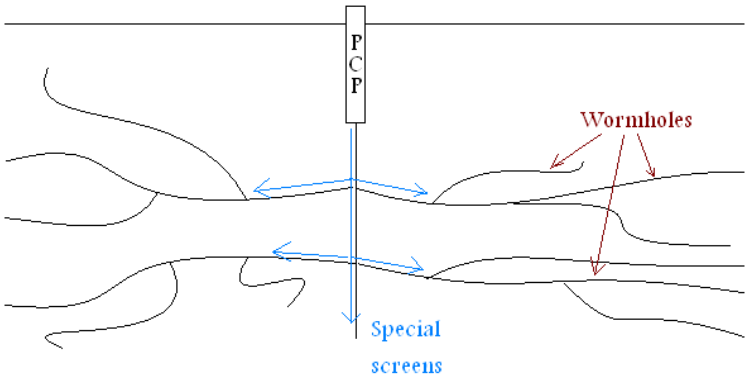

Figure 2-12: Forming wormholes using special screens

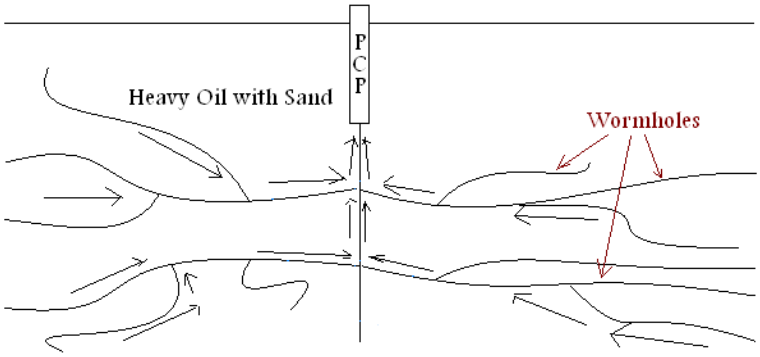

Figure 2-13: Producing heavy oil with sand

CHOPS has special requirements for reservoirs, such as shallow buried depth, unconsolidated formation, easy-to-produce sand, low reservoir pressure, moderate solution gas-oil ratio, and high oil viscosity with some edge-bottom water providing drive energy (Wang *et al*., 2005). However, regardless of the reservoirs condition, CHOPS will be inevitably faced with many problems such as sand production and surface oil/ sand treatment. This will simultaneously increase oil production cost. Consequent engineering technical problems mainly include:

- malfunctioning/ damaging of production tools, for example, progressing cavity pump is clogged or stuck, which may reduce its service life;
- wellbore sand settling will result in work-over and frequent sand washing operation, which will increase work-over expense greatly;
- surface gathering pipelines are easy plugged during heavy oil production with sand; and
- oil/ sand separating and processing equipments are required on surface due to sand production with produced crude oil.

There are several mechanisms responsible for the production rate enhancement in CHOPS wells:

- When the sand matrix is unconstrained (no screens or other impediments) and is allowed to move with the viscous fluids into the well bore, the basic permeability is increased, and the oil mobility is thereby enhanced.

- Continued sand production from a CHOP well leads to the growth of a disturbed zone, most likely a channelled and remoulded zone filled with slurry of sand, water, oil and gas. The zone increases porosity and permeability, and the well behaves as if it has an increased drainage radius. Production enhancement from this effect alone should approach a factor of 4 or 5 after large quantities of sand have been produced. Late in life this could be 1,000 to 15,000 bbls of sand per well.

- CHOPS production uses foamy oil drive from the solution gas with intentional sand production. Wells are subjected to aggressive drawdown, and gas evolves as bubbles in the porous matrix. However, a continuous gas phase is not formed due to the high fluid viscosity; gas remains as bubbles that expand in response to pressure decline during flow. Hence, the bubbles act as an “internal drive” driving the slurry to the well at a greater velocity than predicted by conventional fluid flow theories. Foamy oil develops in a zone that propagates outward from the well, following the growth of the disturbed and remoulded zone. This extends the zone of highest pressure gradient far from the well, where it destabilizes more sand. Operating below the bubble point means a dramatic increase in production rate and recovery.

- Heavy oil reservoirs can have high skin effects due to plugging of pore throats with precipitated asphaltenes and mobilised fine-grained particles and clays. CHOPS continually shears and disturbs the sand grains, which prevents pore throat plugging. As the disturbed zone of hyper-porosity and permeability extends away from the wellbore, the wellbore skin becomes increasingly negative.

Figure 2-14 shows the history of Luseland Field in Saskatchewan that was converted to CHOPS production in 1994~1998, showing the huge increase of production rate after applying the CHOPS technology.

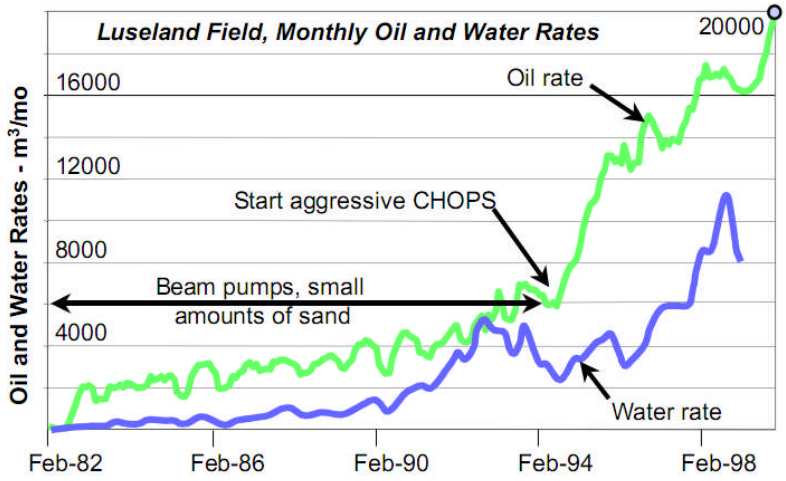

Figure 2-14: Field improvement through CHOPS (Dusseault, 2002)

2.2.2.2 Water Flood

Waterflooding is one of the most common, simple, and efficient secondary recovery methods. It is used to drive a front of heavy oil from one vertical well towards another vertical producing well, as shown in Figure 2-15. Waterflooding is usually initiated in pressure depleted or nearly depleted reservoirs. Most commonly, solution gas drive reservoirs develop free gas saturation due to pressure depletion. Initially, the reservoir pressure is restored as the gas-filled pore volumes are refilled with the injected water, re-dissolving free gas back into the oil. The oil production response occurs after the fill-up of the gas space. The injected water eventually breaks through at the producing wells; generally, very little water is produced before the peak oil production rate is reached if the reservoir resembles a homogeneous formation. The timing of the oil response and water breakthrough, and the magnitude of the peak oil production rate depend upon the reservoir characteristics and the injection rate.

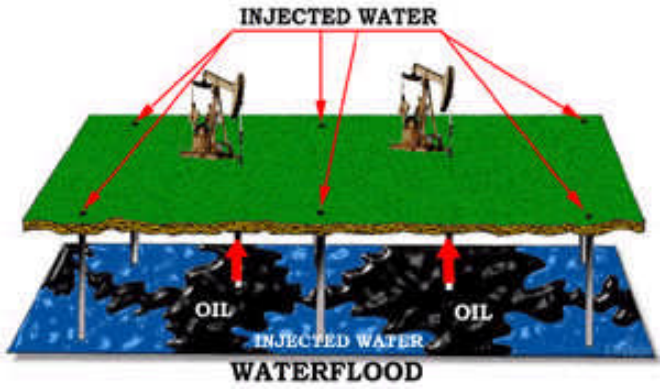

Figure 2-15: Waterflood scheme (Maverickenergy, 2011)

The major challenges in this method are characterizing the fluids and the reservoir, along with monitoring the water front to maximize the production of the heavy oil. Also controlling the sand production throughout a well's productive life requires appropriate sand management.

2.2.2.3 Solvent injection (VAPEX)

Alternatively, means to inject solvent into formation where it makes the oil mobile. One typical application of solvent injection was named VAPEX (vapour assisted petroleum extraction). The basic design of a VAPEX is that two horizontal well pairs are spaced approximately 5 m apart and a gas/solvent mix is injected into the reservoir through the upper well to stimulate gravity-enabled production in the lower well, as shown in Figure 2-16.

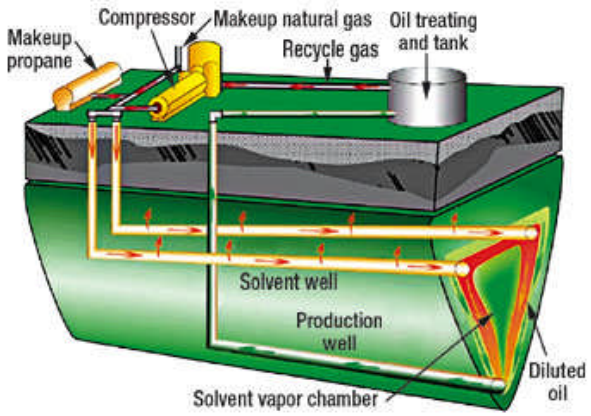

Figure 2-16: VAPEX Concept (World Oil, 2011)

The VAPEX process involves the injection of a vaporized solvent into a horizontal well located in the upper portions of the oil reservoir. Injected mixed gases consist of: methane, CO_2, propane and butane, depending on the reservoir and its rock character (World Oil, 2011). The solvent dissolves (by diffusion/dispersion) into the heavy oil reducing its viscosity and creating an expanding solvent vapour chamber. The diluted oil then drains down the edges of the chamber by gravity to a vertically aligned lower horizontal production well where it is pumped to the surface. In VAPEX, no heat and no water is used. The solvents are made of hydrocarbons that originally come from oil reservoirs so they are not harmful to the reservoir, and they cannot escape the reservoir. The solvents are recovered with the oil and recycled, so they are not released to the atmosphere. The biggest concern when considering this method is the cost of the solvent and the ability to recover it (Clark, 2007).

2.2.2.4 Water – Alternating – Gas Injection (WAG)

As the name suggests, the reservoir is injected with a solvent gas and water alternately to enhance the recovery of heavy oil. The gas acts as a solvent to reduce the heavy oil viscosity and water helps to push the thinner oil towards the producing wells The WAG injection process is intended to recover as much oil from the reservoir as possible. WAG injection has been widely applied since the late 1950s. Gas makes up a large part of the total cost, which makes WAG injection a fairly expensive method except in cases where a gas surplus is available (Statoil, 2011)

2.2.2.5 Pressure Pulse Flow Enhancement Technology (PPT)

It has been found that large amplitude pressure pulses dominated by low-frequency wave energy generate enhanced flow rates in porous media. The mechanism of PPT is by generating local liquid movement into and out of the pores, through the propagation of porosity dilation wave. The dilation wave moves through the porous medium causing small contraction and expansion of

the pores with the passage of each wave helps unblock pores and hence enables higher liquid flow.

2.2.2.6 Microbial Enhanced Oil Recovery (MEOR)

From the 1980's biotechnological research has produced results which can prove helpful to the oil and gas industry. The main aims from these researches were to either reduce pore blockage in the near well bore area or to produce surfactants/ solvents to use in in–situ processes (Clark, 2007). Enzymes from some bacteria have been found to be capable of upgrading the heavy oil making some improvements in controlled surface environments. The surfactants generated biologically by the action of microbes have improved oil recovery in laboratory experiments. However field experiments have not yet been attempted, placing bacteria in the reservoir has not been achieved till now due to the technical challenges that include dispersal into the formation, providing nutrients, competition with existing micro–organisms in the reservoir, all to be achieved without blocking the permeability of the reservoir.

2.2.2.7 Cyclic Carbon Dioxide Stimulation (CCDS)

Cyclic carbon dioxide stimulation involves the injection of CO_2 into heavy oil reservoir to reduce viscosity to a "flow able" level. During what is commonly referred to as the soak period, the well is shut in for a period of weeks or months. The well is then opened after the injected CO_2 has fully dissolved into the oil, an interactive process called miscibility that causes the oil's viscosity to reduce and the oil to expand, thereby allowing a free flow to the well (Halliburton, 2011b).Supercritical CO_2 is an effective solvent with very low viscosity.CO_2 is supercritical at 31^0C and at 1050 psi (Clark, 2007). At the supercritical condition CO_2 is miscible in hydrocarbons. One of its main advantages being that it is inexpensive compared to other solvents used for reducing the viscosity and also for in – situ upgrading of the heavy oil. As remedies to climate change have brought about CO_2 sequestration as a remedy to dispose of the produced CO_2, this technique proves to be a solution to solve

two problems at the same time, one to reduce viscosity during heavy oil production or upgrading and also geological sequestration into the reservoir.

The choice of recovery methods is specific to the reservoir. It requires the evaluation of the well property, geographical factors, environmental issues and economical balance. Different technologies have been found to be suitable for different reservoirs and conditions. CHOPS and PPT have been successful economically in reservoirs less than 15m thick while SAGD is not efficient. CHOPS gives high production rates early in the production life of the reservoir, but SAGD gives better overall hydrocarbon recovery. Whatever the recovery production method selected the ultimate aim of the enhancement is to make the heavy oil more mobile.

After reviewing the production enhancement technologies, it was found that the ultimate goal is to make heavy oil more “mobile”, which could be accomplished by heating, adding solvent (gas/dilution), pressurize the oil or encourage the sand production. Therefore, whatever method chosen, it is vital to understand the multiphase transport behaviour and mechanism in order to enhance the production and assure the transportation.

2.3 Heavy oil transportation

Due to the complex nature of heavy oil, the pipeline transportation has become highly technical operation. One of the major difficulties is the high viscous fluids that require efficient and economical ways to transfer the heavy crude. Heavy crude oils have a density approaching or even exceeding that of water. They are usually extremely viscous, with a consistency ranging from that of maple syrup to a solid substance at room temperature. Heavy crude oils are not pumped easily through the pipelines because of the high concentrations of sulphur and several metals, particularly nickel and vanadium. Crude oils are complex fluids that can cause a variety of difficulties during the production, separation, transportation, and refining of oil (Al-Besharah et al., 1987)

As viscosity is considered to be the dominating factor governs the energy required, most techniques are aimed to reduce its value, so that the size of the pipeline and the pumping requirements are met economically.

Several methods have been deployed to achieve this objective; most of them have been utilized before for enhanced flow of medium and conventional oils, while others are in development stage. These solutions consist either in reducing the viscosity (heating, dilution, oil-in-water emulsion, partial upgrading) or in lowering the friction in the pipe (Core Annular Flow). Each method is described below:

2.3.1 Heating

The heating method of crude to raise its temperature and thereby improving its flow properties is a proven and very popular method for enhancement of flow. This method has been used in Venezuela since 1955 (Escojido et. al, 1991). Heated pipelines have been in operation in California from 1972 for pumping 14^0 to 16^0 API, by Getty Oil (now Texaco Transportation and Trading Inc.).The crude is maintained at temperatures between 49^0C to 54^0C to keep it within acceptable viscosity limits for transporting.

In subsea pipeline systems, the transport pipelines are heated and this technology could be a viable option for transport. Two configurations for electrical heating of the pipelines are available: a Single Heated electrically Insulated Pipeline (SHIP) where electrical current flows along the pipe; and a pipe-in-pipe subsea pipeline where the oil flows through the inner electrically insulated pipe which is surrounded concentrically by an electrically conductive outer pipe. In the latter, heating is caused by a combination of electrical resistance and magnetic eddy effects associated with transmission of an alternating current through the pipeline (Martínez-Palou et al., 2011).

The cooling of the oil during transport in the direction of flow causes an increase in viscosity as a result of decreasing the volumetric flowrate, which will cause shorter transportation distance as shown in Figure 2-17.

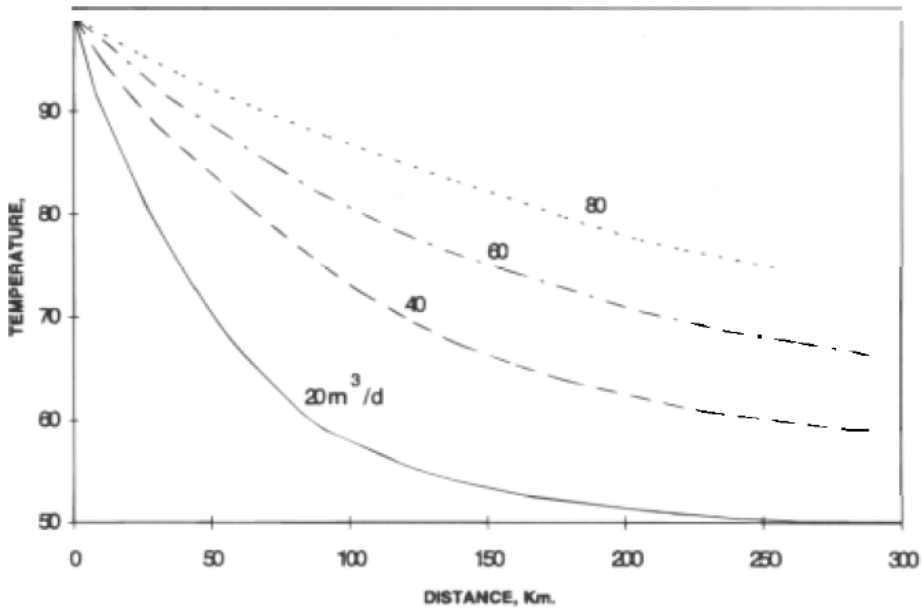

Figure 2-17: Viscosity distribution for heated pipeline at different flow rates

(Guevara et. al, 1997)

Low flow rates force rapid decrease in temperature associated to low fluid velocity this demands more pumping pressure to enable transport as shown in Figure 2-18. The flow rate at which the crude is pumped decides the distance between pumping stations. The design of hot oil pipelines puts forward a number of considerations that has to be made which include the temperature at which the optimum viscosity is achieved, heat loss and whether or not insulation is required, the minimum flow rate to prevent plugging, expansion of pipeline and startup and shutdown operations (Escojido et. al, 1990).

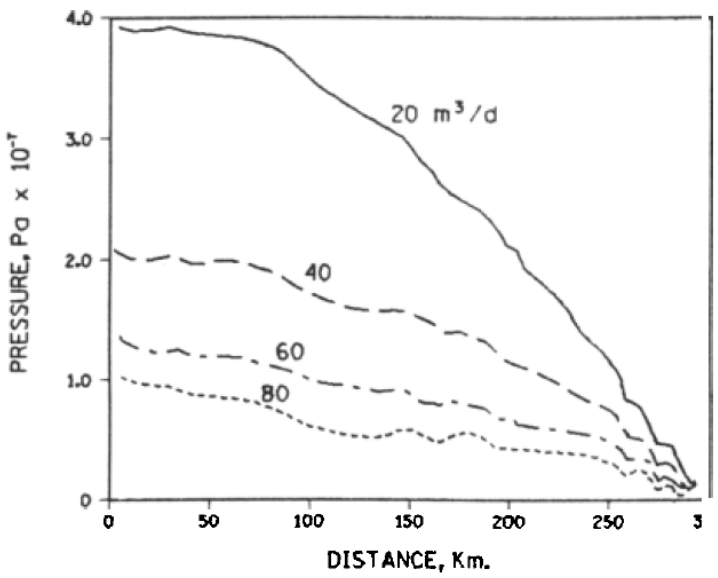

Figure 2-18: Pressure Distribution for a typical heated oil line at different flow rates (Guevara et. al, 1997)

2.3.2 Dilution

Dilution is an advanced method of reducing the energy required for transporting heavy oil through pipelines. The viscosity of the heavy crude is reduced by blending with less viscous hydrocarbons such as condensate, naphtha, kerosene and light crude oil. This method is being used in Canada, Venezuela and USA for heavy oil transport.

From Figure 2-19, it is evident that the volume fraction of the diluent influences the viscosity exponentially bringing about a drop in the effective viscosity of the mixture after blending. This brings to notice that even in small fractions the diluent has significant effect on the viscosity of the mixture makes it a very effective method of enhancement. The pressure loss can be calculated with reference to the viscosity value corresponding to the percentage of diluent in the mixture

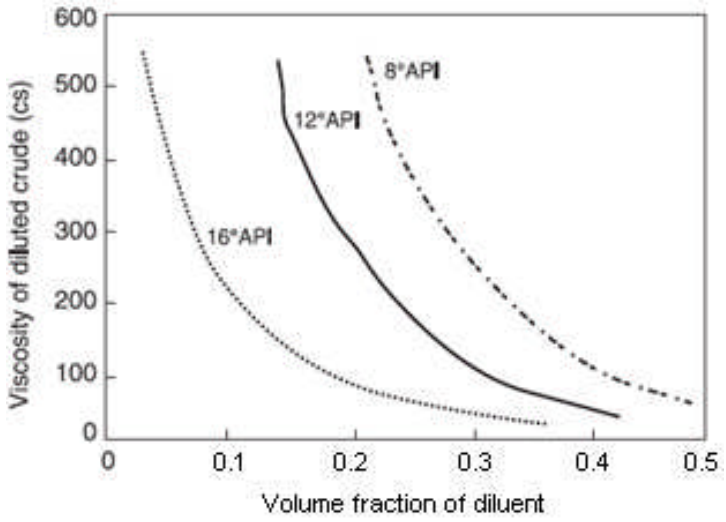

Figure 2-19: Effect of dilution with condensate on crude oil viscosity for different API gravities (Saniere et. al, 2004)

Condensates have been utilized in the enhancement of heavy oil transport in Canada since the 1980's for almost all its transport purposes (Argiller et al., 2005). Condensate used for blending of heavy oil and bitumen, because it is very effective and does the job as well as or better than any other known product, and until very recently has been in adequate supply, at reasonable cost (Urquhart, 1985).

One of the main problems affecting this technology is the availability of the condensates. If the condensates are not available in the field, other suitable alternatives are the manufacturing of diluents, using light crude or recycling of diluents.

Diluents can be manufactured from light crude from fractions usually used to produce gasoline, jet fuels and middle distillates. Naphtha is a good alternative to using condensates (Urquhart, 1985) due to its high API gravity; it shows very good compatibility with asphaltenes and can be recycled easily. Dilution with Naphtha has been used in Canada and Venezuela (Saniere et.al, 2004).Light crudes with API gravity ranging from 35^0 to 45^0 can be used directly although greater volumes are required (Escojido et.al, 1990).Both the cases require larger pipeline capacities which add to initial costs. A fraction as high as 30% in

volume of diluent is necessary and implies large pipeline capacity (Saniere et.al, 2004). Recycling the diluent implies recovery downstream and reinjection upstream, which requires additional pipelines and therefore more investment.

2.3.3 Oil in Water Emulsions

In this method the crude oil is transported in the form of an emulsion. As both fluids are immiscible, the emulsion can take many shapes as shown in Figure 2-20 (Oil-in-water, water-in-oil, and water-in-oil-in-water). However for oil viscosity reduction, the heavy oil is suspended in water in the form of micro spheres stabilized by chemical additives; thereby achieving an overall reduction is viscosity of the mixture. This method has been used in Venezuela since 1980.

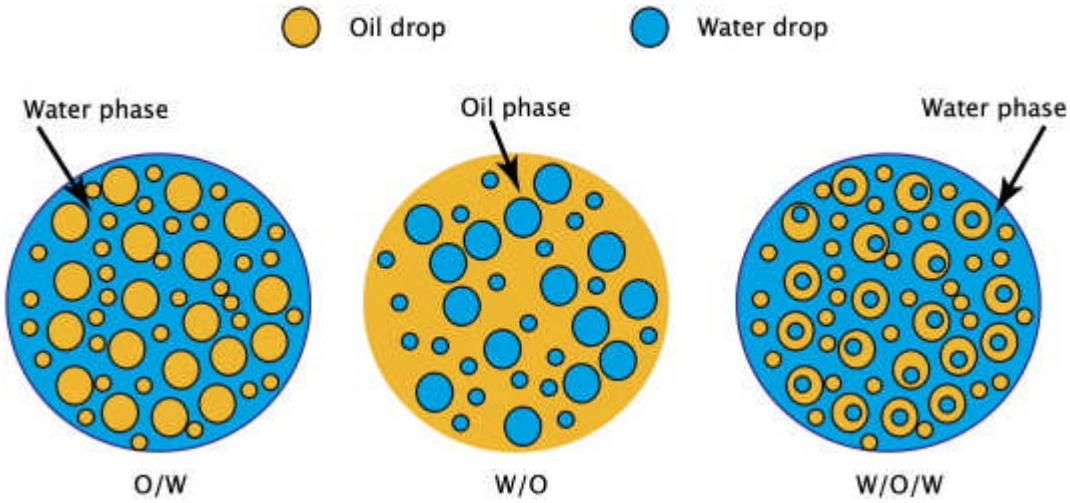

Figure 2-20: Emulsions found in petroleum production and transport (Martínez-Palou et al., 2011)

One of the main concerns of this method is its stability as it must withstand severe handling through pumps, valves and accessories therefore suitable chemical must ensure the stability of the emulsion under different conditions. The most relevant are temperature hydrocarbon/water ratio, water salinity and pH.

From Figure 2-21, the viscosity decreases exponentially with water content, the curve plays very important role to select the optimum amount of water to be present in the emulsion.

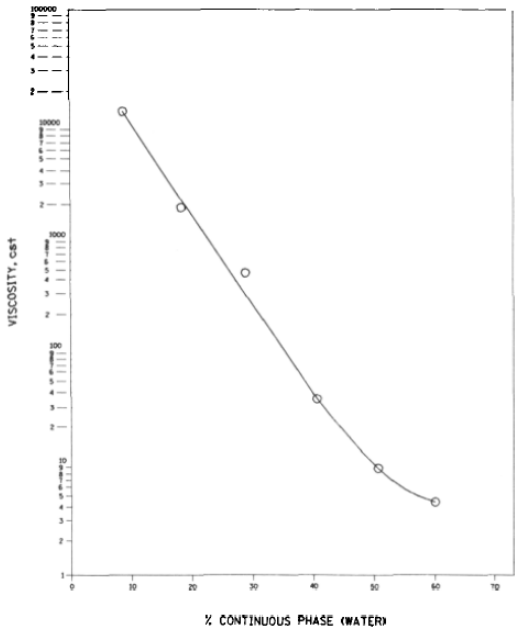

Figure 2-21: Viscosity versus % continuous phase for emulsions

(Escojido et. al, 1990)

A typical emulsion is composed of 70% crude oil, 30% aqueous phase and 500-2000 ppm of chemical additives. The resulting emulsion has a viscosity in the 50-200cP range at pipeline operating conditions and is particularly stable. This method is applied in Venezuela with the commercialization of ORIMULSION® product, emulsion sold as a fuel for electric power plant (Saniere et al., 2004).

TRANSOIL is a technology used for transporting heavy crude oils as oil in water emulsions. It was pioneered by BP Research International (BPRI) and Intevep, of the Venezuelan National Company in 1983.The application of this technology lies in the formation of HIPR (high internal phase ratio) emulsions, this allows oil droplet size characteristics which define the stability of the emulsion during transportation to be controlled effectively (Stockwell et al., 1988)

2.3.4 Core Annular Flow

In this method of enhancement the less viscous immiscible liquid, water gets introduced into the flow to act as a lubricating layer which absorbs the shear stress that would be generated due to the resistance to the flow of the oil.

The technique was considered long time ago, as Isaacs and Speeds (1904) mentioned the possibility to transport viscous fluids using water lubrication. However, commercial usage was never in operation until the 1970s (Bensakhria et al., 2004). One example is pipeline operated by Shell near Bakersfield, California, claiming to have transported significant amounts of high viscosity crude oil with water lubrication. Other researches were further developed in Venezuela by Maraven and Intevep, affiliated companies of Petroleos de Venezuela (Escojido et. al, 1990)

Since then, several works were dedicated to CAF regime and some reviews have been written (Oliemans et al., 1987; Joseph et al., 1996; Bannwart, 1999, 2001; Ghosh et al., 2009). Nevertheless, the capillary instability breaks the inner core into slugs at low velocity and stratification occurs in the system.

Current research points to the successful generation and possibilities of the core annular flow regime, although more field testing is necessary to confirm the reliability of this method of enhancement. Many studies were creating artificial core annular flow using special nozzles, few nozzle designs are shown in Figure 2-22

Hasson et al. (1970) designed the nozzle in a way that the flow path of lubricant is narrowed gradually. They reported this type of configuration reduced the inlet disturbances and also found that the symmetrical position of the nozzle was more effective; Parda and Bannwart (2001) used a conical injector nozzle. The nozzle inlet diameter was gradually reduced to finally match the pipe diameter and it injected water laterally to put the oil at the centre of the pipe. Grassi et al. (2008) used an injector which introduced water in the annulus while the heavy oil passed through the core region.

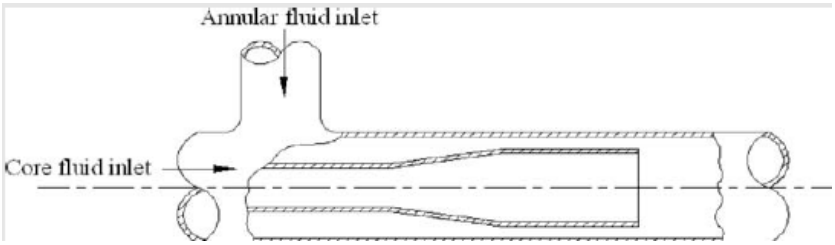

Hasson et al. (1970)

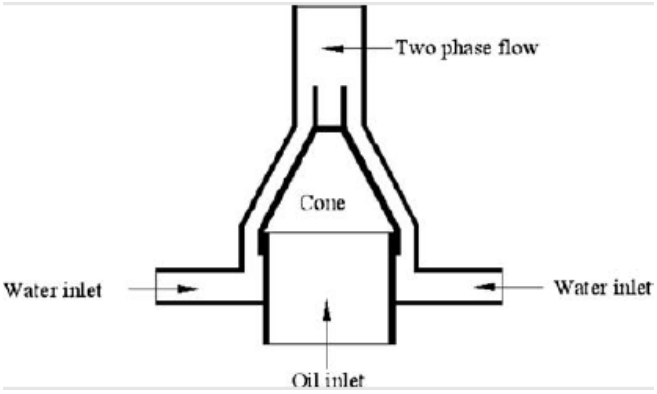

Parda and Bannwart (2001)

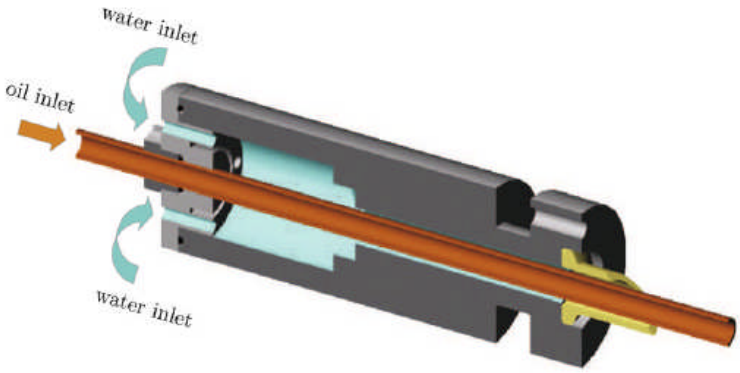

Grassi et al. (2008)

Figure 2-22: Special nozzle designs for CAF

Figure 2-23 is a flow pattern map for oil and water flow in a 2" horizontal pipe. The map conveys the fact that with increase in superficial velocity of oil, a continuous central core of oil flowing inside a film of water (core annular flow) is generated. The water fractions are typically in the range of 10-30% (Saniere et al., 2004).The stability of the flow pattern is weak which tends to break down

into mixed phase pattern. Further increase of the superficial velocity of the oil leads to a thinning and ultimately breaks up forming a direct emulsion of water in oil.

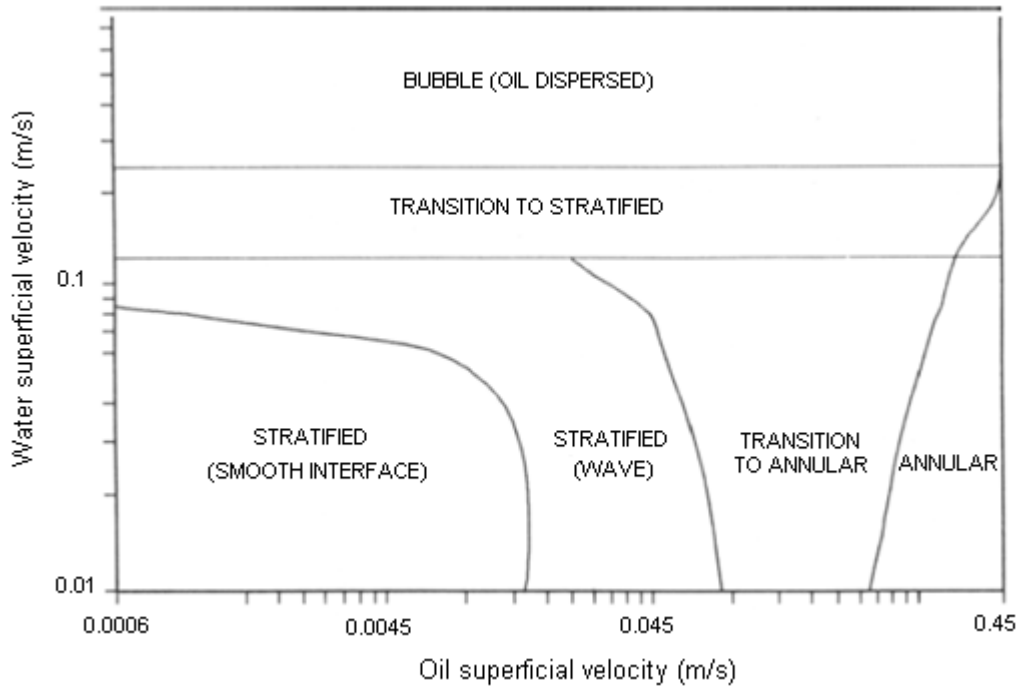

Figure 2-23: Typical Oil water flow pattern map for a 2" horizontal pipe (Escojido et. al, 1990)

The Figure 2-24 gives the pressure loss for annular core flow as a function of the water fraction, for different superficial oil velocities. When the water fraction is increased, the pressure loss decreases down to a minimum. The graph conveys that optimum water fraction in the range 0.08 – 0.12 produces the minimum pressure drop (Guevara et. al, 1997). The maximum reduction of pressure gradient is achieved with the core annular flow pattern. The stratified flow pattern also shows a pressure gradient reduction but much lower than with the annular flow pattern.

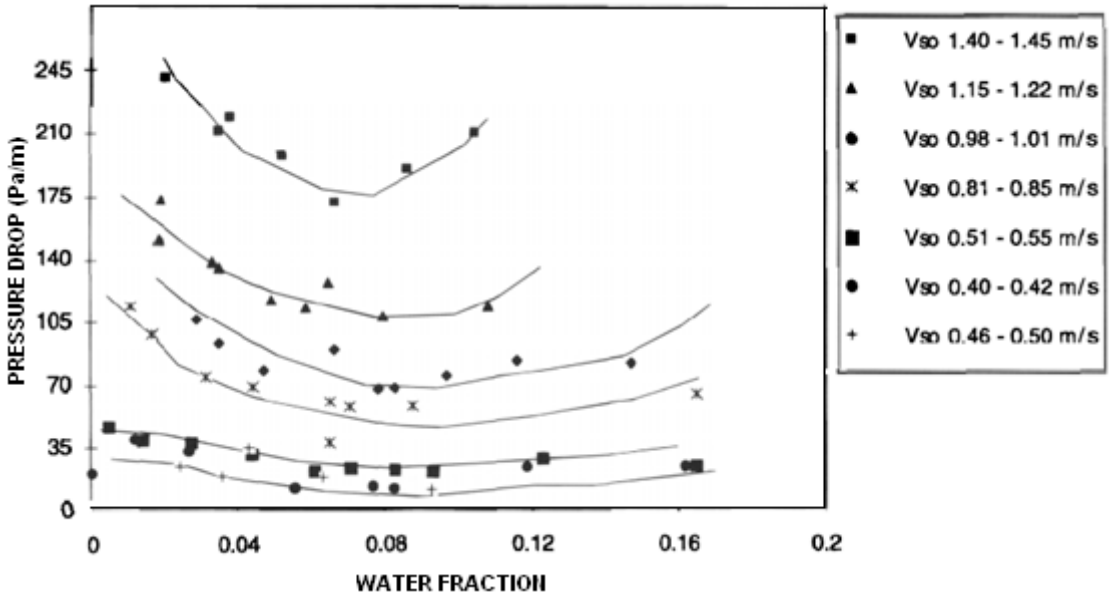

Figure 2-24: Pressure Loss versus Water fraction for different oil superficial velocities (V_{so}) and viscosities (Guevara et. al, 1997)

From earlier works, various reports have concluded on the enhancement produced by the core annular flow regime. Clark and Shapiro (1949) reported that for petroleum with a viscosity of 800 to 1000cP, the injection of 24% water reduced the pressure gradient by a factor of 7.8 – 10.5 and the optimum pressure reduction occurred when 8 – 10% water was injected into the crude oil. Russell and Charles (1959) proposed a theoretical model, according to which the power requirement for pumping oil at viscosity of 1000cP can be reduced almost 500 times by establishing core annular flow. The study mainly aimed at establishing core annular flow as an energy saving process in the transport of heavy oil.

2.3.5 Partial Upgrading

The infield partial upgrading of the heavy crude and bitumen is a new concept. The process is aimed at modifying the crude composition, lowering its viscosity and increasing its API gravity to improve its transportability without significantly altering its refining characteristics.

The Resource Technology Associates (RTA), Boulder, Colorado have reported successful field tests using the Geotrater process which is a thermal treatment of heavy crude oil to upgrade its properties for aid transport (Escojido et. al, 1990). Upgrading technologies such as hydrotreating processes traditionally used in refineries, can be considered for this application. Suitable treatments of this kind were developed by ASVAHL, Association for the Valorization of Heavy Oils (deasphalting process Solvahl, thermal treatment Tervahl process and catalytic hydrotreatment Hyvahl processes) (Saniere et al., 2004).

One of the main advantages of this method is that the upgraded crude can be transported without making changes to the transport pipeline and accompanying systems. The heavy oil to be treated is gathered at upgraders and the processed crude is transported through conventional pipelines. The costs of upgrading is the dominating factor that determines the application of this technology but the cost of upgrading facilities and its operation should be lower to justify the use of this method over others.

2.3.6 Comparison of Transport Methods

Guevara et. al (1997) compares the pressure drop for different heavy oil transport methods in Figure 2-25. The core annular flow methods experiences the lowest pressure drop for similar flow conditions hence implying least power requirement, ironically at the same time, core annular flow is very unstable flow pattern and may be destroyed unless fluid velocities are kept below certain level.

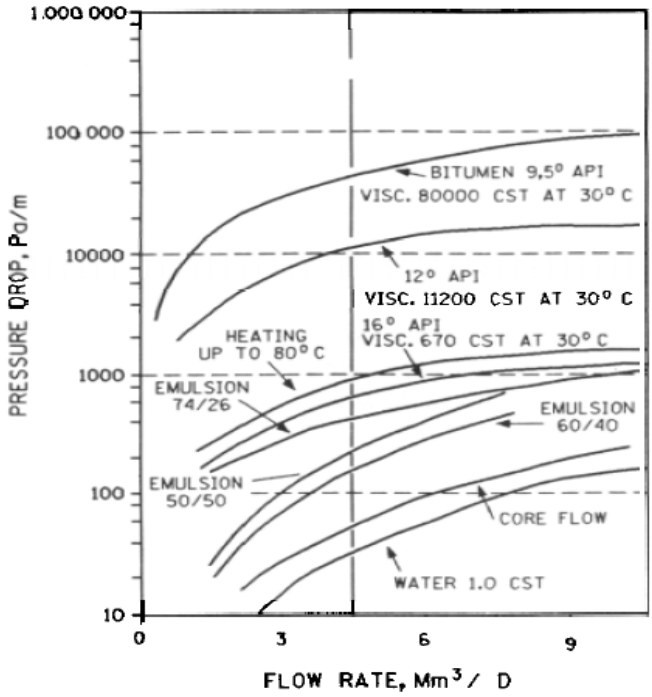

Figure 2-25: Comparison of different Transport Methods (Guevara et. al, 1997)

The stability of the emulsion plays the most important role in the flow stability of the oil in water emulsion method. The chemical additive concentration should be maintained such that the lifetime of the emulsion is long enough to complete its journey along the length of the pipeline, falling short will lead to plugging in the line.

The heating method is very stable considering backups are in place to prevent interruption of the heat supply.

With regard to shut – down and start – up, dilution and emulsion methods are the most adaptable to these changes considering the emulsion is kept stable for that duration.

Emulsion and dilution methods require larger pipelines as compared to others to handle the additional volumes of water, additives and diluent respectively which adds to the costs.

The presence of water in the emulsion cause high concern as this can lead to corrosion of the pipeline. Hence extra measures have to be taken into consideration to prevent corrosion.

Dilution and upgrading methods need very high additional investment for extra facilities. Dilution system requires a diluent recycling system and the upgrading demands high production costs.

Table 2-1 summarizes each method discussed above with their impact in terms of the conditions considered. Each method has its own advantages and disadvantages; it is how their application and characteristics suit the required function.

Heated pipelines may be preferred in warmer parts of the world like Venezuela and California due to low energy requirement for pumping and non – insulated pipes will reduce investment and operating costs. A combined used of diluent and heating can be used in cool countries where diluent availability is low. A lot more research and field testing is encouraged for the core annular flow methods as it has the lowest initial investment and operating costs.

	Heating	Dilution	Annular core flow	Emulsion	Upgrading
Pressure drop	Medium	Maximum	Minimum	Medium	Medium
Flow stability	High	High	High	High	High
Start-up/shut-down operation	Problematic	Flexible	Problematic	Depends on stability of emulsion	Flexible
Required pipe diameter	Normal (conventional flow)	Larger	Normal	Larger	Normal
Corrosion problems	None	None	Potential	Potential	None
Additional investment for additional facilities	Normal (heaters)	High (parallel diluent system)	Normal-High (water supply & disposal system)	Normal-High (water + surfactant supply system)	(field refinery)
Prediction models	Conventional non-isothermal	Conventional isothermal	Empirical & semi-empirical	Laboratory rheological model required	Conventional isothermal

Table 2-1: Comparison of different heavy oil transport methods

(Guevara et. al, 1997)

2.4 Two phase Gas-Liquid flow

The occurrence of two phase liquid-gas flows is very common in pipelines used in petroleum industries, as oil–gas flows are encountered in the production and transport of oil and gas, therefore the capacity to predict the flow patterns and pressure gradients of the flow becomes a very important topic of research.

2.4.1 Flow pattern

The most distinguishing aspect of multiphase flow is a variation in the physical distribution of the phases in the pipe flow, a characteristic known as flow pattern or flow regime. The flow regime depends on the relative magnitudes of the forces acting on the fluids; Such as buoyancy, turbulence, inertia and surface-tension forces, which vary significantly with flow rates, pipe diameter, pipe inclination and fluid properties.

There are some generally accepted descriptions for gas-liquid flow regimes. Concentrating on horizontal and near horizontal pipes, Beggs and Brill (1973) suggested three basic flow regimes: segregated, intermittent and distributed flow. The gas/liquid flow regimes in horizontal pipes are shown in Figure 2-26.

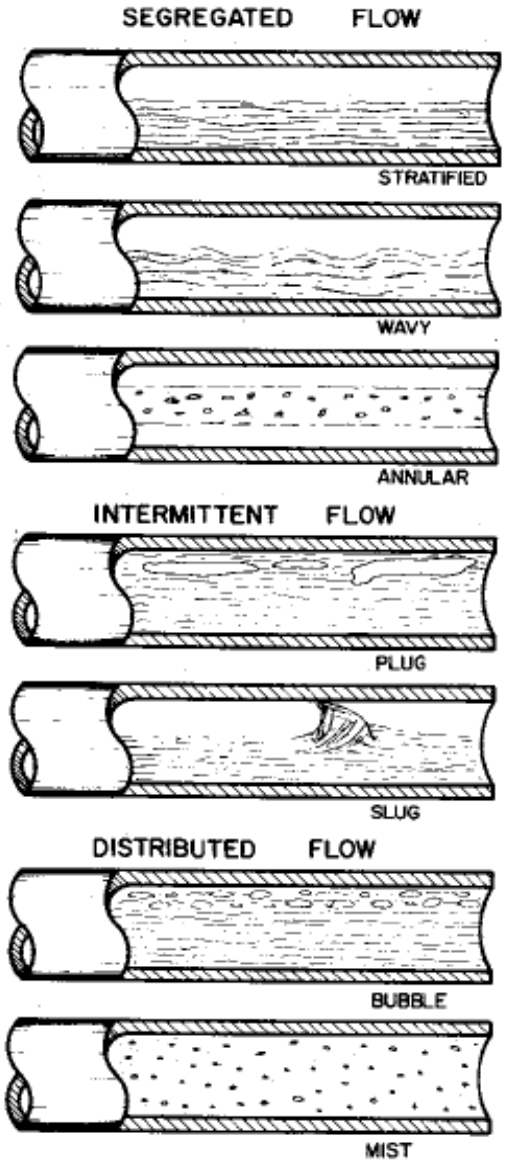

Figure 2-26: Flow patterns for horizontal Liquid – Gas Flows

(Beggs and Brill, 1973)

- **Segregated Flow**

Stratified Flow: The plugs coalesce to produce a continuous gas flow along the top of the pipe with the smooth gas-liquid interface typical of stratified flow.

Wavy Flow: In real situations, the gas-liquid interface is rarely smooth, and ripples appear on the liquid surface. Wavy flow occurs as ripples, this is due to

the gas flowing along the top of the pipe increasing in amplitude with increased gas flow rate.

Annular Flow: This flow regime occurs when gas flow rate is large enough to support the liquid film around the pipe walls. Liquid is also transported as droplets distributed throughout the continuous gas stream flowing along the centre of the pipe. The liquid film is thicker along the bottom of the pipe because of the effect of gravity

- **Intermittent Flow**

Plug Flow: Collisions between the individual bubbles occur more frequently with increasing gas flow rate and they coalesce into elongated bubble (plugs). This is also called elongated bubble.

Slug Flow: When the amplitude of the waves travelling along the liquid surface becomes sufficiently large enough for them to bridge the top of the pipe, the flow enters the slug flow regime. The gas flows as intermittent slugs, with smaller bubbles entrained in the liquid.

- **Distributed Flow**

Bubble Flow: The gas bubbles are dispersed in the liquid phase with higher concentration of bubbles in the upper half of the pipe due to their buoyancy. When shear forces are dominant, the bubbles tend to disperse uniformly in the tube.

Mist Flow: At very high gas velocities, all the liquid may be stripped from the pipe wall and entrained as small droplets in the continuous gas phase.

2.4.2 Studies on liquid viscosity effect

The literature is rich with two phase studies addressing the flow behaviour for low viscosity liquids and gases. However, very limited published work has been done to address high viscosity multiphase flow behaviour. The usage of relative terms (low and high) for viscosity in these studies were associated with values of 1 to 50 cP for low viscosity and anything beyond 100 cP is considered as high viscosity. A summary of the experimental research studies on gas-liquid flows found is given at the end of the section (Table 2-3).

Weisman et al. (1979) studied experimentally the effect of fluid properties and pipe diameter in horizontal pipes. The testing fluids consisted of air-glycerol water solutions with viscosities of 75 to 150 cP. They concluded liquid viscosity has minor effect on flow pattern transition boundaries.

Taitel and Dukler (1987) investigated the effect of pipe length on flow pattern transition boundaries for high viscosity liquids. The liquid (glycerine/water mixture) viscosity ranged from 90 to 165 cP. They concluded that pipe length can play considerable effect of transition boundaries for high viscosity liquids.

Andritsos et al. (1989) have done research into the effect of liquid viscosity on the initiation of gas-liquid slug flow in horizontal configuration. They proposed a mechanism for viscous liquids that slugs arise from small wavelength Kelvin-Helmhotz (KH) waves, which agreed with experimental results. However the new mechanism is applicable to liquids beyond 20 cP only.

Barnea (1991) proposed a combined model of viscous and inviscid KH stability analysis to determine the transition between slug and annular flows. It was shown that the combined model gave good results for different experimental data. As the results were compared to Taitel and Dukler (1976) model, which is the first mechanistic model to predict flow pattern transitions for horizontal and near horizontal gas-liquid flow, it was also shown that Taitel and Dukler (1976) model was valid for different liquid viscosities up to 100 cP.

Barnea and Taitel (1993) investigated the inviscid and viscous KH stability criteria for stratified flow. It was shown that results for low liquid viscosities were different for each analysis; on the other hand, they were similar for high liquid viscosities.

Colmenares et al. (2001) considered pressure drop models for horizontal slug flow for viscous oils. Based on their experimental results, the slug flow pattern enlarged as the oil viscosity increased; also by evaluating slug models, they concluded that the Barnea and Taitel (1993) was best to be used for high viscosity oils, and based on this, a modified model was developed for 480 cP. They concluded that slug length decreased, frequency and liquid film height increased as the liquid viscosity increased.

McNeil and Stuart (2003) experimentally investigated the high viscous liquid phase effect on two phase flow in vertical pipe. The liquid viscosities were ranged from 1 and 550 cP using water and glycerine solution. Annular flow was mostly observed in their study. It was concluded that correlations of entrained liquid fraction and interfacial friction factor for low viscous fluid are inapplicable to highly viscous range. They also developed a new correlation for the interfacial friction factor based on their experimental findings for high viscous fluid.

Gokcal et al. (2006) investigated two phase gas-oil flow in horizontal pipe. The experiments were conducted using viscous oil Citgo Sentry 220 and air. Holdup, flow regime maps, and pressure drop measurements were presented for 4 oil viscosities (181, 257, 378, and 587 cP). As most flow regimes observed was slug flow in addition to stratified wavy and annular flows, it was reported that the frequency of elongated bubbles increased with increasing viscosity while the bubble length decreased. Also, the presented data showed no significant effect of high oil viscosity on the location of transition boundaries. Finally, after comparing the experimental data for pressure gradient and liquid hold up against Zhang et al. (2003) unified and Xiao et al. (1990) mechanistic models, Gokcal et al. (2006) concluded that the models were insufficient for high

viscosity oils and new models should be developed to predict flow patterns, pressure losses, and liquid holdup more accurately.

Al-Safran et al. (2011) studied the slug flow characteristics for high viscosity liquid in horizontal pipe. Based on their experimental results, using viscous mineral oil, the slug front under high liquid viscosity condition was less turbulent due to low Reynolds number with top boundary layer moving faster than the slug body; bubble nose at the back of slug was long and accelerated by the wake of entrained gas pockets which leads to short slug; and liquid film height was large and aerated. A theoretical analysis with proposed empirical slug length model was developed and compared with existing models (Brill et al., 1980; Scott et al., 1981; Norris, 1982; Barnea and Brauner, 1985; Dukler et al., 1985) against experimental data. Although the Al-Safran et al. (2011) model had the best performance, the authors recommended more independent data was needed for further comparison and verifications.

Matsubara and Naito (2011) considered flow patterns identification using aqueous solution of polysaccharide thickener flowed concurrently with air through a test section, which had an ID of 20 mm and 19 m in length. Viscosity of these water solutions varied from 1 to 11000 mPa s with Newtonian viscosity. The results obtained showed that the flow patterns strongly depend on the liquid viscosity, and were not in agreement with previous work by Weisman et al. (1979). Also Taitel and Dukler (1976) model could not predict the flow pattern transition. Therefore different approach is needed to cover flow prediction in highly viscous fluid.

2.4.3 Phenomenological models

The determination and prediction of pressure drop in multiphase flow are vital to the design of industrial transport systems and in chemical or petroleum process. Accurate prediction of pressure drop in multiphase pipeline is of great economic importance but has proved to be very difficult. In this section, several empirical correlations for pressure drop prediction are summarized.

The total pressure drop for given steady state two-phase flow is the sum of pressure drop due to kinetic energy (acceleration) effects, hydrostatic (gravitation) effects and fluid friction effects:

$$\left|\frac{\Delta P}{\Delta x}\right|_{Total} = \left|\frac{\Delta P}{\Delta x}\right|_{Acceleration} + \left|\frac{\Delta P}{\Delta x}\right|_{Gravitation} + \left|\frac{\Delta P}{\Delta x}\right|_{Friction} \quad [3]$$

In steady, fully developed, isothermal flow of an incompressible fluid in a straight pipe of constant cross section, friction has to be overcome as does the static head, unless the pipe is horizontal. However there is no change of momentum and consequently the acceleration term is zero.

- Homogenous flow model

The simplest methods of two-phase flow prediction are the homogenous models. It is assumed that the two-phase flow can be treated as a hypothetical single-phase flow having some kind of average properties. An early example of a homogenous model was that by McAdams et al. (1942) which used values of the mixture density and viscosity to calculate the two-phase pressure gradient using single phase friction correlations.

- Separated flow model (flow-regime independent)

An alternative approach is the use of separated flow methods, where the flow of each phase is considered independently and then a procedure is applied to arrive at the result for the two phase mixture. The traditional method is to predict multiphase flow parameters by fitting correlations to large sets of experimental data. The relationships thus obtained are not easily extended to conditions which are

physically very different from the original experimental systems. Therefore, the correlations obtained in this way are regardless of the gas-liquid flow regimes and have been used as closure for simplified phenomenological models.

In separated flow models, the two-phase frictional pressure gradient is calculated from a reference single-phase frictional pressure gradient $|\Delta P/\Delta x|_{iO}$ with multiplying by the two-phase multiplier Φ_i^2, the value of which is determined from empirical correlations:

$$\left|\frac{\Delta P}{\Delta x}\right|_{\text{Friction}} = \Phi_i^2 \left|\frac{\Delta P}{\Delta x}\right|_{iO} \qquad [4]$$

where i is L or G (i.e. LO denotes liquid only and GO is gas only).

The most famous example of separated flow methods is the work by Lockhart & Martinelli (1949) who proposed a graphical correlation for the prediction of pressure drop and liquid holdup. The experimental work on which the correlation was based on horizontal flow of air-water mixtures at near-atmospheric pressures and with no change of phase and it is inadvisable to use the correlation for other conditions. Since the experiment done in this study was always above atmospheric pressure due to the nature of high liquid viscosity, other models were considered based on flow regime map.

- Models based on flow regime map

A limited number of pressure drop correlation incorporate a crude method of determining the flow pattern from the value of a parameter based on the phase velocities. The pressure drop correlation of Beggs & Brill (1973) and Dukler et al. (1964) used widely in the hydrocarbon industry, both of these methods are described in this section below:

- Beggs & Bell (1973)

Flow pattern	Determining flow regimes	H_{L0}	Parameters calculation
Segregated	$\lambda_l < 0.01$ & $Fr_m < L1$ or $\lambda_l \geq 0.01$ & $Fr_m < L2$	$\frac{0.98\lambda_l^{0.4846}}{Fr_m^{0.0868}}$	$Fr_m = \frac{V_m^2}{gD}$ $\lambda_l = \frac{V_{sl}}{V_m}$ $L1 = 316\lambda_l^{0.302}$ $L2 = 9.252*10^{-4}\lambda_l^{-2.4684}$ $L3 = 0.1\lambda_l^{-1.4516}$ $L4 = 0.5\lambda_l^{-6.738}$
Intermittent	$0.01 < \lambda_l < 0.4$ & $L3 < Fr_m \leq L1$ or $\lambda_l \geq 0.4$ & $L3 < Fr_m \leq L4$	$\frac{0.845\lambda_l^{0.5351}}{Fr_m^{0.0173}}$	
Distributed	$\lambda_l < 0.4$ & $Fr_m \geq L1$ or $\lambda_l \geq 0.4$ & $Fr_m > L4$	$\frac{1.065\lambda_l^{0.5824}}{Fr_m^{0.0609}}$	
Transition	$\lambda_l \geq 0.01$ & $L2 < Fr_m < L3$	$\left(\frac{L3 - Fr_m}{L3 - L2}\right)\frac{0.98\lambda_l^{0.4846}}{Fr_m^{0.0868}} - \left(\frac{Fr_m - L2}{L3 - L2}\right)\frac{0.845\lambda_l^{0.5351}}{Fr_m^{0.0173}}$	

Table 2-2: Determination method of air-water flow regime using Beggs and Brill (1973) correlation

where V_m is the mixture velocity, which is the summation of superficial velocities of each fluid ($V_m = V_{sl} + V_{sg}$). λ_l and H_{L0} are the no-slip and actual liquid holdup in horizontal pipe. The liquid holdup at any pipe inclination, $H_{L\beta}$, is then calculated:

$$H_{L\beta} = H_{L0}\left(1 + c\left(\sin 1.8\,\beta - \frac{1}{3}\sin^3(1.8\,\beta)\right)\right) \qquad [5]$$

β is the pipe inclination from the horizontal axis in radian. Therefore $H_{L\beta} = H_{L0}$ for horizontal flow.

The two-phase density, ρ_{TP} (lb/ft^3), and the two-phase friction factor, f_{TP} is then calculated.

$$\rho_{TP} = \rho_l \lambda_L + \rho_g (1 - \lambda_L) \quad [6]$$

$$f_{TP} = f_{NS} * e^S \quad [7]$$

Here, S is a liquid holdup parameter and f_{NS} is the no-slip friction factor which can be obtained by smooth pipe chart or using the following formula:

$$f_{NS} = \left(2 \log \left(\frac{Re_{NS}}{4.5223 \log Re_{NS} - 3.8215} \right) \right)^{-2} \quad [8]$$

The "no slip" Reynolds number, Re_{NS}, is given by:

$$Re_{NS} = \frac{[\rho_l \lambda_L + \rho_g (1 - \lambda_L)] V_m D}{\mu_l \lambda_L + \mu_g (1 - \lambda_L)} \quad [9]$$

The value of S is governed by the following conditions:

if $1 < y < 1.2$, then

$$S = \ln (2.2 y - 1.2) \quad [10]$$

else

$$S = \frac{\ln(y)}{-0.0523 + 3.182 \ln(y) - 0.8725 [\ln(y)]^2 + 0.01853 [\ln(y)]^4} \quad [11]$$

y is calculated by

$$y = \frac{\lambda_L}{H_{L\beta}^{\ 2}} \quad [12]$$

Finally, the friction pressure gradient (mbar) is calculated:

$$\left|\frac{\Delta P}{\Delta x}\right|_{Friction} = \frac{2 f_{TP} V_m{}^2 \rho_{TP}}{144 g_c D} * 68.948 \quad [13]$$

g_c is conversion factor = 32.2 $lb_m \cdot ft/(lb_f \cdot s^2)$

- Dukler et al. (1964)

The correlation is based on wide range of measured data. Although flow patterns are not considered, the kinetic term is included. The authors proposed an iterative procedure for liquid holdup calculations and can be used for pipe diameters of up to 5.5 in.

Dukler et al. (1964) compiled a data bank consisting more than 20000 measurement data taken from different sources. After carefully culling 2620 pressure drop measurements constituted the basis for the developed correlation, the range of practical applications covered in these measurements came from pipe diameter range of 1 to 5.5 inch and liquid viscosities of 1 to 20 cP. Though several correlations for horizontal two phase flow were developed, the universally accepted one is the constant slip model,

$$f_{TP} = f_{NS} \frac{1}{\left[(\rho_l/\rho_{TP})\frac{\lambda^2}{H_{L\beta}} + (\rho_g/\rho_{TP})\frac{(1-\lambda)^2}{(1 - H_{L\beta})}\right]} \quad [14]$$

$$f_{dukler} = f_{TP} * \left(1 + \frac{y}{1.281 - .478y + 0.444y^2 - 0.094y^3 + 0.00843y^4}\right) \quad [15]$$

where $y = - \ln \lambda$, finally, the friction pressure gradient (mbar) is calculated using equation [13].

2.4.4 Summary

A lot of experimental and theoretical work has been done on the flow pattern analysis of liquid-gas flow. Yet when it comes to high viscosity oil, only limited studies are available and no general results has been obtained or accepted so far. This is mainly due to the limitation of experimental results within high viscosity region. This thesis will cover the effect of viscosity and fluid flowrates on pressure drop and flow pattern for different flow conditions.

Table 2-3 summarizes all the experimental research studies on gas-liquid flows found in this section.

Authors	Pipe ID (mm)	Pipe material	Fluid type	Liquid properties	Comments
Weisman et al. (1979)	11.5, 25, 51	Glass pipe	Air/ water glycerol solution	μ= 75, 150 cP ρ = 1210, 1240 kg/m^3 σ = 65 dyne/cm	Evaluating fluid property and pipe diameter effects on flow transitions. Although deficiencies were found for the data when compared with literature, a revised dimensionless correlations was devised to fit all reliable data
Taitel and Dukler (1987)	38	N.A.	Air/ water glycerine solution	μ= 90, 165 cP	The importance of pipe length on the transition line was demonstrated. 0.9 < V_{sg} < 20 m/s & 0.001 < V_{sl} < 0.6 m/s
Andritsos and Hanratty (1987)	25.2	N.A.	Air/ water glycerine solution	μ= 1, 4.5, 16, 70 cP	Defined three types of instabilities waves: pressure variations in phase with the wave slope, irregular large-amplitude waves and atomization of the liquid are associated with pressure variations in phase with the wave height. Linear stability theory was used to predict conditions for the initiation of these instabilities.
Andritsos et al. (1989)	95.3	N.A.	Air/ water glycerine solution	μ= 1, 20, 100 cP	For high viscous liquids, a stability analysis which recognizes that slugs originate from a train of small-wavelength sinusoidal waves was consistent with the measurements.
Colmenares et al. (2001)	50.8	N.A.	Air/ lube oil	μ= 480 cP	Modified mechanistic model is formulated to predict the pressure drop in horizontal slug flow.
McNeil and Stuart (2003)	100	PVC	Air/ water glycerine solution	μ= 1, 50, 200, 550 cP ρ = 1000, 1190, 1235, 1260 kg/m^3	Studied the effect of viscosity on vertical upward flow. The flow pattern was mainly annular up-flow. Annular flow model was extended by proposing interfacial friction factor for high viscous liquid.
Gokcal et al. (2006)	50.8	Acrylic pipe	Air/ Citgo Sentry 220 oil	μ= 181, 257, 378, 587 cP ρ = 889 kg/m^3	Investigated the liquid viscosity effect on flow pattern, pressure gradient, and liquid holdup. 0.01 < V_{sl} < 1.75 m/s & 0.1 < V_{sg} < 20 m/s
Al-Safran et al. (2011)	50.8	Steel and Acrylic pipes	Air/ viscous mineral oil	μ= 1 - 590 cP	Quantified the effect of liquid viscosity on slug length and developed a dimensional analysis based model to predict the average slug length for high viscosity liquid slug flow.
Matsubara and Naito (2011)	20	Polyphenyl sulphone	Air/ water polysaccharide	μ= 1, 100, 250, 2500, 7500, 11000 cP	Investigated the effect of liquid viscosity on the flow patterns. The flow patterns were strongly depended on the liquid viscosity, 0.002 < V_{sl} < 0.2 m/s & 1 < V_{sg} < 30 m/s

Table 2-3: Review of range of experimental variables for gas-liquid flows

2.5 Two phase Liquid-Liquid flow

The simultaneous flow of oil and water in pipelines is a common occurrence in the petroleum industry. As the offshore oil and gas exploration and production are increasing, more and more pipelines need to be designed to be able transport the well fluid over a long distance. Usually, the fluid delivered by the well contains water, which is already present within the stratum. Water fractions often increase during the producing life of a well. The presence of water must be properly accounted for when designing and predicting the flow behaviour in both wells and pipelines.

Moreover, due to the increasing interests in heavy oil, considerable efforts have been invested in developing pipeline systems for field transport of heavy oil. Although it is a standard practice to locate collection tanks near the heavy oil well site and use trucks as transportation method, many attempts have been made to design an energy efficient and environmental friendly pipeline system.

For a successful design, it is vital to include the detailed information of actual pipe flow into consideration. As in air-liquid flow systems, determination of the flow patterns and pressure loss is a central problem in oil-water two-phase flow analysis. Dynamic flow characteristics of oil-water mixture can be crucial in many aspects, such as: determining the amount of free water in contact with the pipe wall that can cause corrosion/erosion problems, collecting the correct interpretation of the response of production logging instruments, and enhancing the performances of separation facilities and multiphase pumps. The oil-water flow patterns were usually determined by the visual observation. However, with the advanced instruments and techniques, different flow pattern parameters (pressure drop, oil/water holdup…etc.) have been measured more accurately, and flow patterns of oil–water flow have been analyzed objectively.

Both the oil-water flow patterns and the pressure loss are strongly dependent on the fluid viscosity. Dusseault (2002) suggested 100cP as a lowest viscosity

value for heavy oil. Therefore, the following review on oil-water studies were divided into two subsections which were dealing with low viscosity oil (<100cP) /water system and high viscosity oil (≥100cP) /water system respectively. A summary of the experimental research studies on liquid-liquid flows found is given at the end of the section (Table 2-6).

2.5.1 Low viscosity oil/water system

As reported by Govier and Aziz (1972), four kinds of flow patterns named bubble (oil dispersed), slug (oil dispersed), (both phases dispersed) and mist (water dispersed) flow were defined in a horizontal pipe with an inner diameter of 26 mm using oil with viscosity of 6.29, 16.8 and 16.8 cP and density of 834 kg/m^3 (Charles et al., 1961).

Arirachakaran et al. (1989) observed Stratified flow, Mixed flow, Annular flow, Intermediate flow and Dispersed flow, five flow patterns of oil-water flow in two horizontal tubes with 41 and 26 mm ID.

In their flow pattern map, intermediate flow existed under very narrow flow conditions. Nadler and Mewers (1997) conducted similar investigations in a horizontal straight pipe with 59 mm ID They distinguished flow patterns and presented a flow pattern map, but did not observe intermediate flow.

Significant progress has been made in understanding the flow patterns of the light oil–water flow in recent years. New and more comprehensive flow patterns based on published data were proposed by Trallero (1995). He studied oil-water flow pattern in a 50cm ID, 15.54 m horizontal pipe, both experimental and theoretically. Six flow patterns were identified and described in details, as shown in Figure 2-27.

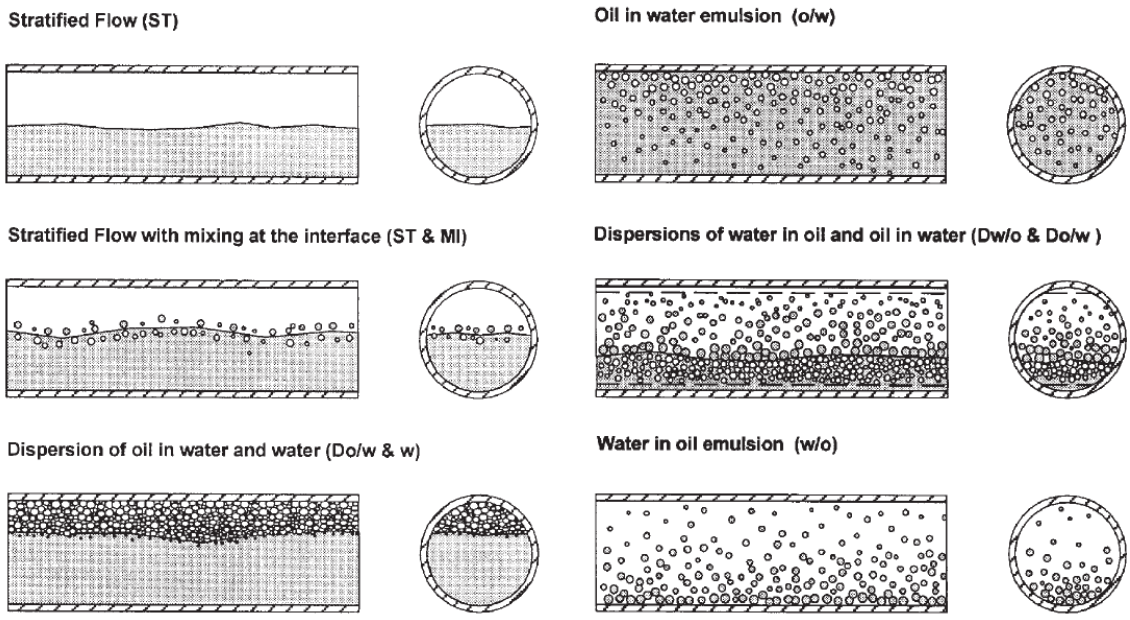

Figure 2-27: The oil–water flow patterns (Trallero, 1995)

- Segregated flow
  - Stratified flow (ST)
  - Stratified flow with mixing at the interface (ST&MI)
- Dispersed flow
  - Water dominated
    - Dispersion of oil in water and water layer (Do/w & w)
    - Oil in water emulsion (o/w)
  - Oil dominated
    - Dispersion of oil in water and water in oil (Do/w & Dw/o)
    - Oil in water emulsion (w/o)

For low oil and water superficial velocities, the flow is gravity dominated and the phases are segregated. The oil/water interface is smooth initially, even though the water phase could be in transition to the turbulent flow pattern (ST). A further increase in the flow rates will cause the appearance of interfacial waves.

Water droplets exist in the oil layer and oil droplets in the water layer (ST&MI). Both water and oil droplets remain close to the interface.

Dispersions will always form when the motions of two immiscible liquids are sufficiently intense. An emulsion is a stable dispersion and it is used to describe a tight dispersion or when the discontinuous phase is totally dispersed. There are water-in-oil (W/O) dispersions and oil-in-water dispersions (O/W). It can be considered as a homogeneous mixture only at sufficiently high mixture velocities. The droplet size distribution depends on fluid properties, superficial velocities, pipeline length and orientation. When an O/W dispersion changing to a W/O dispersion, it is called a phase inversion, and that point when it occurs called the inversion point.

For intermediate superficial velocities, the forces associated with the motion are not sufficient to maintain all the droplets suspended, and some of them eventually settle. The more dense droplets accumulate at the bottom of the pipe while the less dense droplets rise to the top. In these regions, if the droplet concentration is sufficiently high, a coalescing process begins and a continuous layer of the dispersed phase is formed. For large water superficial velocities, the flow is water dominated. Water vortices appearing at the interface enter the oil layer and tend to displace it. However, the water flow energy is still insufficient to distribute larger oil droplets along the cross section of the pipe. Then, the upward buoyancy force prevails, and a dispersion of oil in water over a water layer (DO/W and W) is developed. On the other hand, oil is the dominant phase for small input water fractions. The interfacial mixing region grows with an increase in velocity, and the two types of dispersions coexist (DW/O and DO/W).

Trallero's flow pattern classification and prediction were widely used by many researchers dealing with low viscosity oil-water systems (Valle and Utvik, 1997; Rodriguez and Olimans, 2006; Vielma et al., 2007 and Atmaca et al., 2008). It was found that Trallero's flow pattern predicted the oil-water flow patterns quite well in horizontal and slightly inclined oil water flows (Rodriguez and Olimans,

2006; Vielma et al., 2007 and Atmaca et al., 2008). However, they reported some discrepancy at the transition boundaries at ST and ST&MI flow patterns which they believed was caused by the different experimental conditions.

Chen and Guo (1999) classified the oil/water two-phase flow according to their observations and analysis. The flow patterns schematically shown in Figure 2-28 were categorized into four patterns, which can be distinguished as follows:

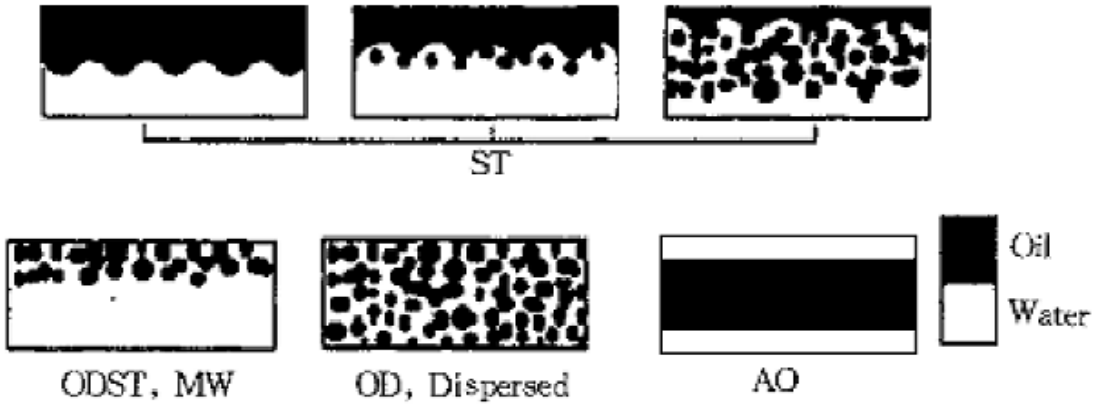

Figure 2-28: Classification of oil—water flow patterns in coiled tubes (Chen and Guo, 1999).

- Stratified Flow Fattern (ST)

Stratified flow pattern occurs within the lower mixture velocity conditions. It is characterized by the existence of a distinct interface between the oil and water phases and a continuous liquid film flowing along the tube wall for each phase. Oil flows at the upper part of the tube, while water flows at the lower part. (i) Since both two-phase velocities are sufficiently low, there exists a distinct interface. No blending of the two phases around the oil/water interface was found. Waves on the oil/water interface were always observed: long-wavelength waves due to the gravitational force. (ii) Increasing the velocity of the two-phase mixture, the momentum transferred between the oil and water phases through the interface is increased. At certain condition, some amount of the continuous oil phase becomes dispersed oil droplets near the interface. Further increasing the

velocity of the mixture, the amount of the oil droplets increases and the thickness of the continuous oil layer decreases.

- Oil-Droplet Stratified Flow (ODST)

Oil-droplet stratified flow occurs at the higher water fraction conditions. Within this flow pattern, the oil phase, characterized by different size droplets, exists within the continuous water phase. Due to buoyancy, all the oil droplets agglomerate at the upper part of the tube, while the water phase flows at the lower part.

- Oil-Dispersed Flow (OD)

All the oil phase is present as oil droplets and distributed homogeneously in the continuous water phase. This flow pattern occurs under higher mixture velocity and higher water cut conditions.

- Annular Oil Flow (AO)

Annular oil flow occurs under higher oil flow rate and lower water flow rate. The oil phase flows along the tube wall as a continuous phase, while water flows in the core of the tube as water droplets and water filaments.

Angeli and Hewitt (2000) carried out oil–water flow pattern experiments with two different pipe materials (steel and acrylic), and four flow patterns were observed both in acrylic and steel pipe, as shown in Figure 2-29:

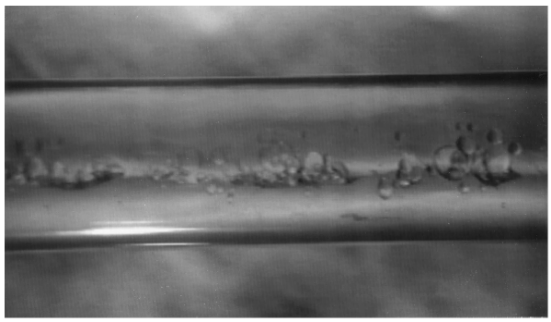

Stratified Wavy with Drops (SWD)

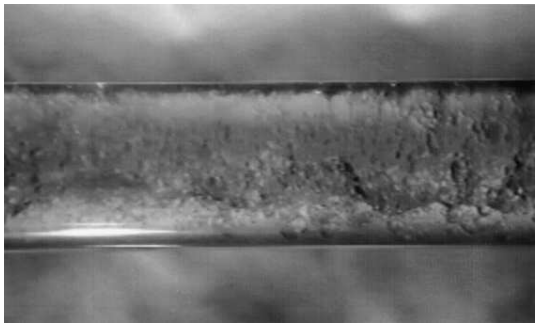

Three Layer (3L) flow pattern

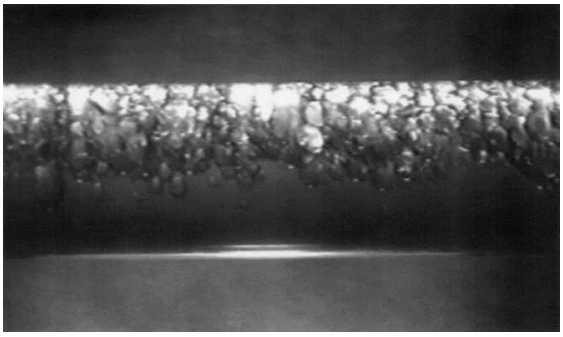

Stratified Mixed with water layer (SM/water)

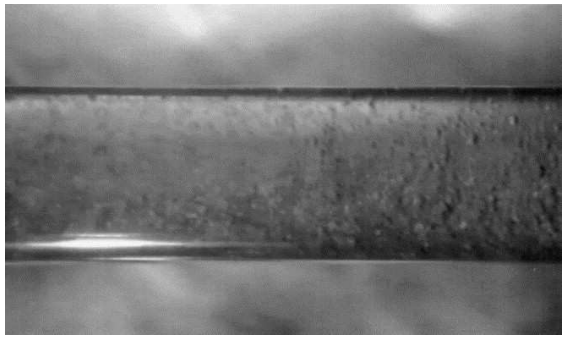

Mixed (M) flow pattern

Figure 2-29: The oil–water flow patterns (Angeli and Hewitt, 2000)

Stratified Wavy flow pattern (SW): Two fluids flowed in separate layers on the top and bottom of the pipe according to their densities and their interface was disturbed.

Three Layer flow pattern (3L): Distinct continuous layers of oil and water were observed at the top and bottom of the pipe respectively but in the interface there existed a layer of drops while drops of each phase could appear within the other phase.

Stratified Mixed flow pattern (SM): Here one phase was continuous while the other was in the form of drops occupying only part of the pipe. At high water fractions, where water was the continuous phase, there was a layer of oil drops at the top of the pipe (SM/water flow pattern), while at low water fractions,

where oil was the continuous phase, there was a layer of water drops on the bottom of the pipe (SM/oil flow pattern).

Fully Dispersed or Mixed flow pattern (M): here one phase was dispersed more or less uniformly into the other and occupied a whole pipe cross section.

During their experiment, they found that the flow patterns in the steel pipe were in general more disturbed than those in the acrylic pipe and there was only a very narrow stratified wavy region in the steel tube while the mixed region started at lower velocities than in the acrylic tube. They also found that in the acrylic pipe the oil continuous flow patterns (Stratified Mixed/oil, Three Layer) persisted over a wider range of mixture velocities and water fractions than in the steel pipe due to different wettability of the two pipe materials from the oil and the water. Based on those facts, they concluded that the wall roughness and the different wettability characteristics of the two pipe materials would affect the oil–water patterns.

Abduvayt et al.'s (2006) experiments involved the study on oil – water flows using a 40m long pipe test section with internal diameter 106.4mm and different orientations (0, 0.5±, 3±, and 90± degrees). A total of twelve flow patterns were identified which are grouped under three basic types, segregated, semi – segregated and semi – dispersed flow. The mentioned flow patterns have been identified and reported as shown Figure 2-30, the flow patterns have been classified under each group as:

- Segregated flow
  - Stratified smooth (ST – S),
  - Stratified wave (SW),
  - Stratified roll wave (SR),
  - Oil at top of pipe and water (O/TP & W), and
  - Oil with water film and water (O – WF & W).

- Semi – Segregated Flow
  - Stratified with water droplets in oil and water (ST – WD/O & W),
  - Stratified with water droplets in oil and oil droplets in water (ST – WD/O & OD/W),
  - Stratified roll wave with water droplets in oil and water (SR – WD/O & OD/W), and
  - Stratified long roll with oil droplets in water and water droplets in oil (SLR – OD/W & WD/O).
- Semi – Dispersed Flow
  - Dispersion of water in oil and water (DW/O & W),
  - Thin oil line at the top of pipe and fine dispersion of oil in water (ThO/TP & FDO/W), and
  - Fine dispersion of water in oil and fine dispersion of oil in water (FDW/O & FDO/W).

The flow regime map was generated for the superficial oil and water velocities as shown in Figure 2-31

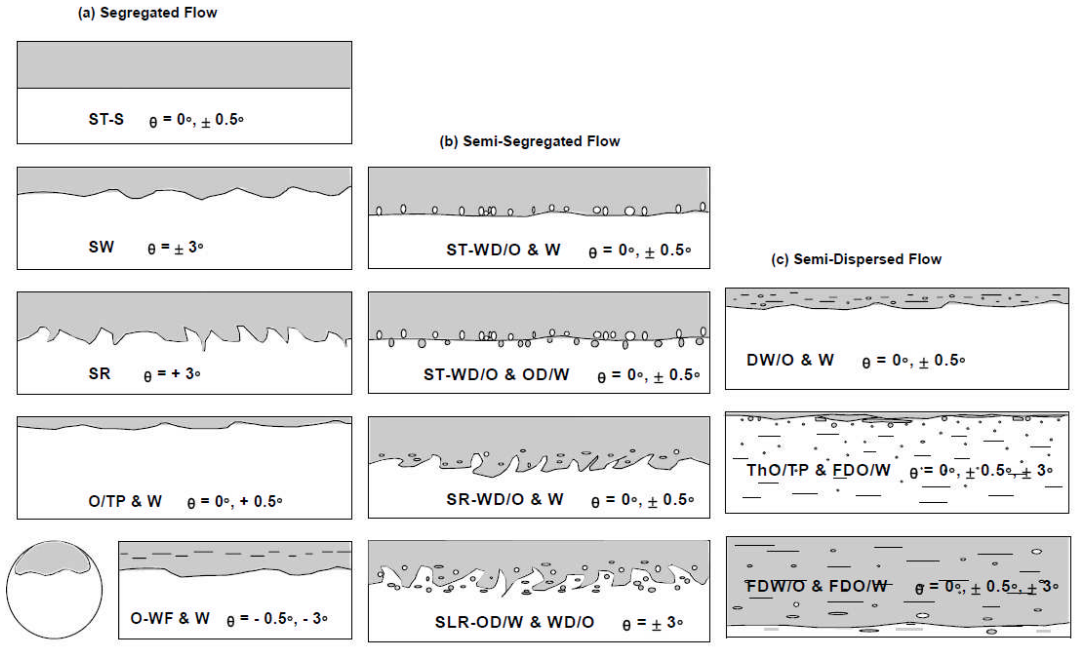

Figure 2-30: Flow patterns for Oil – Water flow in horizontal pipes

(Abduvayt et al., 2006)

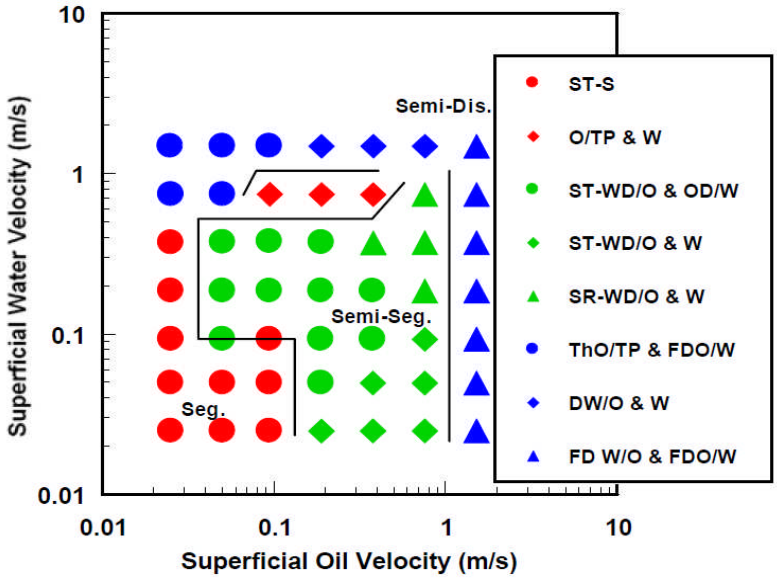

Figure 2-31: Flow Regime Map for Oil – Water flow in horizontal pipes (Abduvayt et al., 2006)

2.5.2 High viscosity oil/water system

- Arirachakaran et al. (1989)

The experiments were conducted on oil – water flows for viscosities of 4.7, 58, 84 and 115cP for 41 mm internal pipe diameter and viscosities of 237 and 2116cP for 26 mm pipe diameter. The experiments and undertaken using water fractions from 0.05 to 0.9 and mixture velocity of 0.5 to 3.7m/s. The experiments were aimed at obtaining pressure drop, flow patterns, flow rates, water fraction, holdup, and mixture temperature. The flow patterns observed were defined and a generated flow patter map were given as shown in Figure 2-32.

The phase inversion point prediction was determined as key parameter in the design of oil-water dispersion system. Increasing oil viscosity decreased the required input water fraction to invert an oil-water dispersion system. Also mixture velocity, which was a very important parameter in the flow pattern determination, did not have significant effect on the inversion concentration for an oil-water system as long as the flow regime was laminar.

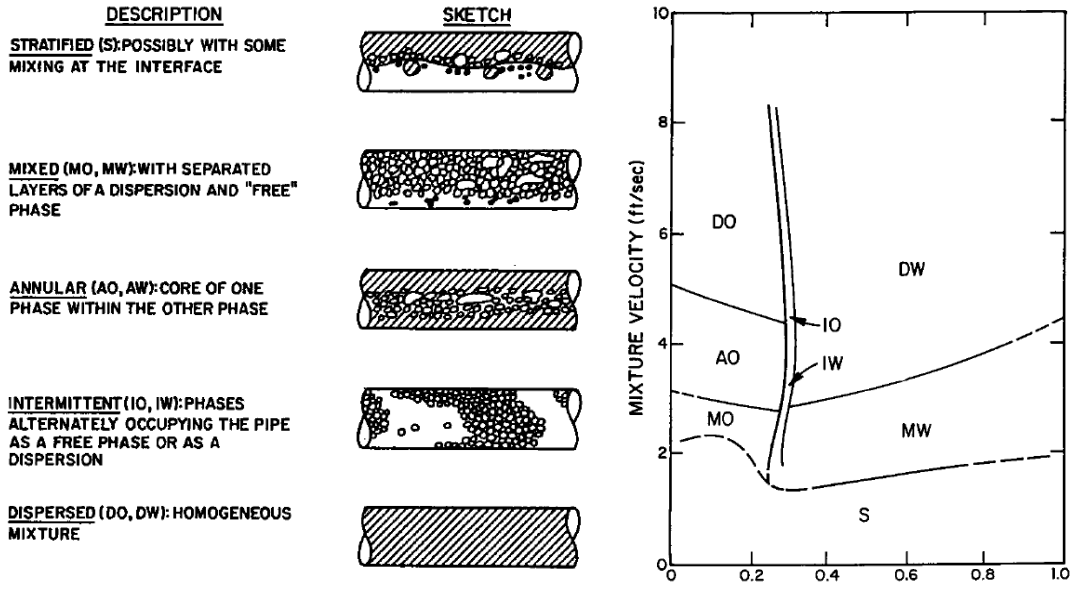

Figure 2-32: Oil – Water schematic drawing and flow patterns (Arirachakaran et. al, 1989)

- Bai et al. (1992)

Bai et al. (1992) performed experiments with cylinder oil (μ = 600 cP and ρ = 905 kg/m^3) and water, using a 9.5 mm diameter pipe in vertical upward/downward and horizontal flow. The flow patterns were sketched in Figure 2-33 - Figure 2-35 and formed by (Joseph and Renardy, 1993; Joseph et al., 1997). They identified a new flow type namely bamboo waves (Figure 2-33, c) in upward flow and corkscrew waves (Figure 2-35, f) in horizontal flow.

The pressure gradient, which is dependent on the flow type, for Bai et al. (1992) is shown in Figure 2-36. The authors reported that the minimum pressure gradients are found for flow types near to PCAF; wavy flows are energy efficient and the input ratio can be controlled to achieve maximum efficiency.

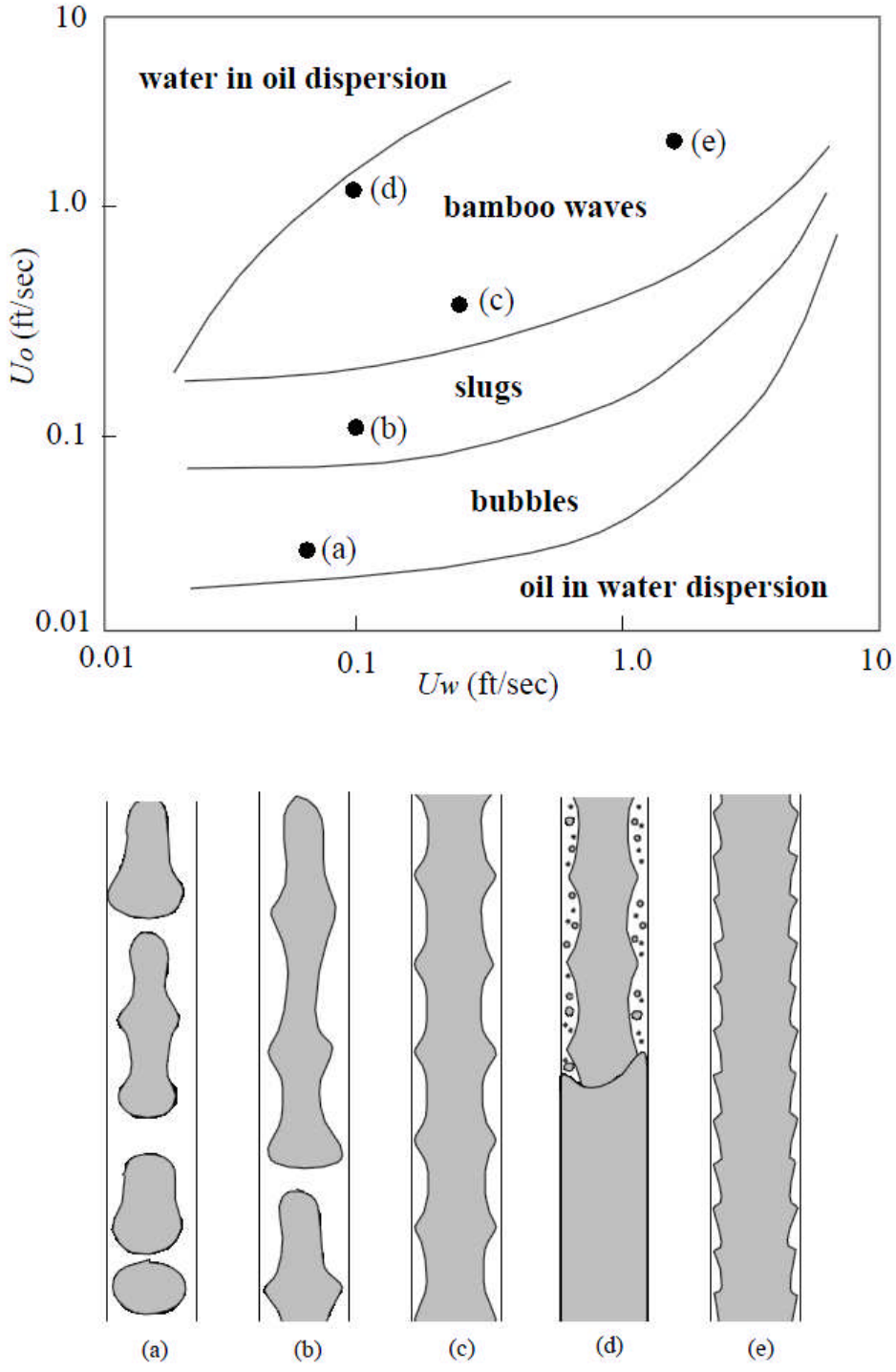

Figure 2-33: Schematic of vertical upward flow (Joseph and Renardy, 1993)

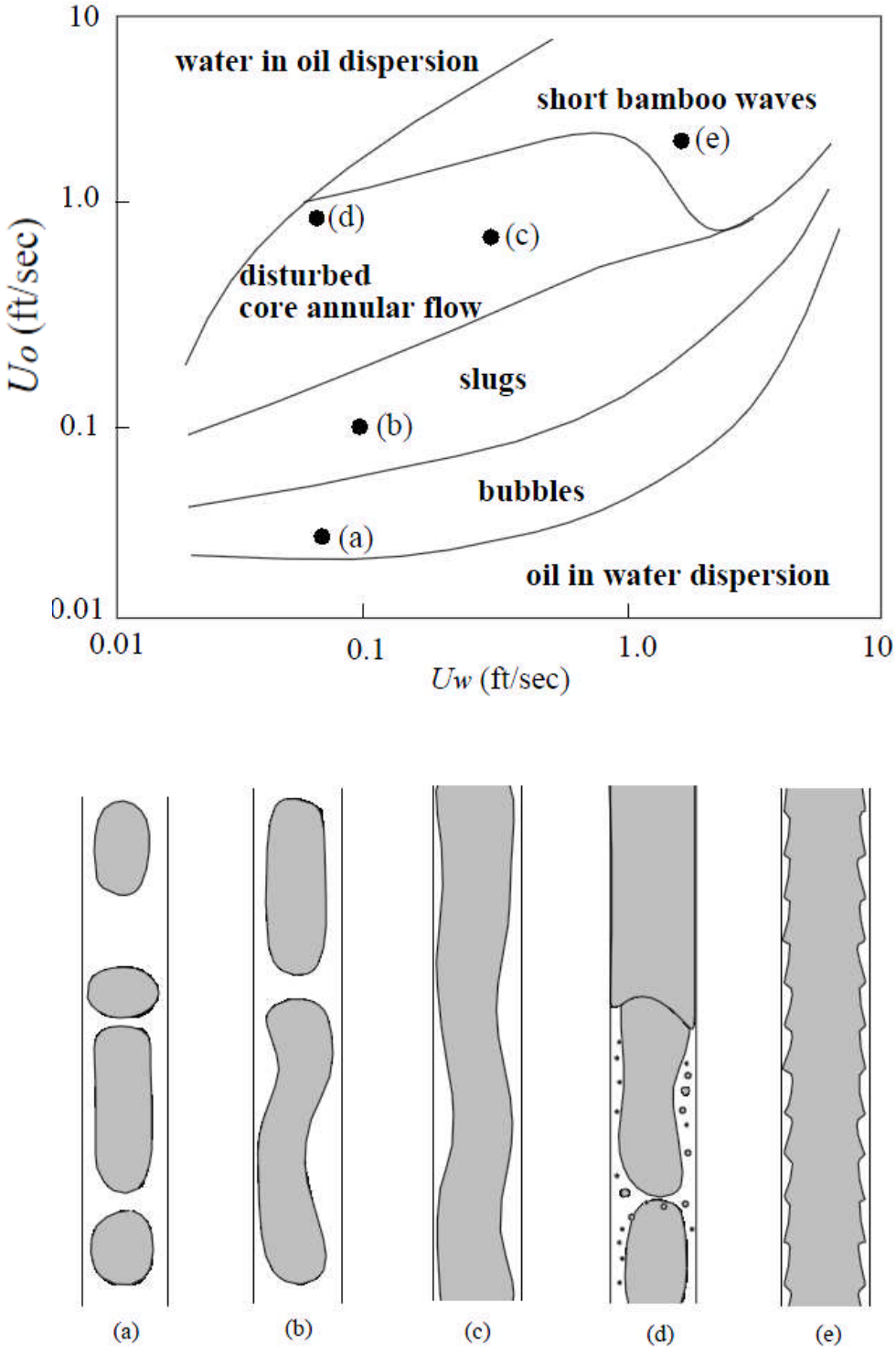

Figure 2-34: Schematic of vertical downward flow

(Joseph and Renardy, 1993)

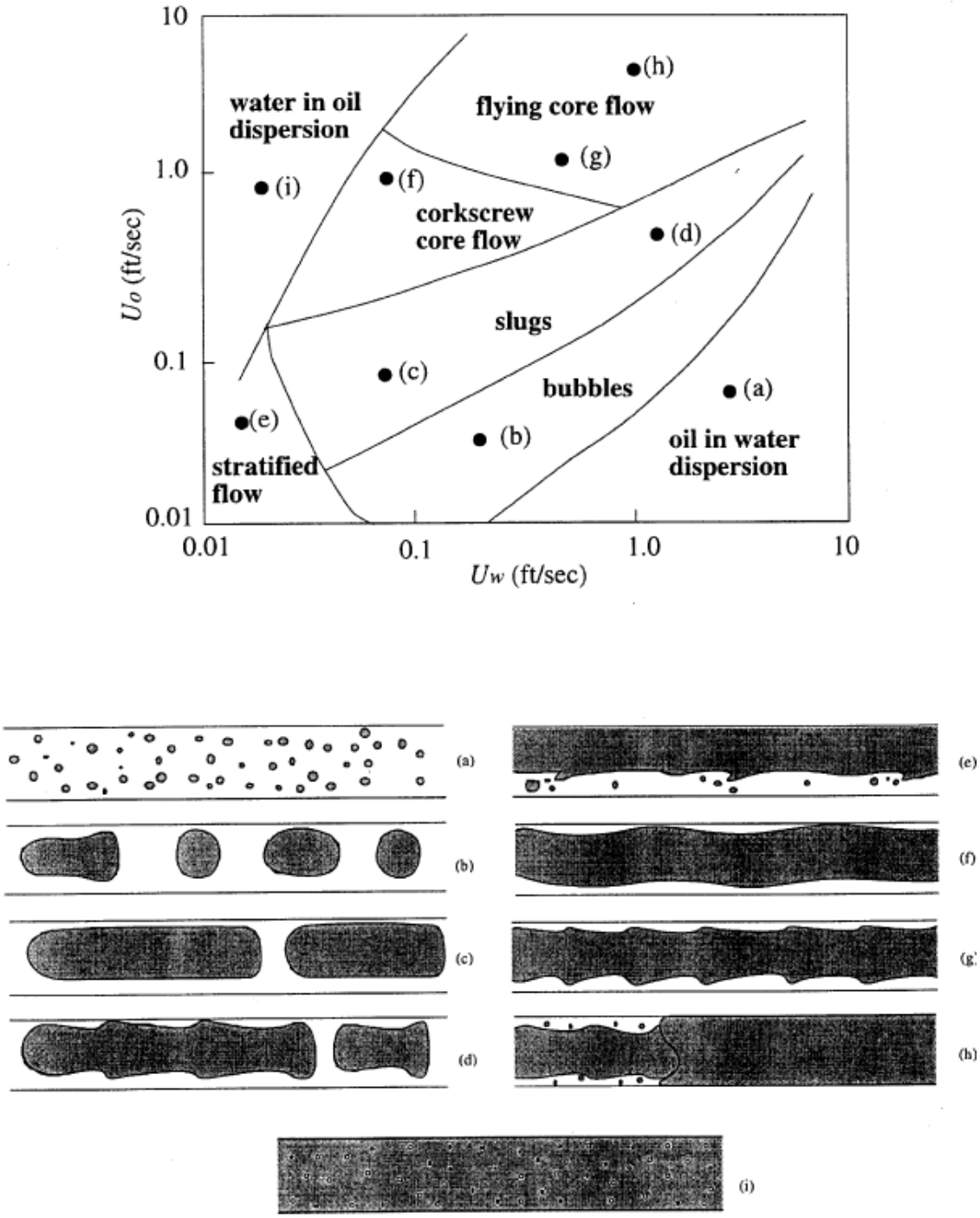

Figure 2-35: Schematic of horizontal flow (Joseph et al., 1997)

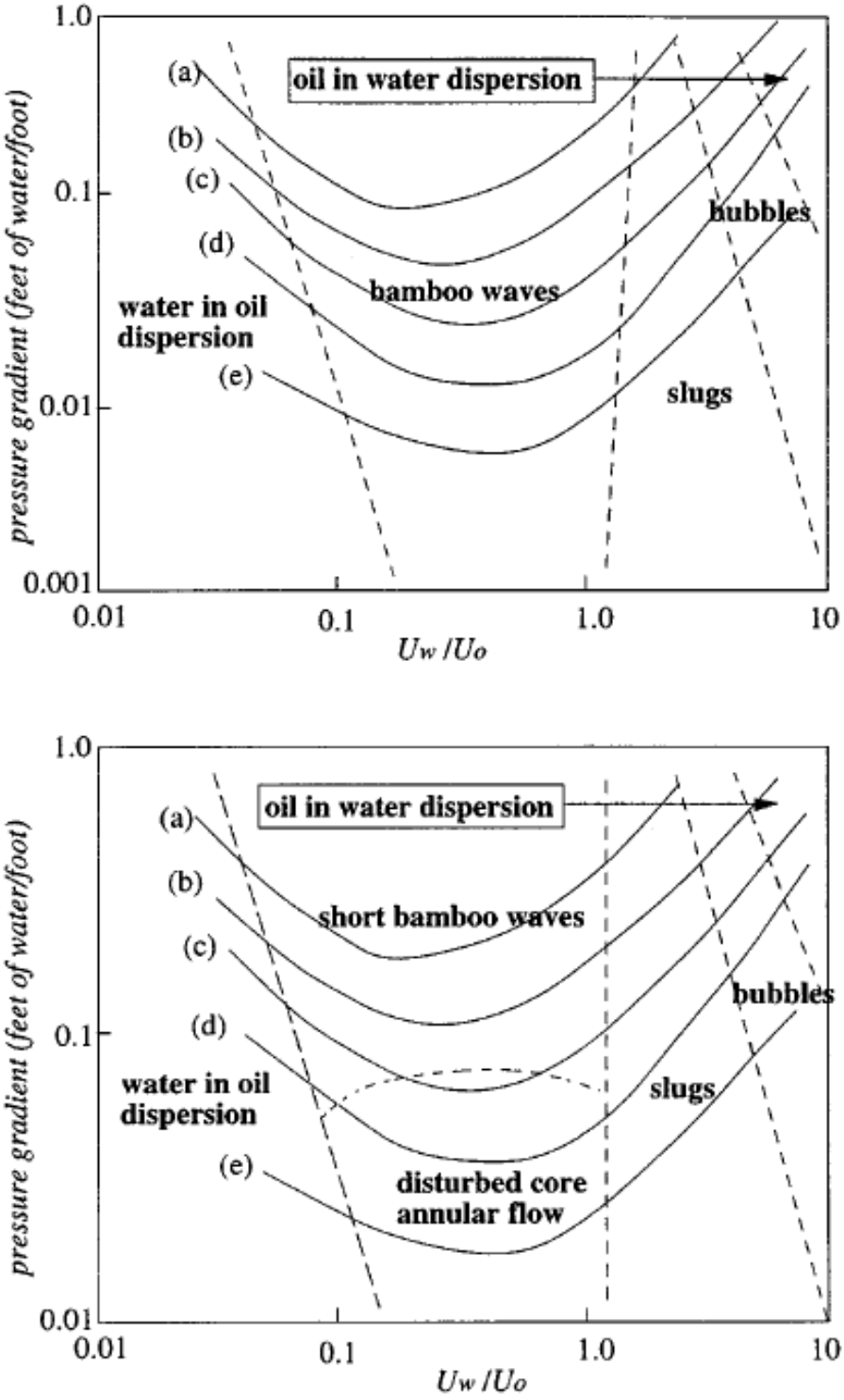

Figure 2-36: Pressure gradient versus the inverse input ratio for different V_{so} in ft/sec: (a) 0.31 (b) 0.61 (c) 0.91 (d) 1.51 (e) 2.27. (top) represents up-flow and (bottom) represents down-flow (Bai et al 1992).

- Bannwart (1999)

Based on experimental data for heavy oil-water flow inside steel and cement horizontal tubes, with ID of 26.7 and 23.9 mm respectively, a simple model for pressure drop in the core annular flow region was formed. The experiments were done at room temperature using fuel oil with μ_o = 2700cP and ρ_o = 989 kg/m^3. It was noted that the system was cleaned from any fouling action caused by the oil after each run.

The author concluded that since oil-water CAF flows are often wavy with turbulent water flow in the annulus, PCAF theory was inappropriate to consider and two simple correlations were proposed to describe the frictional pressure drop in a horizontal pipe for oleophobic and oleophilic pipes. The correlations were based on water fraction and pressure drop for single phase water flow in the same pipe at the flow rate of the mixture. Figure 2-37 Show the Experimental pressure drop against modified flow rate, $Q^* = Q\ C_w^{-n}$, for steel (left) and cemented tube.

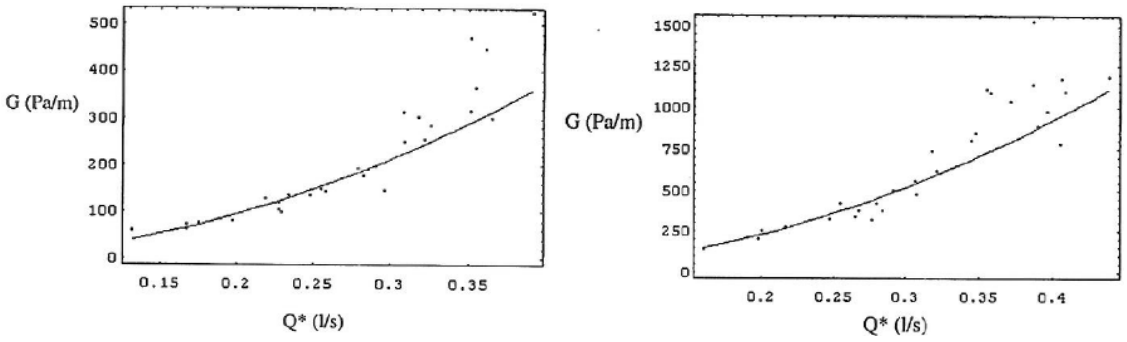

Figure 2-37: Experimental pressure drop against modified flow rate for steel (left) and cemented tube (Bannwart, 1999)

- Bannwart et al. (2004)

Bannwart et al. (2004) studied on the flow patterns formed by heavy crude oil (initial viscosity and density 488 mPa s, 925.5 kg/m^3 at 20 °C and water inside vertical and horizontal 28.4 mm ID pipes. To prevent the oil from touching the pipe wall, a special water injection nozzle was used to add water to the pipe

circumference and oil by the centre. These flow patterns were believed to tend to occur in heavy oil-water flows at low water input fractions. His work has been categorized into WAF due to that he also covered other flow patterns while observed CAF in his work.

For horizontal flow, the following flow patterns were observed, as shown in Figure 2-38

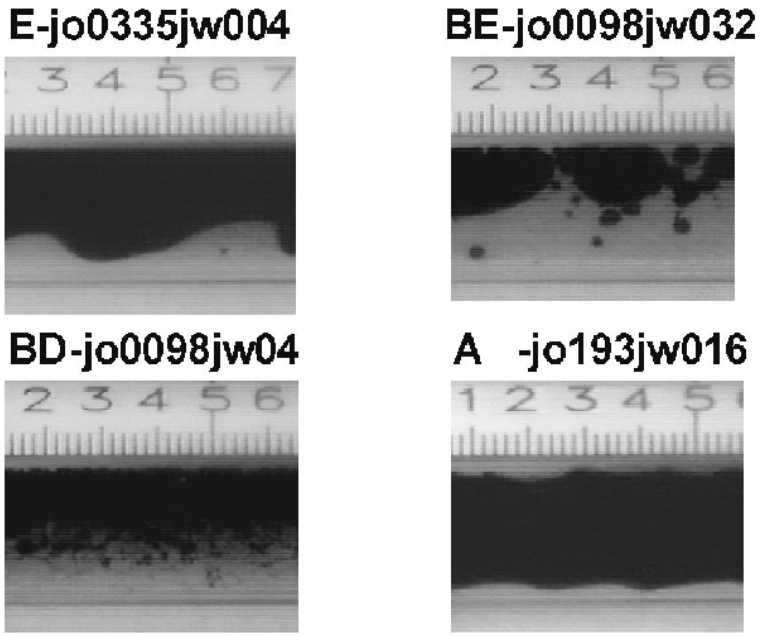

Figure 2-38: Flow patterns in horizontal pipe observed by Bannwart et al. (2004)

where: -

- E: Stratified
- BE: Bubbles (stratified)
- BD: Dispersed bubbles (high flow rates)
- A: Annular.

Apart from the base flow patterns, which were very similar to gas-liquid flow patterns in horizontal pipes, they also defined some sub-patterns with the help of video recording:

- BDE: dispersed stratified bubbles
- BDH: homogeneously dispersed bubbles
- AOE: wavy annular stratified
- AP: perfect annular (nearly smooth interface)

For vertical flow, the following flow patterns were observed, as shown in Figure 2-39:

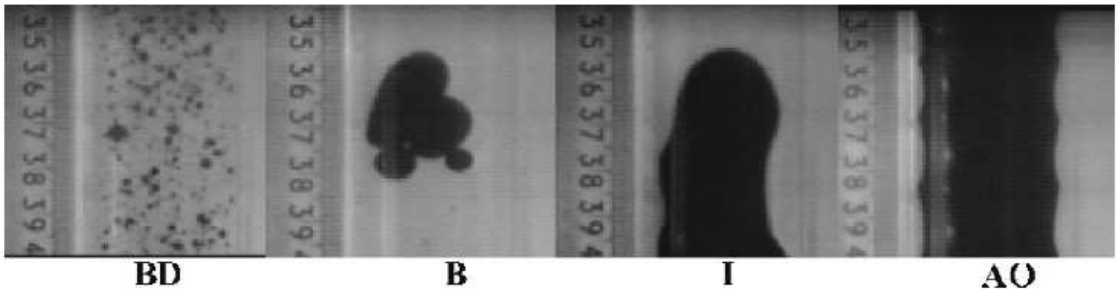

Figure 2-39: Flow patterns in vertical pipe observed by Bannwart et al. (2004)

where: -

- B: Bubbles
- BD: Dispersed bubbles
- I: Intermittent
- A: Annular

Also by using a high speed video camera, they defined sub-patterns flows for annular flow as follows:

- AO: wavy annular ‘‘bamboo waves’’
- AOD: disturbed wavy annular (transition to intermittent)
- AOP: perturbed wavy annular (oil bubbles in annulus)
- AP: perfect annular (nearly smooth interface)

Finally, he defined some combined flow patterns due to bubble dispersion at each flow pattern, as shown in Figure 2-40

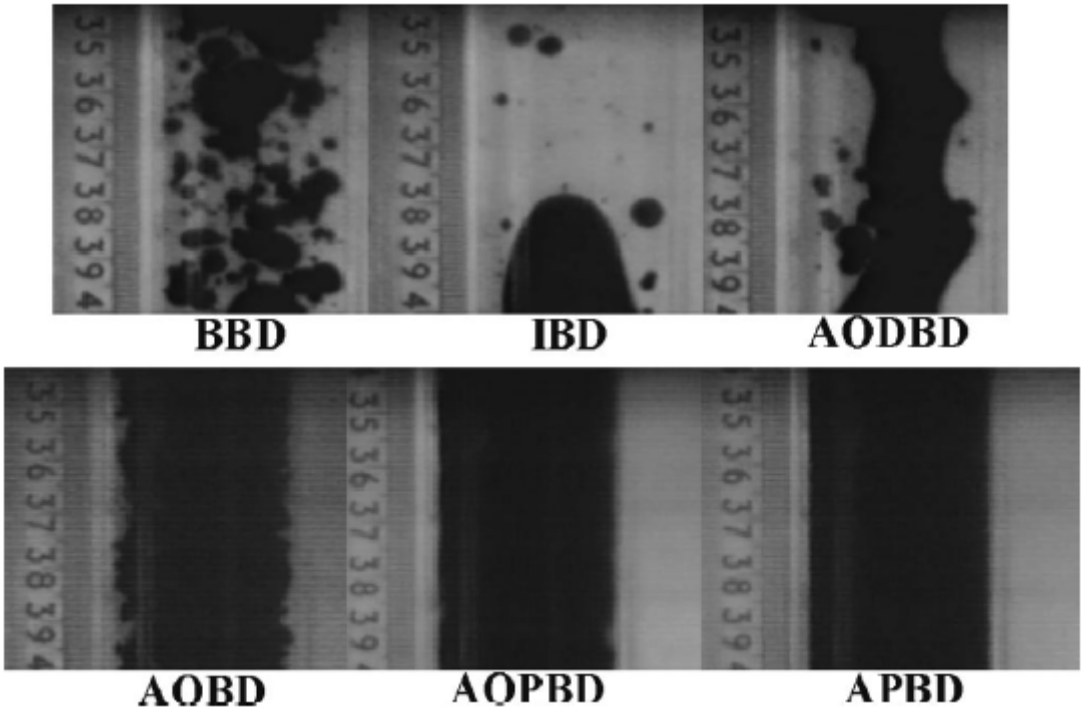

Figure 2-40: Combined flow patterns in vertical pipe observed

(Bannwart et al., 2004)

where: -

- BBD: Bubbles + dispersed bubbles
- IBD: Intermittent + dispersed bubbles
- AODBD: Wavy disturbed annular + dispersed bubbles
- AOBD: Wavy annular + dispersed bubbles
- AOPBD: Wavy perturbed annular + dispersed bubbles
- APBD: Perfect annular + dispersed bubbles

The horizontal and vertical flow maps with respect to the superficial liquid velocities were given as shown in Figure 2-41 and Figure 2-42.

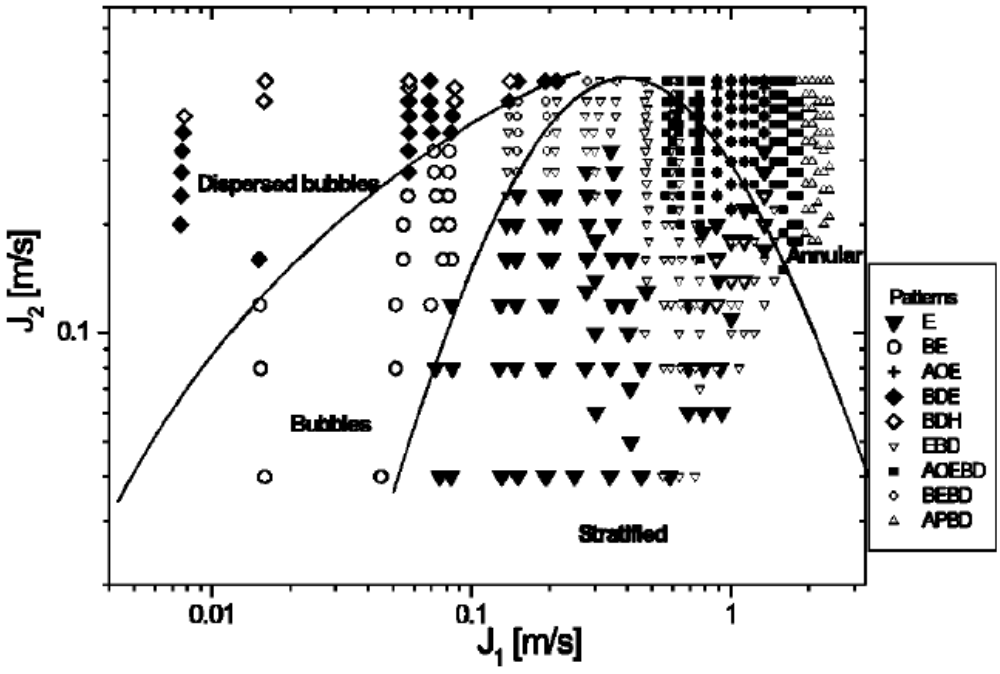

Figure 2-41: Horizontal flow map (Bannwart et al., 2004)

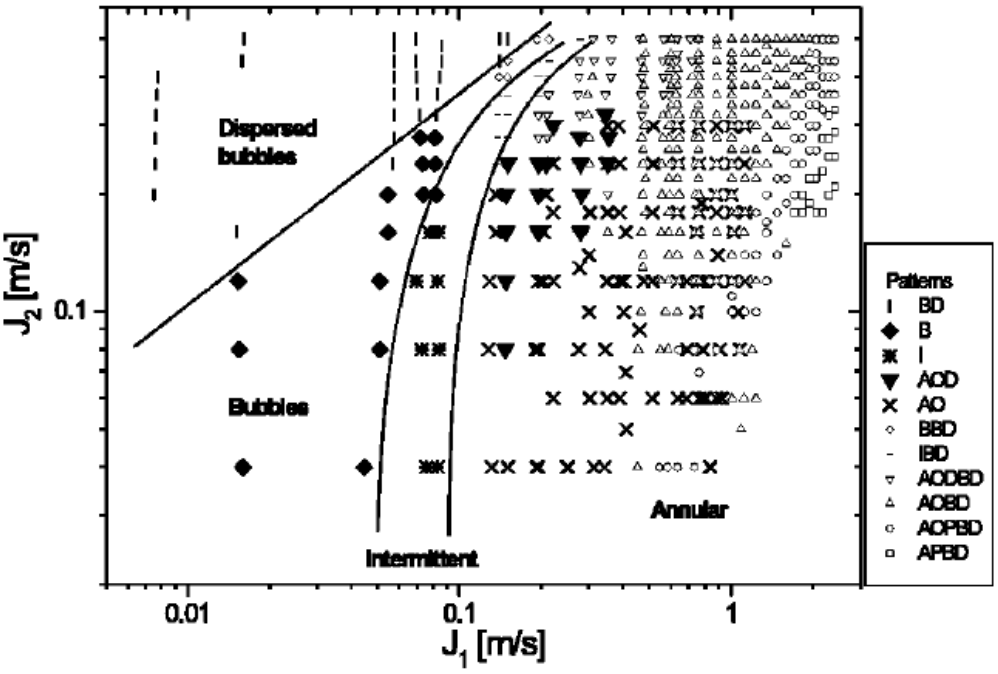

Figure 2-42: Vertical flow map by (Bannwart et al., 2004)

- Grassi et al. (2008)

The authors studied experimentally the pressure drops and flow-pattern maps associated to the flow of oil and water in horizontal and slightly inclined pipe, where the chosen liquids are characterised by an oil-to-water viscosity ratio of about 800:1 at 20 °C, oil density equal to 886 kg/m^3 and interfacial tension of 0.05 N/m. Various theoretical models have been examined with their findings, however particular attention was given to core annular flow two-fluid model and oil-in-water dispersion homogeneous no-slip model.

Examples of different flow regimes observed in their experiments is given in Figure 2-43.The flow-pattern maps obtained in the described set-up show large core-annular flow and oil-in-water dispersion regions, as shown in Figure 2-44; only few occurrences of wavy stratified and none of smooth stratified flow have been observed, due to the small Eötvös number characterizing the system; elongated oil-in-water bubbles have also been observed in small but well-defined regions of the flow-pattern maps.

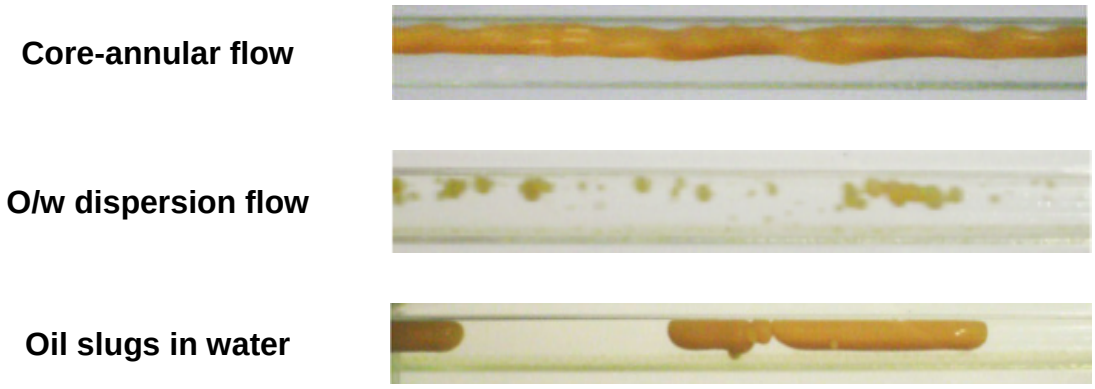

Figure 2-43: Different observed flow regimes (Grassi et al., 2008)

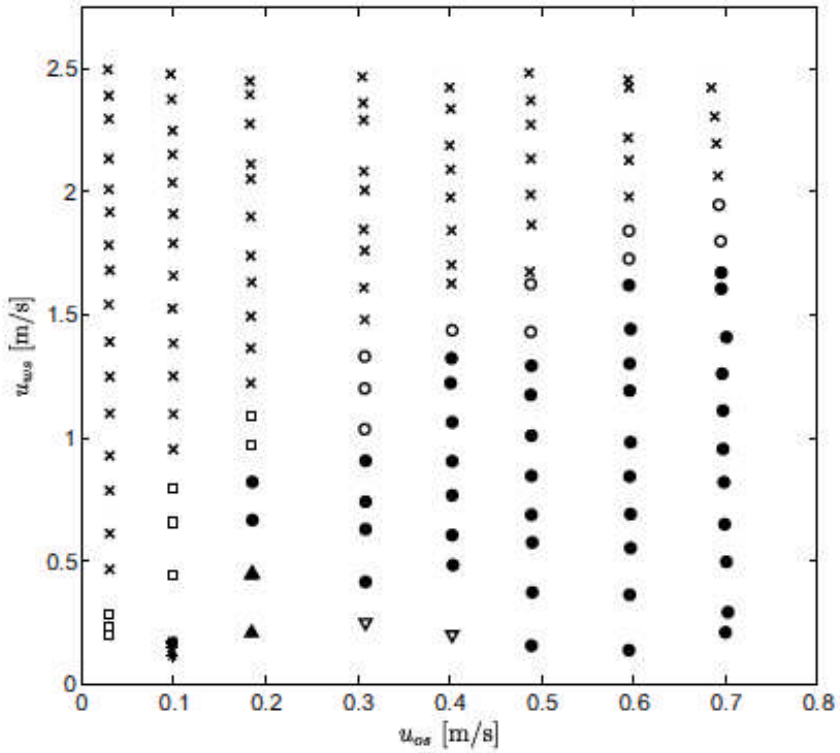

Fig. 3. Experimental flow-pattern map (0°). u_{ws}, u_{os}: water and oil superficial velocities. ▲ = *stratified flow*; × = *dispersion of oil in water*; • = *core-annular flow*; □ = *plug/slug flow*; ▽ = *stratified flow and dispersion of oil in water*; ○ = *core-annular flow and oil in water dispersion*; ⋆ = *oil film at the wall and inner dispersion of oil in water.*

Figure 2-44: Horizontal flow pattern map (Grassi et al., 2008)

Pressure drops on a 1.5 m segment of the test pipe have been measured (see Figure 2-45); the results have then been compared to the values predicted by traditional formulae for the single-phase flow of water at the same mixture velocity with transition boundary prediction in Brauner (2002) with good agreement, accuracy around 20%, as shown in Figure 2-46. They also concluded that the choice of the effective viscosity expression in the implementation of oil-in-water dispersion homogeneous model does not appear to affect significantly the final prediction.

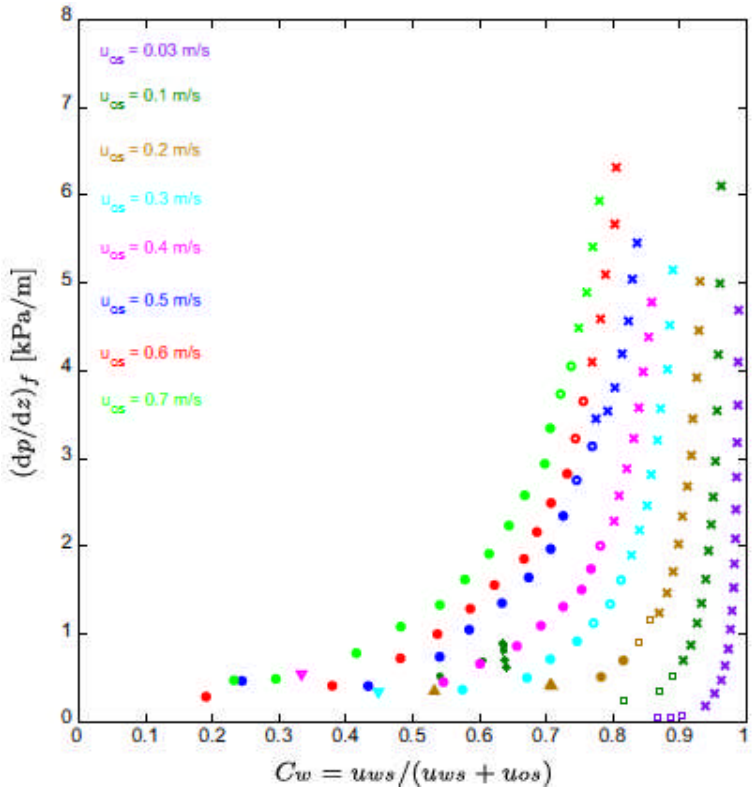

Figure 2-45: Measured pressure drop in horizontal flow against water cut (Grassi et al., 2008)

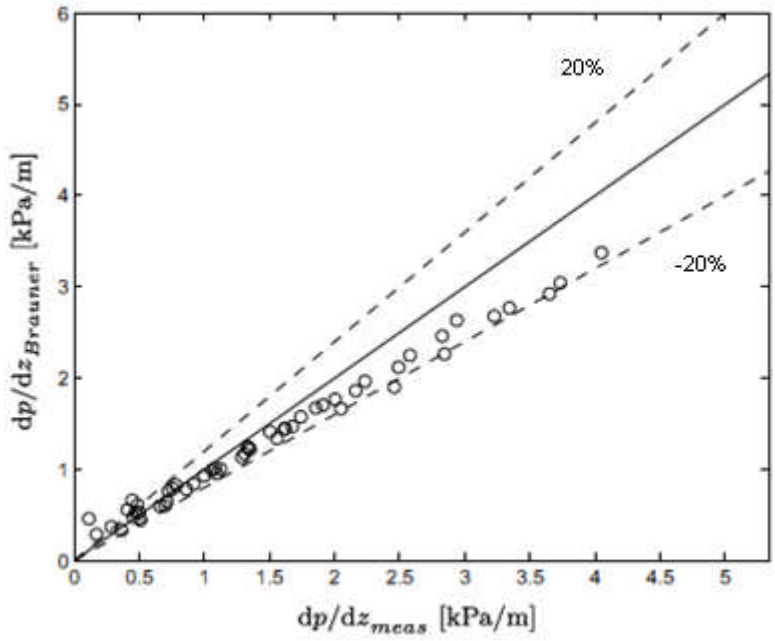

Figure 2-46: Experimental pressure gradient comparison against Brauner's (2002) model for core annular flow (Grassi et al., 2008)

- Vuong et al. (2009)

Vuong et al. (2009) studied the flow patterns formed by heavy crude oil (with viscosity of 230, 440, 1070 cP and density of 884.4 kg/m^3) and water inside vertical and horizontal 2 inch pipes. Four flow patterns were identified, as shown in Figure 2-47

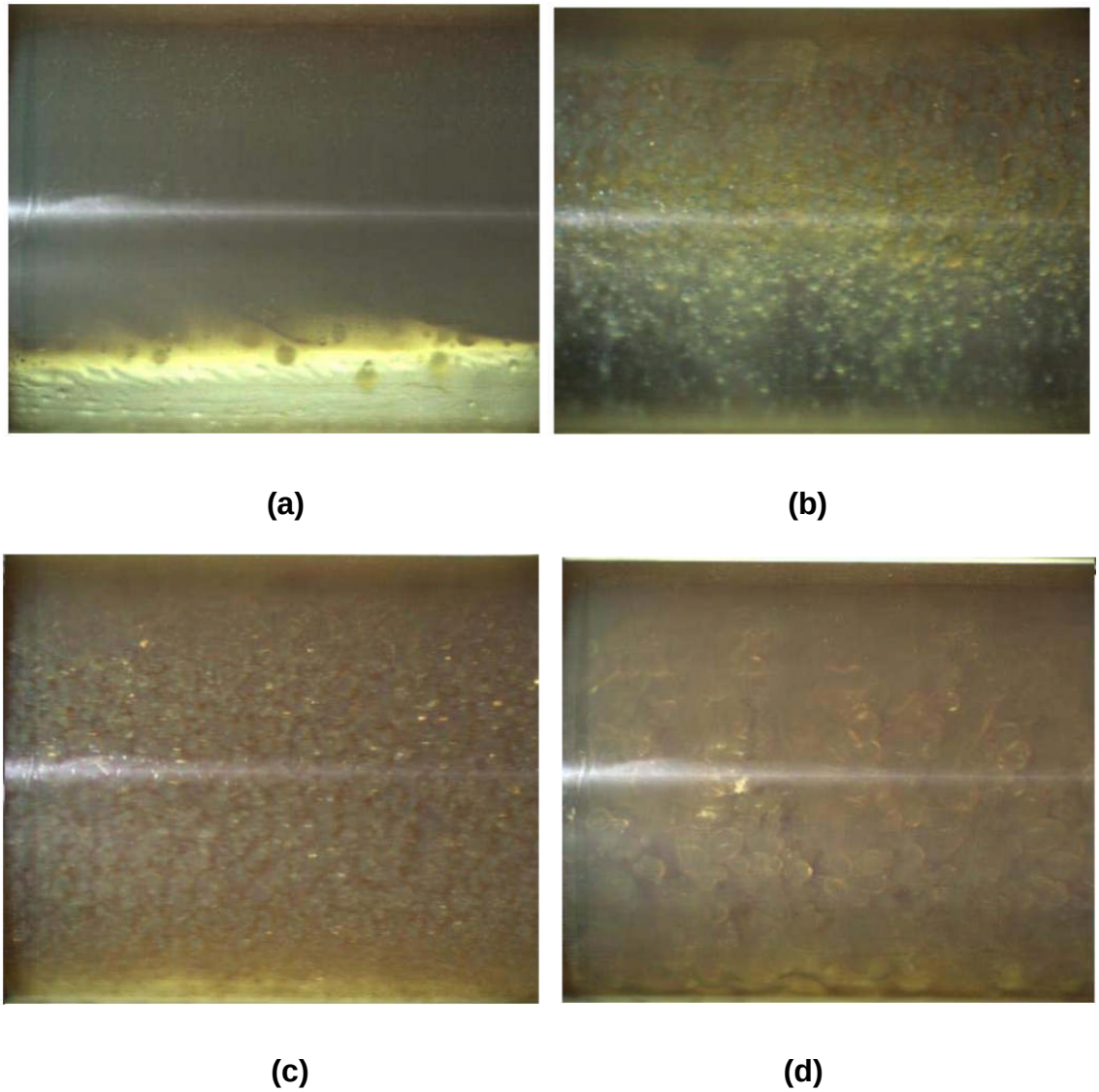

(a) **(b)**

(c) **(d)**

Figure 2-47: Flow patterns in horizontal pipe observed (Vuong et al., 2009)

(a) Stratified Wavy with Oil Droplets at Interface (SW&OI)

This flow pattern was found to be similar to Stratified with Mixing at Interface (ST&MI) identified by Trallero (1995). Oil and water flow were observed as two separated layers with oil flowing at the top and water flowing at the bottom of the pipe. Some waviness and oil droplets are observed at the interface. This flow pattern was only found at low oil and water flow rates.

(b) Dispersion of Oil in Water over a Water Layer (DO/W&W)

As the water flow rate increased, the water phase became continuous with dispersed oil droplets at the upper part of the pipe; while a free water layer flows could be found at the pipe bottom.

(c) Full Dispersion of Oil in Water (DO/W)

By further increasing water and oil flow rates, the free water layer disappeared. Water was the external phase with oil droplets distributed from bottom to top of the pipe.

(d) Dispersion of Oil in Water and Oil Film (DO/W&OF)

The behaviour of DO/W&OF was similar to DO/W and DO/W&W in the way that oil dispersed in continuous phase water, while a thin oil film was visually observed on the pipe wall. This is probably related to the wettability of the pipe wall.

The flow regime map was generated for a viscosity of 1070cP as shown in Figure 2-48, while the pressure gradient for the horizontal flow is shown in Figure 2-49. The higher flow rates cause higher pressure gradients. The presence of oil film on the wall increases the pressure gradient. Higher water velocity causes high shear stress which thins the oil film on the pipe wall, the oil film breaks up into droplets, thereby making the flow more water dominant at the pipe wall. This transition reduces the pressure gradient.

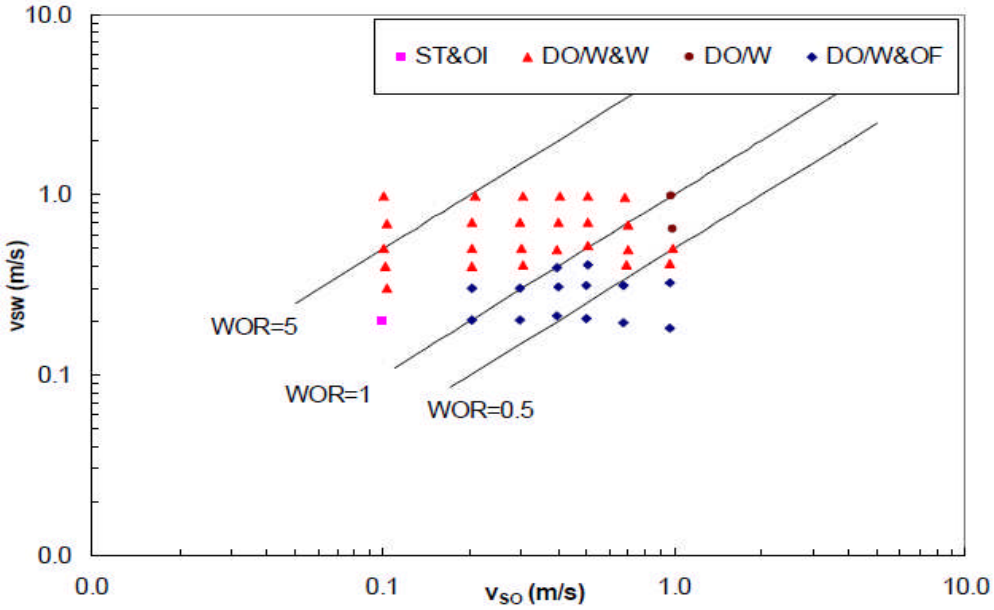

Figure 2-48: Flow patterns in horizontal pipe observed (Vuong et al, 2009)

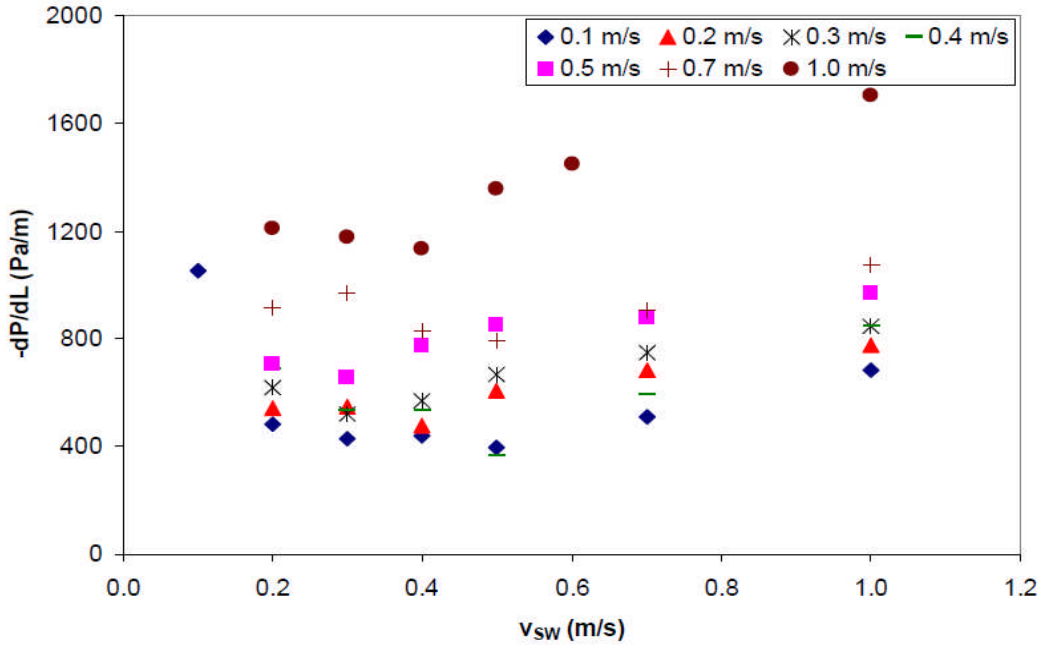

Figure 2-49: Pressure gradient for the horizontal flow (Vuong et al, 2009)

- Strazza et al. (2011)

Strazza et al. (2011) studied the existence of highly viscous oil–water core annular flow in horizontal and slightly inclined systems. The flow maps obtained for different pipe inclinations showed slight difference when compared to the work by Rodriguez and Oliemans (2006) due to the substantial balance between buoyancy and superficial tension forces as indicated by the characteristic Eötvös number. Brauner's predictions of CAF transition boundaries were compared to the experimental data and showed good agreement, especially in the light of the criterion generality. The model requires as input data a critical oil hold-up value to compute the transition boundary. This value was obtained from hold-up measurements.

Core-annular flow pressure gradients were presented in term of reduction factor to emphasize the advantage of this flow regime. As noted by other authors, such as Brauner (2002), core-annular pressure gradients are comparable to the ones with water flowing alone in the pipe at the mixture velocity. Experimental pressure gradients were then compared to the predictions provided by three different models (Brauner,1991; Arney et al., 1993; and Bannwart, 1999). All models showed good agreement with the experimental data.

Finally, hold-up data have been presented and compared with the correlation proposed by many correlations. The correlation proposed by Arney et al. (1993) was in good agreement with the experimental data. From hold-up data, the phase velocities was computed to show that the oil core was always faster than the annulus, i.e. the slip parameter is always larger than 1.

2.5.3 Phenomenological models

Pressure drop is a vital factor in pipeline design. Better understanding on the existing oil-water prediction models will be helpful to realise the mechanism behind the flow behaviour and for further model development.

2.5.3.1 Core Annular Flow

Here is a strong tendency for two immiscible fluids to arrange themselves so that the low viscosity constituent is in the region of high shear. Water-lubricated transport of heavy viscous oil is a technology from based on this principle, which the water migrate close to the pipe wall where the high shear region is, thus lubricating the flow. Lubricated flow in an oil core is called core annular flow (CAF).

Few models have been established to predict the pressure drop associated with CAF pattern for horizontal flow, with application to heavy oil transportation. However many discrepancies were found in two-phase pressure drop prediction. In this section, four models are presented and applied to the acquired CAF data to examine their validity and help understanding the mechanism behind the flow behaviour.

2.5.3.1.1 Arney et al. (1993)

This model is based on concentric cylindrical core-annular flow and takes into account of turbulence. However, it neglects the effects which serve to increase the frictional losses such as core waviness and eccentricity. Since the mixture velocity accompanied with CAF in our facilities was always turbulent, the friction factor associated is defined as:

$$f_{\mathrm{Arney}} = \frac{0.316}{\mathrm{Re}_{\mathrm{Arney}}^{0.25}} \tag{16}$$

The modified Reynolds number, $\mathrm{Re}_{\mathrm{Arney}}$ is defined as

$$\mathrm{Re}_{\mathrm{Arney}} = \frac{\rho_m V_m D}{\mu_w}\left[1 + \eta^4\left(\frac{\mu_w}{\mu_o} - 1\right)\right] \quad (17)$$

where μ_w and μ_o are the water and oil dynamic viscosities respectively; ρ_m is the calculated average density using the mixing rule and defined as

$$\rho_m = (1-\eta^2)\rho_w + \eta^2\rho_o \quad \text{with} \quad \eta = \sqrt{(1-H_w)} \quad (18)$$

The previous equation shows the need of hold up data to calculate the average density of the two fluids. In the same work done by the author, a correlation was derived based on data collected from the literature to relate the water volume hold-up, H_w, to the water input fraction(i.e. water-cut, C_w) and given by

$$H_w = C_w[1.35 - 0.35C_w] \quad (19)$$

The final form of the pressure gradient model is obtained by:

$$\frac{dP}{dx} = 0.5\frac{f_{\mathrm{Arney}}\rho_m V_m^2}{D} \quad (20)$$

2.5.3.1.2 Brauner (2002)

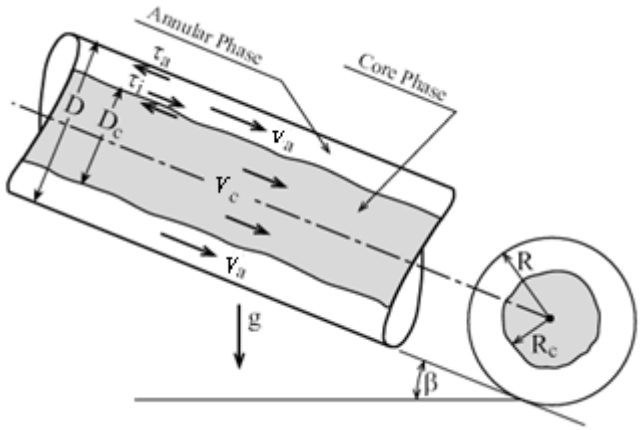

Figure 2-50: Schematic description of CAF configuration (Brauner, 2002)

A simple practical model for general annular concurrent liquid-liquid flow, which is not restricted to laminar flow regimes, can be obtained using the two-fluid approach (Brauner, 1991). Based on the schematic description of CAF, Figure

2-50, the combined momentum equation for the core (c) and annular liquid (a) (obtained after eliminating the pressure drop) reads:

$$\frac{4}{D(1-\widetilde{D}_c^2)}\left[-\tau_a+\frac{\tau_i}{\widetilde{D}_c}\right]+(\rho_a-\rho_c)g\sin\beta=0 \tag{21}$$

where $\widetilde{D}_c^2$ is the core fluid in-situ hold up and $\beta > 0$ and $\beta < 0$ for downward and upward flow, respectively. However, since our case is for horizontal flow, $\beta = 0$. The associated densities are $\rho_a = \rho_w$ and $\rho_c = \rho_o$, the wall shear stress τ_a and interfacial shear stress τ_i are expressed in terms of the phases average velocities V_a, V_c and the corresponding friction factors f_a, f_i. The appropriate structure for these closure relations has been identified (Brauner, 1997) as:

$$\tau_a=\frac{1}{2}f_a\rho_aV_a^2\ ;\ f_a=C_a\left[\frac{\rho_aD(1-\widetilde{D}_c^2)V_a}{\mu_a}\right]^{-n_a} \tag{22}$$

$$\tau_i=\frac{1}{2}f_i(V_c-c_iV_a)V_c\ ;\ f_i=F_iC_c\left(\frac{\rho_cD_cV_c}{\mu_c}\right)^{-n_c} \tag{23}$$

where $c_i = v_i/V_a$ and v_i is the interfacial velocity. For laminar annular phase $c_i = 2$, while for turbulent annular phase $c_i \approx 1.15$ to 1.20. The constants $C_{a,c}$ and $n_{a,c}$ are set according to the flow regime in each phase ($C = 16$; $n = 1$ for laminar flow and $C = 0.046$; $n = 0.2$ for turbulent flow). The coefficient F_i denotes possible augmentation of the interfacial shear due to interfacial waviness. However, in core-flow, the liquids interface is characterized by long smooth waves and appears less roughened than in annular gas-liquid flows. Also, as the velocities of the two liquids in core flow are comparable, the modelling becomes even less sensitive to the estimation of the interfacial friction factor, where F_i can be set to 1. Using mass balances on the annular and core phases yields to the following non-dimensional equation for the core diameter:

$$(1-\widetilde{D}_c^2)\widetilde{D}_c^{n_c-5}\left[1-\widetilde{D}_c^2(1+c_i\widetilde{Q})\right]-X^2+Y(1-\widetilde{D}_c^2)^3=0 \tag{24}$$

The dimensionless parameters are $\widetilde{Q}=\frac{Q_a}{Q_c}$, X^2 (Martinelli parameter), and Y:

$$X^2 = \frac{C_a Re_{as}^{-n_a}}{C_c Re_{cs}^{-n_c}} \frac{\tilde{Q}^2}{\tilde{\rho}} = \frac{(\frac{dP}{dx})_{as}}{(\frac{dP}{dx})_{cs}} \quad ; \quad Y = \frac{1}{2} \frac{(\rho_a - \rho_c)}{\rho_c} \frac{Dg\sin\beta}{U_{cs}^2} \frac{1}{C_c Re_{cs}^{-n_c}} \tag{25}$$

where $\tilde{\rho} = \frac{\rho_c}{\rho_a}$ and Re_{as}, Re_{cs} are the superficial Reynolds numbers of the annular and core liquids respectively. Again, Y should equate to zero since our case is for horizontal flow (i.e. β = 0) .Finally, a summary of the in two fluid models for core diameter and pressure drop for CAF (laminar core) is presented in Table 2-4.

Parameter	Laminar core-Laminar Annulus (L-L)	Laminar core- Turbulent Annulus (L-T)
X^2	$\frac{\mu_a}{\mu_c}\tilde{Q}$	$\frac{0.046}{16}\frac{\mu_a}{\mu_c}\tilde{Q}\,Re_{as}^{0.8}$
c_i	2	1.15 to 1.2
$\tilde{D}_c^2$	$\frac{1+\tilde{Q}-\sqrt{(1+\frac{\mu_a}{\mu_c}/\tilde{Q})\tilde{Q}}}{1+2\tilde{Q}-\frac{\mu_a}{\mu_c}\tilde{Q}}$	$\frac{1+\tilde{Q}c_i/2\left[1-\sqrt{\left(1+\frac{4X^2}{\tilde{Q}^2{c_i}^2}\right)}\right]}{1+\tilde{Q}c_i+X^2}$
$\frac{dP}{dx}$	$\frac{\mu_a/\mu_c}{\tilde{Q}}\left[\frac{1+2\tilde{Q}-\frac{\mu_a}{\mu_c}\tilde{Q}}{1-\frac{\mu_a}{\mu_c}+\sqrt{(1+\frac{\mu_a}{\mu_c}/\tilde{Q})}}\right]^2$	$X^2\left[\frac{1+\tilde{Q}c_i-X^2}{\tilde{Q}c_i/2-X^2+\sqrt{\frac{\tilde{Q}{c_i}^2}{4}+X^2}}\right]^2$

Table 2-4: Core diameter and pressure drop for laminar core (Brauner, 2002)

The Two-fluid model for CAF is a simple practical tool for evaluating the potential pressure drop reduction and power saving in concentric CAF. However, the predicted pressure drop via this model may underestimate measured values in CAF operation. Possible reasons for deviations are the increase of the wall friction due to surface irregularities, fouling of pipe walls by a wavy core interface at high oil rates, and eccentric (rather than concentric)

core flow. Accounting for these effects in the framework of the two-fluid model requires appropriate modifications of the closure laws used for the wall and/or interfacial shear stresses.

2.5.3.1.3 Bannwart (2001)

Bannwart proposed phenomenological models to predict the pressure drop during liquid–liquid flow through horizontal as well as vertical pipes. The analysis was an improvement over Perfect Core Annular Flow model (PCAF, refer to Joseph and Renardy, 1993) and accounted for the effect of turbulence in the annular fluid and wavy interface. It also included the effect of buoyancy for vertical system. The results showed higher oil flow rate required less amounts of water for the minimum pressure gradient. He further suggested that the flow configuration was favoured by interfacial tension, which played a major role in stabilizing the flow.

For horizontal annular flow, he proposed:

$$\frac{dP}{dx} = b\left(\frac{\rho_w V_m D}{\mu_w}\right)^{-n} \frac{\rho_w V_m^2}{2D}\left[1-\left(1-\frac{\rho_o}{\rho_w}\right)\varepsilon\right]^{1-n}\left[1-\left(1-\frac{\mu_o}{\mu_w}\right)\varepsilon\right]^{-n} \quad (26)$$

where b and n are curve fitting constants (which can be adjusted to account for pipe wall conditions in the friction law of the actual flow), and ε is the volume fraction of the core (oil volume fraction) which can be described in the following equation:

$$\varepsilon = \frac{1}{1+s_{i,o}\frac{V_{sw}}{V_{so}}} \quad (27)$$

Where $s_{i,o}$ is the experimental determined slip value between the two fluids.

2.5.3.1.4 Rodriguez et al. (2009)

The authors propose a refine pressure loss prediction model for CAF which includes a slip ratio term that implicitly accounts for the buoyancy of the oil core.

The model depends on two parameters that can be either adjusted to fit pressure drop data, when the behaviour of the pipe wall cannot be predicted, or set to theoretical values for smooth and clean pipes. Its physical basis is the observation that the pressure drop in core-annular flow is comparable to that of the annulus fluid (usually water) alone in the pipe at mixture flow rate.

Accordingly, a two-phase multiplier is proposed which accounts for the slip between the two phases and the physical properties of the two fluids. The model also depends on the in-situ volumetric fraction of the core fluid, which can be readily calculated via the kinematic wave theory for laminar or turbulent annulus flow. The model allows for the adequate representation of different annulus flow regimes, kinematic effects and wall conditions, including fouling. The final form of the pressure drop model is obtained by:

$$\frac{dP}{dx} = b\left(\frac{\rho_w V_m D}{\mu_w}\right)^{-n} \frac{\rho_w V_m^2}{2D}\left[1-\left(1-\frac{\rho_o}{\rho_w}\right)\varepsilon\right]^{1-n}(1-\varepsilon)^{-n}\left[1+(s-1)\varepsilon\right]^{n-2} \quad (28)$$

Again, Blasius' friction law coefficients, b and n, can be set to known single phase parameters or adjusted to fit pressure drop data, since these parameters are affected by wall properties (roughness, fouling and wettability). Also the effects of wavy interface and dispersion of oil droplets in the water annulus can be taken into consideration by fitting the Blasius' friction law coefficients. The model is valid for either upward-vertical or horizontal core-annular flow, which can be more adequate than the two-fluid model.

- Occurrence of Core Annular Flow (CAF)

Typically, waves always appear on the surface of the oil core and “they appear to be necessary for levitation of the core off the wall when the densities are different and for centring the core when densities are matched” (Flores et al., 1997). These flows were called wavy core annular flow (WCAF). Perfectly centred core flows (PCAF) of density matched fluids are possible but rarely stable.

Experiments (Ooms et al., 1984; Oliemens et al., 1987; Bai et al., 1992; Arney et al., 1993; Bannwart, 2001; Bannwart et al., 2004; Benshakaria et al., 2004) generally indicate the following conditions to be satisfied for CAF flow pattern to occur in a pipe:

a. the core phase must be much thicker than the annulus;

b. the injection of the thinner fluid must happen in such a way so as to create a continuous lubrication layer around the thicker fluid; thus, the last occupies the centre of the tube surrounded by a thin water annulus adjacent to the wall, which at the same time must keep the core from touching the pipe wall.

Miesen et al. (1992) stated that owing to the complicated hydrodynamics of CAF, the buoyancy on the core can be counterbalanced by pressure and viscous forces, resulting in stable flow. By using their 2 and 8 inch test loop for variation of viscosities (between 3900cP and 27000cP), they observed and studied the waves on the oil/water interface, and concluded that for lubricating CAF with thin annulus, three conditions must be achieved:

1. Very large viscosity ratio between the two fluids.

2. Large Reynolds number for the fluid in the annulus.

3. Wave speeds in the interface must close to the speed of the core fluid.

The above conditions were refined by Bannwart (2001), as CAF will tend to occur in a pipe when the two fluids have relatively similar densities and very different viscosities. He presented three criteria as necessary requirements for existence of core–annular flow:

1. The oil velocity in the core has to be higher than the water velocity in the annulus, considering the slip ratio between the two fluids. This criterion can be represented with superficial velocities by:

$$V_{so} > s\, V_{sw} \tag{29}$$

Where s is the slip ratio (i.e. the ratio of the velocity of oil to water). This criterion represents the stability condition of two liquid in CAF with the same densities having more viscous fluid placed at the core and occupies most of the pipe cross-section area.

2. Joseph et al. (1984) concluded that viscous-dissipation principle was not always true for the tendency of the less viscous fluid to encapsulate the more viscous one and, by applying numerical solution to linear stability analysis, showed stability can be better with more viscous fluid occupying most of the pipe; also by examining gas-liquid annular flow, Joseph et al. (1996) extended the stability theory to a count for turbulent flow using effective viscosity; Bannwart (2001) considered the stability of a viscous liquid flowing at the core, surrounded by a turbulent annulus flow, and assuming the fluids are well separated (i.e. there is no water in the core and no oil in the annulus), the criterion was represented by:

$$\mu_o > \mu_w + 0.0005\rho_w V_{sw} D \quad \text{for} \quad \frac{\rho_w V_{sw} D}{\mu_w} > 2000 \tag{30}$$

This expresses a necessity condition to prevent the annulus turbulence from breaking up the core continuity.

3. Using the idea of Brauner and Moalem Maron (1998), who proposed a flow classification for horizontal flow based on an Eötvös number (low numbers gives favour to annular flow pattern), a theoretical interface shape in fully developed core flow was considered and the effect of peripheral flow in the annulus was included. The stabilization of CAF in a pipe was shown possible when

$$8 > \frac{\pi \Delta\rho g D^2 \varepsilon}{4\sigma} \tag{31}$$

This criterion represents the limiting condition that the force associated with the interfacial curvature gradients balances the buoyancy force on the core. If this condition is not obeyed, then stratification is most likely to occur instead of CAF.

A comparison of the results of different researchers with the criteria (2) and (3), as the slip is needed to consider criteria (1), are presented in Table 2-5 . While criterion (2) is satisfied in practice for, criterion (3) is not. The stratification condition, instead of CAF, was predicted for Trallero (1995) and Vuong et al. (2009) which reported the same findings for their tests.

Authors	Pipe size & properties	RHS value of Criterion		CAF observed
		(2) for v_w=0.5 m/s	(3) at ε = 0.5	
Oliemans (1987)	D = 50 mm; μ_o = 3000cP; ρ_o = 975 kg/m^3; ($\sigma_{assumed}$ = 30 dyn/cm)	14	8	Yes
Trallero (1995)	D = 50.1 mm; μ_o = 29.6cP; ρ_o = 850 kg/m^3; σ = 36 dyn/cm	14	40.3	No
Bannwart (1999)	D = 23.9 mm; μ_o = 2700cP; ρ_o = 989 kg/m^3; σ = 30 dyn/cm	7	0.8	Yes
Bannwart et al. (2004)	D = 28.4 mm; μ_o = 488cP; ρ_o = 925.5 kg/m^3; σ = 29 dyn/cm	8	8	Yes
Vuong et al. (2009)	D = 52.5 mm; μ_o = 1070cP; ρ_o = 884.4 kg/m^3; σ = 30.4 dyn/cm	14	40.4	No

Table 2-5: Predictions and observations of CAF in horizontal pipes

2.5.3.2 Stratified Flow

Charles and Lilleleht (1966) used the empirical parameters X and Φ, suggested by Lockhart and Martineli (1949) for gas-liquid flow, to represent pressure gradient data of stratified liquid-liquid flows. The X and Φ were defined as:

$$X^2 = \frac{(\Delta P/\Delta x)_o}{(\Delta P/\Delta x)_w} \qquad \Phi^2 = \frac{(\Delta P/\Delta x)_{TP}}{(\Delta P/\Delta x)_o} \tag{32}$$

where $(\Delta P/\Delta x)_o$ and $(\Delta P/\Delta x)_w$ are the pressure gradients for oil and water phase alone respectively; and $(\Delta P/\Delta x)_{TP}$ is the pressure gradients for two phase oil-water flow.

Stapelberg and Mewes (1994) also applied this method and try to interpret their data in two pipes with different parameters. Their results showed a single model is not sufficient to correlate the pressure gradient data in the entire liquid-liquid flow pattern.

Brauner et al. (1998) considered that the surface phenomena may dominate and presented a straightforward extension of the two-fluid model for analyzing oil–water stratified flow with curved interfaces. The validity of the model and its practical significance for analyzing stratified flows were evaluated in view of experimental data of the in situ flow configuration and the associated pressure drop in an oil– water system reported by Valle and Kvandal (1995).

Vedapuri and Jepsen (1997) developed a three-phase segregated flow model, the water layer; oil layer and mixed layer in between are treated as three different phases with their own distinct properties.

Shi et al. (2003) proposed a four-phase segregated flow model for oil–water flows in horizontal and near horizontal pipelines based on Vedapuri and Jepsen (1997) model. Oil–water flows were treated as four segregated phases: pure oil, water in oil phase (Dw/o), oil in water phase (Do/w) and pure water. This model also assumed that both the oil in water and the water in oil were a homogeneous pseudo phase, with a uniform density and viscosity, and with no-slip between the two phases in the dispersion. Shi et al. (2003) pointed out that the four-phase segregated model was able to predict the water film height and holdup as well as pressure gradient. However, the biggest error by applying the segregated model is around the inversion point due to discontinuities in the equations which could cause numerical instability.

2.5.3.3 Dispersed Flow

For dispersed oil–water flows, the homogeneous model is usually applied. In this model averaged properties of the mixture will be adopted, and it obeys the usual equations of single-phase flow. The main problem in applying this approach is in the calculation of effective mixture viscosity. In general, the viscosity of an emulsion is governed by a number of factors: viscosity of the continuous phase, viscosity of the dispersed phase, volume fraction of the dispersed phase, shear rate, temperature, average droplet size and size distribution of the dispersed phase droplets, and interfacial tension.

2.5.3.4 Water Assist Flow (WAF)

As a new and developing technology, WAF was only studied by limited number of researchers:

McKibben et al. (2000a) and others stated a tentative description of flow pattern when heavy oil or bitumen is transported in pipeline:

- The pipe wall becomes coated with a layer of oil.
- An oil rich zone develops in the central portion of the pipe.
- A water rich sheath forms and this sheath separates the rapidly moving core from the oil which stuck to the pipe wall. Water provides the lubrication that allows the flow to occur at greatly reduced pressure drop.
- The pipeline pressure is dependent on the thickness and the shape (waviness) on the pipe wall

McKibben et al. (2000a) conducted experiments with lubricating and crude oil (viscosity range: 32.5~11200 cP and density range 884~985 kg/m^3) and water at low velocities, using a 53 mm diameter pipe.

Three series tests were conducted to study the flow pattern. The first series of experiments were performed by using viscous lubricating oil (viscosity range: 620~690 cP and density range 884~885 kg/m^3), and water to which methanol had been added to reduce the water density. The total flowrate was 6 l/min. By

visualizing the flow through a glass observation section, two flow patterns were observed:

1. Water dispersed as large slugs in oil when the low water-to-oil ratios occurred. And then a transition happened after the water-to-oil ratio reached around 20%.
2. Stratified flow with a high velocity water stream flowing below a low velocity oil stream.

The second series of experiments were performed by using viscous lubricating oil (viscosity range: 5300~11000 cP and density range 971~976 kg/m^3). The effective loop length is 38 m and flowrate ranged from 4~16 l/min. Also two flow patterns were obtained:

1. Flows in which the pressure gradient fluctuated between high values, consistent with single phase oil flow and very low values.
2. Flows in which the pressure gradients was steady and very low.

Pressure gradients analysis indicated that the slug inside was not like the traditional slug behaviour. The pressure reduction was not due to water at pipe wall as in CAF, but is associated with water slugs which envelop oil. Using the anemometer voltage recording of temperature fluctuation in the pipe at different positions, the tentative picture of flow behaviour, which called envelop slug flow, was proposed as show in Figure 2-51:

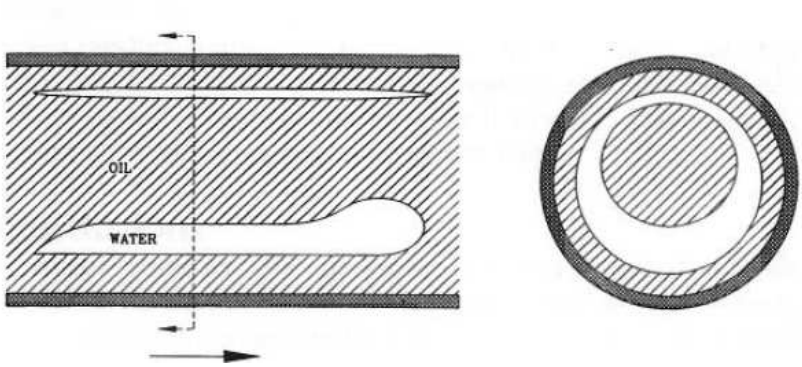

Figure 2-51: Hypothetical water/oil blob in pipe cross-section

(McKibben et al. 2000a)

The aim of third set of tests (viscosity range: 325~7300 cP and density range 952~972 kg/m^3) was to examine the effects of crude oil and the length of pipe. The tests were conducted at 12 L/min flowrate and in 38~68 m effective loop length. After analyzing the anemometer voltage recording, the flow pattern for this set of test was found similar to that found in series 2 tests, which indicated that the oil viscosity does not seem to affect the flow pattern significantly. They concluded that no existence of stratified flow was due to that steel wettability for oil to steel pipe is higher than that for water to steel.

McKibben et al. (2000a) also introduced the densimetric Froude Number, Fr, to account for the effects from both mixture velocity and water cut. The densimetric Froude Number is based on the mixture velocity and in the form of:

$$Fr = \frac{V_m}{\sqrt{gD\left(\frac{\rho_w - \rho_o}{\rho_w}\right)}} \tag{33}$$

where V_m is the mixture velocity of oil and water, D is pipe diameter, and ρ_w and ρ_o are water and oil density respectively.

A boundary line was generated to indicate the transition between water assist flow region and where water assist flow is not achieved, as shown in Figure 2-52.

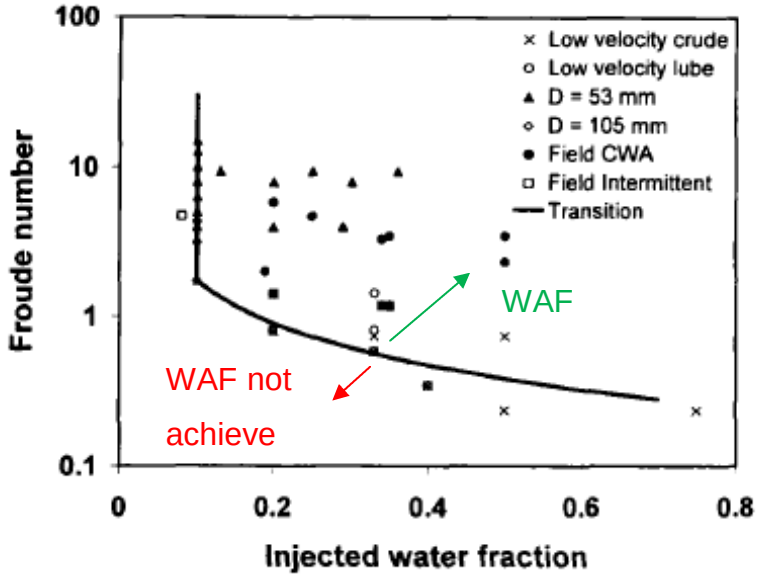

Figure 2-52: Transition for water assist flow from McKibben et al. (2000b)

The experimental data in this work will be used to validate the transition line from McKibben et al. (2000b). To be consistent with the previous interpretation, the operating conditions, where the pressure gradients only experience little/no further reduction by addition of water, are considered as the WAF. Otherwise, WAF is not achieved.

2.5.4 Summary

Although a lot of experimental and theoretical work has been done on the flow pattern analysis of liquid-liquid flow, no general results has been obtained or accepted so far. This is not only due to the changes in fluid properties, flow conditions and pipe geometry, but also complexity of interactions between different phases. Therefore, further effort is still needed in this area. This thesis will cover the effect of viscosity and water cut on pressure drop and flow pattern for different flow conditions.

Table 2-6 summarizes all the research studies on oil-water flows in this report:

Authors	Pipe ID (mm)	Pipe Material	Pipe Orientation (degrees)	Oil Viscosity (cP)	Oil Density (kg/m3)	Comments
Charles et al. (1961)	26.4	Cellulose acetate-butyrate	0	6.29, 16.8, 65	834	Studied the flow patterns, holdup ratios, and pressure gradients. $0.03 < V_{so} < 1.2$ m/s & $0.03 < V_{sw} < 1.1$ m/s
Ooms et al. (1984)	51, 200	PVC	0	2300, 3200, 3300	970	CAF modeling with the attention for buoyancy force and ripples on the core.
Oliemens et al. (1987)	50	PVC	0	3000	975	Considered the turbulent lubricating film model to predict the pressure gradient. $0.3 < V_{so} < 2.25$ m/s & $0.02 < V_{sw} < 0.6$ m/s
Arirachakaren et al. (1989)	26, 41	PVC, Steel	0	4.7, 58, 84, 115, 237, 2116	852	Studied the phase inversion, flow patterns, and pressure gradients. $0.35 < V_m < 3.7$ m/s
Bai et al. (1992)	9.5	PVC	±90	600	905	Investigated the stability of CAF, flow patterns within CAF, holdup, dispersion and phase inversion.
Arney et al. (1993)	15.9	Glass, PVC	0	600, 2700	985	Studied the pressure gradient, holdup, and developed a model based on concentric cylindrical CAF.
Trallero (1995)	50.1	Acrylic	0	29.6	850	Studied the pressure gradient, flow patterns, holdup, and developed flow pattern transition prediction model. $0.01 < V_{so} < 1.7$ m/s & $0.03 < V_{sw} < 1.7$ m/s
Valle and Kvandal (1995)	37.5	Glass	0	2.3	794	Investigated the pressure gradient and dispersion characteristics.
Valle and Utvik (1997)	77.9	Glass	0	1	741	Studied the flow pattern, slip between phases, and pressure gradients.
Nadler and Mewes (1997)	59	Perspex	0	22~35	841	The effect of emulsification and phase inversion on pressure gradient for different flow regimes was investigated. $0.1 < V_{so} < 1.6$ m/s & $0.1 < V_{sw} < 1.6$ m/s

Table 2-6: Review of range of experimental variables for liquid-liquid flows- part 1/3

Authors	Pipe ID (mm)	Pipe Material	Pipe Orientation (degrees)	Oil Viscosity (cP)	Oil Density (kg/m3)	Comments
Bannwart (1999)	26.7, 23.9	Steel, Cement	0	2700	989	Considered the pipe wall effect in term of attracting or repelling the oil from the surface on pressure gradient. $0.18<V_{so}<0.6$ m/s & $0.02<V_{sw}<0.25$ m/s
Flores et al. (1999)	50.8	Acrylic	90, 75, 60, 45	20	850	Studied the flow patterns and proposed a mechanistic model to predict the flow pattern transition. $0.04<V_{so}<1.3$ m/s & $0.04<V_{sw}<1.3$ m/s
Angeli and Hewitt (2000)	24.3	Acrylic, Stainless Steel	0	1.6	801	Studied the flow patter, phase distribution, and holdup. $0.2<V_m<3.9$ m/s & 6 < water cut < 86 %
McKibben et al. (2000a)	53	Steel	0	325~11200	884~985	Examined the water existence effect in well-bore flow conditions. They Predicted CAF with oil coating and developed WAF criterion.
Bannwart (2001)	22.5	PVC	0, 90	2700	989	Investigated the existence of stable core. Developed a model for volume fraction and pressure gradient for CAF based on mass and momentum balances.
Benshakaria et al. (2004)	25	Steel	0, 90	4740	800	Studied the effect of water as a lubrication to enhance the flow. The pressure gradient was dropped by more than 90%.
Abduvayt et al. (2004)	106.4	PVC	0, ±0.5, ±3, 90	1.88±0.19	800	Studied the flow patterns, hold up, slip, and pressure gradient. $0.02<V_{so}<1.5$ m/s & $0.02<V_{sw}<1.5$ m/s
Bannwart et al. (2004)	28.4	PVC	0, 90	488	925.5	Studied the flow patterns and the occurrence of CAF. $0.007<V_{so}<2.5$ m/s & $0.04<V_{sw}<0.5$ m/s

Table 2-6: Review of range of experimental variables for liquid-liquid flows- part 2/3

Authors	Pipe ID (mm)	Pipe Material	Pipe Orientation (degrees)	Oil Viscosity (cP)	Oil Density (kg/m3)	Comments
Rodriguez et al.(2006)	82.5	Stainless Steel, Perspex	0, ±1, ±2, -5	7.5, 800	830, 1060	Studied the flow patterns, pressure gradients, and oil/water holdups. $0.02<V_{so}<3$ m/s & $0.02<V_{sw}<2.55$ m/s
Vielma et al. (2007)	50.8	Acrylic	0	15	850	Studied the flow patterns, pressure drop, phase fraction, and droplet size as a function of flow patterns. $0.025<V_{so}<1.75$ m/s & $0.025<V_{sw}<1.75$ m/s
Atmaca et al. (2008)	50.8	Perspex	0, ±1, ±2, -5	15	858.75	Studied the flow patterns, pressure drop, holdup, phase distribution, and slippage between phases. $0.025<V_{so}<1.75$ m/s & $0.025<V_{sw}<1.75$ m/s
Grassi et al. (2008)	21	Transparent polycarbonate	0, ±15	533, 653, 800	886	Investigated the pressure drops and flow patterns experimentally and compared against different prediction models. $0.02<V_{so}<0.7$ m/s & $0.02<V_{sw}<2.7$ m/s
Vuong et al. (2009)	52.5	Steel	0, 90	230,440,1070	884.4	Investigated viscosity effect on the flow patterns, holdup, and pressure drops. $0.1<V_{so}<1.0$ m/s & $0.15<V_{sw}<1.0$ m/s
Wang et al. (2010)	25.4	Steel	0	620.8, 628.1	854.8, 952.66	Investigated the pressure drops, flow patterns, and phase inversion phenomenon. $0.1<V_m<1.15$ m/s & $0.1<$ water fraction <0.7
Strazza et al. (2011)	21, 22	Plexiglas, glass	-10 ~ 15	900	886	Investigated the Exist of CAF, pressure drops, and holdup and compared against different prediction models.

Table 2-6: Review of range of experimental variables for liquid-liquid flows- part 3/3

2.6 Three phase Liquid-Liquid-Gas Flows

Similar to the oil-water flow, the simultaneous flow of oil, water and gas in pipelines is also a common occurrence in the petroleum industry, which is due to that, either water is naturally produced with oil and gas or water is injected to maintain the pressure of an oil reservoir. Therefore, oil-water-gas flow is very common phenomena happening in wellbore and surface gathering system. However, the studies on oil-water-gas flow are still limited without any general acceptance. In this section, the definitions for oil-water-gas flow patterns were summarized based on the observations from different researchers. Moreover, several pressure prediction methods were reviewed. A summary of the experimental research studies on liquid-liquid flows found is given at the end of the section (Table 2-7).

2.6.1 Flow Patterns in Oil- Water- Gas Flow

- Acikgoz et al. (1992)

The first comprehensive classification of three phase flow patterns and flow pattern map (Figure 2-53) was proposed by Acikgoz et al. (1992). The mapping parameters used were superficial water and gas velocities with separate maps for each oil velocity (J_o). These mapping parameters were used by other later workers (Pan et al., 1995; Woods et al., 1998).

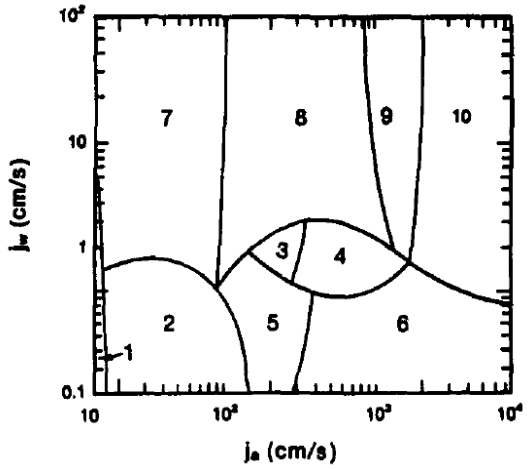

J_o = 4.3 cm/s

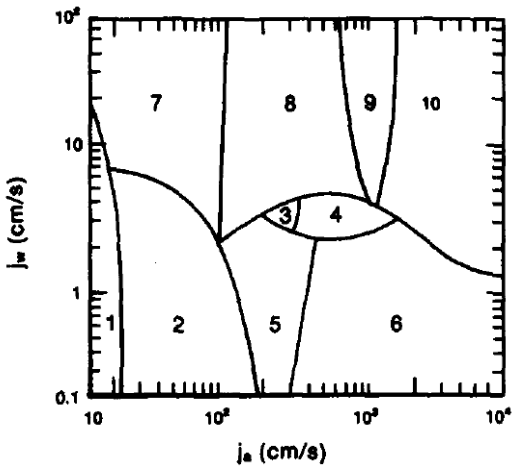

J_o = 9 cm/s

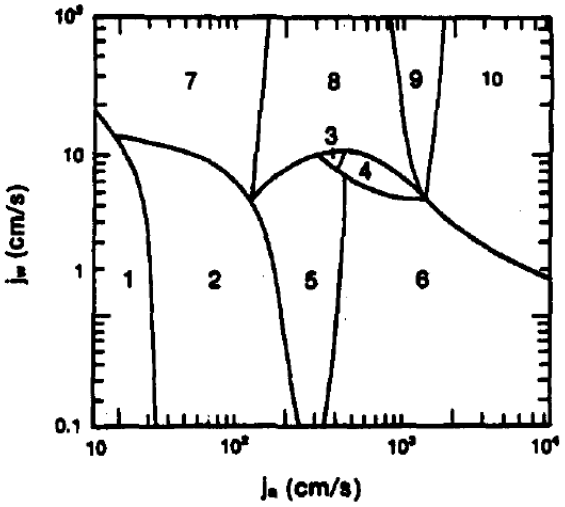

J_o = 24 cm/s

Region	Flow regime
1	Oil-based dispersed plug flow
2	Oil-based dispersed slug flow
3	Oil-based dispersed stratified/wavy flow
4	Oil-based separated stratified/wavy flow
5	Oil-based separated wavy stratifying-annular flow
6	Oil-based separated/dispersed stratifying-annular flow
7	Water-based dispersed slug flow
8	Water-based dispersed stratified/wavy flow
9	Water-based separated/dispersed incipient stratifying-annular flow
10	Water-based dispersed stratifying-annular flow

Figure 2-53: Oil-water-air three phase flow patterns classifications and flow pattern map (Acikgoz et al., 1992)

Schematic drawings of the different classifications mentioned above are shown in Figure 2-54 to Figure 2-58

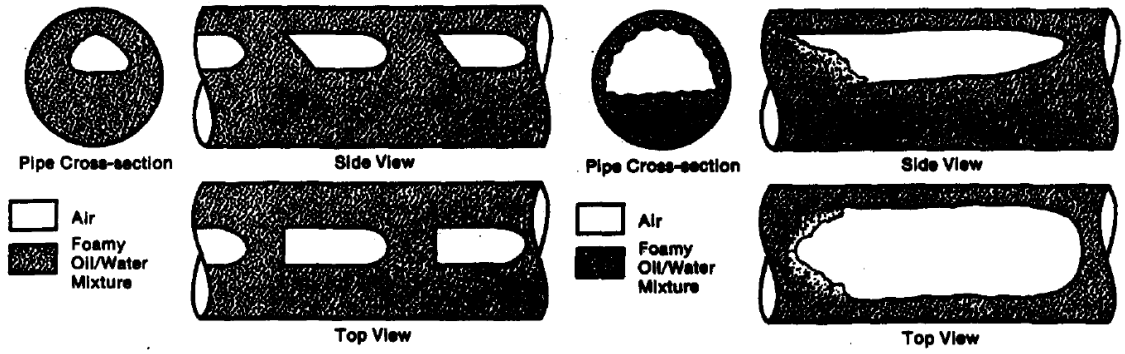

(a) **(b)**

Figure 2-54: Schematic of oil-based dispersed plug (a) / slug (b) flow (Acikgoz et al., 1992)

- Oil-based dispersed plug flow (Figure 2-54, a)

For relatively low water and air superficial velocities oil-based dispersed plug flow was observed. At these flow rates, water mixed with oil causing a liquid mixture which was foamy in appearance.

- Oil-based dispersed slug flow (Figure 2-54, b)

As increasing the air superficial velocity, it was observed that the air phase began to drive the liquid phases. This implied that we were in the slug flow pattern. In the slug flow region the oil-based liquid phase appeared to be foamy. In contrast with plug flow, however, the trailing edge of the large air bubbles was not sharply defined.

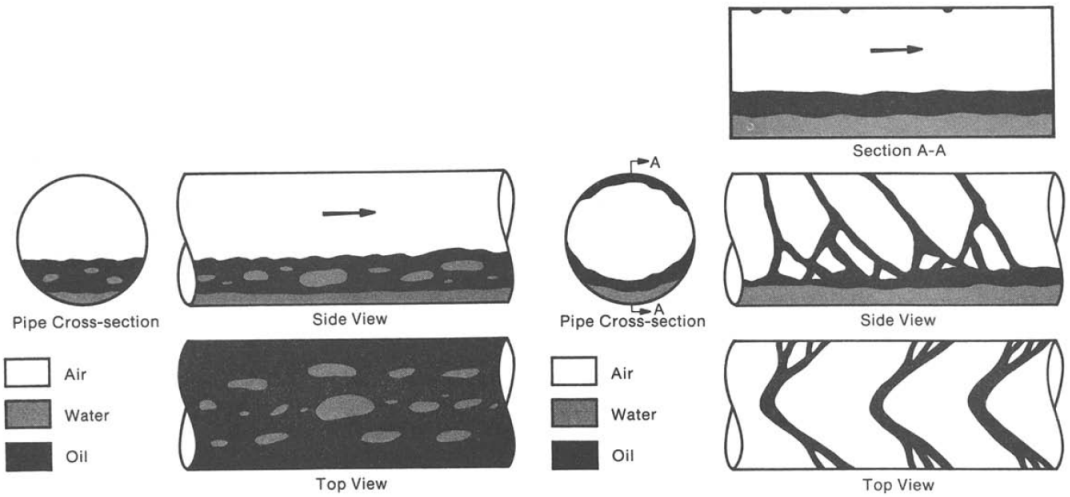

(a) **(b)**

Figure 2-55: Schematic of oil-based dispersed (a) /separated (b) stratified (wavy) flow (Acikgoz et al., 1992)

- Oil-based dispersed stratified/wavy flow (Figure 2-55, a)

In this flow pattern, stratification and gravitational phase separation was observed. On top of a continuous layer of water, there was an oil-based mixture having relatively large water droplets in it. In this region of the three-phase flow pattern map, small-amplitude surface waves were observed on the oil/water layer.

- Oil-based separated stratified/wavy flow (Figure 2-55, b)

The oil and water phases were completely separated. Due to gravitational stratification, the oil phase flowed on top of the water phase; also a complicated wave structure appeared on the top of the pipe. Ripple waves were also observed on the interface between the oil and water phases.

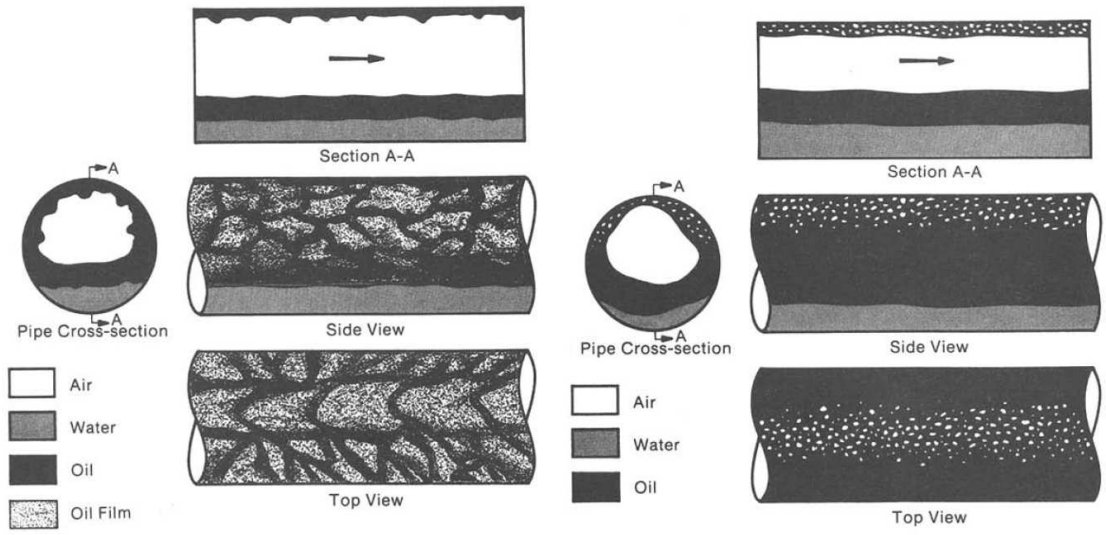

(a) **(b)**

Figure 2-56: Schematic of oil-based separated-wavy (a) / separated-dispersed (b) stratifying-annular flow (Acikgoz et al., 1992)

- Oil-based separated - wavy stratifying-annular flow (Figure 2-56, a)

The upper oil structures observed in separated stratified/wavy flow became denser in this flow pattern and were connected with a thinner oil film, which caused continuous wetting of the upper pipe wall. However, stratification still played a dominant role for this flow pattern.

- Oil-based separated- dispersed stratifying-annular flow (Figure 2-56, b)

By increasing the air flow rate, the variations in the oil film thickness on the upper pipe wall, which characterized the previous flow pattern, disappeared. Small air bubbles in the oil film were observed towards the top of pipe. As in the previous flow pattern, stratification effects were still evident.

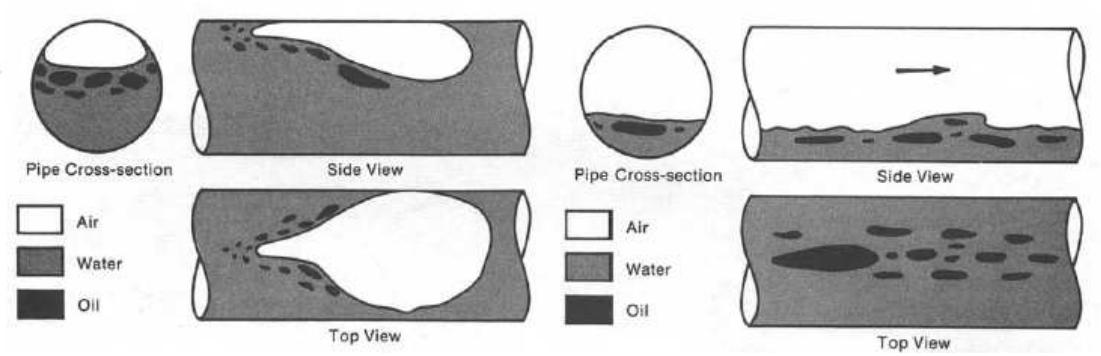

(a) **(b)**

Figure 2-57: Schematic of water-based dispersed slug (a)/ stratified wavy (b) flow (Acikgoz et al., 1992)

- Water-based dispersed slug flow (Figure 2-57, a)

For relatively low air and high water flow rates, air bubbles with very distinct tails were observed. For this flow pattern, the air phase was the driving phase. A relatively high concentration of oil droplets in the regions was observed following the air bubbles. As increasing the air flow rate, the clear boundaries between the air plug tails and water phase were replaced by a frothy appearance at the back of the air plugs.

- Water-based dispersed stratified wavy flow (Figure 2-57, b)

This flow pattern looked similar to a two-phase stratified/wavy flow with the exception of the dispersed oil droplets.

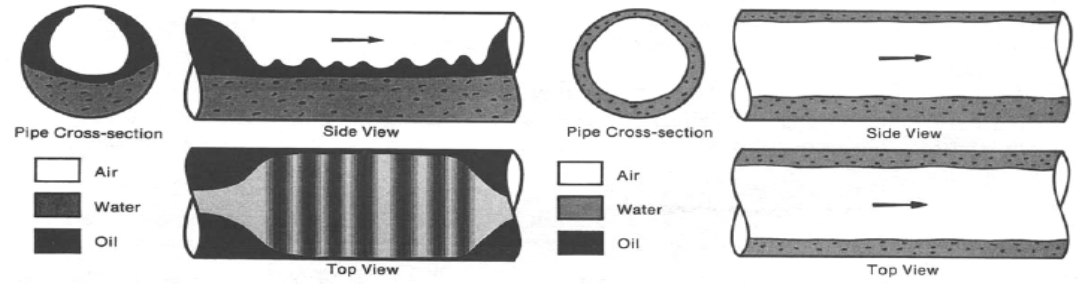

(a) **(b)**

Figure 2-58: Schematic of water-based separated dispersed incipient (a)/ dispersed (b) stratifying-annular flow (Acikgoz et al., 1992)

- Water-based separate dispersed incipient stratifying-annular flow (Figure 2-58, a)

As the air flow was increased the relatively, small waves were found replaced by a new structure which including roll waves. Moreover, liquid "phase" separation occurs, presumably due to gravitational and shear effects.

- Water-based dispersed stratifying-annular flow (Figure 2-58, b)

In this flow pattern, the pipe perimeter was wetted continuously by a water-based film which contained small oil droplets dispersed in it. The water film thickness differences between the top and the bottom of the pipe were most noticeable at lower superficial air velocities, and became smaller on increasing the air flow rate. Except for the dispersed oil droplets, this flow pattern was found very much like two-phase stratifying-annular flow.

- Taitel et al. (1995)

Taitel et al. (1995) developed theoretical method to predict flow pattern map for three phase oil-water-air flows. This method was based on the momentum balances for each phase in a stratified flow. By elimination of the pressure loss, two equations are obtained, which can be solved iteratively to get the volume fractions of each phase. The transition criteria from stratified flow was taken from Taitel and Dukler (1976), namely that the liquid level is unstable when

$$V_g - V_o > \left(1 - \frac{h_L}{D}\right)\sqrt{\frac{(\rho_o - \rho_g)gA_g}{\rho_g S_j}} \qquad (34)$$

where V_g and V_o are the corresponding average velocities in the gas and the oil layer, h_L is the total liquid level, ρ_o and ρ_g are the gas and the oil density, g is the gravitational acceleration, A_g is the cross sectional area of the gas layer and S_j is the chord length of the gas–liquid interface in the cross section of the pipe. When $h_L / D \geq 0.35$, slug flow will exist, while annular flow will occur at $h_L / D < 0.35$. Only flow pattern changes in the gas liquid system were

considered in this model. The boundary slug flow to annular flow might be strongly dependent on the fluid properties like surface tensions, wetting angles and viscosities.

- Chen and Guo (1999)

Chen and Guo (1999) carried out the oil-water-air experiments in coiled tube with the input water fraction greater than 50%. The water behaved as a continuous phase and oil always dispersed in the continuous water phase. Four main flow patterns were observed, as shown in Figure 2-59:

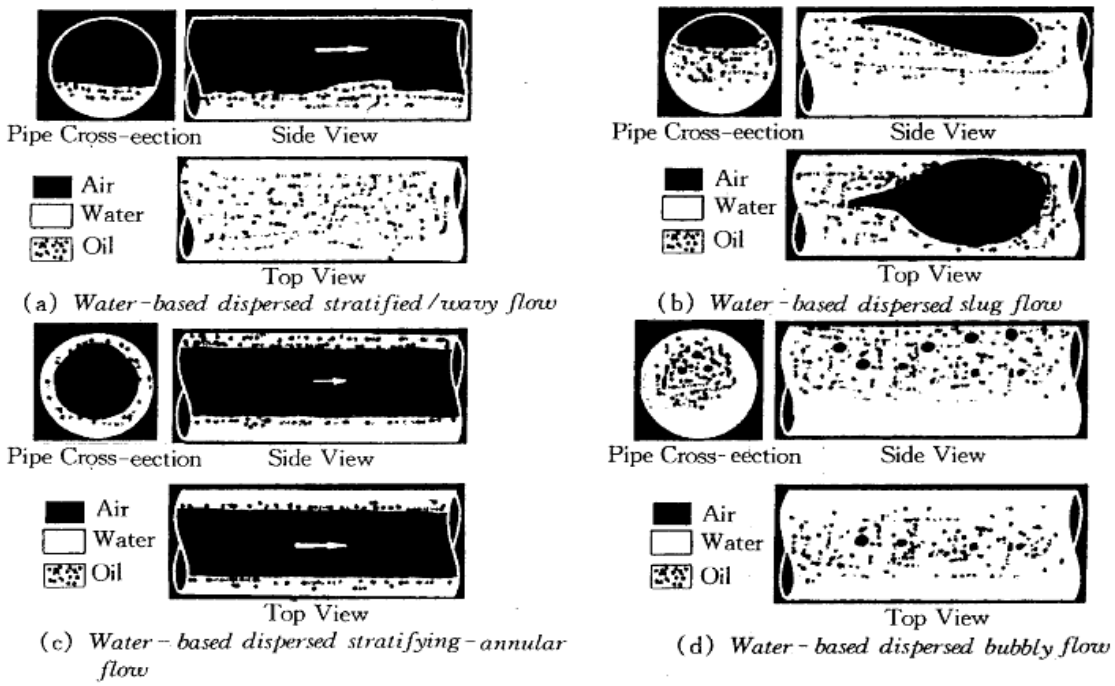

Figure 2-59: Classification of oil-water-air three-phase flow patterns in coiled tubes (Chen and Guo, 1999)

- Water-based dispersed stratified/wavy flow (Figure 2-59, a):

This flow pattern were observed similar to two-phase stratified flow, in which the air and liquid were separated completely while the air flowing at the upper side of the test section, or it was an intermediate stratified flow in which the top of the tube wall was wetted sometimes by the liquid in curved tubes.

- Water-based dispersed slug flow (Figure 2-59, b):

For relatively low air and high water flow rates, air bubbles with very distinct tails were observed. For this flow pattern, the air phase was the driving phase. A relatively high concentration of oil droplets in the regions following air-bubbles was observed. With increasing air flow rate, the distinct boundaries between the air plus tails and the water phase were replaced by a froth appearance at the back of the air plug.

- Water-based dispersed stratified annular flow (Figure 2-59, c):

The pipe perimeter was observed to be wetted continuously by a water-based film containing small dispersed oil droplets. The difference in water film thickness between the top and bottom of the pipe was most noticeable at lower superficial air velocities, and became smaller with increasing air flow rate.

- Water-based dispersed bubbly flow (Figure 2-59, d):

Similar to a two-phase bubbly flow, oil droplets were found dispersed in water.

- Spedding et al. (2005)

Under the broad classification as oil dominated (OD) or water dominated (WD) based on the dominant liquid phase, Spedding et al. (2005) made additional classifications for intermittent, stratified or annular type patterns. The oil dominated co-current patterns observed in his work is shown in Figure 2-60:

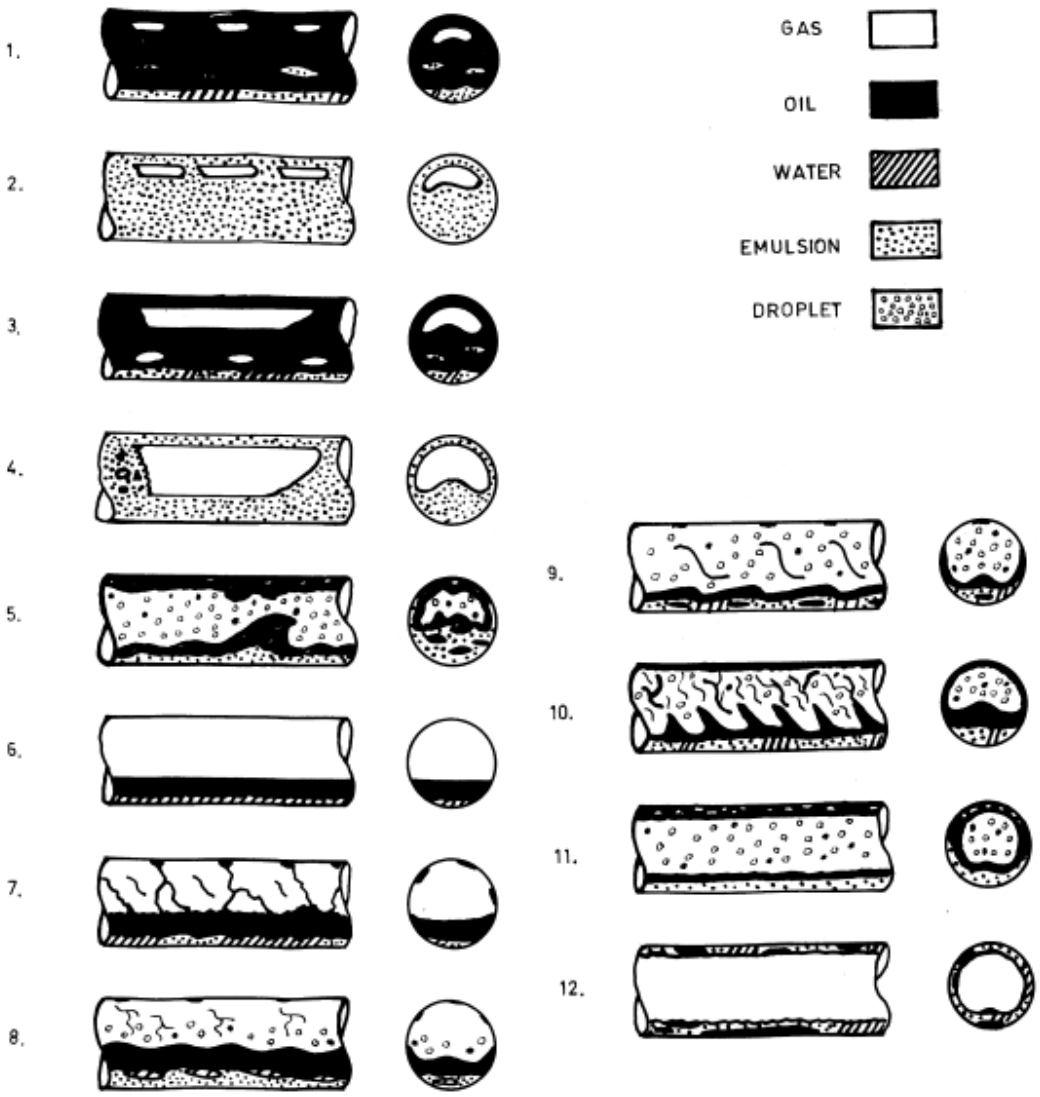

Figure 2-60: Oil dominated flow patterns and inversion for three phase horizontal co-current pipe flow (Spedding et al., 2005)

At low gas rates, when the liquid phases were the main driving component, the patterns were either plug separated (1) or plug dispersed (2) flows. In the latter case the liquid phase had a foaming white appearance while in the former case there was a degree of liquid phase separation. Increasing the gas rate resulted in either the slug separated (3) or the slug dispersed (4) patterns being formed. Oil attached on the pipe wall was found drained downwards forming complex wave structures on the pipe side wall. The blow through slug (5) pattern appeared as increasing the gas flowrate. The interaction between gas and liquid phase were considerably high. In addition an oil film was

present on the upper pipe wall over which droplets of water drained away under gravity.

When the initial liquid rate level was below the pipe centre line, the smooth stratified (6) and stratified wavy separated (7) patterns or dispersed as in the stratified roll wave dispersed (8) and the stratified roll wave dispersed droplet (9) flows were observed. In the smooth stratified pattern, small amplitude waves were only observed on the oil/water interface. As increasing the gas flowrate, the droplet of oil were also observed on the upper surface of the pipe. By further increasing the gas flowrate, annular separated (10) or annular dispersed (11) flows were observed. And then the inversion point was approached, where the transition occurred from oil dominated flow to water dominated flow.

The water dominated co-current patterns observed is shown in Figure 2-61:

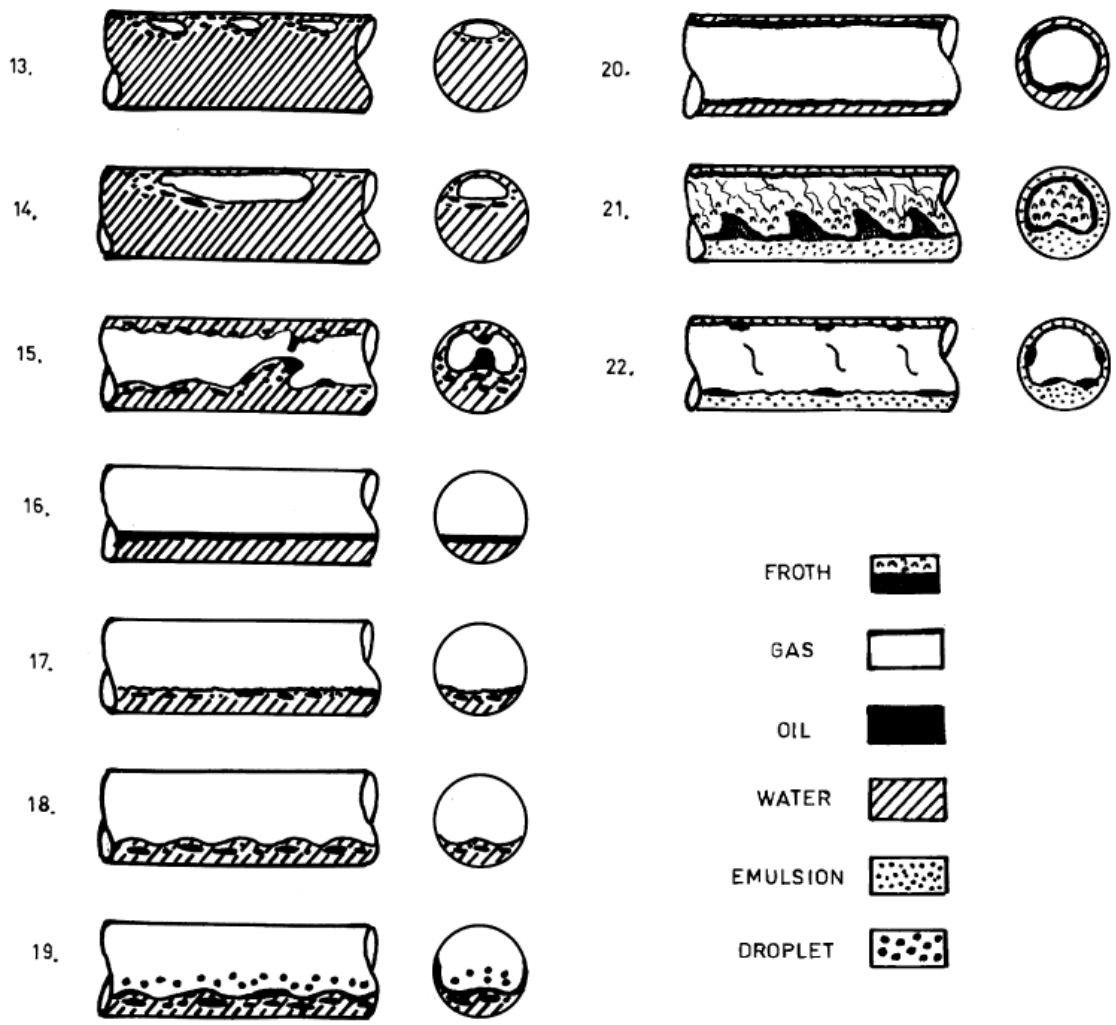

Figure 2-61: Water dominated flow patterns and inversion for three phase horizontal co-current pipe flow (Spedding et al., 2005)

The water dominated intermittent flows (13–15) were found all of the dispersed type, with the oil droplets within the water continuum. For the dispersed plug (13) and the dispersed slug (14) patterns, the oil droplets were observed tending to accumulate at the tail of gas bubbles. The blow through slug (15) pattern retained the essential features of pattern 5. For the water dominated stratified patterns (16–19), the smooth stratified (16), stratified ripple dispersed (17) and the stratified roll wave dispersed (18) patterns possessed a very similar appearance to that of the equivalent two phase gas/water patterns. However, the dispersion of oil droplets was observed within the water. For the stratified roll wave droplet (19), the surface waves on

the liquid tended to be more complex than with the equivalent oil dominated pattern. The annular patterns were observed as either separated as in the annulus water annular oil (20) pattern or dispersed as either the annular froth (21) or the dispersed annular (22) patterns.

- Keskin et al. (2007)

Keskin et al. (2007) also proposed a new classification of oil-water-air three phase flow patterns by combining the terms from air-water flow and oil-water flow. 12 individual three phase patterns were identified in horizontal pipe under their test condition, as shown in Figure 2-62:

- Stratified-Stratified (ST-ST)

This flow pattern occurred at low oil and water flow rates but gas flow rate could be high enough to observe wavy gas-oil interface. A few droplets at the interface might be seen.

- Stratified-Dual Continuous (ST-DC)

Oil and water flow rates were still low enough for intermittent flow. In most cases, gas-oil interface had wavy structure. Oil and water phases were found separated with an interface above which water/oil droplets dispersing in continuous oil/water phase.

- Stratified-Oil Continuous (ST-OC)

Wavy structure was observed the whole time at gas-oil interface due to high gas flow rates. Oil was the only continuous liquid phase and water was completely dispersed in oil. This flow pattern was observed for relatively low water fractions.

- Stratified-Water Continuous (ST-WC)

Water fraction should be high enough for complete oil in water dispersion for this flow pattern. High gas flow rate causes a wavy gas-water interface.

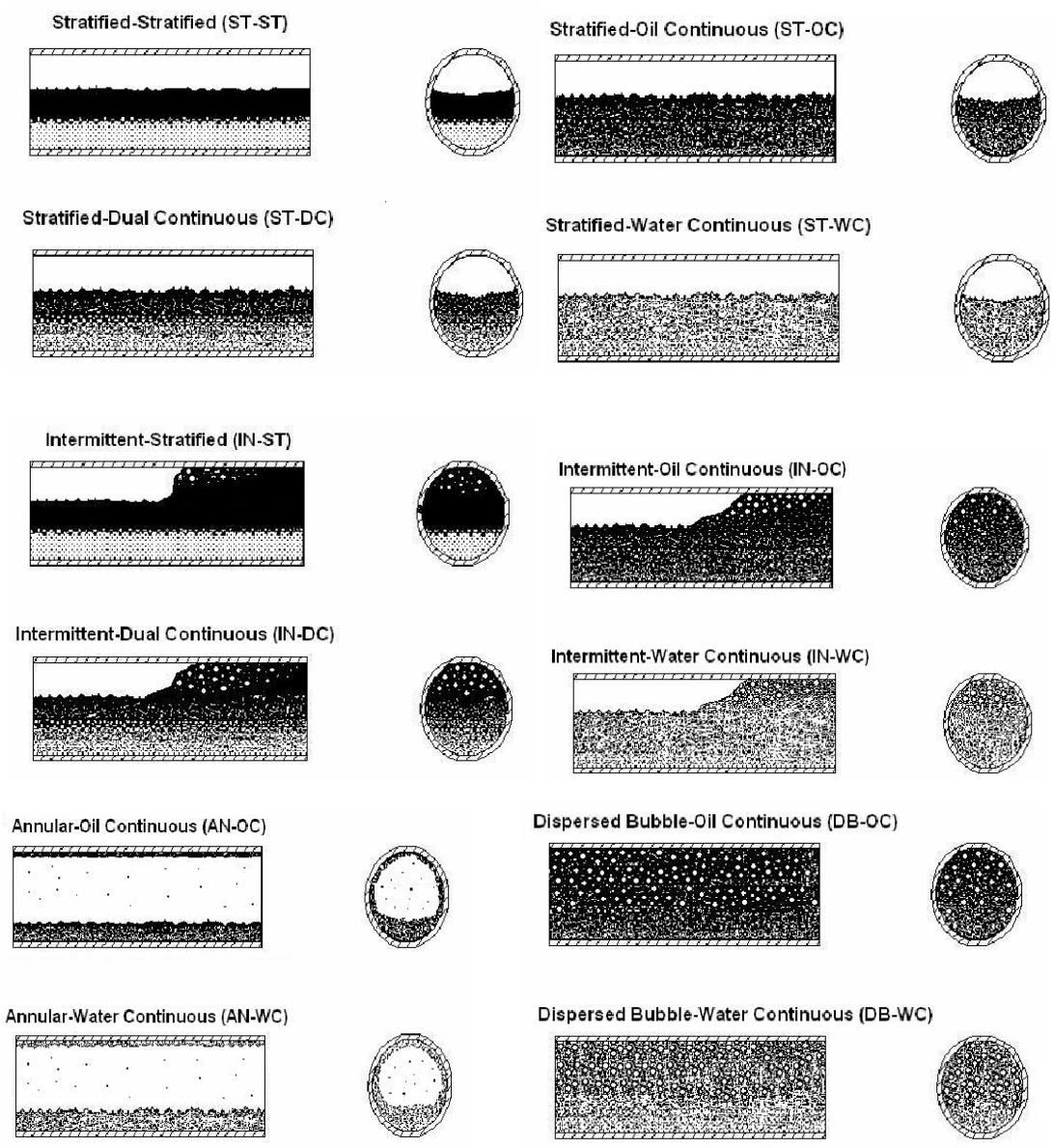

Figure 2-62: Oil-water-air three phase flow regime classification by Keskin et al. (2007)

- Intermittent-Stratified (IN-ST)

Elongated bubble was observed due to the low gas flow rates for this flow pattern. Few droplets appeared at the oil-water interface.

- Intermittent-Dual Continuous (IN-DC)

Depending on the water fraction, oil continuous layer with dispersed water droplets and water continuous layer with dispersed oil droplets were observed simultaneously.

- Intermittent-Oil Continuous (IN-OC)

This flow pattern was observed at low water fractions with relatively high liquid flow rates. Gas-liquid flow pattern was generally slug flow. The only continuous liquid phase was oil and water is completely dispersed in oil.

- Intermittent-Water Continuous (IN-WC)

Due to the relatively high water fraction, oil is completely dispersed in continuous water phase. Slug flow is observed.

- Annular-Oil Continuous (AN-OC)

Annular flow occurs at very high gas velocities. The gas phase flows were found acting as a core at the centre of the pipe and the liquid phase flows as a film around the pipe wall. Even if the liquid velocities are low, they tended to mix and one liquid phase disperses in the other due to the high turbulence. When the oil fraction is high, the continuous liquid phase is oil and water is completely dispersed.

- Annular-Water Continuous (AN-WC)

When the gas liquid flow pattern is annular flow and the water fraction is higher than the oil fraction, water is the continuous phase and oil is completely dispersed in water.

- Dispersed Bubble-Oil Continuous (DB-OC)

At very high liquid flow rates, gas phase is dispersed in continuous liquid phase as discrete bubbles. The gas-oil-water flow pattern is dispersed bubble-oil continuous (DB-OC) If the continuous liquid phase is oil.

- Dispersed Bubble-Water Continuous (DB-WC)

The gas phase was dispersed as bubbles and the oil phase was dispersed as droplet in continuous water phase for this flow pattern.

- Bannwart et al. (2009)

Bannwart et al. (2009) carried out the experiments to study the oil-water-air flow patterns using crude oil (3400 cP, 970 kg m^{-3} at 20 °C) in both horizontal and vertical pipeline. The gas–water and oil–water flow patterns are separately classified, as shown in Figure 2-63:

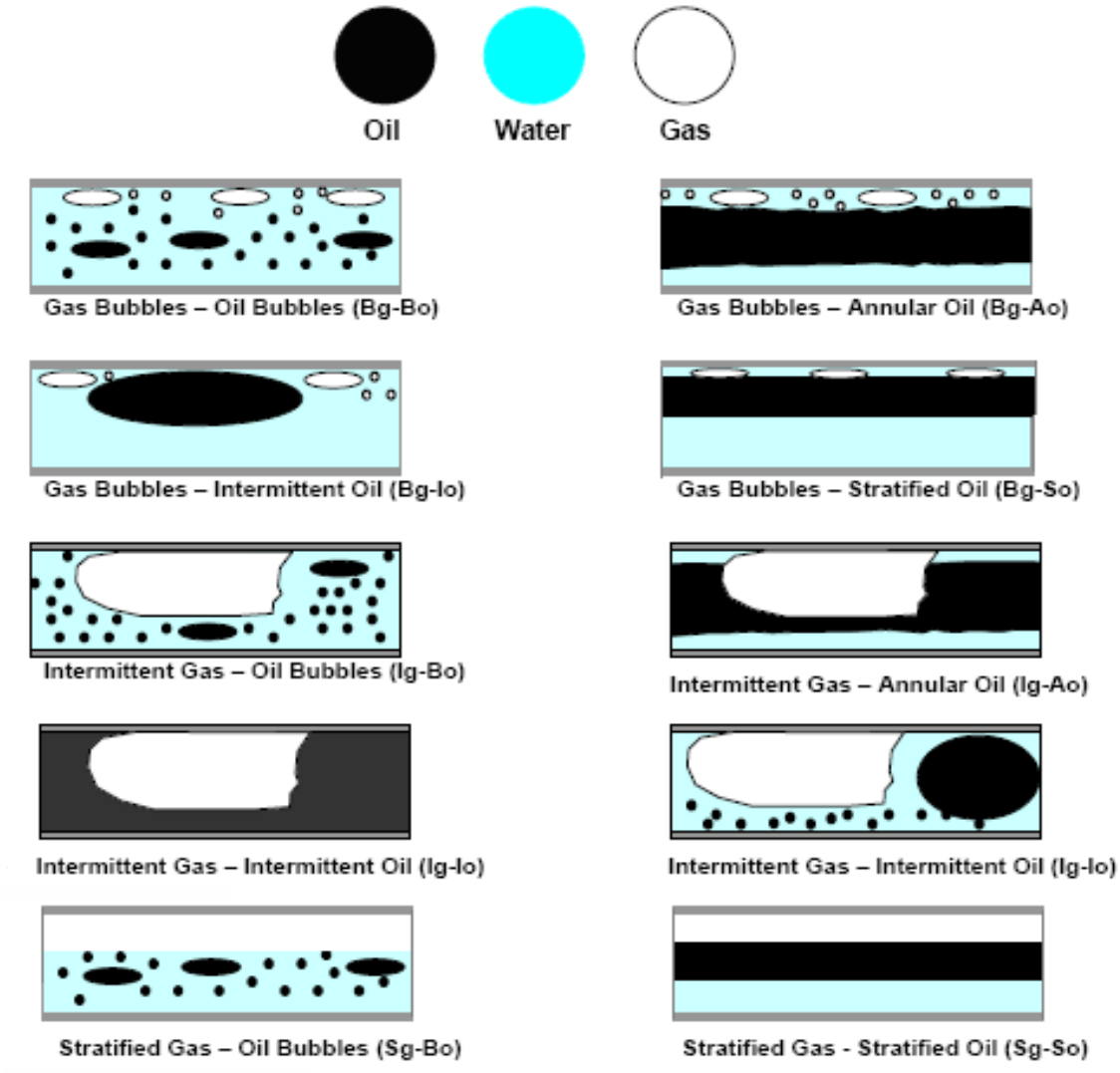

Figure 2-63: Three-phase patterns for horizontal water-assisted flow of heavy oil in the presence of a gas phase (Bannwart et al., 2009)

- Bubble gas–Bubbles oil (Bg–Bo)

Gas bubbles dispersed in water at the top of the pipe due to buoyancy effect. Almost spherical oil bubbles dispersed in water following the water velocity profile.

- Bubble gas–Annular oil (Bg–Ao)

Gas bubbles dispersed in water at the top of the pipe and continuous oil phase in the pipe's core surrounded by water (core annular flow). At high oil and low water flow rates, the gas bubbles might be trapped within the oil–water interfacial waves.

- Bubble gas–Intermittent oil (Bg–Io)

Oil bubbles become bigger and start to coalesce; the relatively large oil bubbles were found close to the top of the pipe due to buoyancy effect.

- Bubble gas–Stratified oil (Bg–So)

Continuous oil phase flowing were observed very close to the top of the pipe due to buoyancy effect. Nevertheless, due to wettability effect a thin water film on the top wall was detected, which explains the observed high speed of the oil phase.

- Intermittent gas–Bubbles oil (Ig–Bo)

Relatively large gas bubbles were seen separated by water slugs (slug flow). The latter consisted of a dispersion of oil bubbles in water.

- Intermittent gas–Annular oil (Ig–Ao)

Relatively large gas bubbles are seen flowing through the water and are separated by water slugs. Continuous oil phase in the pipe's core were found surrounded by water.

- Intermittent gas–Intermittent oil (Ig–Io)

Gas bubbles and oil bubbles were separated by water slugs. Sometimes an emulsion of oil in water might form due to the agitation caused by the gas.

- Stratified gas–Bubbles oil (Sg–Bo)

Gas–water stratified flow; wavy structures at the interface may occur. Almost spherical oil bubbles dispersed in water flowing mainly at the top of the water phase.

- Stratified gas–Stratified oil (Sg–So)

At lower water and intermediate oil and gas flow rates a gas–oil–water stratified flow was observed. Wavy structures at the interfaces may occur.

The vertical flow patterns in high viscosity solid/liquid flow can be categorised into six main types, as illustrated in Figure 2-64:

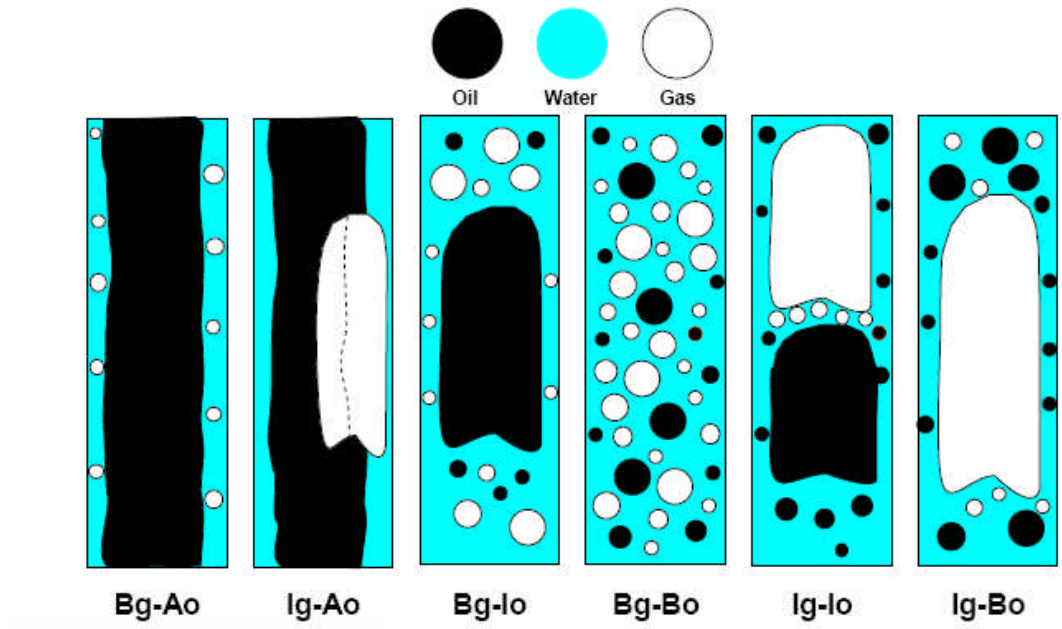

Figure 2-64: Three-phase patterns for vertical water-assisted flow of heavy oil in the presence of a gas phase (Bannwart et al., 2009)

- Bubbly gas – Annular oil (Bg-Ao): Similar to heavy oil-water core flow, except that here gas bubbles are seen in the water phase. The oil-water

interface was typically sinuous. This pattern occurred at high oil and low gas superficial velocities.

- Intermittent gas – Annular oil (Ig-Ao): The gas phase formed large bubbles which partly surrounded a still continuous oil core. This pattern occurred at high oil and moderate gas superficial velocities.
- Bubbly gas – Intermittent oil (Bg-Io): The small bubbles of gas and the large bubbles of oil were observed. This pattern occurred at moderate oil and low gas superficial velocities.
- Bubbly gas – Bubbly oil (Bg-Bo): This pattern was observed seen at low oil and gas superficial velocities, but only when the water superficial velocity was higher than 0.3 m/s, which was enough to disperse the oil into bubbles.
- Intermittent gas – Intermittent oil (Ig-Io): The gas and oil both formed large bubbles which were very close to each other. Detailed observation showed that the oil bubble was sucked towards the low pressure wake was found behind the gas bubble. This pattern occurred at high gas and oil superficial velocities and also for moderate gas and oil superficial velocities.
- Intermittent gas – Bubbly oil (Ig–Bo): At high gas superficial velocities the gas forms large, high speed bubbles and the oil is dispersed into small bubbles. This pattern was typically pulsating, indicating a transition to annular gas-liquid flow.

Comparing the works on the oil-water-air flow patterns, it can be found that the definition of each flow pattern depends on different criterion from different researchers. However, Spedding et al. (2008) point out that no existing horizontal flow map is robust enough to predict accurately for a wide range of geometries, physical properties and flow rate of different phases.

2.6.2 Prediction Models for Pressure Drop in Oil – Water- Air Flows

Since the experimental data for oil-water-air flow were limited, limited prediction models have been proposed to date. Due to the complexity of the flow patterns for oil-water-air flow, the current models proposed were either empirical or mechanistic dealing with one or two specific oil-water-air flow patterns with some assumptions.

2.6.2.1 Empirical Correlations for Oil-Water- Air Flows

- Stapelberg and Mewes Correlation (1994)

Stapelberg and Mewes (1994) were focus on slug flow patterns in oil-water-air flows, aiming to extend frequently-used two-phase models to three-phase flow by assuming two immiscible liquids flow in a horizontal pipe together with the gas. The following assumptions were made:

1. The slugs are formed, from stratified flow, in a similar process to that in two-phase gas-liquid flow. The oil and water flow through the tube in layers corresponding to their density. Thus, the formation of the slug is a result of the forces acting at the interface between the oil and gas.
2. The liquid height and the average velocity of the gas are calculated from the momentum balance for three-phase stratified flow. Therefore, it is assumed that the oil and water flow through the tube as a homogeneous mixture.

In this way, the parameters required for the calculations of the slug frequency can be determined as functions of the Lockhart Martinelli parameter, which was redefined as the ratio of the pressure losses in two-phase (oil-water) and single phase (gas) flow and given by:

$$\Phi^2 = \frac{\gamma^2_{\text{liquid}} \left(\Delta P/\Delta x\right)_{\text{liquid}}}{\left(\Delta P/\Delta x\right)_{\text{gas}}} \tag{35}$$

Where Φ denotes the Lockhart-Martinelli parameter of three-phase flow, γ^2_{liquid} denotes the correction value for two phase flow of oil and water.

- Poesio et al. model (2009)

Poesio et al. (2009) proposed a hybrid Lockhart-Martinelli method with two fluid models (LM2FM). A two-fluid model for the computation of pressure drop for liquid–liquid flow was generated first, and then it was used in Lockhart–Martinelli model for the computation of the overall pressure drop:

$$X^2 = \frac{(\Delta P/\Delta x)_{liquid}}{(\Delta P/\Delta x)_{gas}} \tag{36}$$

$$\Phi_{liquid}{}^2 = \frac{(\Delta P/\Delta x)_{3\text{-phase}}}{(\Delta P/\Delta x)_{liquid}} \qquad \Phi_{gas}{}^2 = \frac{(\Delta P/\Delta x)_{3\text{-phase}}}{(\Delta P/\Delta x)_{gas}} \tag{37}$$

$$\Phi_{gas}{}^2 = 1 + CX + X^2 \qquad \Phi_{liquid}{}^2 = 1 + \frac{C}{X} + \frac{1}{X^2} \tag{38}$$

where $(\Delta P/\Delta x)_{liquid}$ is pressure loss for water and oil, which obtained by solving two fluid model for liquid–liquid (oil-water) core annular flow; and the parameter C is kept constant at 15 without any fitting.

2.6.2.2 Pressure Drop Prediction Models for Stratified Oil-Water-Air Flows

Neogi et al. (1994) used three phase momentum balance equations to predict the pressure drop for oil-water-air stratified flows. The similar approach was also carried out by Taitel et al. (1995) and Khor et al. (1997); Later, Spedding et al. (2008) improved this method by using the actual rheological data for emulsion and the Colebrook-White relation to estimate the interfacial roughness. The oil-water-gas flow system they assumed is illustrated in Figure 2-65:

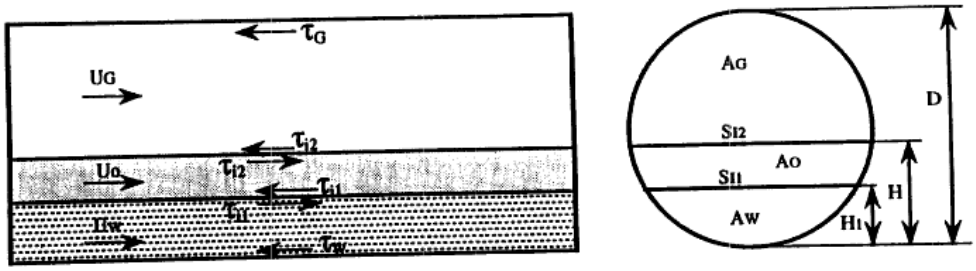

Figure 2-65: Oil-water-air three-phase stratified flow geometry (Neogi et al., 2009)

2.6.2.3 Unified Model from Zhang et al. (2005)

Zhang et al. proposed a unified model for oil-water-gas flow based on the similar concept (Zhang et al., 2003) he proposed for gas-liquid two phase flow. The equations of slug flow were used not only to calculate the slug characteristics, but also to predict transitions from slug flow pattern to other flow patterns. However, the effective physical properties needed to be used and closure relationships were implemented in his model (such as gas-liquid interfacial friction factor, liquid entrainment fraction in gas core, gas void fraction in oil and water in slug body, slug translational velocity and length). In addition, new closure relationships such as oil-water mixing or inversion were also proposed. The following flow patterns can be predicted using his model:

- Oil-water-air three phase stratified flow
- Oil-water two phase stratified flow
- Slug flow with fully mixed oil and water
- Annular flow with fully mixed oil and water
- Bubbly flow with fully mixed oil and water

It can be conclude from the review above, the pressure prediction methods are very limited to date. The most common way is using Lockhart Martinelli parameter and two fluid models with improved closure relationships. The reviewed methods can only be applied to limited cases of oil-water-air flow patterns observed during experiments. More work is required in establishing

the method to account for transition flow patterns, the slippage among different phases, wall wettability for oil and interfacial tension/dynamics.

Table 2-7 summarizes all the research studies on oil-water-air flows in this report:

Authors	Pipe ID (mm)	Pipe Orientation (degrees)	Oil Viscosity (cP)	Oil Density (kg/m3)	Range of velocities (m/s)
Acikgoz et al. (1992)	19	0	116.4	864	$0.15 < V_{sg} < 50$ $0.043 < V_{so} < 0.24$ $0.004 < V_{sw} < 0.66$
Stapelberg and Mewes (1994)	23.8-59	0	31	886	-
Taitel et al. (1995)	50	0	1, 100	800	-
Chen and Guo (1999)	39	0	132-179	861-871	$0.45 < V_{sg} < 19.02$ $0.014 < V_{so} < 0.91$ $0.018 < V_{sw} < 1.85$
Spedding et al. (2005)	25.9, 50.1	0	12.2, 39.5	828.5, 854.2	-
Keskin et al. (2007)	50.8	0	13.5	858	$0.1 < V_{sg} < 7$ $0.02 < V_{so} < 1.5$ $0.01 < V_{sw} < 1$
Bannwart et al. (2009)	28.4	0, 90	3400	970	$0.01 < V_{sg} < 2.5$ $0.02 < V_{so} < 1.5$ $0.04 < V_{sw} < 0.5$
Poesio et al. (2009)	21, 28, 40	0	900, 1200	886	$0.06 < V_{sg} < 4$ $0.03 < V_{so} < 0.7$ $0.1 < V_{sw} < 2.6$

Table 2-7: Summary of research studies on oil-water-air flows reviewed.

2.7 Three phase Liquid-Liquid-solid Flows

Due to the complexity of the mixture flow, only few published research papers were found in the literature regarding three phase liquid-liquid-solid flows in pipelines. What makes it more difficult is the presence of heavy viscous oil in the mixture.

In comparison with the high velocities required for effective sand transport in conventional slurry pipelining applications and the high pressure gradients required for sand transport with laminar Newtonian flows (i.e., heated oil and oil/diluents systems), it is known that the water-assisted flow regime has significant potential for improved sand transport. However, the flow regime itself is not very well understood. Terms such as “annular flow” and “core annular flow” tend to understate the complexity of the flow regime that occurs during water-assisted flow of heavy crude oils and bitumen in field pipelines. Better understanding is needed toward the water-assisted flow regime and an effective method for predicting sand transport rates for this regime. As work progresses in these two related areas, the risk factors will be reduced and heavy oil and bitumen producers will be in an increasingly better position to take advantage of the true potential of this emerging technology.

- Sand- High Viscous Liquid Flow in Pipeline

The only published investigation regarding to sand transport in a high viscous fluid was carried out by Gillies et al. (1994) in Saskatchewan Research Council (SRC). These were single phase tests with viscous oil with viscosity of 7500cP. In these tests, it was noticed that a bed never formed in the system as the solids were always transported when fluids were circulating. It was concluded that it was attributed to the excessively high shear in the flow.

Two-phase laminar flow model (Gillies et al., 1999) can be used to determine sand transport and accumulation conditions for heated oil pipelines, diluent pipelines, and cold production flows. It is known that high pipeline pressure

gradients are required for sand to be transported with laminar flow of Newtonian fluids.

- Sand- Water- High Viscous Liquid Flow in Pipeline

Other published studies were done on turbulent flow model, which has found extensive application in the design of pipelines that use water as the carrier fluid to transport solids. Examples include the oil sand industry's ore hydro-transport lines and tailings pipeline systems. Relatively high pipeline operating velocities are required to ensure that the turbulent mixing forces are strong enough to prevent sand from settling out during operation of horizontal slurry pipelines.

As reported by Zorgani, 2010, a recent research work was carried out in SRC to study the effect of sand addition in heavy oil-water flow and the sand transport condition. The sand addition test was conducted in a 100mm ID pipeline with sand of which has an average diameter of 310 micron. The sand concentrations tested were 6 and 12 % v/v.

It was found that, while adding 6% v/v sand into bitumen froth (total water fraction 33%), the pressure gradient changes were not obvious, while 30% increase in pressure gradients would be expected in slurry flow. Further experimental revealed that the sand addition actually would reduce the pressure gradient. They proposed a "scouring process" as the explanation for the reduction phenomena in pressure gradient, which saying that the sand tend to remove some of the bitumen coating on the pipe wall, thus increasing the pipe cross section area. However, this concept needs to be validated with great care since no sand transport characteristics were observed by any means. It would normally expect there is a maximum sand concentration when the pressure gradient starts to increase sharply due to the blockage. Also, further analysis is required to explore the link between this phenomenon and the CHOPS production method, which do increase the production of heavy oil by encouraging sand production.

In addition, the effect on the sand mobility by increasing water fraction was studied in both lube oil and bitumen forth. The coarse oil-in-water emulsion with sand particles were found and coarse oil drops were found coated in sand particles. In addition, there was still sand movement observed even at the highest water fraction examined (60%), particularly in the upper portion of the pipeline. For bitumen forth tests, sand mobility were found decreasing while the water fraction was increase from 28 to 41% v/v.

2.8 Conclusion

Many large development projects have been targeting heavy oil. The high viscosity of heavy oil poses great challenges for its production and transportation through pipelines.

Based on the literature reviewed above, it was found that the investigation of high viscosity oil (above 1000 cP) in multiphase flow is limited in resources and starving for more. Phenomena encountered in high viscosity oil multiphase flow behaviours are very different from low viscosity oils. The pressure gradient is very critical in pipeline design and energy reduction for transporting the heavy oil from the well head to the reservoir. Most of the previous studies were artificially preventing the oil from fouling to minimize the associated pressure with the flow; however this is inevitable in industrial scale.

Most of the available multiphase flow models were developed based on low viscosity oil experimental results. When compared with high viscosity oil data, the models displayed significant differences. Also, oil coating was not considered in modelling aspect for oil/water two phase flows.

Therefore, more work is needed to expand the knowledge in multiphase flow with high viscosity oil in pipelines.

3 Instrumentation and experimental methods

In response to the need for better understanding of multiphase (heavy oil, water, air, and sand) flow, a 1 inch multiphase test rig was designed, constructed, and commissioned in the Process Systems Engineering (PSE) laboratory, School of Engineering, Cranfield University. This study is the first project to use the facility, which was commissioned in March 2010.

3.1 One inch multiphase test facility

3.1.1 Facility specifications

The 1 inch multiphase test facility is designed to operate under single phase and multiphase flows, however the following combinations were used to fulfil the purpose of this study:

- Single phase heavy oil at different viscosities,
- Single phase water only,
- Two-phase heavy oil/air flow,
- Two-phase heavy oil/water flow,
- Three-phase heavy oil/water/air flow, and
- Three-phase water/heavy oil/sand flow.

The simplified P&ID diagram is shown in Figure 3-1, while a photo of the 1 inch multiphase rig is given in Figure 3-2

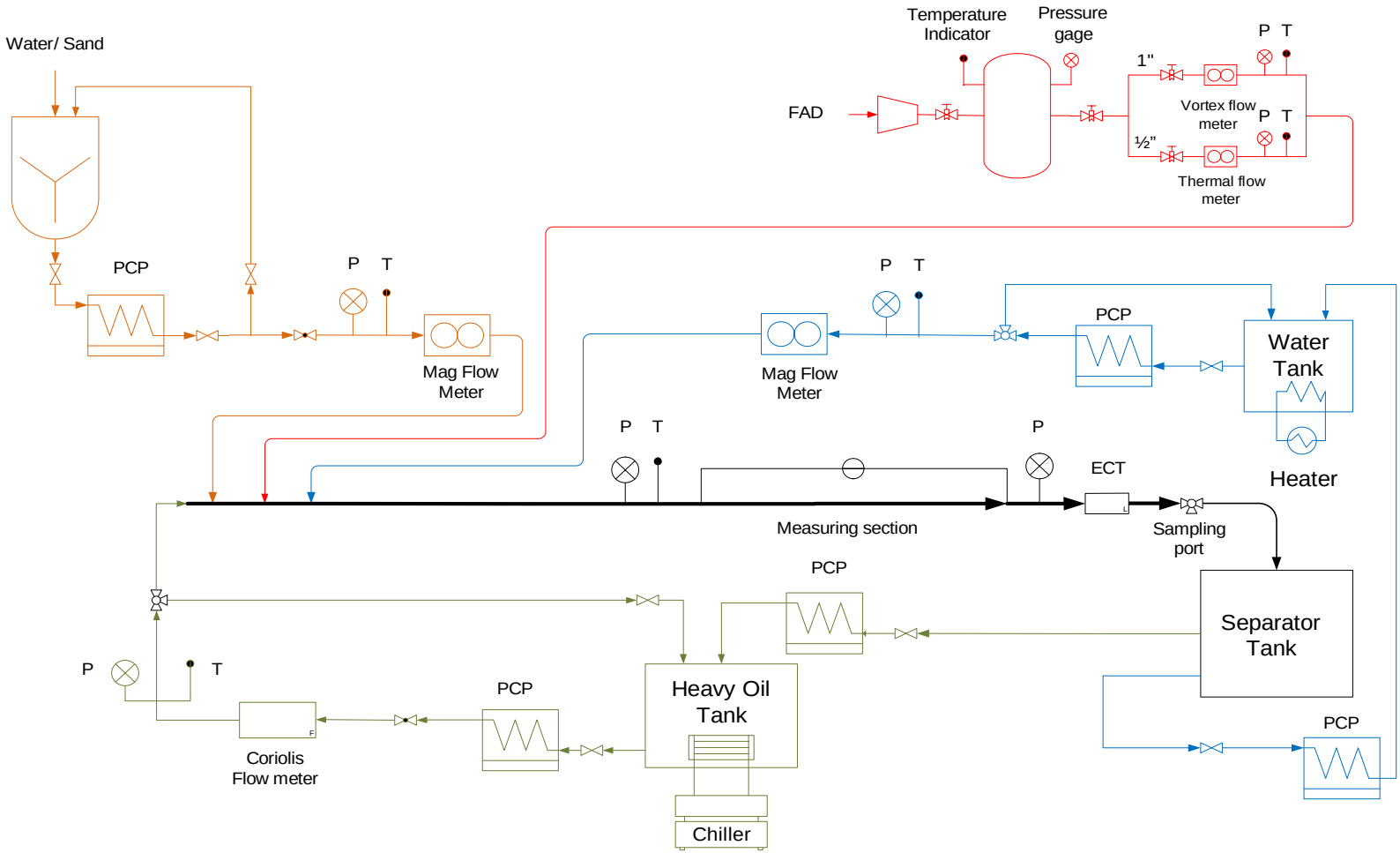

Figure 3-1: Simplified P&ID diagram of 1 inch multiphase test facility

Figure 3-2: The 1 inch multiphase test facility

3.1.1.1 Specification of the Facility

The test rig consists of a 5.5 m horizontal flow line with I.D. = 0.026 m and made from Perspex “clear acrylic”. Several insertion points are costumed to inject heavy oil, air, water, and slurry (Figure 3-3). Flow from the test rigs returns to the open top collecting tank and then back to water or heavy oil tanks. Thus the rigs are operated at near atmospheric pressure.

Figure 3-3: Horizontal Perspex pipe with insertion points

Both single and differential pressure transducers are used in Perspex pipe, positioned at 3 m and 5.17m from the insertion points, to measure the pressure gradient. The differential pressure transducer (GE Sensing PMP 4110 amplified output pressure transducer, pressure range -200 to +200 mbar and accuracy ±0.04 % full scale) is used with experiments associated with relatively small pressure drop (water, slurry, and gas flow). Two singles GE Sensing PMP 1400 industrial amplified pressure transducer, pressure range 6 bar gauge and accuracy ±0.15 % typical) are used to measure all the flows (including heavy oil flow).

Since the temperature affects the viscosity of the heavy oil, the temperatures of the fluids are constantly monitored in the transportation line and in the Perspex pipe. Temperatures are measured using J-type thermocouples with accuracy of ±0.1°C.

Air is supplied from the laboratory compressor. This compressor has a maximum supply capacity of 1275 m^3/hr free air delivery (FAD) and a maximum discharge pressure of 7 barg. A 2.5 m^3 air tank receiver is used to damp down the pressure fluctuation induced by the compressor. From the receiver, air pass through a bank of filters (coarse, medium and fine), a cooler where moisture in the air is stripped, before the flowmeters.

Air flow rate is measured by using two gas flowmeters in order to cover the range of application requires:

- Thermal mass flowmeter, Endress+Hauser t-mass 65F15 DN15 (0.5-inch), with a range of 0 to 2 m^3/hr @ 9 barg;
- Vortex flowmeter, Endress+Hauser Prowirl 72F25 DN 25 (1-inch), with a range of 3 to 100 m^3/hr @ 9 barg;

The gas flowmeters have 4-20 mA HART output that are connected to the data acquisition system.

Water is stored in a tank of 0.15 m^3 capacity. The water temperature is controlled by an external chiller system. The water is pumped by a progressive cavity pump (PCP) through a flexible pipe. The PCP pump has a maximum capacity of 2.18 m^3/hr with safety switch to stop the pump at the maximum discharge pressure of 10 barg. Water flow is metered using an electromagnetic meter, Promag 50P50, DN50, with a range of 0 m^3/hr to 2.18 m^3/hr. The 4-20 mA HART output is connected to the data acquisition system.

Sand and water are mixed in a cylindrical tank of 0.20 m^3 capacity (Figure 3-4). The slurry is mixed by a stirrer with a variable speed controller. The slurry is pumped by a progressive cavity pump (PCP) through flexible pipe. The PCP

pump has a maximum capacity of 2.18 m^3/hr with safety switch to stop the pump at a maximum discharge pressure of 10 barg. Water flow is metered using an electromagnetic meter, Promag 50P50, DN50, with a range of 0 m^3/hr to 2.18 m^3/hr. The 4-20 mA HART output is connected to the data acquisition system.

Figure 3-4: Sand-water mixer tank

Heavy oil is stored in a tank of 0.15 m^3 capacity. The heavy oil temperature is controlled by a chiller system to attain temperature ranges (5°C - 50°C); therefore achieving the desired viscosity range for the run. The Heavy oil is injected by flexible pipe to the test rig by the progressive cavity pump (PCP) through a 1-inch (ID = 25 mm). The PCP pump has a maximum capacity of 0.72 m^3/hr with safety switch to stop the pump at maximum discharge pressure of 10 barg. Heavy oil flow is metered using Coriolis flow meter, Promass 83I50, DN50, with a range of 0 m^3/hr to 0.72 m^3/hr. The 4-20 mA HART output is connected to the data acquisition system.

Bulk flow of heavy oil, water, and sand mixture are collected in a specially designed tank of 0.50 m^3 capacity (Figure 3-5). The separation of the bulk

components is achieved by gravity. The heavy oil is pumped back to heavy oil tank and the water is pumped back to water tank by individual progressive cavity pump (PCP). The PCP pumps have a maximum capacity of 0.72 m^3/hr & 2.18 m^3/hr for Heavy oil and water respectively. Both pumps have a maximum discharge pressure of 10 barg.

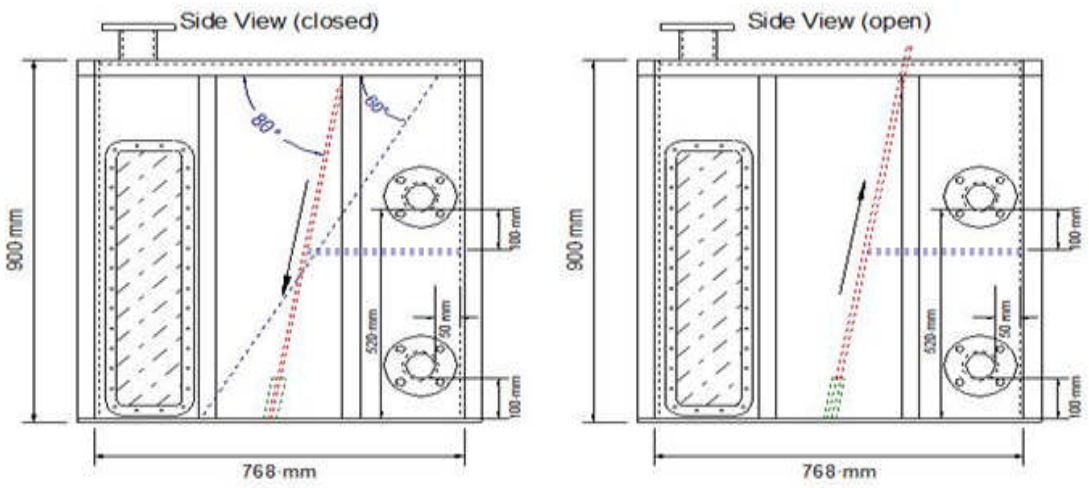

Figure 3-5: Separator tank drawings

Two types of Congleton HST 50 with an average particle size of 270µm and Congleton HST95 with an average particle size of 144µm were used. The bulk sand mass to be investigated cover solids loadings of 1-10% by volume. The sand feeder system consists of a cylinder with a cone shape end hopper of 0.20 m^3 capacity and a stirrer. The water/sand mixture is pumped to the main flow line by a variable speed PCP pump. The PCP pump has a maximum capacity of 2.18 m^3/hr and a maximum discharge pressure of 10 barg. The mixer is designed to maintain a stable flowrate for 5 minutes minimum.

The conditioned raw data from the instrumentations (including flowmeters, pressure transducers, differential pressure transducers and temperature sensors) are sampled and saved onto a PC data acquisition system using a Labview®, version 8.6.1, based system (Figure 3-6). This system consists of the following components:

- An NI USB-6210 connector board (National Instruments) interfaces the output signals from the instrumentations using BNC coaxial cables.
- A standard PC system (2.40 GHz Dell, VOSTRO1320, Intel ® Core ™ 2 Duo CPU P8600) with 300 GB hard disk and 4.00 GB of RAM.

Figure 3-6: PC data acquisition system with Labview

Data acquisition software is written in the graphical programming language Labview® 'Virtual Instrument', version 8.6.1. As each test run may generate a considerable amount of data, the software is designed to write data continuously to the computer hard disk. Sensor signals are converted into engineering units before on screen display and storage.

The technical specifications summary for the 1 inch multiphase Test Facility and equipment\instruments are listed in Table 3-1:

Equipment\Instruments	Description	
Flow rigs	Diameter Internal diameter Length of horizontal pipe	1” Perspex 26 mm 5.5m
Operating temperature and pressure	Pressure Temperature	near atmospheric 5°C - 50°C
Flow rates	2 PCP water pump PCP water/sand pump 2 PCP heavy oil pump Air compressor	2.18 m^3/hr @ 10 barg 2.18 m^3/hr @ 10 barg 0.72 m^3/hr @ 10 barg 1275 m^3/h FAD @ 7 barg
Flow meters	Heavy oil flowmeter 2 water flowmeters Air flowmeter	0 – 2.18 m^3/h 0 – 2.18 m^3/h 0 – 2 m^3/h 3 – 100 m^3/h
Sand Hopper Conical Mixer	624mm diameter x 1000mm high Motor: 4 pole, 400v, 3ph, 50 Hz, IP55. 0.75 kW. Drive: Gearbox maximum 300 rpm Shaft: 1002mm long, 40mm diameter. Impeller: SC3, 365 mm diameter Designed for viscosity: 1cps - 200cp specific gravity: 1 solids: sand, s.g. 2.65 particle size: 450µm solids concentration: 15% volume	

Table 3-1: 1 inch multiphase rig technical specifications

3.1.2 Chiller system

An Haake P1-C41P refrigerated circulator by Thermo Electron Corporation (Figure 3-7) was used to control the temperature of the test fluids (heavy oil and water) and reach the desired heavy oil viscosity for the proposed tests. The screen panel allowed setting the temperature with fine adjustment by circulating the refrigerant with a pump. It had a cooling capacity 1kW @ 20°C, 750W @ 0°C, temperature range between -40°C to +200°C, temperature accuracy of ±0.01°C, heater power of 2000W and pumping flow rate of 24 l/min.

Figure 3-7: The refrigerated circulator

The unit can be used to control the temperature of both fluids (heavy oil and water), however the heavy oil is more difficult to achieve a desired temperature due to its nature. Therefore, a specific operating procedure is used to homogenize the temperature distribution in heavy oil tank and achieve the required viscosity for a given test:

1. Connect the chiller with the oil tank as shown in Figure 3-8
2. Place the thermocouple (Pt100) in the oil tank
3. Top up the chiller with the coolant Liquid (Water glycol mix or silicone oil as recommended by manufacturer) when necessary.

4. Set the chiller controller to the desired temperature and turn the chiller on.

5. Close valve 2 and open valve 1 (mixing)

6. Start the oil pump

7. When the desired temperature is reached and the main system is ready to run, open Valve 2 then close valve 1

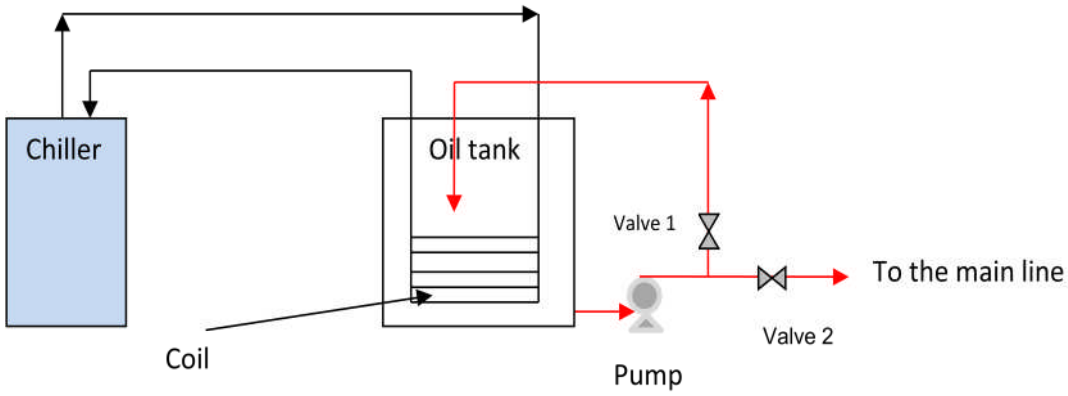

Figure 3-8: Connection between Oil tank and the chiller

The total liquid in the system is 168 litre for the refrigerated circulator unit (150 litre tank, 15 litre bath and 3 litre tubing). The Cooling (or heating) required to reach minimum and maximum operational temperature for the heavy oil from ambient condition was calculated to be nearly 6 hours. However the actual operational temperature was extended to 9 hours to account for heat losses from and to environment.

3.1.3 Electrical Capacitance Tomography (ECT)

Description of ECT equipment

Electrode arrangement and design of the ECT system used are provided and manufactured by Industrial Tomography Systems plc. (ITS), UK. A flexible copper-coated laminate (50 microns thick with 35 micron layer of copper) is etched with the required electrode pattern and then wrapped around the pipe.

The sensor for the 1” diameter pipe is shown in Figure 3-9. The electrodes dimensions as provided by the company are 42 mm in length and 4.38 mm in width. The spaces between the electrodes are 2 mm. The electrode coverage has been sized to cover the entire outer surface of the pipe (1” inner diameter).

Figure 3-9: The 1-inch pipe ECT-sensor

The electrode coverage has been sized to cover the entire outer surface of the pipe of outer diameter 32.15 mm. Axial copper strips separate the electrodes and are connected to the earthed areas at each end of the sensor.

The PCB laminate is wrapped around the non-conducting pipeline or column. Figure 3-10 shows a photograph of a PCB laminate and the size of the electrodes sheet.

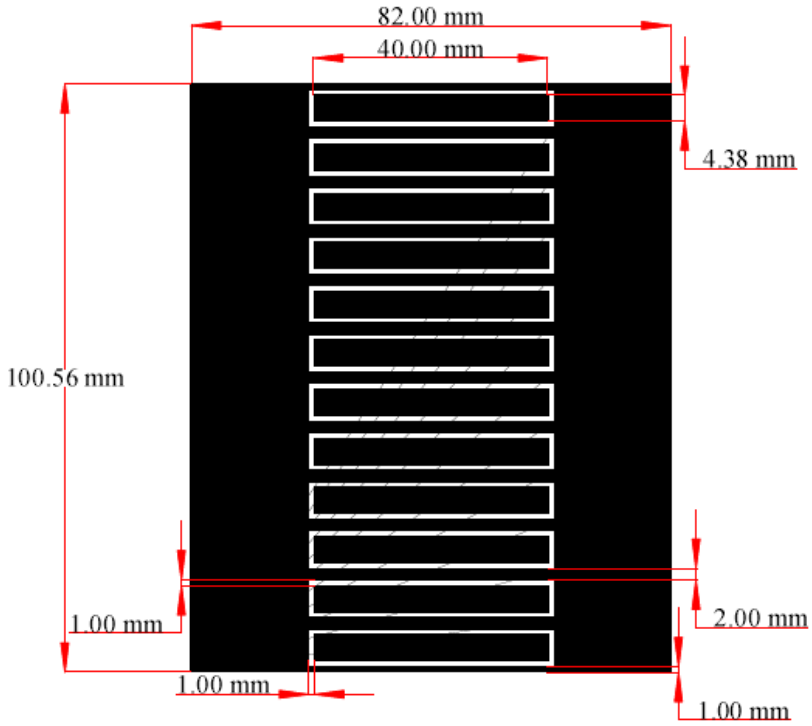

Figure 3-10: ECT-sensor and Electrode dimensions for the 1-inch pipe

The ECT system can be divided into three main components, as shown in Figure 3-11: (1) a sensing system, to measure the capacitances between sets of electrodes; (2) a data acquisition system, to collect and transfer the measured capacitance values; and (3) a computing system to collect the data, reconstruct the image, and display the results. The ECT system gives *ne* (*ne* - 1)/2 unique measurements, where *ne* is the number of electrodes. Thus 66 readings were obtained with a twelve electrode sensor used in this study.

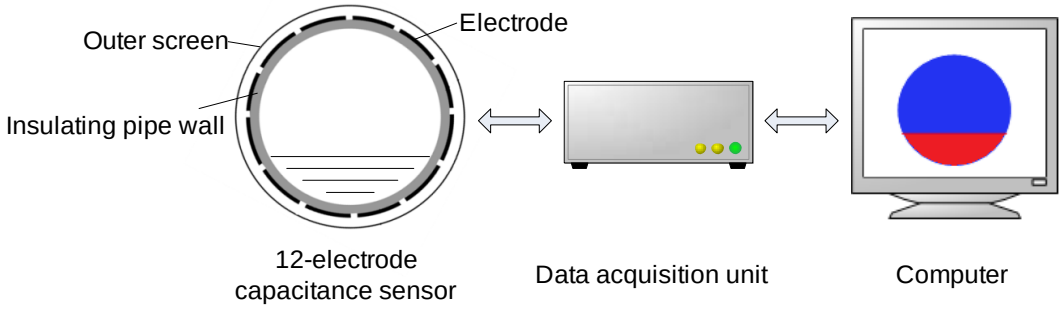

Figure 3-11: The main components of ECT system

Static Calibration for ECT sensor

The purpose of calibrating the ECT sensor was to establish the scale of display with the phase with low permittivity coded as blue and the second phase with high permittivity coded as red. The 1-inch “ECT-sensor” together with the 0.2 m length of Perspex pipe was calibrated based on the following procedures:

The 1-inch Perspex pipe and the ECT-sensor were completely cleaned by a cloth and dried by compressed air before any reference was taken. For gaseous phase, the reference was taken right after the cleaning process. However, for all other liquid phases, the pipe was filled with the desired liquid for calibration. Then sufficient time was allowed to lapse to ensure there were no small gas bubbles inside the liquid phase and all gas bubbles were purged out. Finally, the ECT system was turned into data “images” collecting mode and, as a result, different permittivity references were obtained. Depending on the desired test, each phase was associated with different references, Table 3-2 shows a quick summary for all systems acquired.

Table 3-2: ECT references for all systems

System	First reference (coded blue)	Second reference (coded red)
Air/Oil	Air	Oil
Oil / Water	Oil	Water

3.1.4 Sand extraction system (De-sander unit)

The processed sand in the separator was removed using 1″ TORE ® LANCE Hydraulic Shovel, provided by Merpro Limited (Figure 3-12). It works by feeding it with water via a flexible hose and the operating valve is adjusted to regulate distribution of the water to either the jet pump. The jet pump provides suction and motive force for transportation of the solids whilst the water exiting the

device generates a vortex to fluidise the solids and control the flow of slurry to the jet pump.

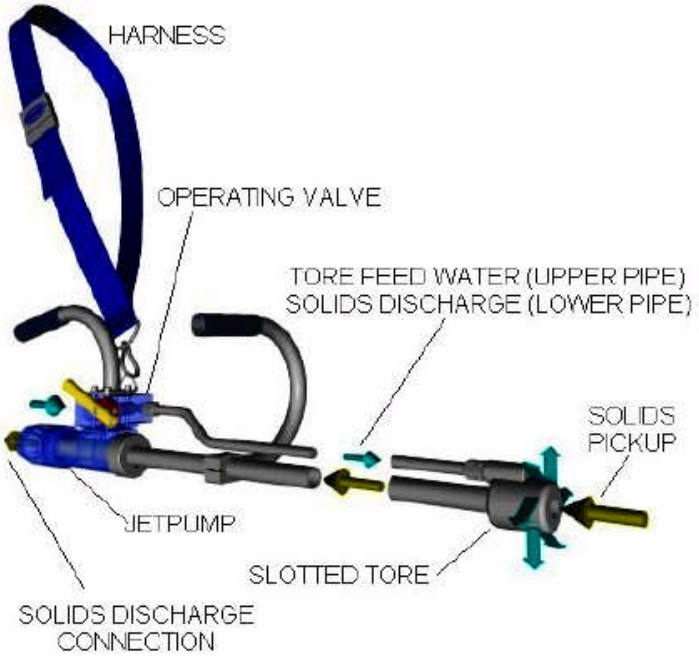

Figure 3-12: TORE ® LANCE Hydraulic Shovel

The de-sander was modified to extract the slurry and filter the water from the sand using a porous bag to re-utilize it again for further sand extraction (Figure 3-13). The pictures of detailed components are shown in Figure 3-14 and Figure 3-15.

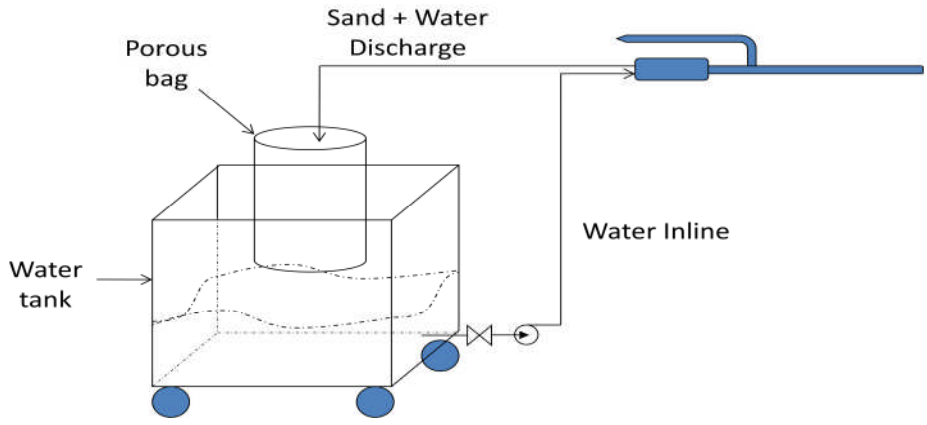

Figure 3-13: Modified de-sander structure

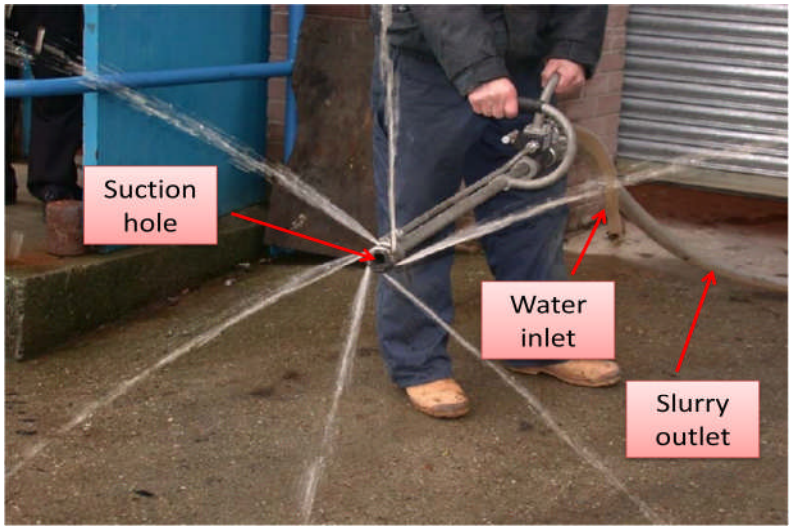

Figure 3-14: TORE ® LANCE in operation

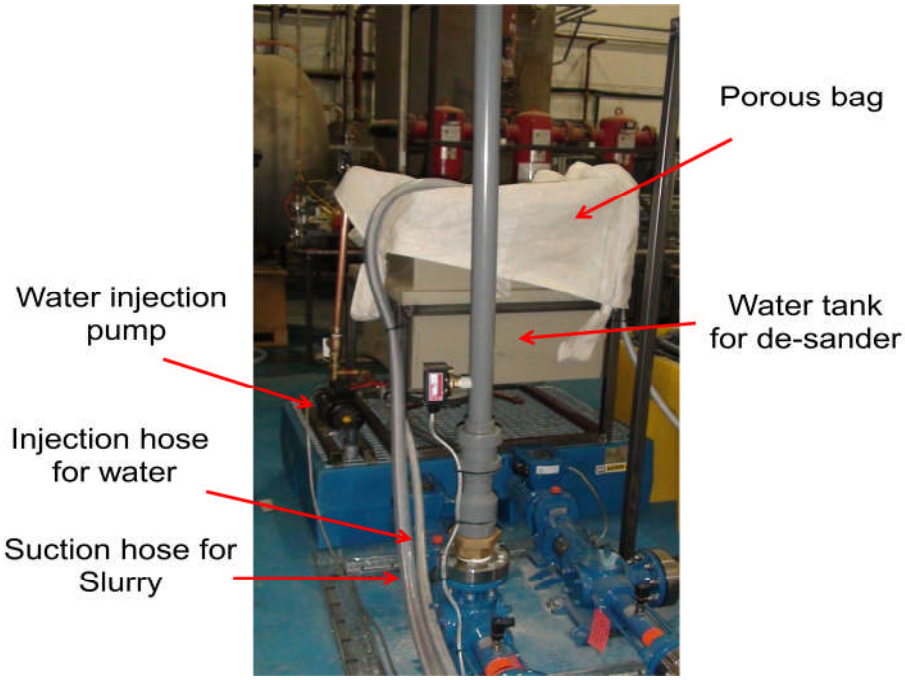

Figure 3-15: Detailed modification arrangement for the de-sander.

3.2 Bench instruments

3.2.1 Viscometer

The viscosity was measured using Brookfield Viscometer (LVDV-I Prime) with 0–100 rpm range and viscosity accuracy and repeatability of ± 1% and 0.2% of full scale (see Figure 3-16).

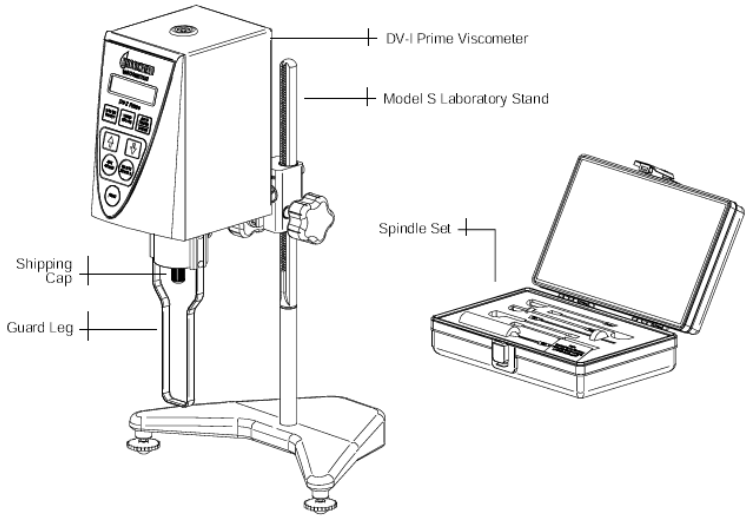

Figure 3-16: Brookfield Viscometer model diagram

The principle of this viscometer is to drive a spindle (which is immersed in the test fluid) through a calibrated spring. The viscous drag of the fluid against the spindle is measured by the spring deflection, which is measured with a rotary transducer. The measurement range (in centipoise) is determined by the rotational speed of the spindle, the size and shape of the spindle, the container the spindle is rotating in, and the full scale torque of the calibrated spring. The data can then be analyzed using the shear stress and shear rate relationship.

3.2.2 Sand sieve unit

The principle of sieving is to pass sand sample through a set of sieves of known mesh sizes (Figure 3-17). The sieves were arranged in descending mesh diameters. The sieves were mechanically vibrated for a fixed period of time (Figure 3-18). Finally the desired sand size was obtained for the experiment.

However, this cannot eliminate the possibility of having different grains size on other range due the different crystallised shapes of the sand. Also the time to sieve the entire sample to the next level can be indefinite due to the bouncing mechanism of the sand particles as being filtered.

Figure 3-17: Sand sieving apparatus

Figure 3-18: Mechanical vibrator.

3.3 Physical properties of heavy oil, water, sand, and air

The three fluids and one solid are used in the 1 inch multiphase facility, namely tap water, Total CYL1000 Straight mineral oil, air, and sand. Though a summary

of the physical properties at atmospheric pressure are listed in Table 3-3, detailed description of the heavy oil and sand are given below

	ρ (kg/m^3)	μ (cP)	Surface tension (N/m)	Flash point (°C)	Pour point (°C)
Air	1.2 (std. cond.)	1.84 (25°C)	—	—	—
CYL1000	931 (15°C)	3800 (25°C)	0.030 (25°C)	310	-9
Tap water	998 (25°C)	1.002 (20°C)	0.072 (20°C)	—	—
Sand	2650	—	—	—	—

Table 3-3: The physical properties of the 1-inch multiphase fluids and solid.

- CYL1000

The temperature effect on Total CYL1000 viscosity was examined from 2 °C; 5 °C up to 50 °C with an increment of 5 °C using Brookfield Viscometer (LVDV-I Prime). The resulted graph is shown in Figure 3-19.

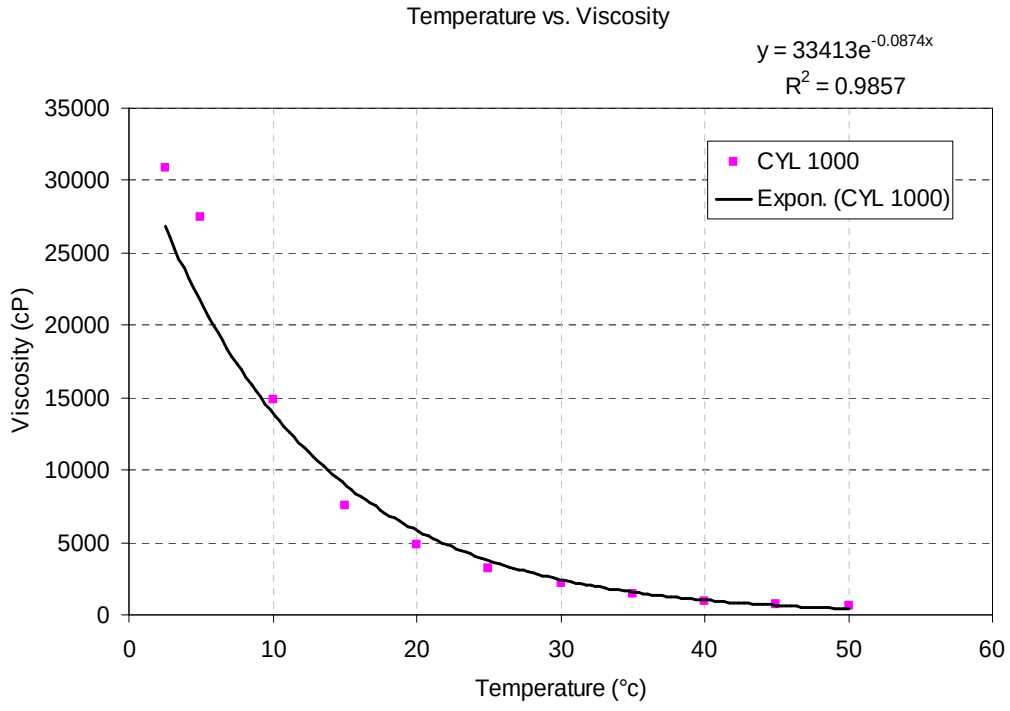

Figure 3-19: Temperature effect on the viscosity

Viscosity is related to the inverse of temperature. Hence, as the temperature of the oil increases, the viscosity decreases. The range of viscosities to be studied in the 1 inch multiphase rig can be achieved using this type of straight mineral oil, thus the temperatures required to achieve 3800cP and 10000 cP are around 25 °C, and 14 °C respectively.

Furthermore, the density of the oil was measured using the Coriolis flowmeter with wide viscosity variations due to the change of temperature.

T_o (°C)	ρ_o (kg/m^3)	μ_o (cP)	ν_o (m^2/s)
25.7	918.8	3572	3.887
22.9	920.5	4557	4.950
16.4	930.1	8022	8.625
13.7	935.0	10146	10.851
10.6	936.8	13286	14.204
8.8	938.4	15539	16.559

Table 3-4: Oil density and viscosity measurements in this work.

- Sand properties

Sand sieve was used to determine the particle size distribution for the sand used in this study (Figure 3-20). The average diameter provided by the manufacturer is approximately 150 microns (HST 95, from WBB Mineral) with a mixture density of 2650 kg/m^3. However the actual measured d_{50}, which is average particle size representing 50% volume or weight fraction, was approximately 144 microns. Samples of different sand grains after being sieved are listed in Figure 3-21.

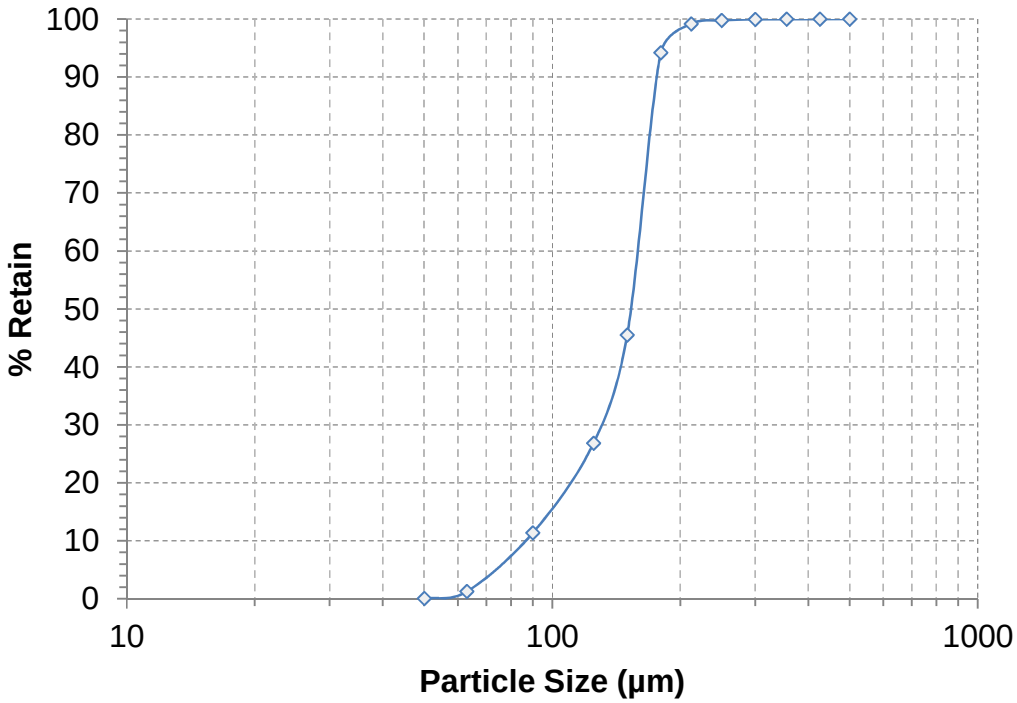

Figure 3-20: Sand size distribution as measure at PASE lab.

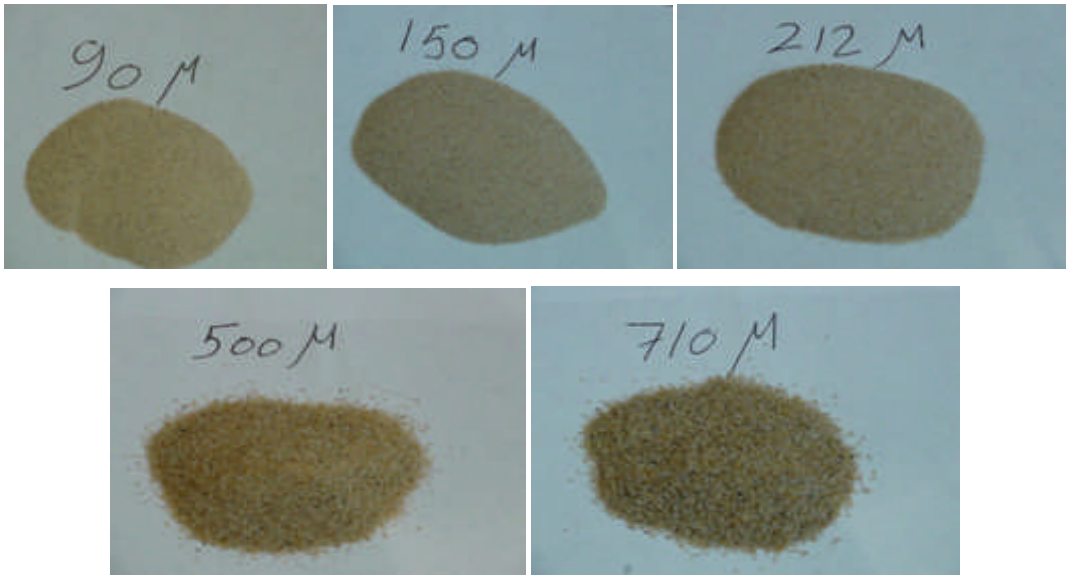

Figure 3-21: samples of different sand grains

3.4 Tests methodologies

Before the start of any test, the horizontal Perspex flow section was cleaned by flushing the system with oil, water, or air (depending on the upcoming test). The separator was also drained from any remains left due to previous experiments after giving enough time to allow the phases to separate from each other, usually around 6 hours. Depending on the type of test, the air was purged out to the atmosphere, water was dumped to external tanks for recycling and fresh tap water was added to the water tank, sand was extracted using the de-sander unit, and oil was recycled back to the oil tank. This was done to allow enough time for the oil/water to reach the desired temperature for a given test using chiller system as mentioned previously.

- Oil-air test procedure

    1. Check whether the desired oil viscosity was achieved using the Coriolis flow meter readings.
    2. Start to inject the system with oil at low flow rate. The Perspex pipe is checked to be fully occupied by single phase oil only before going to the next step.
    3. The desired oil flow rate is adjusted by controlling the speed of the PCP pump and the bypass valve until the required V_{so} is achieved.
    4. Gas is then injected to the system using the gas diaphragm valve. After reaching the desired gas flow rate, the system is given enough time to stabilize the flow.
    5. Raw data is collected for 60 seconds.

- Oil-water test procedure

    1. Check the desired oil viscosity was achieved using the Coriolis flow meter readings.

2. Start to inject the system with oil at low flow rate. The Perspex pipe is checked to be fully occupied by single phase oil only before going to the next step.
3. The desired oil flow rate is adjusted by controlling the speed of the PCP pump and the bypass valve until the required V_{so} is achieved.
4. Water is then injected to the system by opening the water control valve. Bypass valve was used to reach low water flow rate.
5. Adjust the water flowrate using diaphragm valve until the desired V_{sw} is reached. The system is given enough time to stabilize the flow.
6. Raw data is collected for 60 seconds.

- Oil-water-air test procedure

1. Check the desired oil viscosity was achieved using the Coriolis flow meter readings.
2. Start to inject the system with oil at low flow rate. The Perspex pipe is checked to be fully occupied by single phase oil only before going to the next step.
3. The desired oil flow rate is adjusted by controlling the speed of the PCP pump and the bypass valve until the required V_{so} is achieved.
4. Water is then injected to the system by opening the water control valve. Bypass valve was used to reach low water flow rate.
5. Adjust the water flowrate using diaphragm valve until the desired V_{sw} is reached. The system is given enough time to stabilize the flow.
6. Gas is then injected to the system using the gas diaphragm valve. After reaching the desired gas flow rate, the system is given enough time to stabilize the flow.
7. Raw data is collected for 60 seconds.

- Oil-water-sand test procedure

1. Prepare the required concentration of sand using a clean bucket to be loaded into the hopper (sand/water mixing tank).

2. Stir the sand with water in the hopper for at least 5 minutes while operating the bypass to ensure proper (homogeneous) mixing is achieved.
3. Check the desired oil viscosity was achieved using the Coriolis flow meter readings.
4. Start to inject the system with oil at low flow rate. The Perspex pipe is checked to be fully occupied by single phase oil only before going to the next step.
5. The desired oil flow rate is adjusted by controlling the speed of the PCP pump and the bypass valve until the required V_{so} is achieved.
6. Slurry mixture is then introduced to the system by opening the slurry control valve at high slurry flow rate using bypass valve to ensure no sand settling in the pipe during the experiment.
7. Adjust the water flowrate using diaphragm valve until the desired V_{ss} is reached. The system is given enough time to stabilize the flow.
8. Raw data is collected for 60 seconds.

4 Experimental results

In this chapter, the data obtained from the 1 inch heavy oil facility are presented in two sections:

- Different flow patterns for two phase flows, heavy oil- gas and heavy oil-water.
- Pressure gradients for single phase flows (oil and water), two phase flows (heavy oil- gas and heavy oil-water), and three phase flow (heavy oil-water-air and heavy oil-water-sand).

All collected data are given in details and presented in Appendix A.

4.1 Flow patterns

The flow patterns were defined based on analyzing the images obtained with digital HD video camera recorders (SONY HANDYCAM HDR-CX550VE) and ECT system that shows the cross-sectional distribution of the pipe (information of the ECT system was described in chapter 3.1.3).

4.1.1 Heavy oil - gas

Experimental data were acquired for a test matrix consisting 42 flow points by varying superficial fluid velocities and for two viscosities. These tests covered the range of 0.50-10.0 m/s and 0.025-0.30 m/s gas and heavy oil superficial velocities respectively.

- $V_{so} \in \{0.025, 0.035, 0.06, 0.10, 0.20, 0.30\}$ at different viscosities.
- $V_{sg} \in \{0.5, 0.7, 1.0, 1.5, 2.0, 3.0, 5.0, 7.0, 10\}$ at ambient conditions.

Test phases were air (density 1.2 kg/m^3, viscosity 0.0184 cP) and heavy oil with properties of densities ranging from 919 to 933 kg/m^3 and averaged viscosities of 4326cP and 10605 cP respectively. Despite having an oil film coating the pipe wall throughout, the observed flow regimes had similar characteristics to

liquid/gas flow in general. On these bases, the flow pattern map was classified according to Wong and Yau (1997), as shown in Figure 4-1. The solid lines drawn in the diagram are for visualization purposes only.

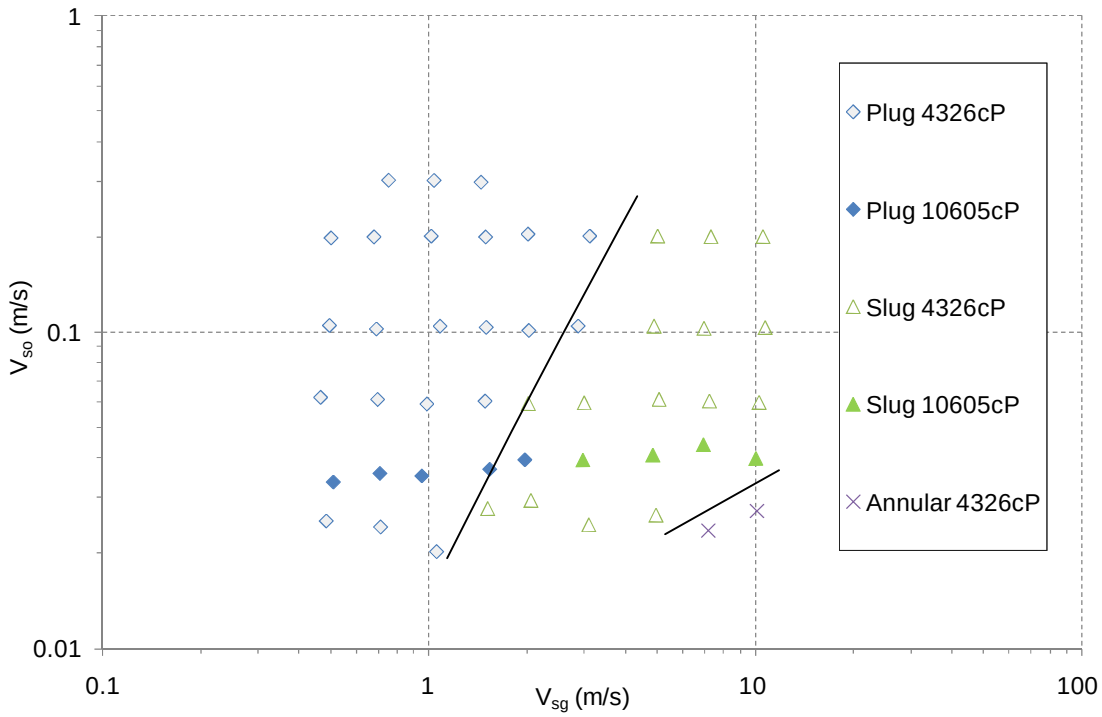

Figure 4-1: Observed flow pattern map for heavy oil and air system for two heavy oil viscosities.

With the exception of the couple of points at very low V_{so} and relatively high V_{sg}, varying the viscosity of the oil showed no significant effect on the flow pattern for the test range concentrate upon the intermittent region and the transition boundaries. Due to the different nature of the tested liquid in this study, it has been thought that a detailed description of the flow would be helpful for potential future analysis of these data.

- Plug flow

The air pocket for lower oil viscosity passes slowly in the system, allowing more time for the coated film on the pipe wall to drop back to the plug tail in the lower section of the pipe. However, thicker oil coating was found when

heavy oil superficial velocity, V_{so}, increased. Entrained air bubbles were observed in the oil coating (Figure 4-2a) and this was thought to be resulted by the entrained gas phase in the plug body. Nevertheless, this was not observed for high oil viscosity as the oil coating film was much thicker and no air bubbles were observed in the pipe (Figure 4-2b), this is expected since increasing the viscous forces over the capillary forces contributes toward lowering the porosity at the interface between the flowing fluids, which minimizes the entrained gas bubbles into the plug body. It was noted that the air pocket for this condition was smaller and more frequent when compared to relatively lower oil viscosity. This finding is in agreement with Gockal et al. (2006) as he found that the frequency of elongated bubbles increased with increasing viscosity while the bubble length decreased, also Al-Safran et al.(2011) showed through a model that due to large film thickness in front of the slug/plug, small velocity profile, and centreline velocity at the back of the slug body, a shorter mixing zone and reattachment distance are developed; as this will shorten the required slug/plug length to achieve a fully developed velocity profile resulting in a short minimum stable air pockets.

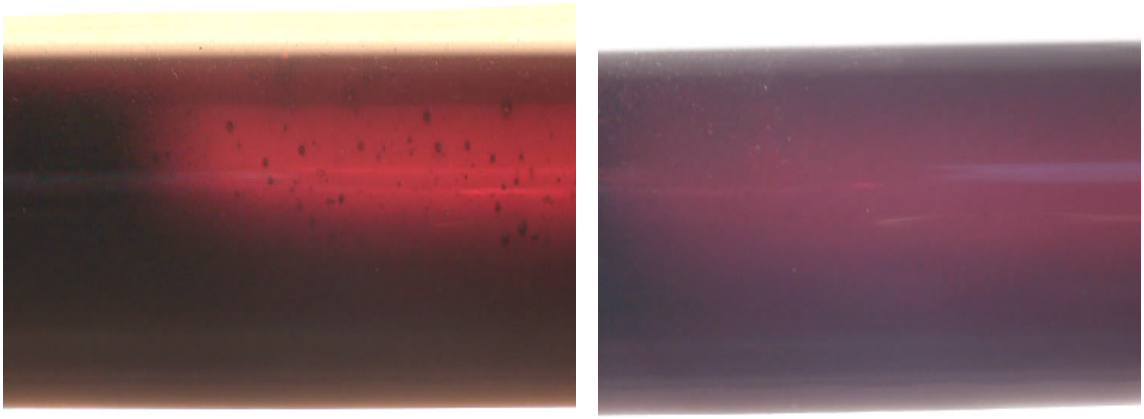

(a) 4326 cP

(b) 10605 cP

Figure 4-2: Plug flow for heavy oil and air system at different viscosities.

By increasing the superficial gas velocity, V_{sg}, the plug body travels much faster in the pipe with high impact force at the pipe outlet leading to

- Slug flow

A possible definition of a slug is a liquid mass travelling in a pipe being driven by the difference in the dynamic pressure (the driving force) between the gas in the front and back. Similar to plug flow, the increase of V_{so} led to thicker oil coating, as shown in Figure 4-3, also the entrained air bubbles were observed to be attached to the pipe wall for V_{sg} around 3 m/s.

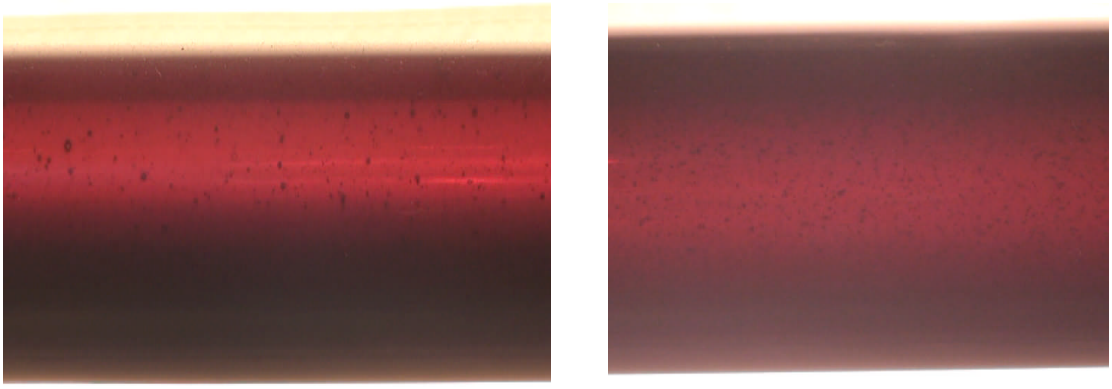

(a) Thin oil coating

(b) Thick oil coating

Figure 4-3: Slug flow for heavy oil and air system at 4326 cP heavy oil viscosity.

However when V_{sg} was further increased, the generated dynamic pressure from the gas pocket in the slug tail becomes very strong that it started to destroy the smooth oil coating into stationary ripples (Figure 4-4). This phenomenon occurred as a transition phase between slug flow and

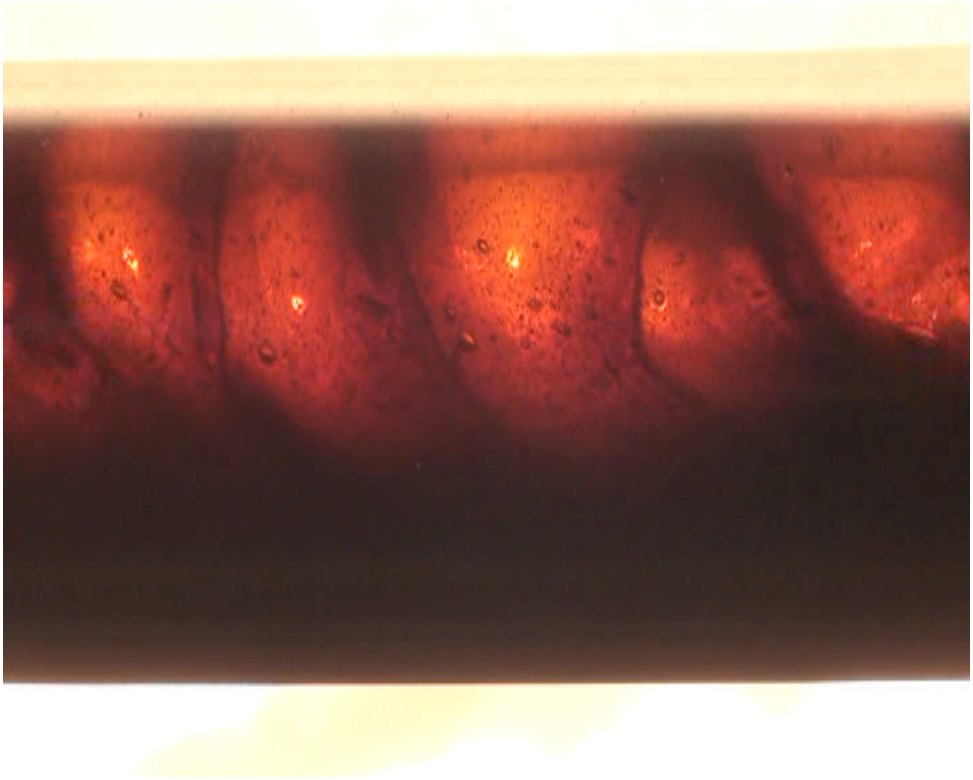

Figure 4-4: Slug flow for heavy oil and air system at 4326 cP heavy oil viscosity.

- Annular flow

The conventional description for this flow is when gas flow is high enough to support the liquid film around the pipe walls. However for this study, since the oil coating is sustained across all examined flows, annular flow occurs when gas flow rate is high enough to penetrate continuously through heavy oil phase. Figure 4-5 shows the irregular shape of the generated dynamic ripples due to very high gas flow rate, it is also noted that heavy oil film is thicker in the bottom of the pipe because of the effect of gravity.

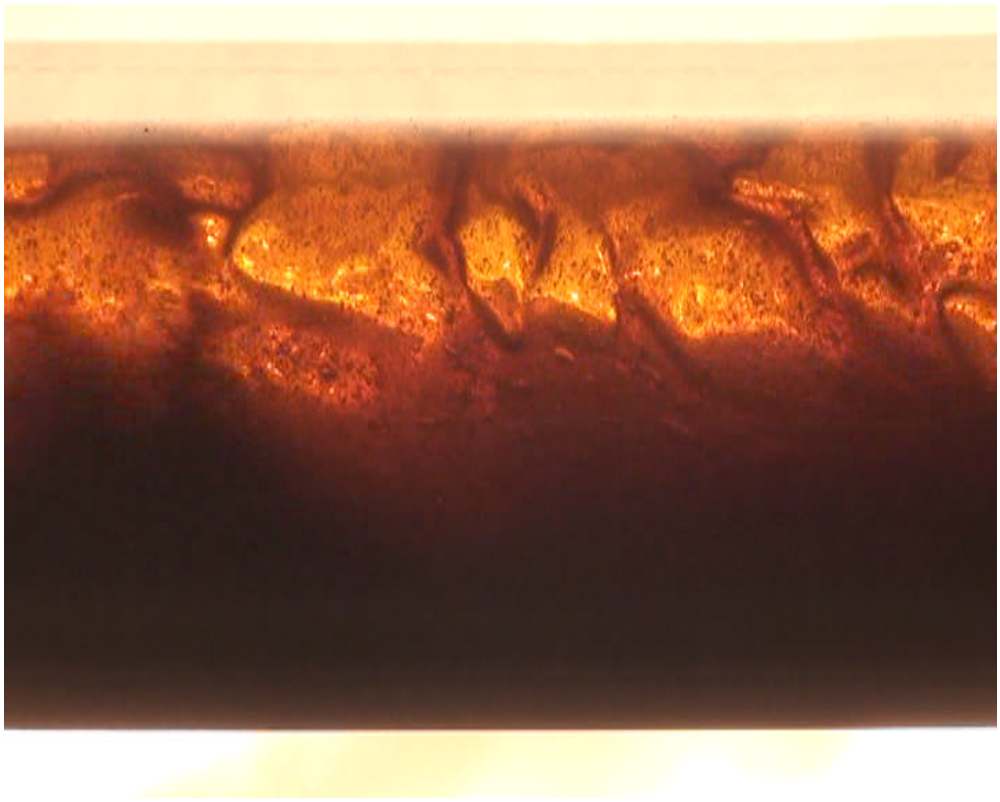

Figure 4-5: Annular flow for heavy oil and air system.

The experimental flow pattern observations were compared with Beggs and Brill (1973) flow map model. Figure 4-6 shows the transition boundaries did not match with experimental observations. The intermittent flow prediction region seems to account only for plug flows, while slug flow found in the present experiments scattered in 3 different regimes. This was expected as Beggs and Brill (1973) model was based on water/gas experiments in 1 & 1.5 inch pipe diameters and inclination effect. New models should be developed to predict flow patterns more accurately for high viscosity oils.

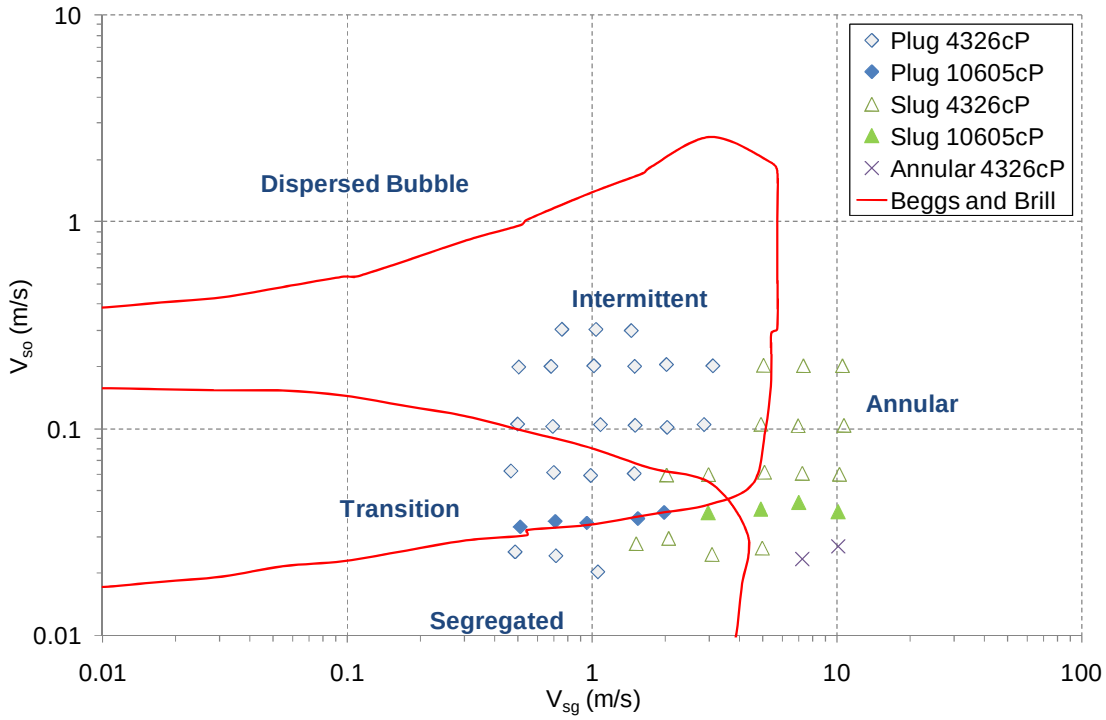

Figure 4-6: Beggs and Brill flow pattern map comparison

An effort was made to use the ECT technology towards distinguishing the different phases across the pipe dynamically. The attempt was not fully successful due to the low sampling rate of the acquired system, as the motion of the intermittent flow had a high slug/plug frequency, ECT system showed high potential in giving qualitative information about the flow patterns and phase distribution in the pipe (Appendix B).

4.1.2 Heavy oil - water

Three main flow patterns were initially categorized using conventional definition (oil continuous, water continuous, and transition phase). However unlike the classifications found in the literature for oil/water flow patterns (Trallero, 1995; Bannwart et al., 2004; Vuong et al., 2009), the flow patterns of heavy oil/water in this research were found to be different and five new classifications (Figure 4-7) were proposed based on the visual outputs, and driven from the main three flow patterns; Oil film coating on the wall were observed for all flow patterns.

The summary description of each abbreviation for the observed flow patterns are listed in Table 4-1, while Figure 4-8 and Figure 4-9 show the typical images and corresponding schematic drawings of these flow patterns.

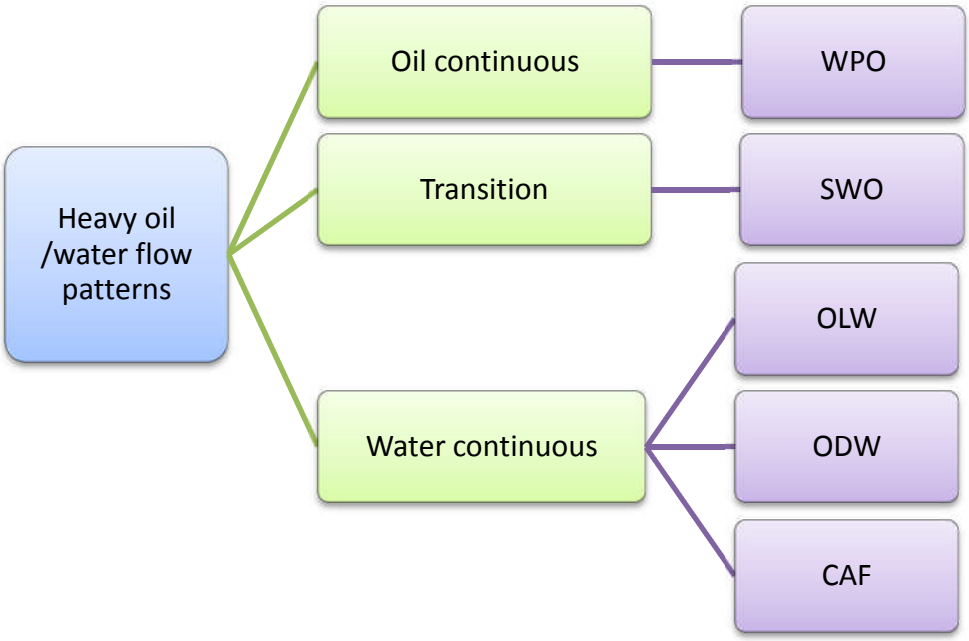

Figure 4-7: Classification of observed heavy oil/water phase flow patterns

Abbreviation	Description
WPO	Water Plugs in Oil continuous phase.
SWO	Spiral motion of Water & Oil.
OLW	Oil Lumps in Water continuous phase.
ODW	Oil Dispersion in Water continuous phase.
CAF	Core Annular Flow.

Table 4-1: Two phase abbreviations used for heavy oil/water flow

Water Plugs in Oil continuous phase (WPO) were obtained at low heavy oil and water flow rates, the heavy oil phase was observed to be dominant with periodic short plugs/slugs of water travelling through the pipe. These plugs would get longer as a result of increasing the water flow rate**.** Though not visually observed by McKibben et al. (2000a), this flow pattern was

hypothesized by the authors as envelop slug flow using voltage records from a rotatable L-shaped hot-film anemometer probe.

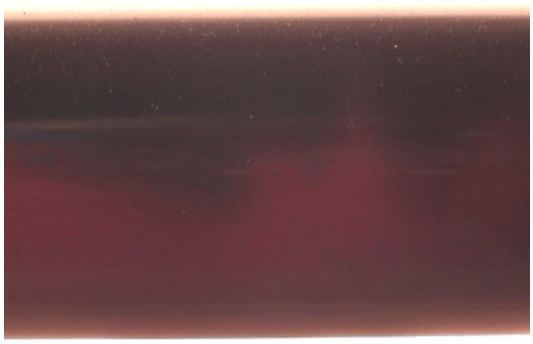

WPO

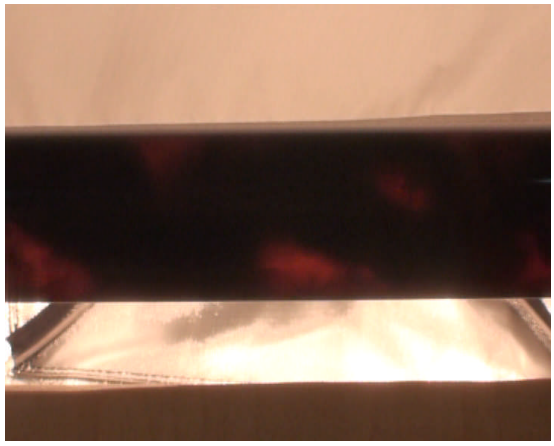

SWO

OLW

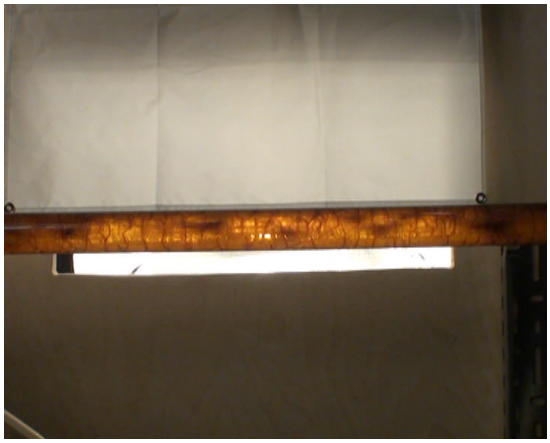

ODW

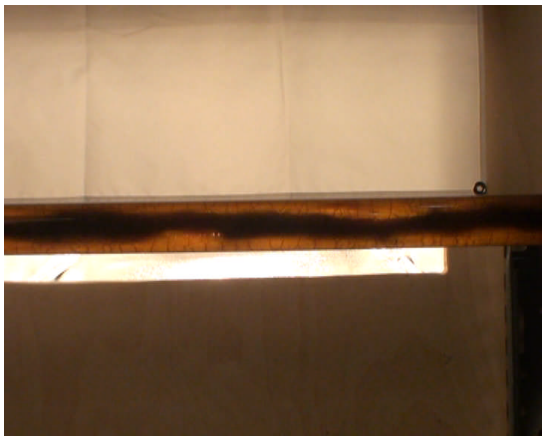

CAF

Figure 4-8: Typical base flow patterns recorded in the horizontal pipe

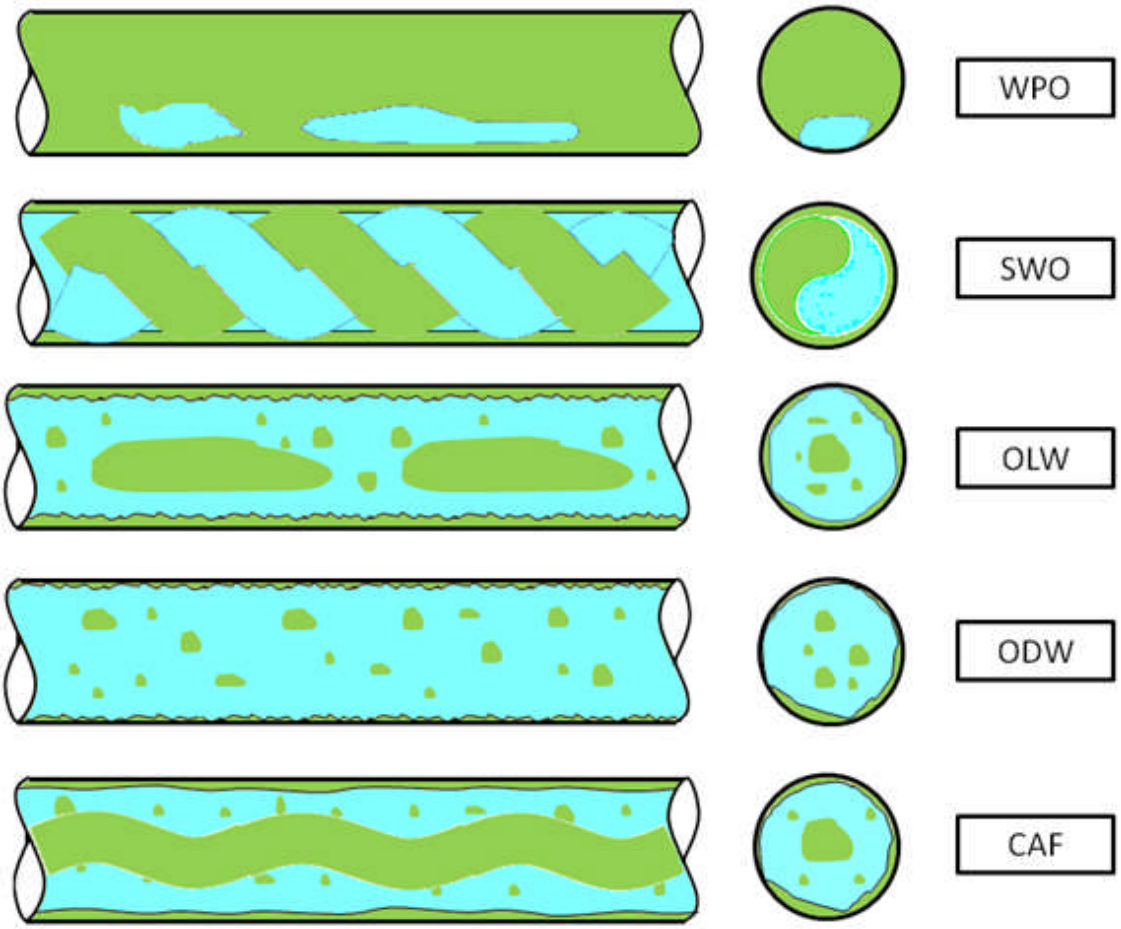

Figure 4-9: Schematic drawings of the mineral engine oil and water flow patterns

By further increasing the water flow rate, though not clearly observed through the fluids due to the dark colour of the heavy oil and the thick coating of oil on the inner pipe wall, the individual water plug starts to connect and move in swirling motion forcing the heavy oil flow to swirl as well in the pipe, forming **Spiral motion of Water & Oil (SWO).** At this stage, it is believed that the transition of flow continuous pattern is occurring from oil to water, and by Arirachakaran et al. (1989) explanation of phase inversion, this can be referred to as transition/ (unconventional) inversion phase. By further increasing the

water flow rate, the agitated motion of the swirl starts to break the continuity of oil into individual lumps in water continuous phase.

Oil Lumps in Water (OLW) is characterized by packages of coalesced oil chunks in water phase, and could also be considered as an intermittent flow pattern with oil coating. However due to the high water flow rate associated with this flow pattern, the oil started to tear off leaving thinner coating in the pipe wall surface. Also ripple motions were observed on the oil film coating, it is suspected that interfacial tension, slip ratio between the water and oil film, and oil viscosity were contributing into this motion. As sufficient velocity difference across the interface between the water flow and oil coating existed in this flow.

Further increase of the water flow rate breaks up the coalescent oil chunks into smaller drops, scattered in water continuous phase with thinner oil film on the pipe wall, generating **Oil Dispersion in Water (ODW)**.

However, if oil flow rate was increased at the transition phase (SWO), **Core Annular Flow (CAF)** will occur instead. The flow was described as wavy continuous heavy oil travelling in the core and surrounded by water (lighter viscous liquid) in the annulus with oil coating on the pipe wall. The oil thickness in the core was found to be determined by the water flow rate, where increasing the water flow resulted into thinner oil in the core for the same oil flow rate. The wavy core motion and core eccentricity were formed by the effect of density difference between the two liquids and stabilizing hydro-dynamic forces (Ooms et al., 1984; Oliemans and Ooms, 1986; Brauner, 2002). Also Kelvin-Helmholtz instability should be considered as there was sufficient velocity difference across the interface between the water flow and oil flow in the core.

Although this flow pattern has similar description to the CAF found in the literature; the uniqueness of this pattern observed in the present work is having oil coating on the inner-pipe wall associated with this type of flow. This proves that retention of water film at the pipe wall is not essential to obtain CAF flow

pattern in a pipe, and the condition of the pipe wall to attract or repel oil to its surface (oleophilic or oleophobic) may not be significant to achieve CAF.

The superficial velocities associated with the described patterns above are shown in the flow pattern map of Figure 4-10. The solid lines drawn in the diagram are for visualization purposes only.

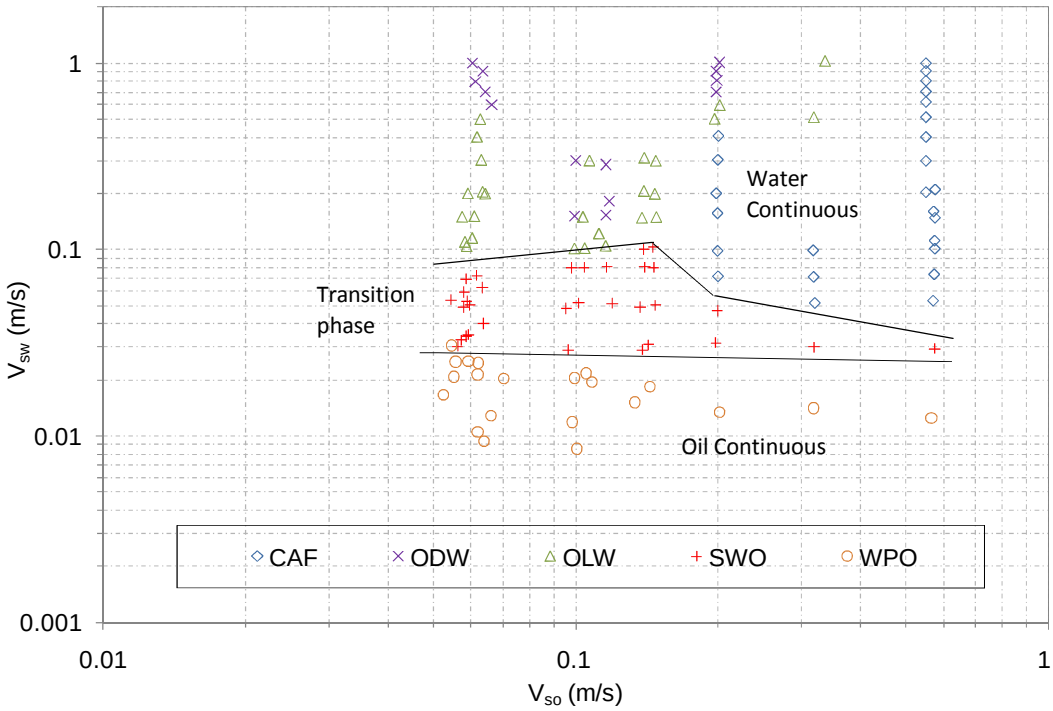

Figure 4-10: Flow regime map for 2-phase (heavy viscous oil/water) flow

The oil viscosity was between 3767 cP and 17070 cP for most of the data points (high superficial oil velocities with higher viscosities could not be achieved due to the high pressure drop associated). Despite the fact that oil coating (fouling) was more difficult to be sheared by the water phase at higher V_{sw}, for very viscous oil conditions (above 10000cP), the variation of viscosity had no significant effect on the observed flow patterns.

Finally, the injected water temperature was varied and controlled to study its influence on the generated flow pattern, a simple comparison between two cases ($T_o \approx T_w$ and $T_o < T_w$) is shown in Figure 4-11. While both cases had

heavy oil temperatures around 8°C, the water temperatures were altered with temperatures difference around 1°C and 11°C respectively, the flow patterns observed remained the same for both cases.

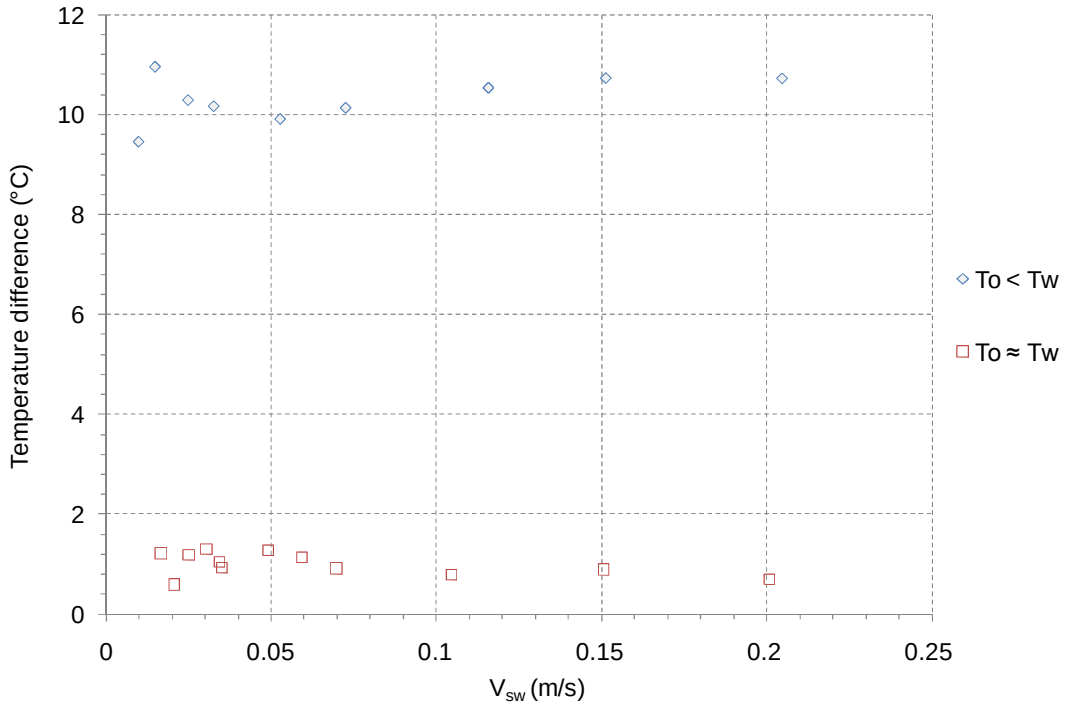

Figure 4-11: Two different temperature variations tests for different superficial water velocity at V_{so} = 0.10 m/s

The ECT technology was used to distinguish the different phases across the pipe dynamically for heavy oil/water flow. The system did not perform as well when compared to heavy oil/air flow as water presence distorted the sensitivity matrix which is needed to reconstruct the output image (Appendix B).

4.2 Pressure gradient

The pressure gradients were calculated based on measuring the difference of two single pressure transducers for heavy oil single phase, two phase, and three phase related flows, while differential pressure transducers were used for water associated phase flow. It should be noted that differential pressure transducers could not be used with flows associated with heavy viscous oil due

to the high pressure drop exerted in the pipe as it is out of range of the instrument capabilities. Although controlling the flow rates of each fluid was difficult, due to the systems back pressure and pressure driven by pumps for liquid flows (PCPs), most problems were solved by controlling the pressures of injected fluids through choking mechanism of both injection and bypass valves.

4.2.1 Single phase results (liquids)

For water, the pressure gradient was obtained for many liquid velocities ranging from 0.2 m/s to 1.2 m/s and examined against 4 different correlations (Colebroke "Darcy", 1939; Swamee and Jain, 1976; Haaland, 1983; and Chen, 1979) as shown in Figure 4-12. The results from the comparison showed a good agreement with the measured values. Therefore, the same correlations were chosen to substitute the measured data sets for further investigations. The liquid used was tap water with a density around 998 kg/m^3 and a viscosity of 1.005 cP at ambient conditions.

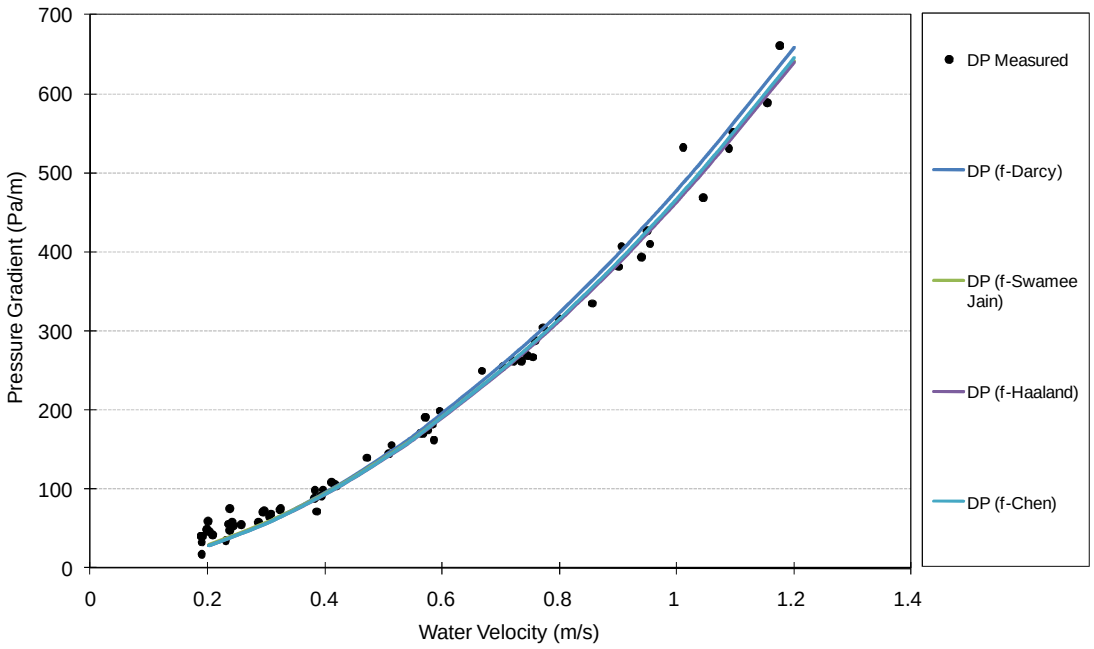

Figure 4-12: Pressure gradient comparison between experimental results and different correlations for water

As for the heavy oil single phase measurements, the pressure gradients were obtained for different liquid velocities and viscosities, ranging from 0.04 m/s to 0.58 m/s for V_o and 3150 cP to 12583 cP for μ_o. Figure 4-13 shows the comparison calculated pressure gradient for laminar flow as the Reynolds number was always less than 1300.

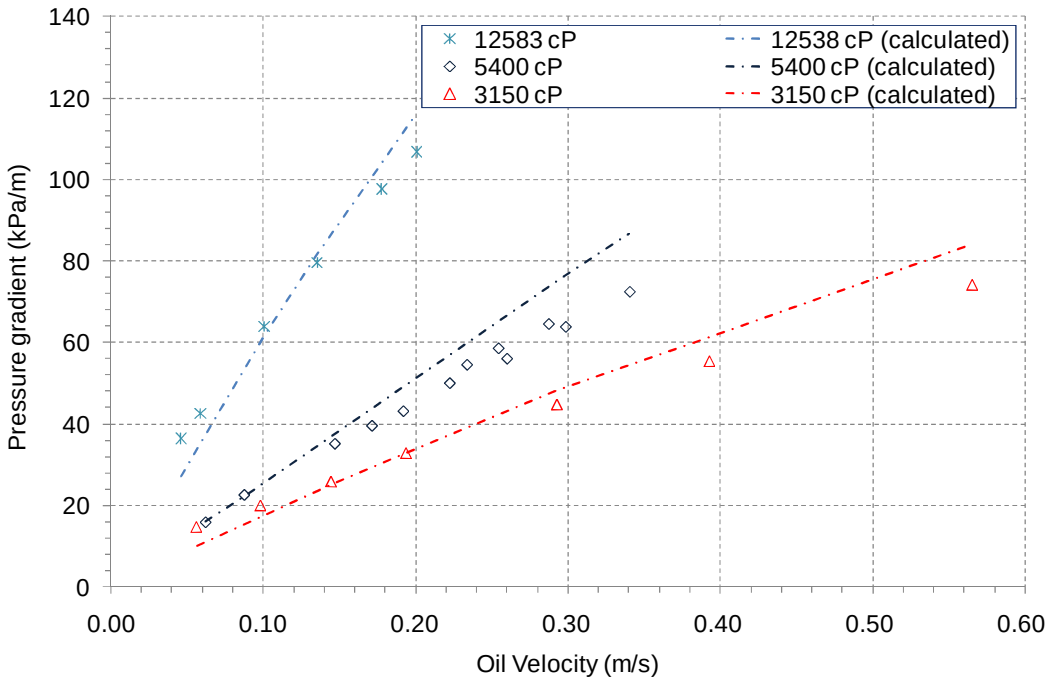

Figure 4-13: Pressure gradient comparison between experimental results and calculated values for different heavy oil viscosities

The results from the comparison showed a good agreement with the measured values with small (gradual) deviation for higher examined velocities. Table 4-2 shows the difference percentage error found between the measured and calculated pressure gradient for heavy oil viscosity of 3150 and 12583cP. The trend for deviation is consistent as the calculated value is under predicting the measured value for low heavy oil flow rate, however the difference becomes smaller as more oil is pumped to the system; finally the calculated pressure gradient value over estimate the measure value for relatively high V_o.

Two reasons were thought to cause this deviation: the nature of the oil to behave as non-Newtonian fluid, where viscosity is shear stress dependent (shear thickening and shear thinning); and the temperature change of the flowing oil in the system due to surrounding temperature difference, which would change to the property of the oil.

Oil Viscosity 3150cP				Oil Viscosity 12583cP			
V_o (m/s)	Pressure gradient (kPa/m)		P.E. (%)	V_o (m/s)	Pressure gradient (kPa/m)		P.E. (%)
	Measured	Calculated			Measured	Calculated	
0.06	14.7	10.0	-32.1	0.05	36.5	27.1	-25.6
0.10	20.0	17.3	-13.3	0.06	42.6	35.6	-16.5
0.14	25.9	25.1	-2.9	0.10	64.0	61.5	-3.9
0.19	32.8	33.0	0.6	0.14	79.7	81.7	2.5
0.29	44.7	48.2	7.8	0.18	97.7	104.1	6.5
0.39	55.4	61.5	11.0	0.20	106.7	116.3	8.9

*P.E. is the percentage error.

Table 4-2: Comparison between measured and calculated pressure gradients for single phase heavy oil at 3150 cP and 12583cP

4.2.2 Two phase results

4.2.2.1 Heavy oil – gas

The pressure gradients were obtained based on measuring the difference of two single pressure transducers for heavy oil/air flow. An example set is presented to demonstrate the effect of flow patterns toward the measured pressure gradient; Figure 4-14 shows the signal output against time for (a) plug, (b) slug, and (c) annular flow at constant V_{so} and μ_o (0.025m/s and 4326cP respectively). The readings were recorded for 60 seconds with 250Hz sample rate and the measuring distance between the two transducers was 2.17m.

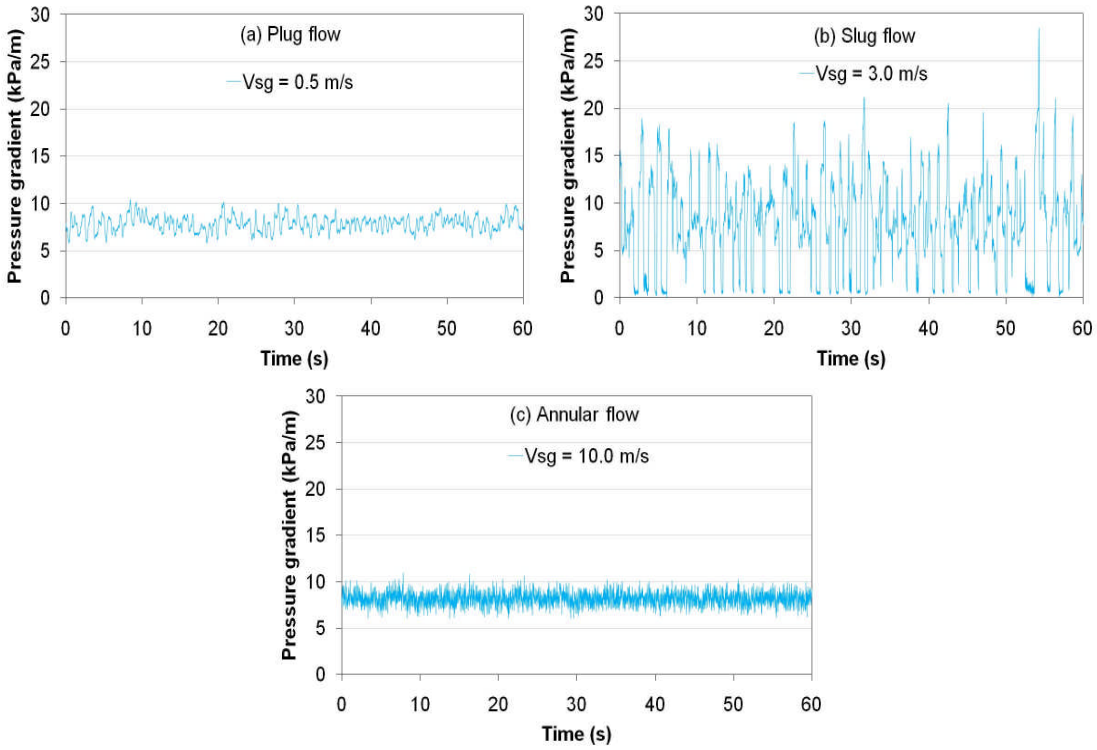

Figure 4-14: Transient pressure gradient comparison for V_{so} = 0.025 m/s and μ_o =4326cP at different V_{sg} representing (a) plug, (b) slug, and (c) annular flow

The graphs above show different pressure gradient fluctuations for each associated flow pattern. At low V_{sg}, the plug flow tends to have low frequency to the generated pressure gradient signal (mean = 7.897 kPa/m and Standard Deviation, SD = 0.81) as shown in Figure 4-14a. However as higher V_{sg} is introduced to the flowing mixture, the energy associated with slug flow that reflects the difference in the dynamic pressure between the gas in the front and back of the liquid body (mean = 7.87 kPa/m, SD = 4.68) is clearly shown in Figure 4-14b; as the signal becomes more disturbed by the driven forces. Finally, the dynamic pressure gradient output returns to the small level of fluctuations but with much higher pitch (mean = 8.196 kPa/m, SD = 0.65) as it reaches the annular flow(Figure 4-14c); this reflects the high turbulent flow of gas and the ripples founded in the heavy oil film for the pipe wall.

Despite the difference in magnitudes for the averaged signals at different μ_o, the trend of transient pressure drop outputs were found to be similar for each flow

pattern. As shown in Figure 4-15, both plug (mean = 37.094 kPa/m, SD = 0.73) and slug (mean = 29.17 kPa/m, SD = 7.25) flow signals have the same tendency when compared with the graphs obtained for lower μ_o for the same flow pattern (i.e., Figure 4-14 a & b).

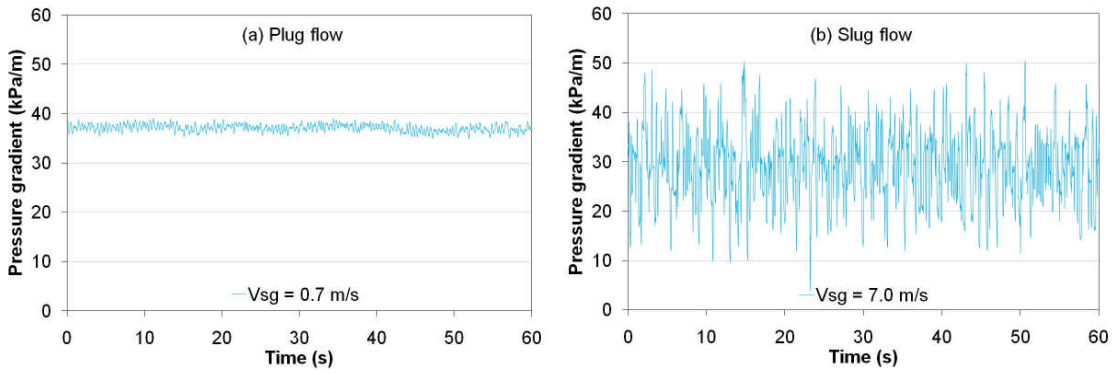

Figure 4-15: Transient pressure gradient comparison for V_{so} = 0.035 m/s and μ_o =10605cP at different V_{sg} representing (a) plug and (b) slug

On the other hand when V_{so} increases for the same μ_o, the coated film becomes thicker. This would make the gas pocket associated with intermittent flow travel closer toward the centre of the pipe. Figure 4-16a shows high frequency and even higher pitch for plug flow (mean = 38.325 kPa/m, SD = 1.59) when compared with the same type of flow at lower V_{so} (i.e., Figure 4-14a and Figure 4-15a). And the same phenomenon is found again for slug flow (mean = 34.599 kPa/m, SD = 4.43), as shown in Figure 4-16b.

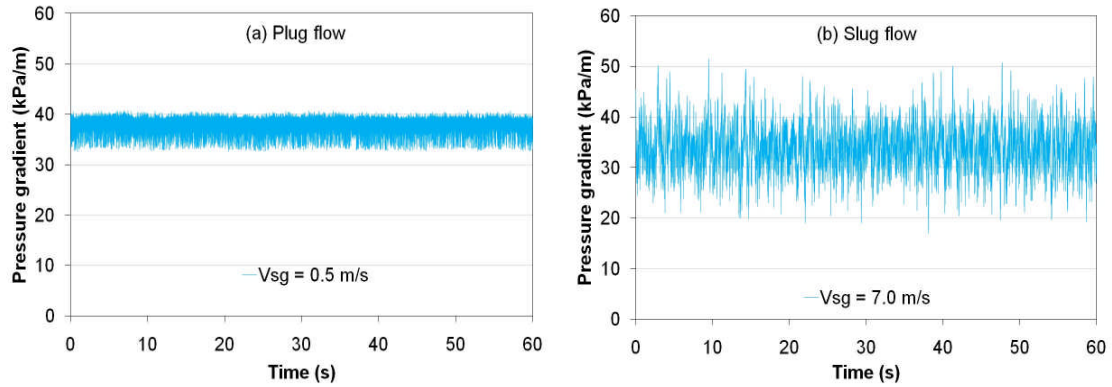

Figure 4-16: Transient pressure gradient comparison for V_{so} = 0.20 m/s and μ_o =4326 cP at different V_{sg} representing (a) plug and (b) slug

The injection of gas to the heavy oil flow was examined against the pressure gradient for four different superficial heavy oil velocities for an averaged heavy oil viscosity of 4326 cP; Figure 4-17 shows the effect of gas flow for V_{so} around 0.03, 0.06, 0.10, and 0.20 m/s. For V_{so} below 0.10 m/s, no significant effect toward the pressure drop was found. However, a variation of ±7.5% was found for V_{so} equal and above 0.10 m/s. This is again thought to be an effect caused by the thicker oil coating associated with higher heavy oil flow rate. It is also noted that the measured pressure gradient values were dependent on the flow pattern; as plug flow showed relatively higher pressure gradient values than slug flow.

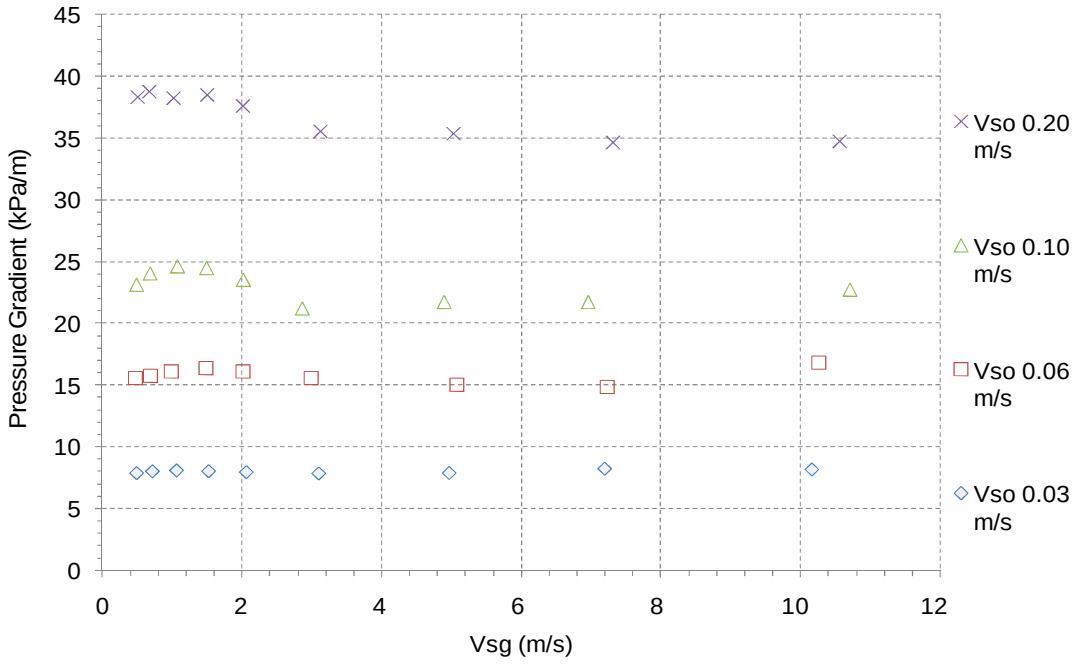

Figure 4-17: Gas injection effect on pressure drop for different V_{so} and averaged μ_o = 4326 cP

Since the pressure drop variation is relatively small for the examined range of V_{sg}, an averaged value was considered for each V_{so} and compared against the pressure gradient obtained for heavy oil single phase flow. Table 4-3 shows the difference percentage error found between the measured two phase heavy oil-air pressure gradients and calculated pressure gradient single phase flow of

heavy oil at averaged μ_o = 4326 cP. The trend for deviation is consistent with what was found earlier for heavy oil single phase (see Table 4-2) as the calculated value first under predict the measured value, then becomes equal around 0.15 m/s, and finally starts to over predict at higher $V_{so.}$ This is again linked to nature of the oil and surrounding temperature effect on the flowing mixture as discussed previously for the heavy oil single phase flow.

V_{oil} (m/s)	oil Viscosity (cP)	Measured pressure gradient for heavy oil-air flow (kPa/m)	Calculated pressure gradient for heavy oil flow (KPa/m)	P.E. (%)
0.025	3949	7.99	4.71	-41.1
0.061	4742	15.65	13.60	-13.1
0.103	4572	23.00	22.39	-2.7
0.227	4130	39.56	44.07	11.4

Table 4-3: Pressure gradients comparison between heavy oil flow and heavy oil-air flow

Finally, the injection of gas to the heavy oil flow was tested again at relatively heavier viscosity oil, averaged around 10605 cP, and compared next to calculated pressure gradient in single phase heavy oil flow around 0.04 m/s, as shown in Figure 4-18. Two observations were deduced by examining the graph:

1) the trend of the pressure drop was dissimilar to the previous tests as it was decreasing with the increase of gas flow; this is mainly due to the sharp decrease of heavy oil viscosity throughout the run as has started around 12564 cP at low V_{sg} and decreased all the way to 9341cP by the end of the experiment at high $V_{sg.}$ The heavier viscosity oil causes thicker oil coating layer, that decreases the effective flowing diameter for the gas pocket to travel through the pipe, and finally contributes to the increase in pressure gradient, and vice versa.

2) the single phase heavy oil calculation is underestimating the averaged measured pressure gradient by 14 kPa/m (P.E. equates to -42.4 %); this is consistent to the nature of the oil and surrounding temperature effect with high viscosity on pressure drop measurements and should expect lower difference with higher heavy oil superficial velocity. However, gas injection tests could not

be performed on V_{so} beyond 0.04 m/s due to high system pressure and limitation of the compressed air supply.

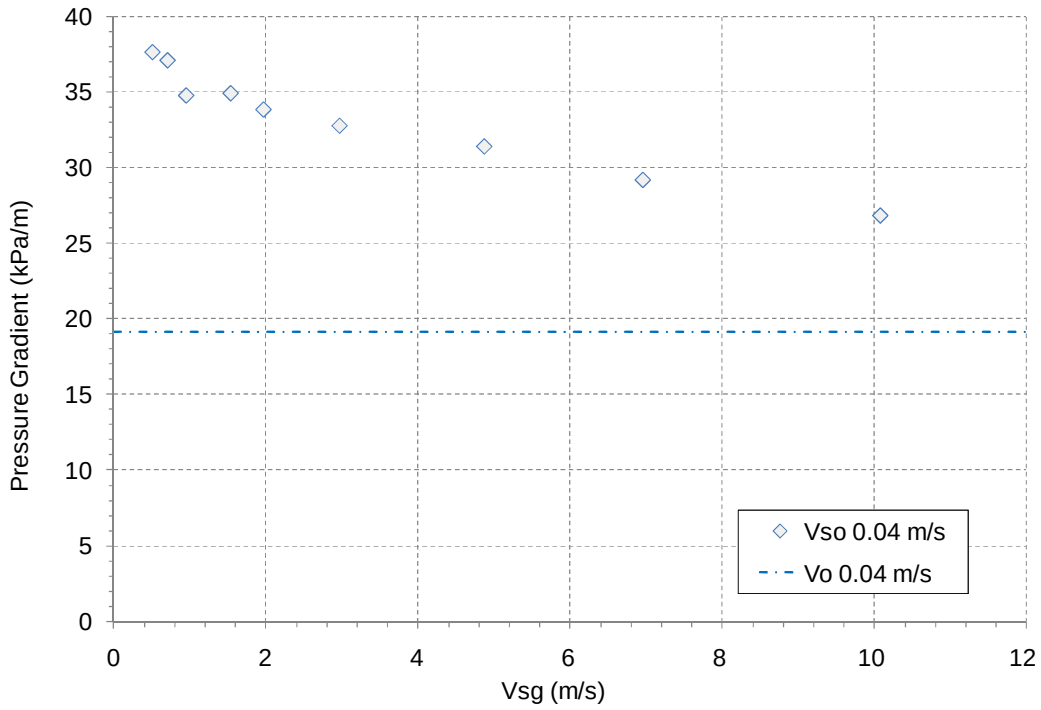

Figure 4-18: Gas injection effect on pressure drop for V_{so}= 0.04 m/s and μ_o ranges from 12564 to 9341 cP

4.2.2.2 Heavy oil – water

The pressure gradients were calculated based on measuring the difference of two single pressure transducers for heavy oil/water mixture flow. Although controlling the flow rates of each fluid was difficult, near transition phase, due to the sharp drop of system pressure as the water was being injected; this was solved by controlling the pressures of injected fluids through choking mechanism of both injection and bypass valves. An example set of steady controlled runs for heavy oil at 13332 cP, V_{so} = 0.10 m/s, and different V_{sw} is shown in Figure 4-19. The readings were recorded for 60 seconds with 250Hz sample rate. The graph shows reduction of pressure in the system as water is introduced to the heavy oil single phase flow; however this reduction would be insignificant after considerable amount of water, V_{sw} = 0.05 m/s for this example, as the pressure signal reaches near the atmospheric pressure value. This can be associated with the lubrication mechanism with more water introduced to the system.

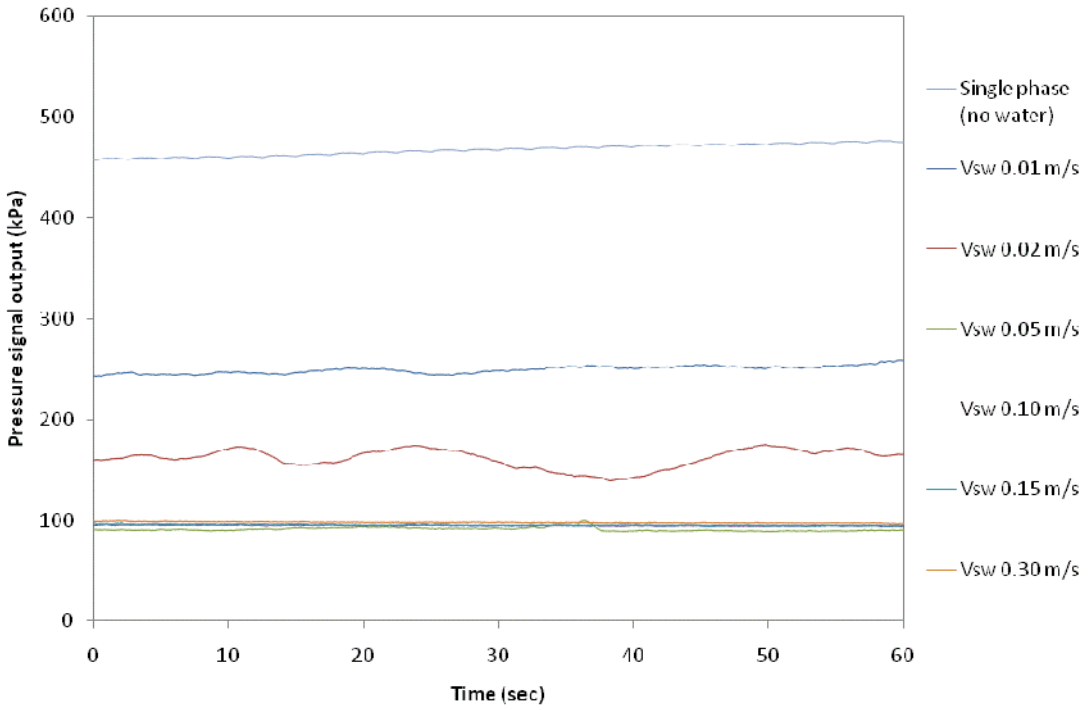

Figure 4-19: Pressure signal comparison at V_{so} = 0.10 m/s

The resulted pressure gradient for the same set of runs is listed in Figure 4-20. Similarly to the system pressure, a reduction in the pressure gradient is observed as water is introduced to the heavy oil single phase flow; and its significance would be minimal beyond a certain V_{sw} value, 0.05 m/s for presented run, on system pressure. The fluctuations in the pressure gradient for very low V_{sw} (0.01 m/s and 0.02 m/s) are mainly due to being in WPO flow pattern, which is oil dominant flow. This is in agreement with McKibben et al. (2000a) hypothesized water/oil blobs envelope as they concluded the reduction of pressure gradient is associated with water slugs which envelop some oil and transport it at low pressure gradients, and these low pressure gradient regions combine with the water free zones with high pressure gradient to produce a time-averaged pressure gradient reduction.

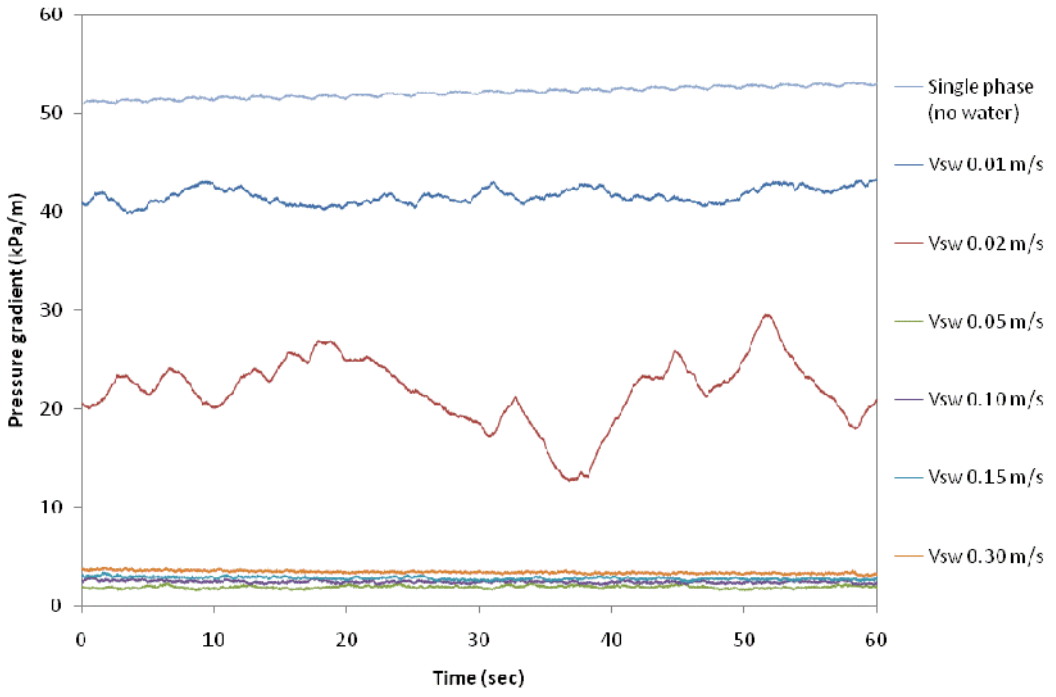

Figure 4-20: Pressure gradient comparison at V_{so} = 0.10 m/s

The existence of water plugs in oil phase travelling in continuous pulse behaviour affected the stability of the pressure at different locations along the pipe, which led to slight change of system pressure at these locations. This

should be avoided in operation as sudden changes in pressure gradients could impose considerable cyclic stresses on pipe-work, ultimately leading to pipe failure.

However, this phenomenon becomes more stable as higher water cuts (calculated as the ratios of the water in the fluid mixture) are obtained in the system, shifting the flow pattern to transition and then to water dominant flow.

The water cut effect was studied on pressure drop for heavy oil viscosity of 3911 cP and superficial heavy oil velocity of 0.06 m/s as shown in Figure 4-21. It is shown that the pressure drop remains high when the flow is dominated with oil (i.e. WPO). However, as more water is introduce to the mixture, the pressure gradient decreases in the transition phase (i.e. SWO). Finally when the flow becomes dominated with water, the pressure gradient starts to increase with the increase of water flow rate.

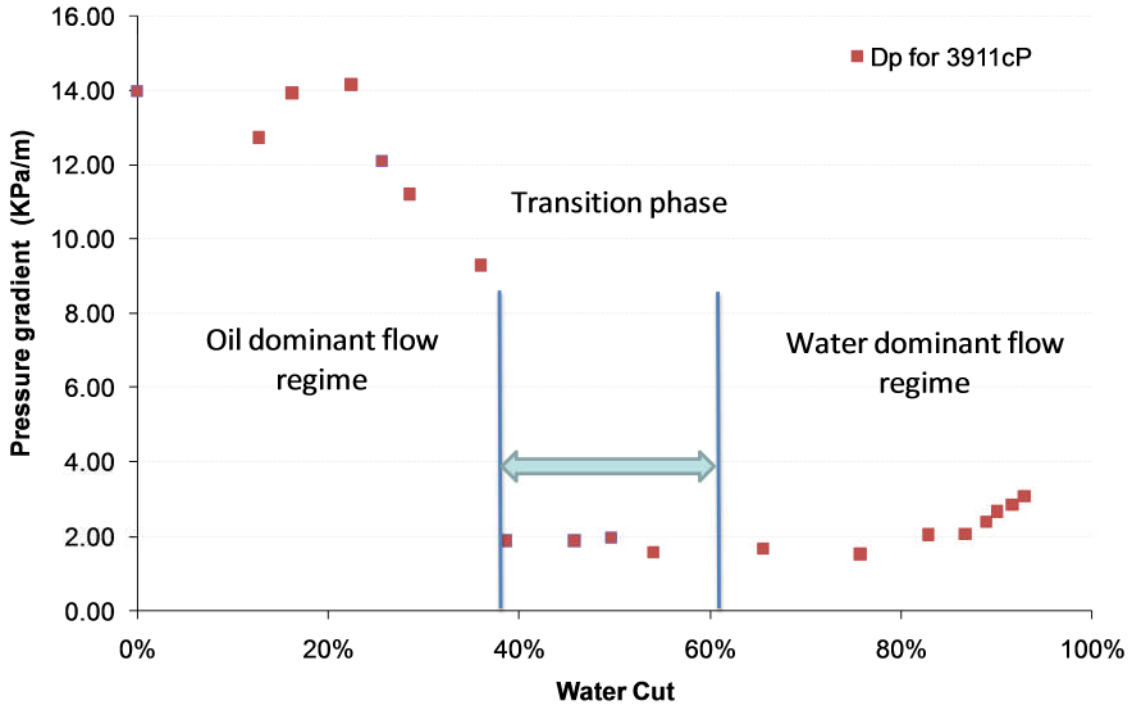

Figure 4-21: Water cut effect on pressure drop for V_{so}= 0.06 m/s

The water cut effect was examined on pressure drop for different superficial heavy oil velocities and viscosities (3911, 8325, 13205, and 15979 cP) as shown from Figure 4-22 to Figure 4-25. Again as would be expected, the pressure gradient decreases with increasing water flow rate for all viscosities. The graphs show the lowest pressure gradient is obtained around 40% water cut or less, however the effect of water cut is insensitive to the viscosity of the heavy oil. The water cut associated to the minimum pressure gradient obtained and beyond shall be referred to as **Water Assist Flow (WAF).** It is noted that slight increase to the pressure gradient is associated with higher water cuts; this is associated with the increase of velocity as the pressure drop is proportional to the square of velocity. Therefore, the pressure gradient reduction due to the water cut is now overtaken by the increase of velocity.

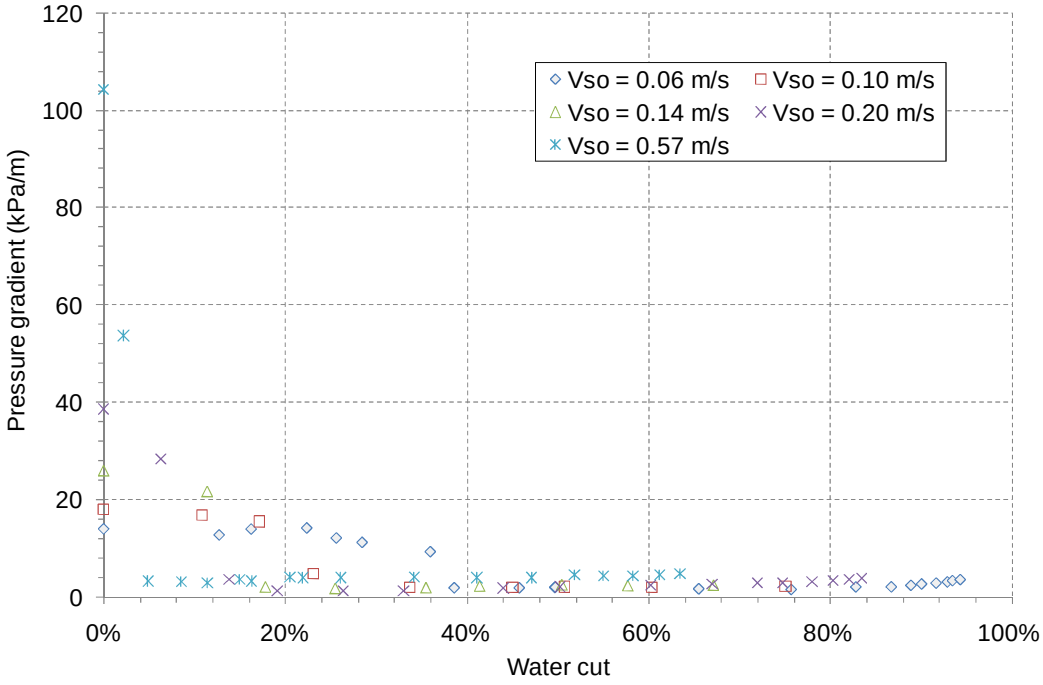

Figure 4-22: Water cut effect on pressure drop for heavy oil viscosity of 3911cP

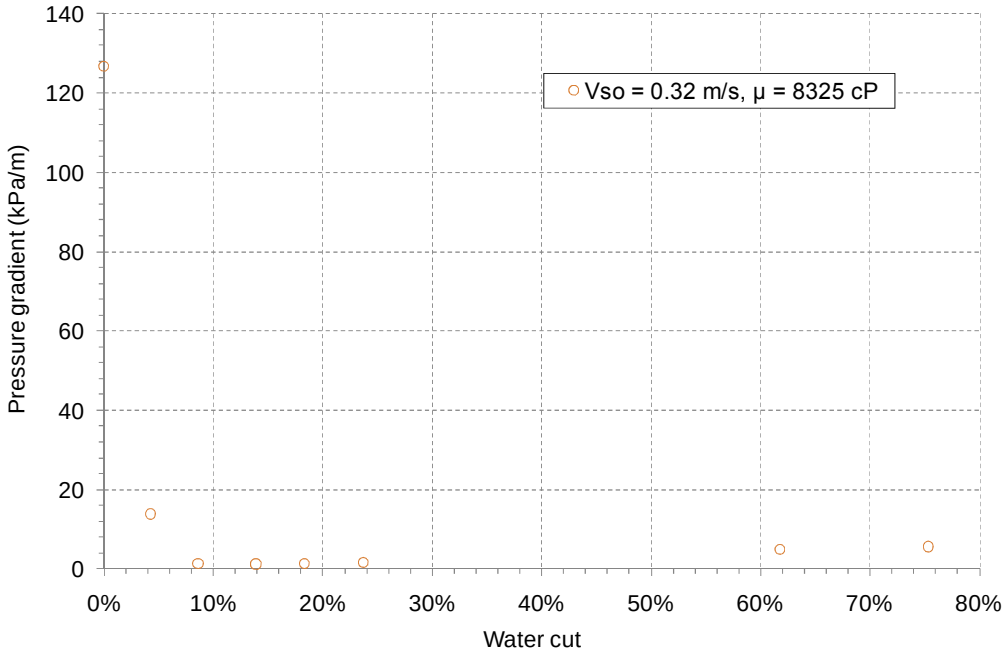

Figure 4-23: Water cut effect on pressure drop for heavy oil viscosity of 8325cP

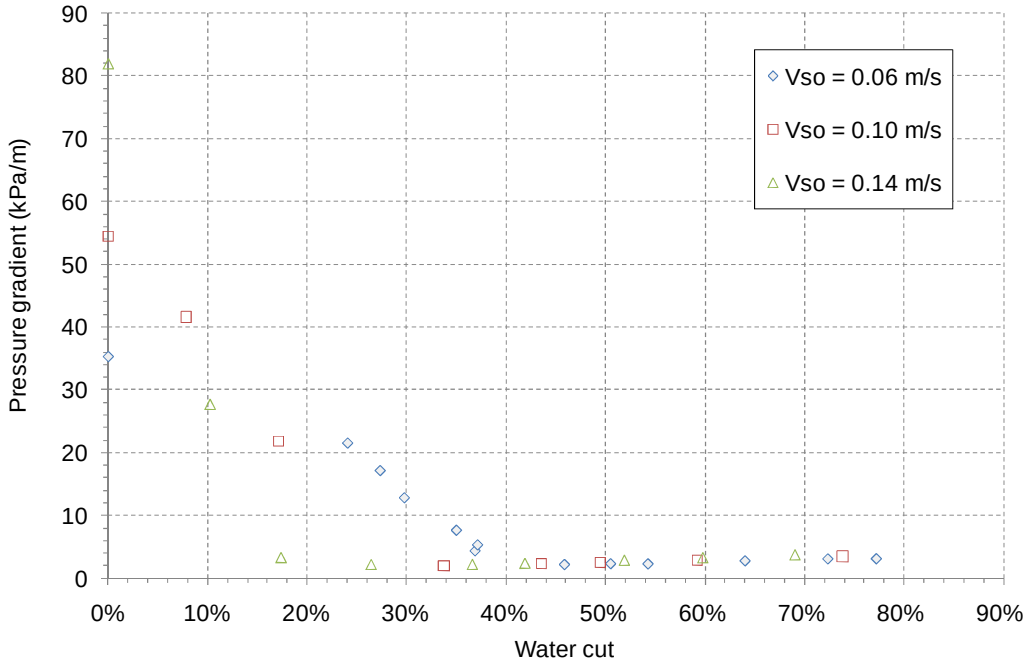

Figure 4-24: Water cut effect on pressure drop for heavy oil viscosity of 13205 cP

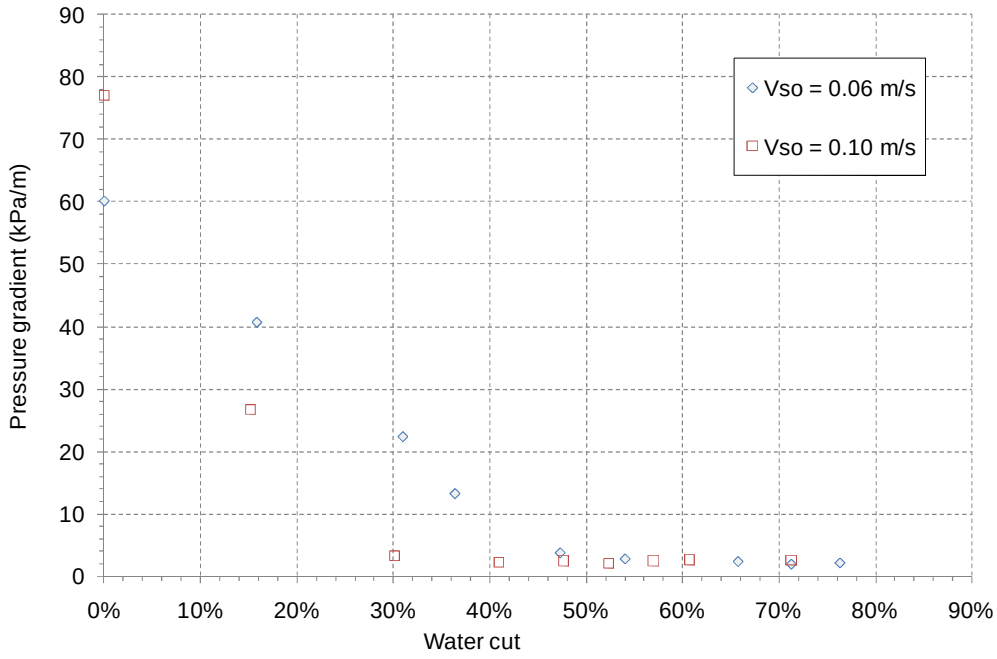

Figure 4-25: Water cut effect on pressure drop for heavy oil viscosity of 15979 cP

Depending on the superficial oil velocity, the WAF can be obtained at different water cuts, as shown from Figure 4-26 to Figure 4-31. The figures show the WAF condition is obtained around 40, 30, 19, 16, 8 and 4 % water cuts for 0.06, 0.10, 0.14, 0.20, 0.32, and 0.57 m/s V_{so} respectively. Though pressure gradients started to drop by introducing water to the heavy oil flow, represented on the y-axis at water cut = 0%, for viscosities beyond 10000 cP at all conditions, it has been observed that inconsistency occurred for relatively lower heavy oil viscosity (3911 cP).

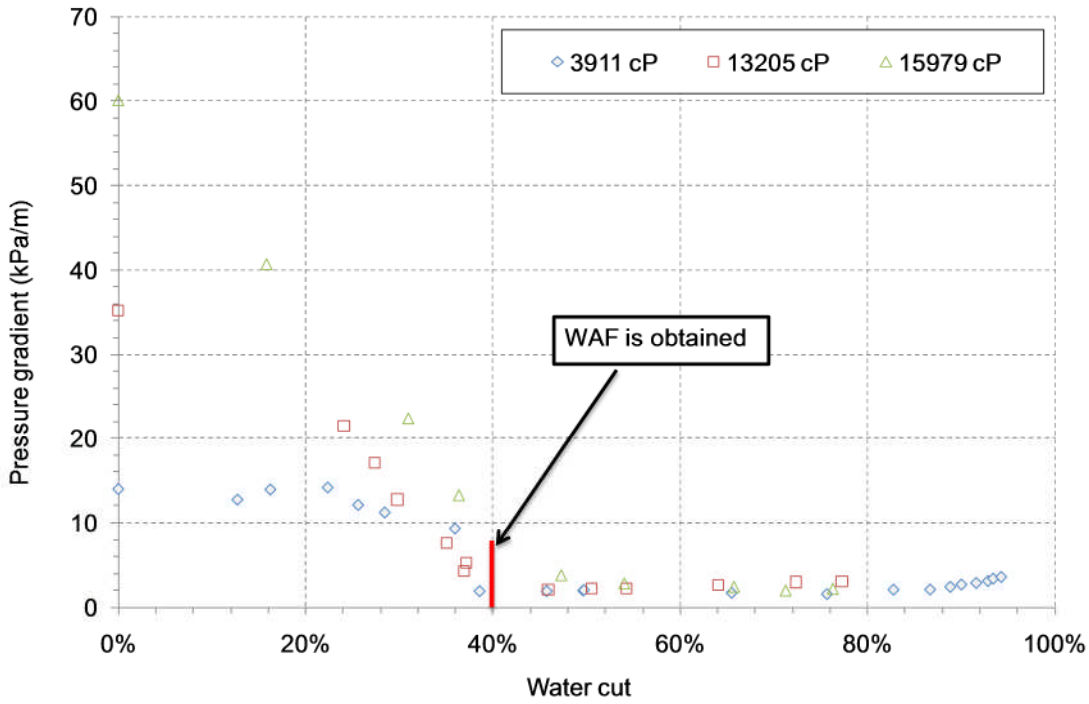

Figure 4-26: Measured pressure gradient versus water cut with various viscosities at V_{so} = 0.06 m/s

For relatively low heavy oil viscosity (3911 cP), the pressure gradient maintained around the single heavy oil value for water cuts less than 22, 18, and 15% for 0.06, 0.10, and 0.14 m/s V_{so} respectively before it started to reduce. This was thought to be caused by the difficulty of achieving the exact superficial oil velocity for all the runs, which contributes strongly on low pressure drop values.

However, as shown in the graphs, the effect of oil viscosity change at that range on pressure gradient is more significant than the contribution effect of water injection to the system at that region, as would be expected since all flows observed in that region were WPO (oil dominant phase).

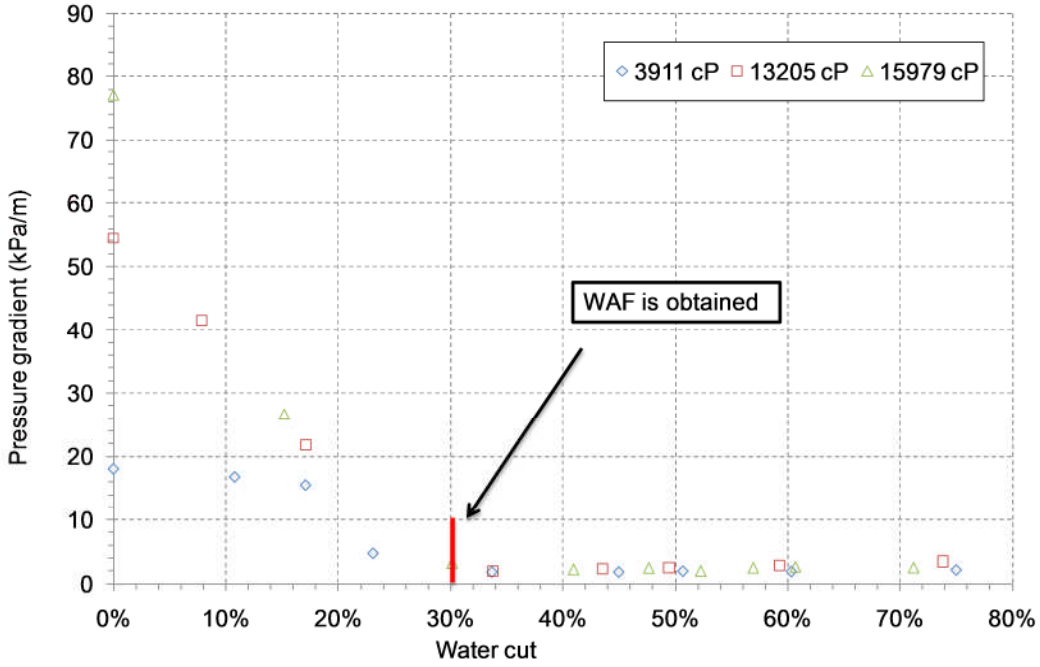

Figure 4-27: Measured pressure gradient versus water cut with various viscosities at V_{so} = 0.10 m/s

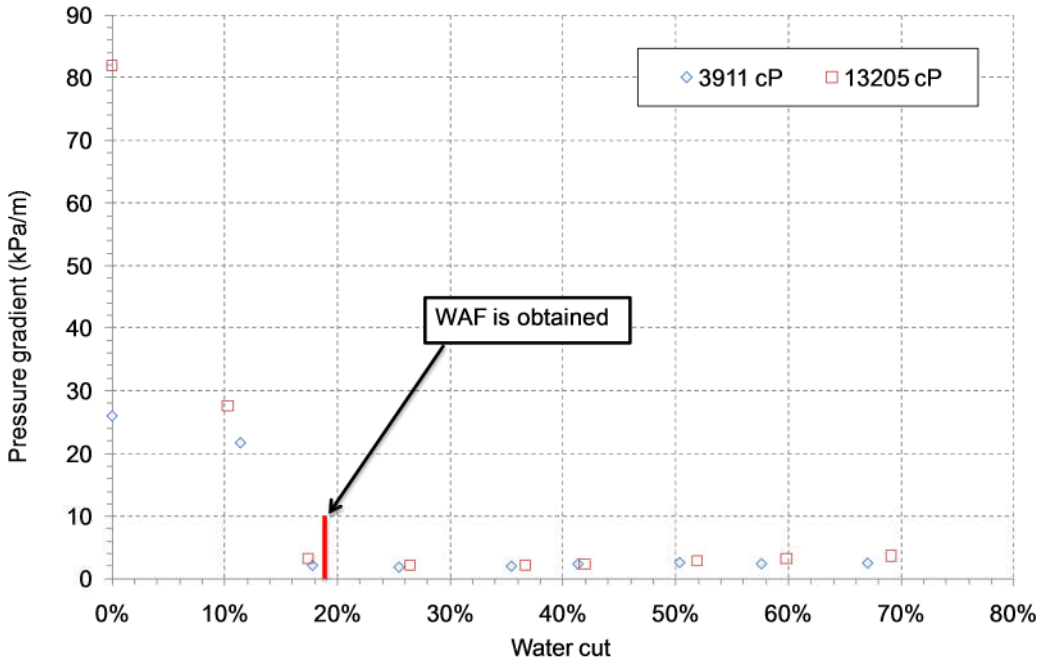

Figure 4-28: Measured pressure gradient versus water cut with various viscosities at V_{so} = 0.14 m/s

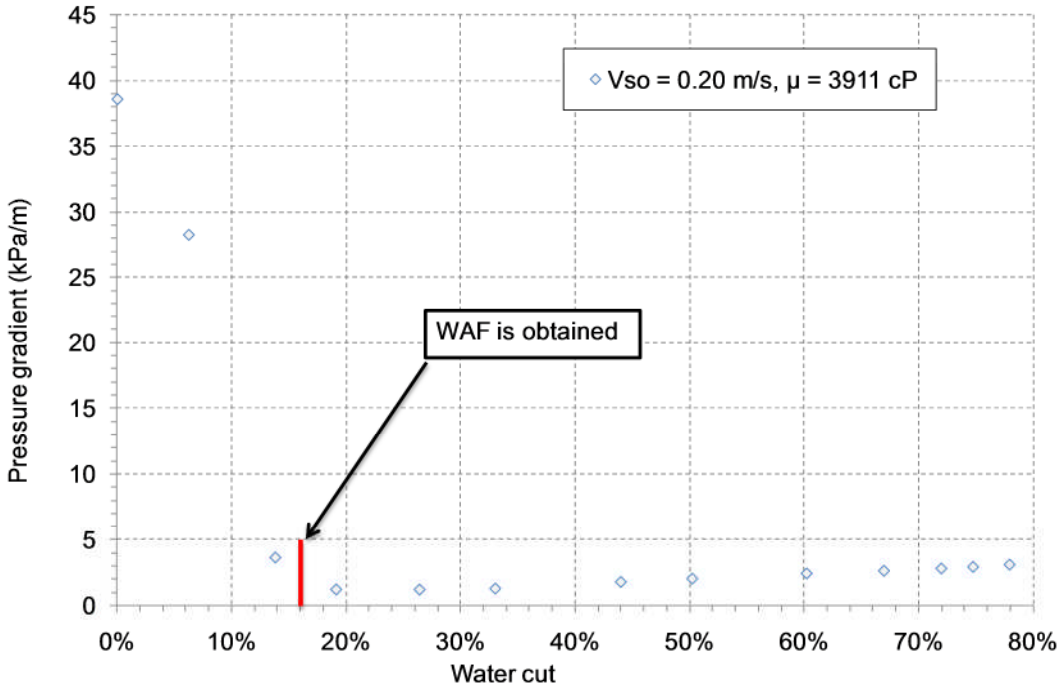

Figure 4-29: Measured pressure gradient versus water cut at V_{so} = 0.20 m/s

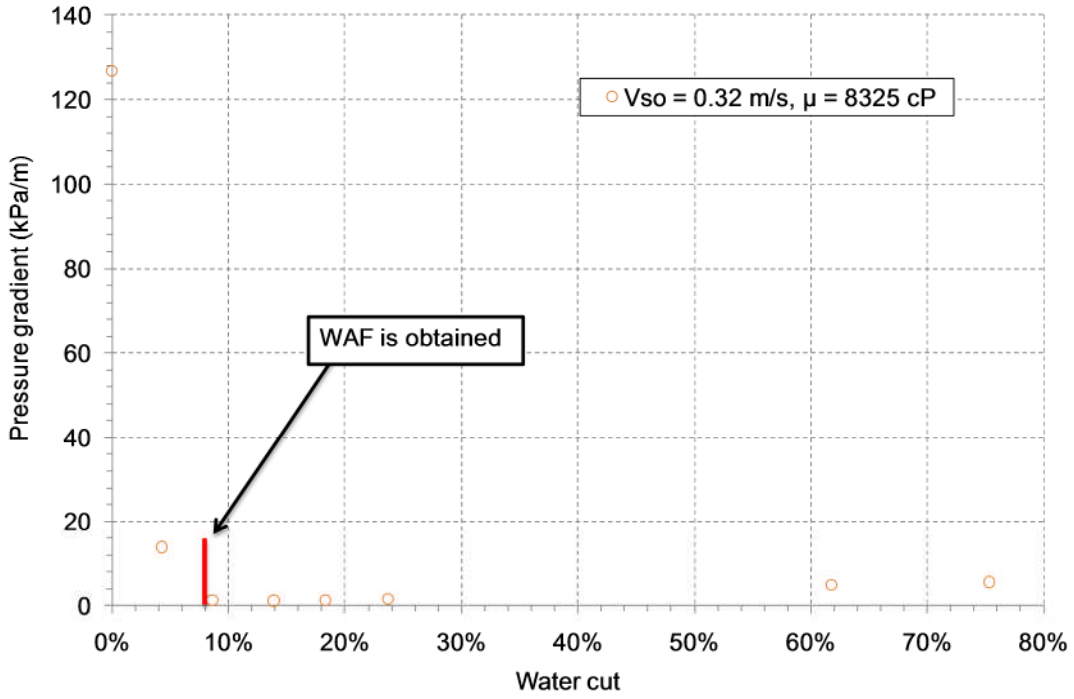

Figure 4-30: Measured pressure gradient versus water cut at V_{so} = 0.32 m/s

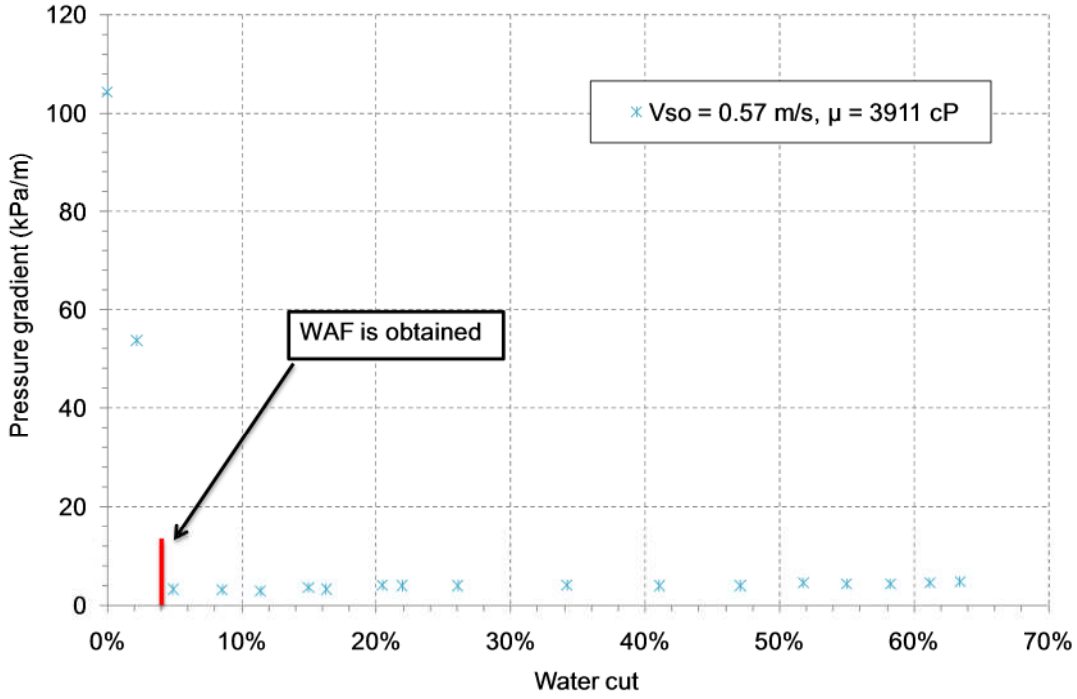

Figure 4-31: Measured pressure gradient versus water cut at V_{so} = 0.57 m/s

The minimum pressure drop achieved for all sets of data is shown on the 2-phase (heavy viscous oil/water) flow regime map (Figure 4-32). Water cut lines are drawn to emphasis the relationship against V_{so}, as the water cut value decreases with the increase of oil flow. The graph shows that WAF can be achieved around V_{sw} = 0.05 m/s, corresponding to 1300 Reynolds number for water, in the SWO flow regime.

As different methods of water injection (i.e. vertically and horizontally) were initially tested and no considerable effect was found toward the observed flow patterns or pressure gradient, It was concluded that neither the viscosity of the heavy oil nor the method of water injection play significant rule toward reaching WAF.

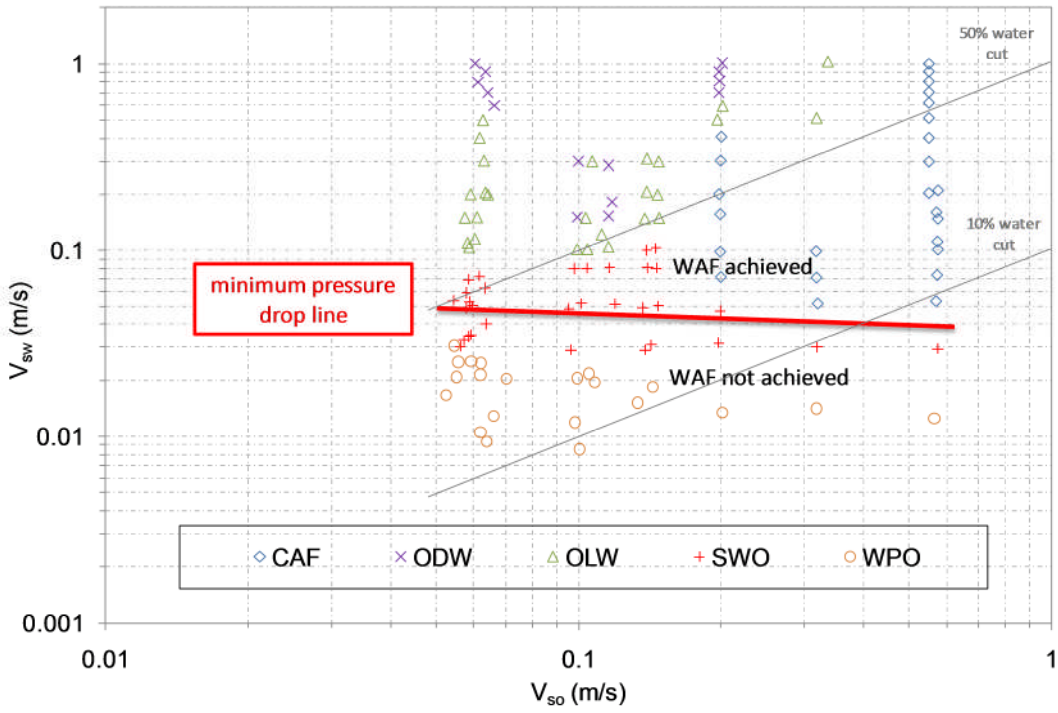

Figure 4-32: WAF occurrence line on 2-phase (heavy viscous oil/water) flow regime map

To examine the effect of oil coating the pipe-wall, the data collected for heavy oil/water in the water dominant regime (i.e., OPW, ODW, and CAF) can be compared against water flow at the corresponding mixture velocity. Figure 4-33 shows huge pressure gradient difference between the single phase water flow and corresponding flow of heavy oil and water mixture. This difference, ranging from 1.5 to 3.5 kPa/m, can be mainly linked to oil coating observed in the pipe as it will reduce the hydraulic diameter of the total flow and increase the pipe wall roughness. Although this will significantly influence the increase of pressure gradient, the differences between the different flows (OPW, ODW, and CAF) will contribute as well due to change of oil in-situ ratio for each flow. Finally, the viscosity of the oil will also affect the pressure gradient, as higher viscosity oil will lead to higher pressure drop in the system.

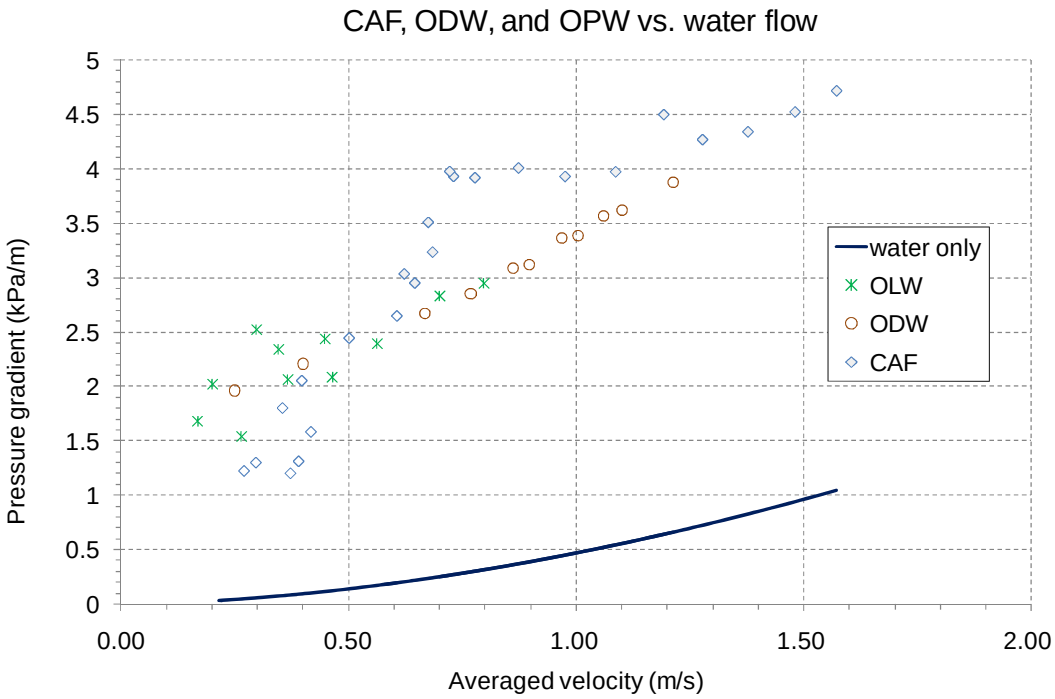

Figure 4-33: Pressure gradient comparison between water dominant (2-phase) flow patterns and single phase water flow

4.2.3 Three phase results

4.2.3.1 Heavy oil – water – gas

The heavy oil-water-air pressure gradients were acquired for a matrix consisting 144 flow points by varying heavy oil viscosities and superficial fluids' velocities. These tests covered the range of 0.06-0.14 m/s, 0.02-0.20 m/s, and 1.0-10.0 m/s superficial heavy oil, water, and gas velocities respectively. The purpose of this matrix is to examine the effect of gas flow to the mixed two phase flow (heavy oil-water) for three very distinguished flows (oil continuous, water continuous, and transition phase). The heavy oil viscosities covered for these tests were around 3300cP and 12700cP.

- $V_{so} \in \{0.06, 0.10, 0.14\}$.
- $V_{sw} \in \{0.02, 0.05, 0.20\}$.
- $V_{sg} \in \{0.5, 0.7, 1.0, 1.5, 2.0, 3.0, 5.0, 7.0, 10\}$.

The data of the pressure gradient are presented in graphical format, where they are compared against two phase (heavy oil-water) flow in figures. The lines connecting the experimental data points are shown to indicate the trend of the pressure gradient behaviour for each condition. However, the whole data set are presented in tabular form in Appendix A for future reference. The data are categorized based on heavy oil density, fluids superficial velocities, temperature, heavy oil viscosity, inlet and outlet pressures and temperatures, and pressure drop.

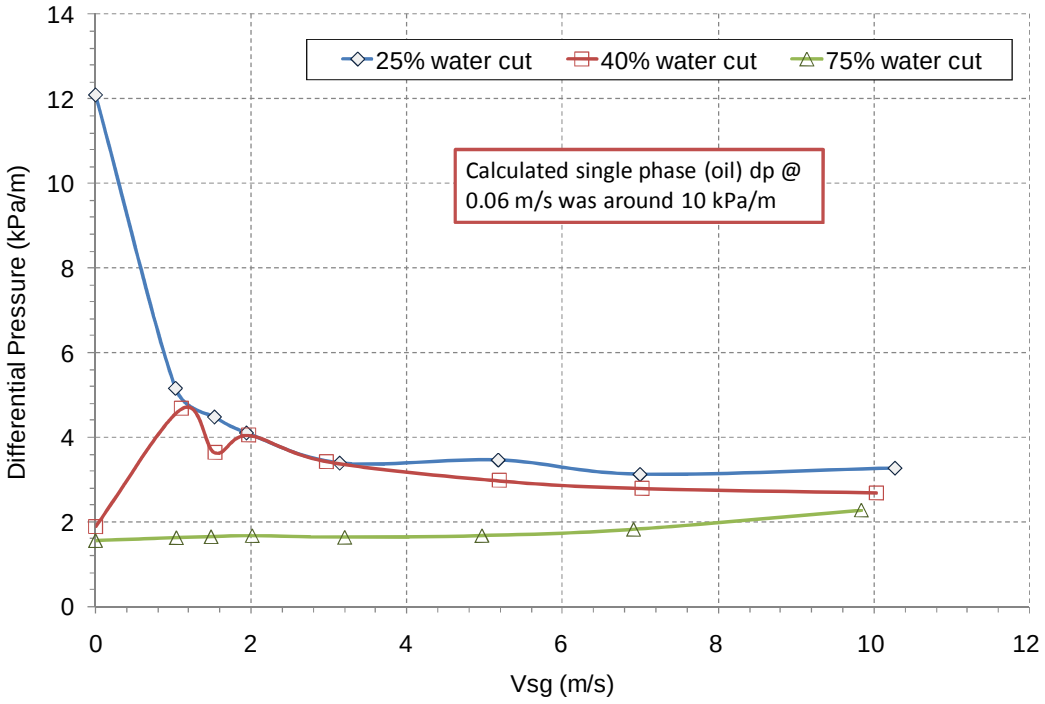

Figure 4-34: Gas injection effect on measured pressure gradient for different water cuts at averaged V_{so} = 0.06 m/s and μ_o =3286 cP

Figure 4-34 shows the effect of gas injection to the heavy oil-water mixture at 25, 40, and 75% water cuts for V_{so} = 0.06 m/s and μ_o =3286 cP. At the highest water cut (water continuous phase), the gas injection showed a small increase to the pressure gradient. However for lowest water cut (oil continuous phase), the pressure gradient dropped significantly. Finally, for the transition phase, 40% water cut, the pressure drop tends to follow the behaviour of oil continuous phase at first, where the pressure gradient rises to that level, and then starts to drop back to lower values. It seems that the pressure gradient for all 3 cases tend to converge to 3 kPa/m.

Similar behaviour was found for heavy oil-water mixture at 18, 31, and 67% water cuts for V_{so} = 0.10 m/s and μ_o =3411 cP (Figure 4-35). Although a rise in the pressure drop convergence value was noted for lowest water cuts (oil continuous flow). It is thought that heavy oil film is contributing toward this surge as more heavy oil is accounted at this condition in the system.

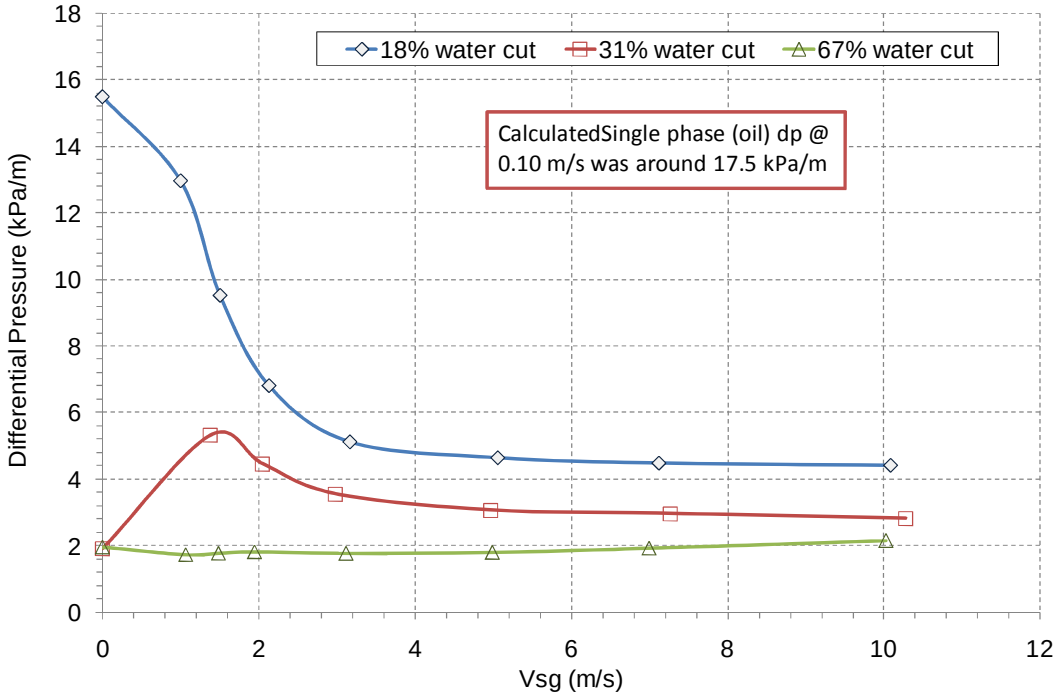

Figure 4-35: Gas injection effect on measured pressure gradient for different water cuts at averaged V_{so} = 0.10 m/s and μ_o =3411 cP

Finally, Figure 4-36 shows comparable trend at water continuous, and transition phase flow for V_{so} = 0.14 m/s and μ_o = 3270 cP. Yet at oil continuous flow, the pressure gradient starts to pick up as more V_{sg} was injection beyond 2.0 m/s. A change of flow pattern was observed at this condition when compared to the previous sets of experiments.

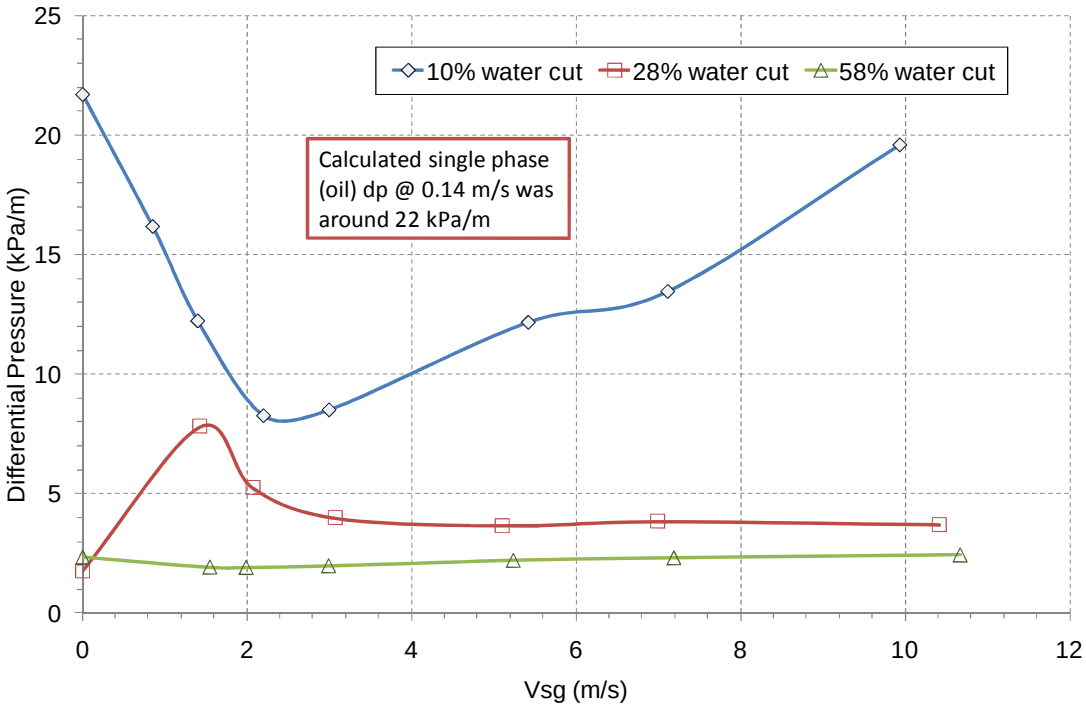

Figure 4-36: Gas injection effect on measured pressure gradient for different water cuts at averaged V_{so} = 0.14 m/s and μ_o = 3270 cP

To study the effect of viscosity toward the three phase sets, the previous set of experiments were repeated for relatively higher heavy oil viscosity. Figure 4-37 shows the effect of gas injection to the heavy oil-water mixture at 25, 40, and 75% water cuts for V_{so} = 0.06 m/s and μ_o =12495 cP. At the highest water cut (water continuous phase), the gas injection showed no significance change to the pressure gradient. However as the water cut was reduced to the transition phase at 40% water cut, the pressure gradient remained around the same value for low V_{sg}; however it increased significantly when V_{sg} reached beyond 3 m/s, and then started to gradually decrease again for high V_{sg}. Finally, for the oil continuous phase, 25% water cut, the pressure drop tends to reach its maximum value at V_{sg} around 2.0 m/s; however it gradually decreases as more gas flow rate got injected to the mixture.

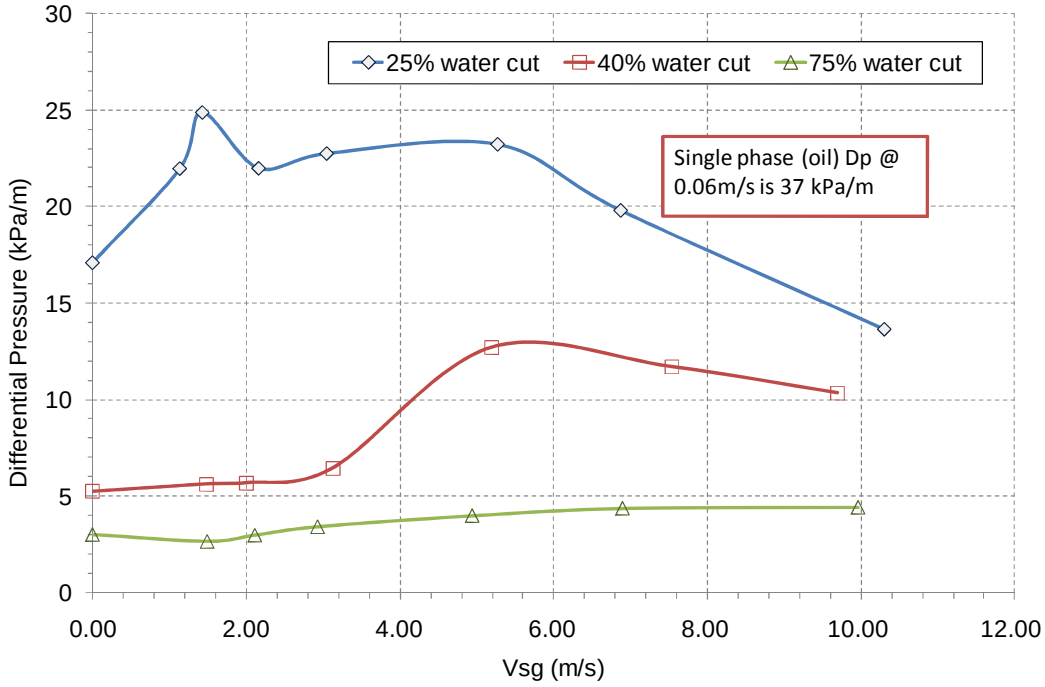

Figure 4-37: Gas injection effect on measured pressure gradient for different water cuts at averaged V_{so} = 0.06 m/s and μ_o = 12495 cP

When V_{so} is increased to 0.10 and 0.14 m/s for oil viscosity of 12739 and 12949 cP respectively, Figure 4-38 and Figure 4-39, similar trends were found for both as water continuous and transition phase were gradually increasing at small rate with gas injection; as for the oil continuous phase, the pressure drop tends to reach its maximum value at V_{sg} around 2.0 m/s and it gradually decreases as more gas flow rate got injected to the mixture.

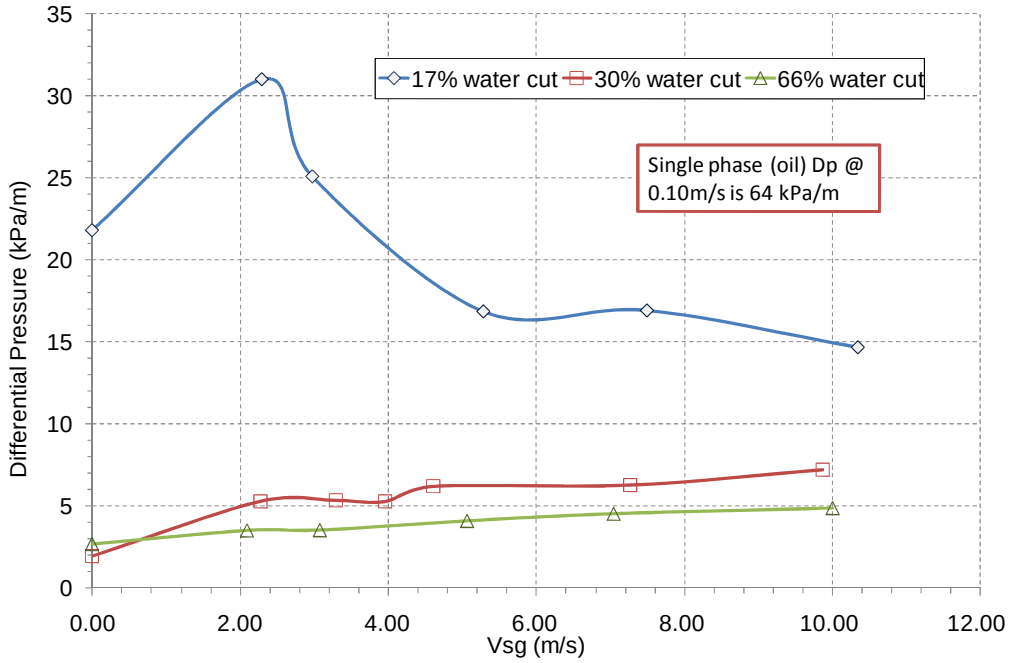

Figure 4-38: Gas injection effect on measured pressure gradient for different water cuts at averaged V_{so} = 0.10 m/s and μ_o = 12739 cP

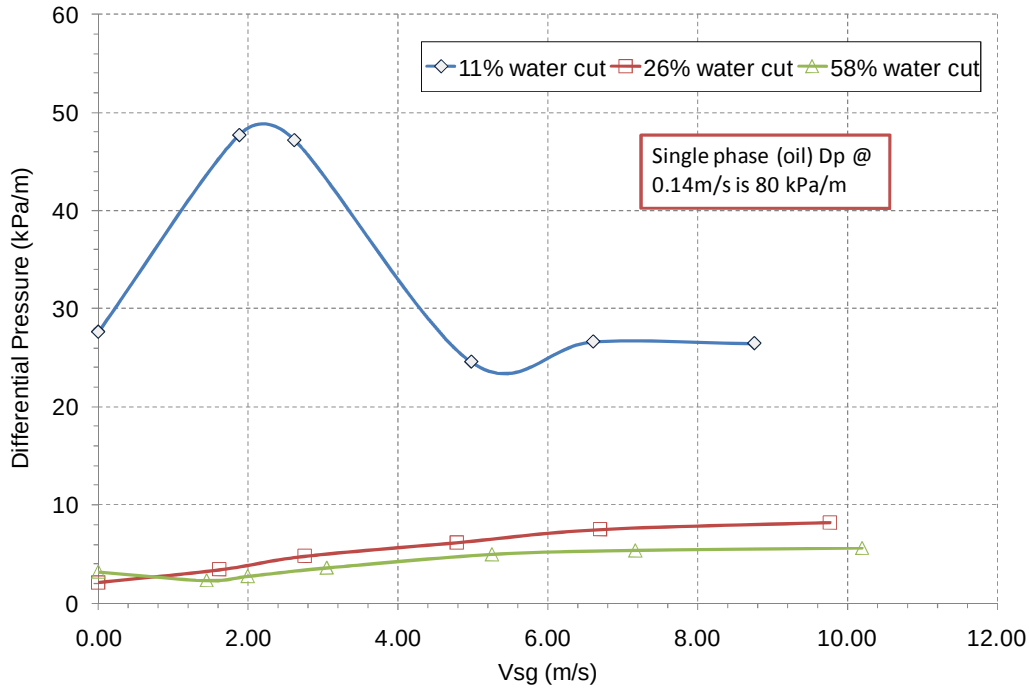

Figure 4-39: Gas injection effect on measured pressure gradient for different water cuts at averaged V_{so} = 0.14 m/s and μ_o = 12949 cP

Since the trend is different from the same experiments done at lower viscosity for transition phase flow and even more for oil continuous phase flows, it is believed that the high viscosity of the oil is playing huge role toward the oil film coating on the pipe wall and the flow behaviour under these conditions.

4.2.3.2 Heavy oil – water - solid

The heavy oil-water-solid pressure gradients were acquired by varying superficial slurry velocities and solid concentration at two fixed V_{so} (0.10 and 0.14 m/s). These tests covered the range of 0.20-1.22 m/s for V_{ss} and 3 different solid (sand) concentrations (1, 5, and 10%). We should note that sand was observed to settle in the pipe for relatively small mixture velocities (V_{mix} around 0.40 m/s), however that is another parallel work at Cranfield university concerning the sand movements in pipelines (Zorgani, 2011). The scope of this study is to examine the effect of sand presence in the mixed two phase flow (heavy oil-water). The tests were carried to cover the water continuous range only due to the facility limitations. The heavy oil viscosity covered for these tests was around 8200cP.

Table 4-4 shows a simple comparison for two V_{so}, different sand concentration conditions at similar obtained water cuts. The measured pressure gradient was increased with higher sand concentration. This can be related to higher frictional resistance due to the sand existence.

V_{SO} (m/s)	Water cut (%)	V_{mix} (m/s)	Sand concentration (%)	Pressure gradient (kPa/m)
0.10	75.0	0.41	0	1.32
	75.1	0.40	1	1.35
	75.7	0.50	5	2.22
	75.9	0.79	10	3.18
0.14	73.0	0.55	0	1.96
	72.8	0.54	1	2.11
	73.5	0.66	5	2.64
	72.7	0.82	10	3.65

Table 4-4: Pressure gradients comparison for different sand concentrations at the same water cuts

The data of the pressure gradient are presented in graphical format, where they are compared against two phase (heavy oil-water) flow for two fixed V_{so}, 0.10 and 0.14 m/s, in Figure 4-40 and Figure 4-41 respectively. while1% sand case had similar pressure gradient values to the heavy oil-water two phase (no sand) condition due to the difference of μ_o between the runs, as all sand cases were operated around 8200 cP while no sand case had an averaged heavy oil viscosity of 10620 cP. The effect of sand existence in the mixture was concluded as higher pressure gradient values for more sand concentration in the system. This is thought to be related to the increase of mixture density with the increase of sand concentration in the mixture fluid.

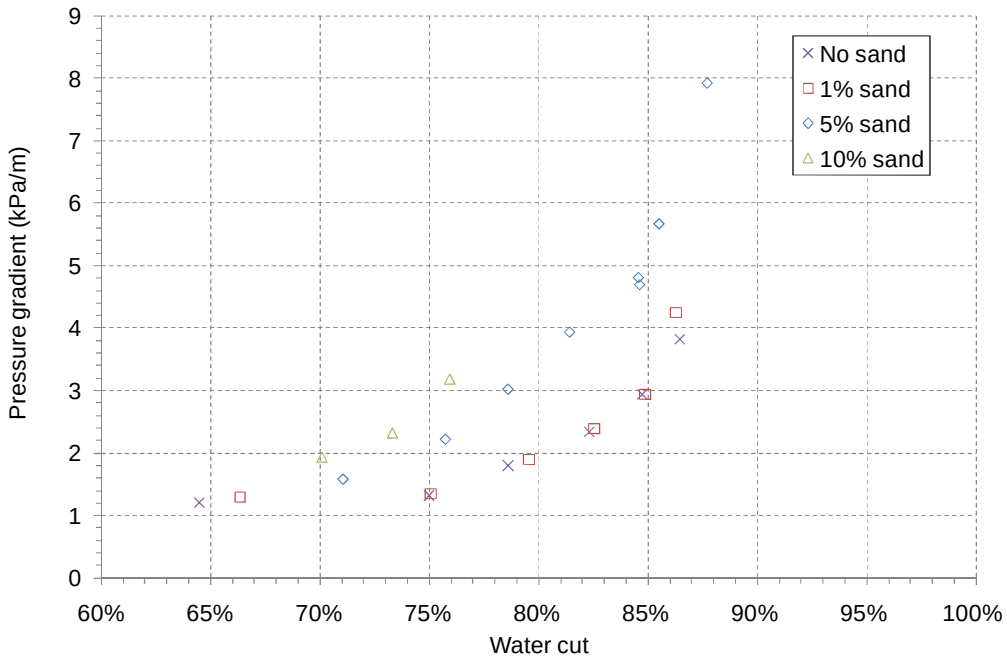

Figure 4-40: Sand concentration effect on measured pressure gradient for different water cuts at averaged V_{so} = 0.10 m/s and μ_o = 8200 cP

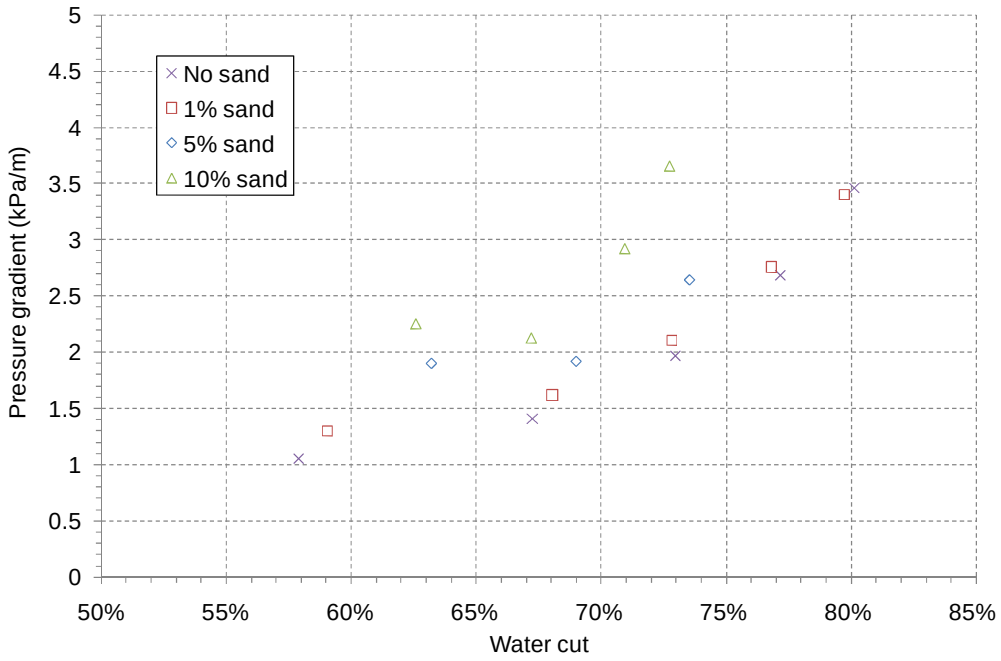

Figure 4-41: Sand concentration effect on measured pressure gradient for different water cuts at averaged V_{so} = 0.14 m/s and μ_o = 8200 cP

5 General discussion and analysis

The general purpose of this study is to determine the effect of each phase found in the reservoir (i.e., gas, water, and solids) against the pressure gradient. The aim to reduce the pressure gradient is essential for pipe design criteria and reduction of the overall required pumping energy; as both are important to deliver the heavy oil from the reservoir to the production sites and refineries.

5.1 Two phase flow

In conventional liquid-gas systems, pressure gradient values were found to be increasing with the increase of gas flow. However in this study, it was found that the change in pressure drop was different for high viscous oil. As a result of acquiring data from water-gas experiments during the commissioning of the 1 inch multiphase test facility, a simple comparison between heavy oil-gas system (μ_o = 4225 cP) and water-gas system at V_l =0.20 m/s obtained experimentally is given in Figure 5-1. The graph shows gradual increase for water while heavy oil has a small decrease of pressure gradient with higher gas flow rates.

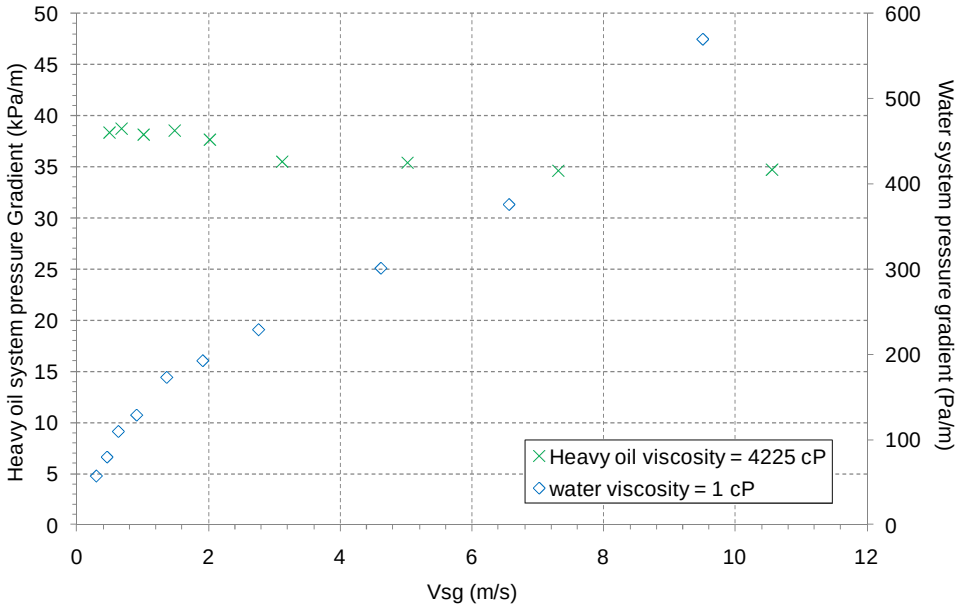

Figure 5-1: Pressure drop trend for liquid-gas system of two different substances (heavy oil and water) at 0.20 m/s liquid superficial velocity.

As mentioned before, this is thought to be an effect caused by the thicker oil coating associated with higher heavy oil flow rate. It was noted that intermittent flow pattern was observed for both cases in this comparison.

The consistency of thicker film coating for higher viscosity conditions was reported by Al-Safran et al.(2011), as they described, along with wavy structure and large entrained bubbles, under high superficial gas velocity.

They also reported that low viscosity liquids (182 cP) have turbulence and mixing in the slug front due to high slug Reynolds number. On the other hand, they found less turbulent with the top boundary layer moving faster than the slug body and entraining large bubbles in high viscosity liquids (590 cP). This is believed to be true as lower slug Reynolds number is associated with this study, however such a mechanism could not be verified due to the significant thick oil film associated with high viscous oil, yet large liquid film height was noticed for heavy oil and gas flow.

The aerated heavy oil can be assumed to have different properties based on deviated behaviour from lower viscous liquids. This was thought to be caused by the gas bubbles in the liquid phase as well as the thick coated film in the gas pocket zone; therefore future physical models should consider these findings for predicting pressure gradients high viscosity liquids.

Finally, based on the results of this study and the findings from the literature, the injection of air to the heavy viscous oil on its own is not the best method to reduce the pressure gradient in the pipe, thus not enhancing the flowing mixture.

On the other hand, the introduction of water to the heavy oil flow reduced the pressure gradient greatly as was shown in result section (Chapter 4.2.2.2). However, many new findings were resulted from the heavy oil-water flow and needed to be explained, compared, and linked to the literature; therefore two individual sub-chapters are presented as follows:

5.1.1 Comparison with published flow patterns from the literature for horizontal heavy oil-water flow

The literature review showed that no generalized flow pattern map for two immiscible liquids in horizontal flow exists; also the information about the flow patterns for heavy viscous oil is exceptionally limited.

The experimental flow pattern map was compared with three different authors; as Trallero (1995) data was compared by many other authors (Yang et al., 2004; Vielma et al., 2007; and Atmaca et al., 2008); while Bannwart et al. (2004), and Vuong et al. (2009) had relatively higher viscosities for their observations. Table 5-1 shows the general conditions and the fluid properties compared with the current study.

Authors	Pipe ID (mm)	Pipe material	μ_o (cP)	ρ_o (kg/m^3)	σ (dynes/cm)	Flow velocity (m/s)
Current study	26	Perspex	3767 to 17070	938.9 to 918	29.7	V_{so} = 0.05-0.58 V_{sw} = 0.008-1.0
Trallero (1995)	50.1	Acrylic	29.6	850	36	V_{so} = 0.01-1.7 V_{sw} = 0.04-0.5
Bannwart et al.(2004)	28.4	PVC	488	925.5	29	V_{so} = 0.007-2.5 V_{sw} = 0.04-0.5
Vuong et al.(2009)	52.5	Steel	220 to 1070	884.4	30.4	V_{so} = 0.1-1.0 V_{sw} = 0.15-1.0

Table 5-1: General conditions and fluid properties compared with this study

In the same region of interest, Trallero (1995) divided his flow map charts into 4 categories: Stratified flow (ST), Stratified with Mixing Interface (ST&MI), Dispersion of Oil in Water over Water Layer (DO/W & W), and Dual Dispersion "dispersion of oil in water and Dispersion of water in oil" (DO/W & DW/O).

Experimental flow pattern map in this study is compared against Trallero (1995) in Figure 5-2

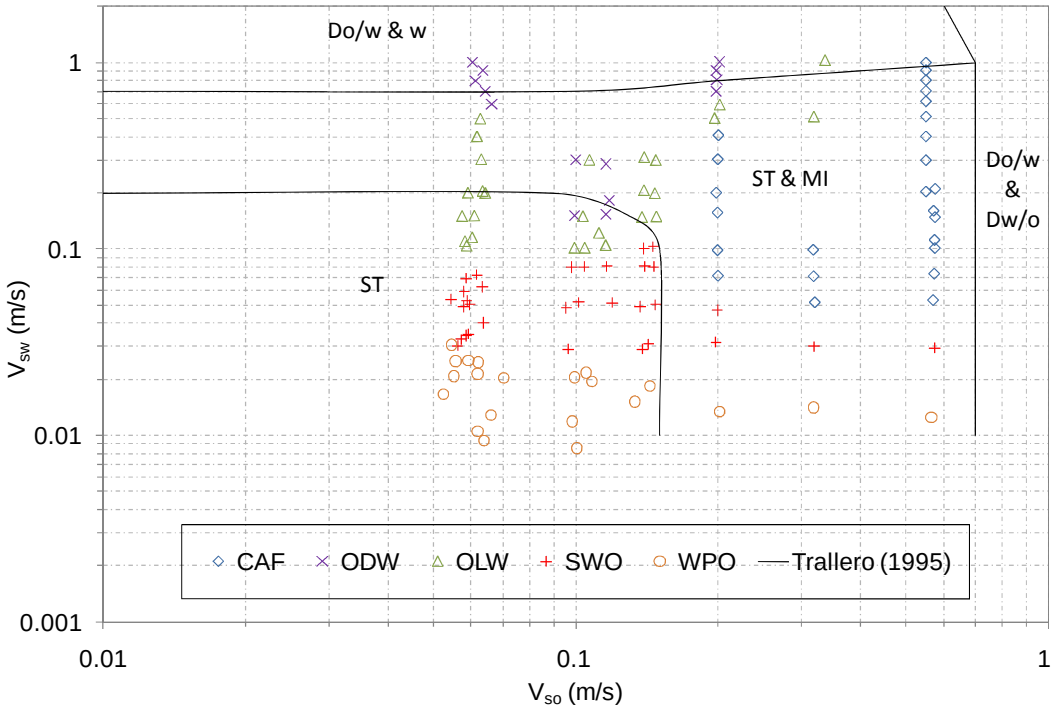

Figure 5-2: Comparison of the experimental flow pattern map with Trallero (1995) typical horizontal flow pattern

It was expected that due to the huge difference between the fluid properties of the two studies, the experimental data in this study would not be located within the Trallero's (1995) boundaries. The similarity only exists around Do/w&w region, as the dispersion of oil in water was due the diffusion of coalescent oil into smaller droplets generating at high V_{so} , the present data showed similar behaviour at that region (ODW) with the exception of having oil coating at the annulus.

With closer pipe sizes and similar fluid properties in their studies (density and interfacial tension), Bannwart et al. (2004) categorized the flow patterns into four main flow patterns: stratified, bubbles, dispersed bubbles (at high water flow rates), and annular. Apart from the oil coating, these categories can be linked sufficiently with the presented data, as both bubbles and dispersed

bubbles are similar to OLW & ODW, the stratified region can be linked with SWO, and finally the annular flow pattern should be compared with CAF. Though more sub-patterns were classified in their study, the experimental data were compared with the main flow patterns for simplicity in Figure 5-3.

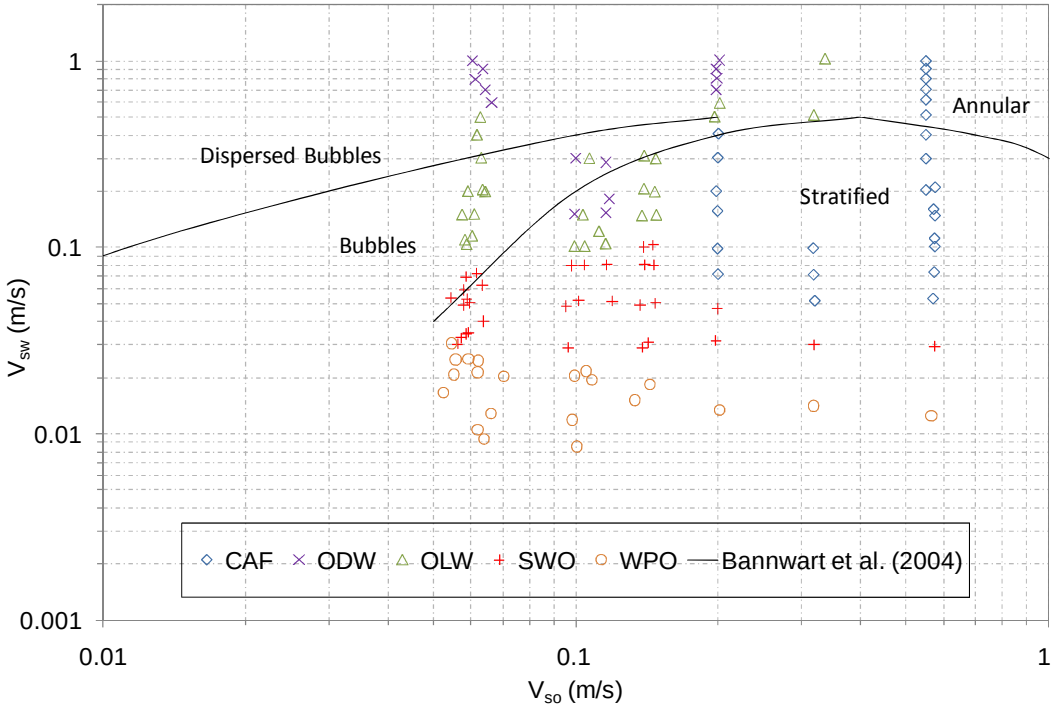

Figure 5-3: Comparison of the experimental flow pattern map with Bannwart et al. (2004) visual Boundary

Despite the transition boundaries, many of the data points, in relatively high water flow rates, are located within their respective regions; as most OLW and ODW are within the bubbles and dispersed bubbles regimes. However this is not the case for the stratified regime, as it intersects with many OLW and CAF found in the current study, if the regime were to be minimized and account for the transition phase only (SWO), then the visual boundary of Bannwart et al.(2004) would be more applicable. It is thought that the large difference of oils viscosity between the two experiments and the pipe wall wettability, olephobic or hydrophilic, played significant role in determining both the transition boundary between the stratified and annular regime, as well as the swirl motion occurring instead of the conventional stratified flow.

More recent study was done by Vuong et al. (2009), as they defined four main flow patterns using sapphire window on a spool piece (yet only three overlap with our region of interest):

1. Stratified Wavy with Oil Droplets at Interface (SW&OI) is similar to the flow pattern (ST&MI) identified by Trallero (1995),

2. Dispersion of Oil in Water over a Water Layer (DO/W&W) is when water phase becomes continuous with dispersed oil droplets at the upper part of the pipe, and

3. Dispersion of Oil in Water and Oil Film (DO/W&OF) is similar with DO/W&W with visual oil film coating on the pipe wall.

SW&OI can be compared to our transition phase (SWO), while both DO/W&W and DO/W&OF are similar with our ODW and OLW in the water continuous phase.

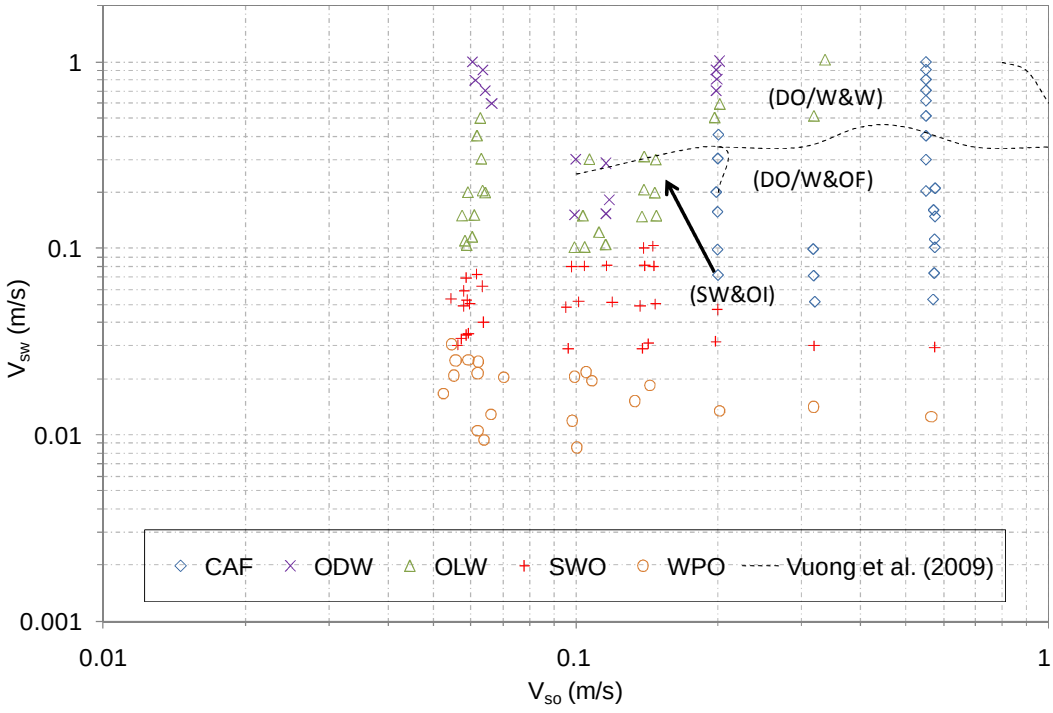

Figure 5-4: Comparison of the experimental flow pattern map with Vuong et al. (2009) visual Boundary

Since lower limit boundary of Vuong et al. (2009) study was determined by the facility limitation at 0.1 m/s for both superficial velocities, SW&OI region was only accounted for small region in comparison with the experimental data of the present work; however if the region was extended for lower V_{so} and V_{sw}, the transition region (SWO) would fairly be located at the same. Also the swirl motion was never reported by the authors, this might be due to the pipe size dissimilarity, and/or, the fluid property difference (especially density). For higher flow rates, though oil coating was found by the authors in their tests, the CAF was never observed.

5.1.2 Comparison with published pressure drops from the literature for horizontal heavy oil-water flow

Though a number of published works have been reported with liquids characterized by low viscosity ratios (Trallero, 1995; Angeli and Hewitt, 2000; Rodriguez and Oliemans, 2006; Vielma et al., 2007; Grassi et al., 2008; Balakhrisna et al., 2010), only limited researches were found in the literature to reflect high viscosity ratios in horizontal flow (Oliemans et al., 1987; Bannwart, 1999; McKibben et al., 2000a).

The experimental data for the pressure gradient were compared to study the effect of the oil density, wettability, and pipe conditions. Most studies had similar oil viscosity around 3000 cP, though Wang et al.(2010) had lower viscosity with similar range of study to examine the phase inversion (i.e. transition phase).

Table 5-2 shows the general conditions and the fluid properties for the authors compared with the current study.

Authors	Pipe ID (mm)	Pipe material	Oil property	μ_o (cP)	ρ_o (kg/m^3)	Flow velocity (m/s)
Current study	26	Perspex	Mineral engine oil	3767 to 17070	938.9 to 918	V_{so} = 0.05–0.58 V_{sw} = 0.008–1.0
Oliemans et al.(1987)	50	PVC	Fuel oil	3000	975	V_{so} = 0.3 – 2.25 V_{sw} = 0.02 – 0.6
Bannwart (1999)	26.7 23.9	Steel Cemented	Fuel oil	2700	989	V_{so} = 0.18 – 0.6 V_{sw} = 0.02 – 0.25
Wang et al.(2010)	25.4	Steel	Crude oil Mineral oil	628.1 620.8	952.66 854.8	V_m = 0.1 – 1.15 w.f.* = 0.1 – 0.7

* w.f. is water fraction

Table 5-2: General conditions and fluid properties compared with this study

Seeing that both Oliemans et al. (1987) and Bannwart (1999) were focussing on the associated pressure drop in CAF with no fouling/coating on the pipe wall, the emphasis of oil coating in this study should to be addressed for all flows associated with water continuous phase (i.e., CAF, ODW, and OPW), shown in chapter 4.2.2.2, Figure 4-33. As discussed previously, big pressure gradient difference between the single phase water flow and corresponding flow of heavy oil and water mixture is observed at water continuous phase. For example at total velocity =0.5 m/s, the pressure gradient was measured around 2 kPa/m in this fouling condition, while the single phase water flow was less than 0.1 kPa/m (also see Figure 4-12 in Chapter 4.2.1); however when we make the same contrast against the findings from Oliemans et al. (1987) in Figure 5-5, the pressure gradient output for the mixture flow was very similar to the water single phase flow.

This was believed to be owing to pipe wall condition, since PVC can be treated as smooth pipe as the pipe roughness for PVC is very minimal (e = 0.0000015 mm). However one might think that pipe ID and density might affect the

pressure gradient, which is true, yet it is believed that the impact of these parameters should not be as significant as the outcome is in this comparison.

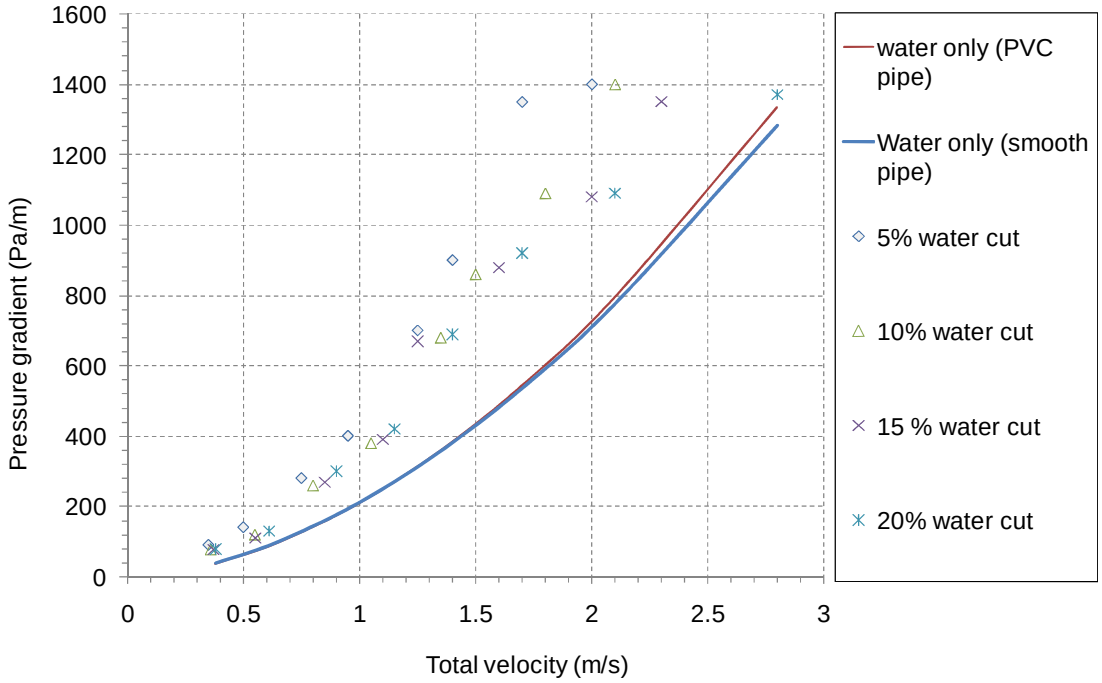

Figure 5-5: Oliemans et al. (1987) pressure gradient data comparison vs. single phase water flow

In fact, the same comparison was done to Bannwart (1999) data to evaluate the pipe material specs, hence pipe wall roughness on the pressure gradient. The obtained pressure gradient data for 1 inch in steel and cemented pipes with predicted values for water single phase flow of smooth pipe are shown in Figure 5-6 and Figure 5-7. For the comparison, the pipe roughness surface was assumed to be 0.00009 mm and 0.0003 mm for steel and cemented pipe respectively.

In Figure 5-6, when the total velocity was smaller than 0.5 m/s, the difference of pressure gradient between the two phase flow and water single phase was less than 100 Pa/m. Though the difference ratio becomes higher at higher mixture velocities, yet it still does not surpass 500 Pa/m when experimenting using steel pipe.

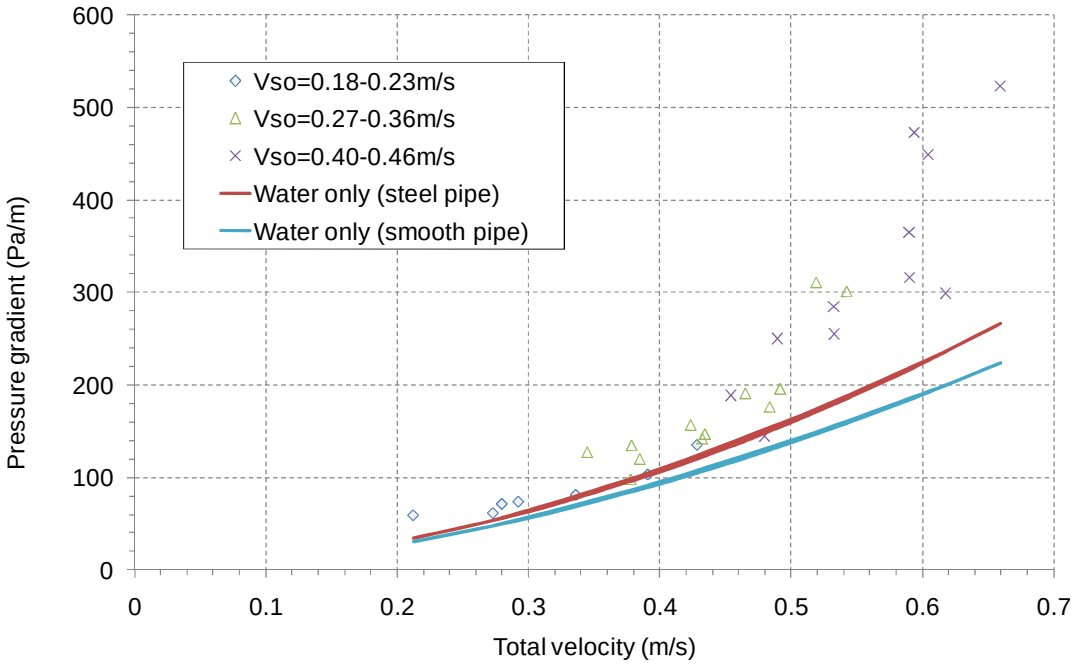

Figure 5-6: Bannwart (1999) pressure gradient data comparison for steel pipe vs. single phase water flow

On the other hand, cemented pipe behaved differently as its higher surface roughness had larger impact on raising the pressure gradient with the total velocity becomes higher (Figure 5-7). The difference was around 800 Pa/m for total velocity of 0.8 m/s. However, this is still much lower than what has been observed in this work, which makes the wall coating/fouling contribution to the pressure gradient much more significant.

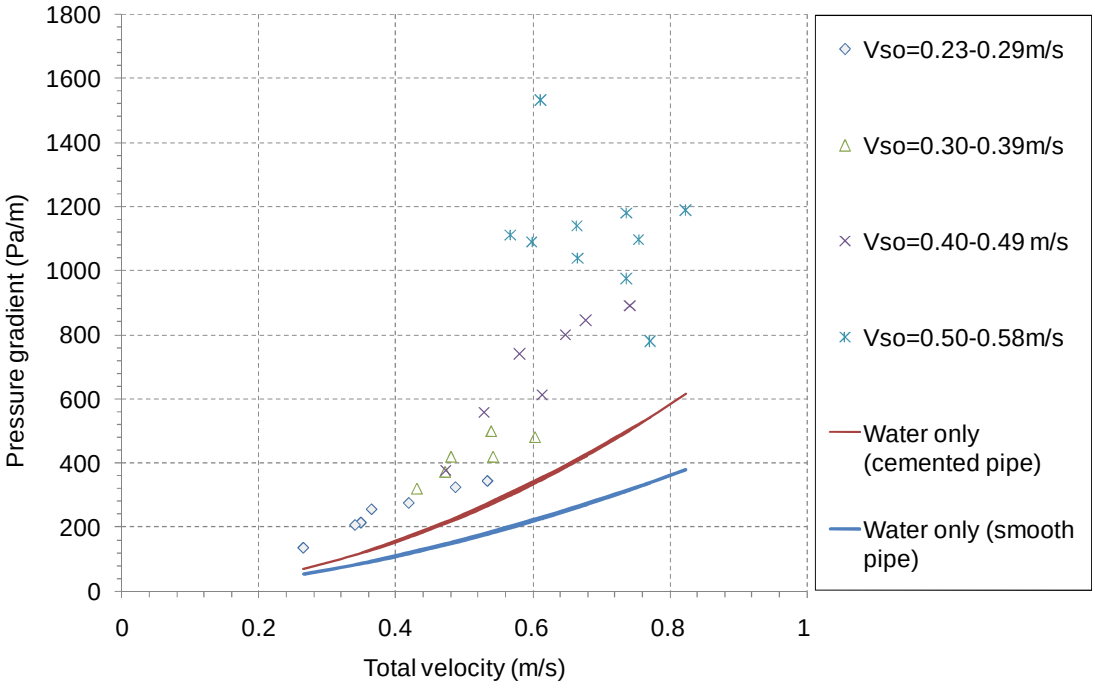

Figure 5-7: Bannwart (1999) pressure gradient data comparison for cemented pipe vs. single phase water flow

One way to quantify the fouling occurrence in the pipe in this work is by considering the Ratio between the Two-phase and Single-phase water (at the same total flowrate) pressure gradients (RTS), defined by Rodriguez et al. (2009) as:

$$\mathbf{RTS} = \frac{\left.\frac{\mathbf{dp}}{\mathbf{dx}}\right|_{\mathbf{oil-water}}}{\left.\frac{\mathbf{dp}}{\mathbf{dx}}\right|_{\mathbf{water}}} \tag{39}$$

Table 5-3 shows the RTS trend as the total velocity of the mixture was increased with 2 fixed oil flows. The resulted ratios between the pressure gradients became smaller as more water was introduced to the mixture, indicating thinner coating on the pipe wall surface as was confirmed by the visual analysis (see chapter 4.1.2). It is worthwhile to emphasize that oil cut is decreasing with lower RTS in this case as a result of introducing more water to the mixture.

V_{so} (m/s)	V_{total} (m/s)	oil cut	Measured pressure gradient for heavy oil-water flow (kPa/m)	Calculated pressure gradient for water flow (kPa/m)	RTS
0.2	0.30	66.7%	1.30	0.06	23.1
	0.50	40.0%	2.45	0.14	17.5
	0.70	28.6%	2.83	0.25	11.3
	1.00	20.0%	3.38	0.47	7.2
	1.20	16.7%	3.87	0.66	5.9
0.57	0.68	83.2%	3.24	0.24	13.5
	0.98	58.4%	3.93	0.45	8.8
	1.28	44.6%	4.27	0.72	5.9
	1.57	36.3%	4.72	1.04	4.5

Table 5-3: RTS comparison at 2 fixed oil flow rates.

Furthermore, RTS value was calculated for different mixture velocity at 3 fixed water flow rates (Table 5-4). The results are similar with the previous comparison, as RTS value decreased with the increase of the mixture flow, indicating less coating on the pipe wall surface as discussed earlier. However due to increase of oil flow is this case, oil cut was boosted to higher values as the mixture flow increased.

V_{sw} (m/s)	V_{total} (m/s)	oil cut	Measured pressure gradient for heavy oil-water flow (kPa/m)	Calculated pressure gradient for water flow (kPa/m)	RTS
0.2	0.26	23.1%	1.54	0.047	32.8
	0.34	41.2%	2.34	0.074	31.6
	0.52	61.5%	2.05	0.095	21.6
	0.77	74.0%	3.9	0.305	12.8
0.5	0.56	10.7%	2.39	0.17	14.0
	0.70	28.6%	2.83	0.25	11.3
	1.09	54.1%	3.97	0.54	7.3
1.0	1.06	5.7%	3.57	0.52	6.9
	1.20	16.7%	3.87	0.66	5.9
	1.57	36.3%	4.72	1.04	4.5

Table 5-4: RTS comparison at 3 fixed water flow rates.

This observation is important as increasing the velocity of any liquid contributed to have less coating on the pipe wall; however maximising the heavy oil flow would be more beneficial in production sites, as both the production rate of heavy oil would be higher and at the same time less fouling/coating on the pipe wall would be associated, as long as sufficient water is presented to maintain the flow in the water continuous phase.

Table 5-5 shows calculated RTS values at different total flow rates for this study and obtained data from the literature. The effect of oil fouling is clearly shown for our acquired data as RTS values rate of change for low V_{total} is much higher when compared against the results of the published work from others.

Collected data	V_{total} (m/s)	Measured pressure gradient for heavy oil-water flow (kPa/m)	Calculated pressure gradient for water flow (kPa/m)	RTS
Current study	0.26	1.54	0.047	32.8
Perspex pipe*	0.50	2.40	0.20	12.0
	1.00	3.38	0.49	6.9
	1.50	4.50	1.00	4.5
Oliemans	0.50	0.14	0.06	2.3
et al. (1987)	1.00	0.40	0.20	2.0
PVC pipe	1.50	0.88	0.45	2.0
Bannwart (1999)	0.30	0.20	0.15	1.3
Cemented pipe	0.50	0.48	0.22	2.2
	0.70	1.00	0.50	2.0
Bannwart (1999)	0.30	0.08	0.06	1.3
Steel pipe	0.50	0.25	0.18	1.4
	0.70	0.52	0.26	2.0

* Oil coating/fouling on the pipe wall surface.

Table 5-5: RTS comparison with the literature for different total flow rates.

The benefit of water addition is not limited to the water continuous phase. In fact, as was shown previously in chapter 4.2.2.2, the addition of water to the heavy oil flow in the oil continuous phase reduced the pressure gradient until it reached the WAF in the transition phase. However at relatively low viscosity

(3911 cP), it has been observed that the addition of water ironically increased the pressure gradient.

Similar behaviour was reported by Wang and Gong (2009) and explained (Wang et al., 2010) as their pressure data tended to increase in low water fractions (i.e. oil continuous phase) in Figure 5-8. They explained this phenomenon by the effective viscosity change of the oil-water mixture and how it can become larger than the viscosity of the oil itself, given that emulsion of water in oil occurred at low water cut. It had non-Newtonian characteristic as the effective viscosity decreases with the increment of mixture velocity, reflecting shear-thinning behaviour of the mixture emulsion.

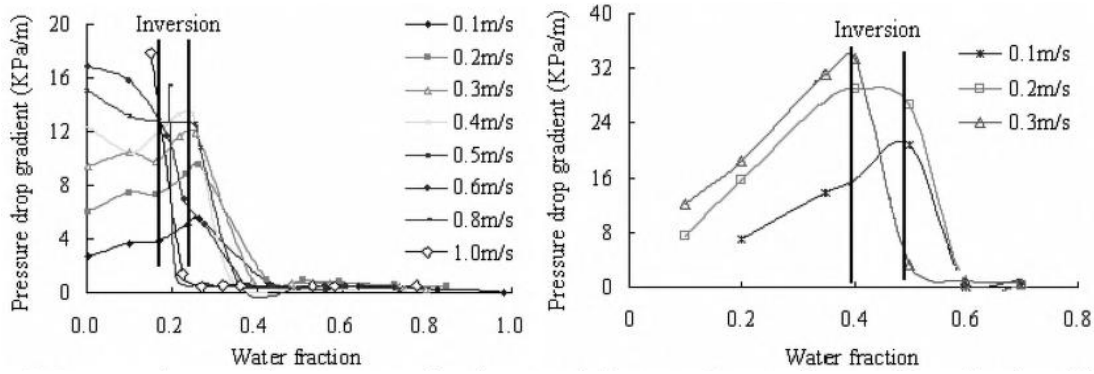

Figure 5-8: Pressure drop gradient vs. water fraction of mineral oil-water (left) and crude oil-water flows (right) (Wang et al., 2010)

However, since this emulsion effect on pressure drop was only observed at 3911 cP oil viscosity in our study and not higher (Figure 4-26, chapter 4.2.2.2), it is believed that the effect of emulsion at low water cut for highly viscous oil (beyond 10000 cP) would be insignificant to the pressure gradient drop. Yet other factors should be considered as the influence of surfactant ingredients and crude oil properties can affect and delay the occurrence of inversion, as asphaltenes and resin have a large hydrophobic hydrocarbon structure containing some hydrophilic functional groups and consequently is surface-active (Wang et al., 2010). Hence, both have potential to form on the water/oil interface, and thus impact the stability of emulsion.

It is noted from Figure 5-8 that their range of WAF is between 20 % to 40 % water cut for mineral oil (left) and 40 % to 60 % water cut for crude oil (right). This might be related to the effect of surfactants, mentioned above, as explained by the authors since both crude oil and mineral oil had approximately the same viscosities. However we should draw attention to the significant difference in density between the two fluids, as it should influence the transition from oil continuous flow to inversion (transition) phase.

Another observation is less water cut is needed to achieve WAF for higher mixture velocity. This is in agreement to our finding we concluded that the actual water needed to achieve WAF is strongly dependent on superficial oil velocity, which will affect the mixture velocity accordingly.

Finally, a simple (generalized) method was needed to quantify the advantage of using different substances to transport very viscous oil; similar to the reduction factor defined by Rodriguez et al. (2009), yet in more general form, the Pressure Gradient Reduction Factor (PGRF) is presented which corresponds to ratio difference of pressure gradient between single phase oil to multi phase flow with oil at the same oil flow rate:

$$\mathrm{PGRF} = \frac{\left.\frac{\mathrm{dp}}{\mathrm{dx}}\right|_{\text{oil single phase}}}{\left.\frac{\mathrm{dp}}{\mathrm{dx}}\right|_{\text{multiphase with oil}}} \tag{40}$$

Based on the equation above, if PGRF value become > 1, the numerator will have higher pressure gradient than denominator and it is beneficial to the reduction factor, though the opposite is also true.

The reduction factor was obtained for two phase heavy oil-water flow at different averaged viscosities, Figure 5-9 and Figure 5-10. Depending on the water input fraction, heavy oil viscosity, and heavy oil superficial velocity, the value of PGRF ranged from less than 1 (where the mixture flow had higher pressure

drop value than heavy oil flow) to 100. This wide range was mainly affected by the flowing condition of the mixture.

In Oil continuous flows, the reduction factor was found to be very low. This Indicate that water input was not sufficient to reduce the pressure gradient of the mixture flow. However with more water is pumped to the mixture, the flow pattern starts to change to transition phase and an increase of PGRF was obtained.

As explained previously in Chapter 4, with the right amount of water needed "to lubricate the flowing mixture", the increase of reduction factor depends mainly on the superficial velocity of the heavy oil. However depending on both the viscosity and the superficial velocity of the examined oil in the mixture, the rate of increase for PGRF can go up to 100 in less than 3% change of water cut (Figure 5-10, V_{so}=0.32m/s and μ_o = 8325cP). This is expected as the denominator in equation (40) becomes very large with higher V_{so} and μ_o while the actual reduction of the pressure gradient measured for the transition phase is also sudden, as shown in Chapter 4 Figure 4-23.

In water continuous phase, the graphs show general trend of having higher PGRF values for low water cuts and high V_{so}, while it starts to decrease gradually with higher water cut. This trend is in partial agreement with other authors (Sotgia et al., 2008; Strazza et al., 2011) as they have steeper reduction factor with the increase of water input. This difference was mainly caused by the unique existence of oil coating on the pipe wall in this study; however as the mixture flow starts to strip more oil from the fouling zone, the reduction slope in this work would become alike with work found in the literature.

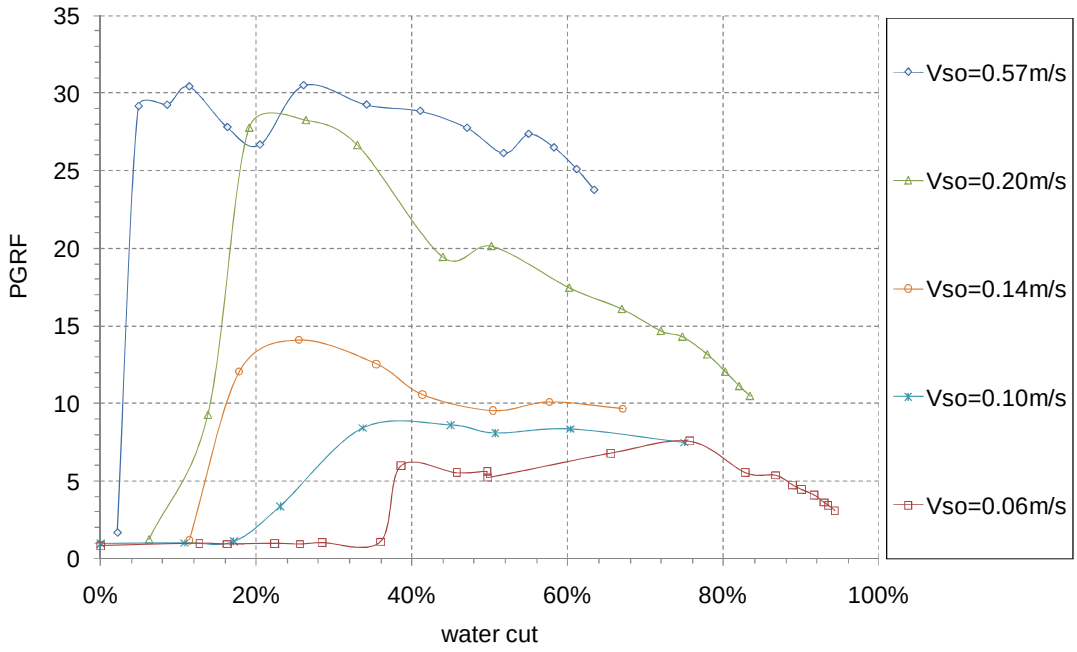

Figure 5-9: PGRF output for 2-phase (heavy oil-water) flow at averaged heavy oil viscosity of 3911cP.

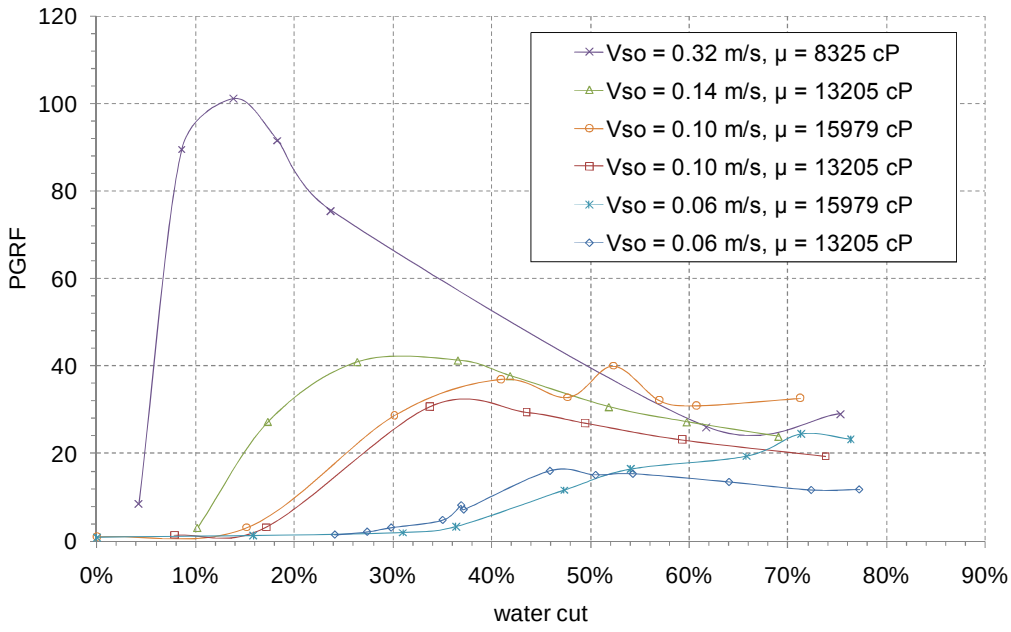

Figure 5-10: PGRF output for 2-phase (heavy oil-water) flow at different heavy oil viscosities.

To summarise the outcome, though most previous work done in the literature try to avoid oil fouling in the pipe to model CAF pattern in pipeline, the work presented in this thesis emphasize the need to replicate the conditions in industrial applications, where occurrence of fouling is almost inevitable. The current study proved that CAF can be obtained with the existence of fouling. Also pressure gradient reduction is not limited to CAF, yet it can be obtained by reaching transition and water continuous flow in general, as WAF covers all the flow patterns associated with it (i.e. ODW, OLW, and CAF). However, it is understandable that the need to maximise the oil production might have the influence to operate at CAF regime as it reaches the highest oil flow rate among all.

5.2 Three phase flow

Though WAF proved to be beneficial to the reduction of pressure gradient (hence reduction of pumping cost), it is not possible to flow oil and water alone in many industrial applications. As oil recovery will have gas presented in the flow and CHOPS will always be associated with large sand concentrations.

The results in section 4.2.3 showed the effect of gas flow and solid existence on the heavy oil and water mixture under different conditions (heavy oil flow rates, water cuts, and heavy oil viscosities). However due to the complexity of the flowing mixture, PGRF method was used to quantify the impact of the mixture flow on the pressure gradient of heavy oil single phase flow. PGRF2 is also introduced to reflect the reduction against heavy oil-water 2 phase flow, as the ratio between the 2-phase to 3-phase flow can be calculated by:

$$\mathbf{PGRF2} = \frac{\left.\frac{\mathbf{dp}}{\mathbf{dx}}\right|_{\mathbf{oil-water}}}{\left.\frac{\mathbf{dp}}{\mathbf{dx}}\right|_{\mathbf{multiphase\ with\ oil}}} \tag{41}$$

Table 5-6 shows the PGRF and PGRF2 obtained in 3 phase flow experiments (heavy oil/water/gas). The reduction factor against single phase flow (PGRF) was always above unity for all phases, though water continuous phase showed best performance as it had highest value among all others. However, to examine the addition of the gaseous phase in the two phase flow, PGRF2 was calculated as well.

PGRF2 showed that the presence of gas in oil continuous phase is ironically beneficial, as this was not the case when gas was introduced to the heavy oil single phase, with values higher than unity. This is thought to be caused by water presence and contribution in the 3-phase mixture. Furthermore, PGRF2 was always lower than 1 in the transition phase, indicating that the pressure gradient measured in the three phase flow was higher than the pressure gradient measurements with corresponding condition of two phase flow; this was expected due to the sensitivity and critical condition associated with this flow, where small change of the flowing conditions can result sudden change of pressure drop as shown previously in Figure 5-9 and Figure 5-10. Finally, the addition of gaseous phase in water continuous flow showed almost no effect as the reduction factor was maintain around unity.

Phase type	V_{so} (m/s)	Water cut (%)	PGRF	PGRF2
Oil continuous	0.06	25	2.7	3.2
	0.10	18	3.0	2.6
	0.14	10	2.0	1.8
Transition	0.06	40	3.0	0.6
	0.10	31	4.7	0.5
	0.14	28	5.0	0.4
Water continuous	0.06	75	5.7	0.9
	0.10	67	9.1	1.1
	0.14	58	10.4	1.1

Table 5-6: PGRF and PGRF2 comparison with different flow types in 3-phase (heavy oil/water/air) flow at averaged μ_o = 3300cP.

The literature indicates (see Strazza et al., 2010) different results for tests done in water continuous phase, as their reduction factor (PGRF2) was always less than unity. This is mainly due to presence of oil coating in the measurements done for 2-phase (heavy oil-water) flow in this study, which will further increase the measured pressure gradient and increase the numerator value in equation (41). We should again emphasize the importance of considering the fouling as it is redundant in industrial applications, as both fouling and oil coating is pipelines is predestined to happen.

Finally the same comparison was done to reflect the addition of solid phase to the heavy oil-water mixture flow. PGRF was above unity for moving sand particles at all examined runs, however the values were getting lower as with the increase of sand concentration. PGRF2 was always lower than unity, indicating that the presence of the solid phase increases the pressure drop respect to the corresponding two-phase (heavy oil-water) flow condition. As reported earlier (Chapter 4.2.3.2), this is thought to be related to the increase of mixture density with the increase of sand concentration in the mixture fluid.

V_o (m/s)	Water cut (%)	Sand concentration (%)	PGRF	PGRF2
0.1	75	0	42.23	1.00
		1	41.31	0.98
		5	25.13	0.60
		10	17.50	0.41
0.14	73	0	28.35	1.00
		1	26.43	0.93
		5	21.10	0.74
		10	15.24	0.54

Table 5-7: PGRF and PGRF2 comparison with different flow types in 3-phase (heavy oil/water/sand) flow at μ_o = 8200cP.

6 Existing models evaluation for two phase flow

6.1 Heavy oil-gas Pressure gradient models

The pressure drop obtained for heavy oil-gas flow was compared against published correlations (Dukler et al., 1964; Beggs and Brill, 1973). All inputs were considered from the injection points for heavy oil properties, while considering the pressurized air properties in the flow line as its density was calculated based on ideal gas equations. Figure 6-1 shows the comparison at very low heavy oil flow rates, V_{so} = 0.03m/s. Although both correlations had good agreement at high gas flow rates with experimental findings; Dukler et al. (1964) correlation over predict the pressure gradient values for V_{sg} < 5.0 m/s, while Beggs and Brill (1973) model under predicted the values for the same range of V_{sg}. This is thought to be due to the wrong prediction of flow regime that these points were covered by Beggs and Bill flow regime map (Figure 4-6, Chapter 4), as it was considering the flow pattern to be segregated while in reality it was observed as intermittent flow. The scattering behaviour of the predicted values around V_{sg} = 2.0 m/s were resulted as an effect of variation of oil injection rate.

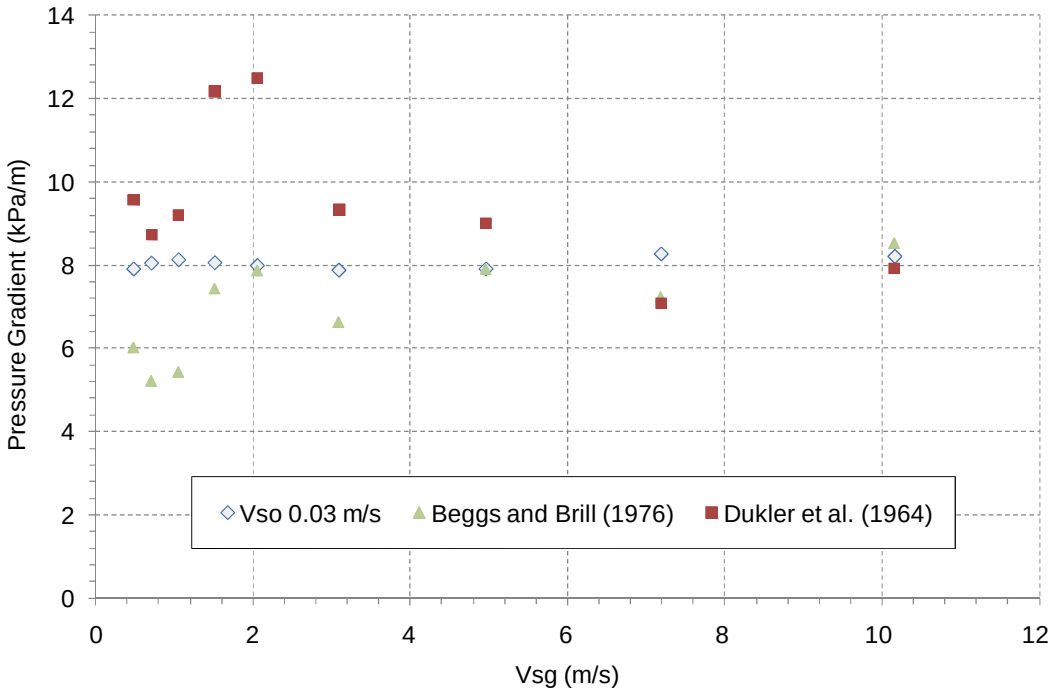

Figure 6-1: Gas injection effect on measured and predicted pressure gradient for averaged V_{so} = 0.03 m/s and μ_o = 3921cP

Table 6-1 shows the result of the correlations predictions for both flow patterns (predicted by Beggs and Brill flow regime map model "segregated" and actual flow observed "intermittent"). Although no significant difference was observed for Beggs and Brill (1973) pressure drop correlation, Dukler et al. (1964) correlation had a higher prediction than it was initially as both correlations were modified to account for this difference, the change has to be addressed to reflect the correct configuration of the tested values.

V_{SO}	V_{SG}	μ_o	Measured Pressure Drop	Intermittent		Segregated	
				Beggs and Brill (1973)	Dukler et al. (1964)	Beggs and Brill (1973)	Dukler et al. (1964)
(m/s)	(m/s)	(cP)	(kPa/m)	(kPa/m)	(kPa/m)	(kPa/m)	(kPa/m)
0.025	0.48	3995	7.90	6.76	11.58	6.03	9.57
0.024	0.71	3981	8.04	6.52	11.22	5.23	8.73
0.020	1.06	3969	8.12	5.46	9.34	5.45	9.20
0.028	1.52	3945	8.05	7.66	13.07	7.44	12.18
0.029	2.06	3909	7.98	7.96	13.46	7.87	12.49
0.025	3.09	3895	7.87	6.91	11.32	6.63	9.33
0.026	4.96	3884	7.90	7.24	11.41	7.90	9.01

Table 6-1: Pressure drop predictions based on both intermittent and segregated flow patterns.

When V_{so} was increased to V_{so} = 0.06 m/s (Figure 6-2), both correlations over estimate the pressure gradient against the measured pressure. Though Beggs and Brill (1973) had similar trend to the measured pressure gradient, while Dukler et al. (1964) gained higher pressure drop values as V_{sg} was approaching 4.0 m/s and then starts to decrease again as it goes beyond that value.

Similar behaviour was achieved by applying the correlations for higher heavy oil flow rates, V_{so} values of 0.10 and 0.20 are shown in Figure 6-3 and Figure 6-4 respectively. The overall predicted vs. measured values for the pressure drop is shown in Figure 6-5, the performance of the two phase models are not very good, in fact the measured pressure gradient values is better predicted using Darcy's equation for laminar single phase flow. It is again believed that heavy oil coating film, from the very high viscous oil, have considerable role toward this difference.

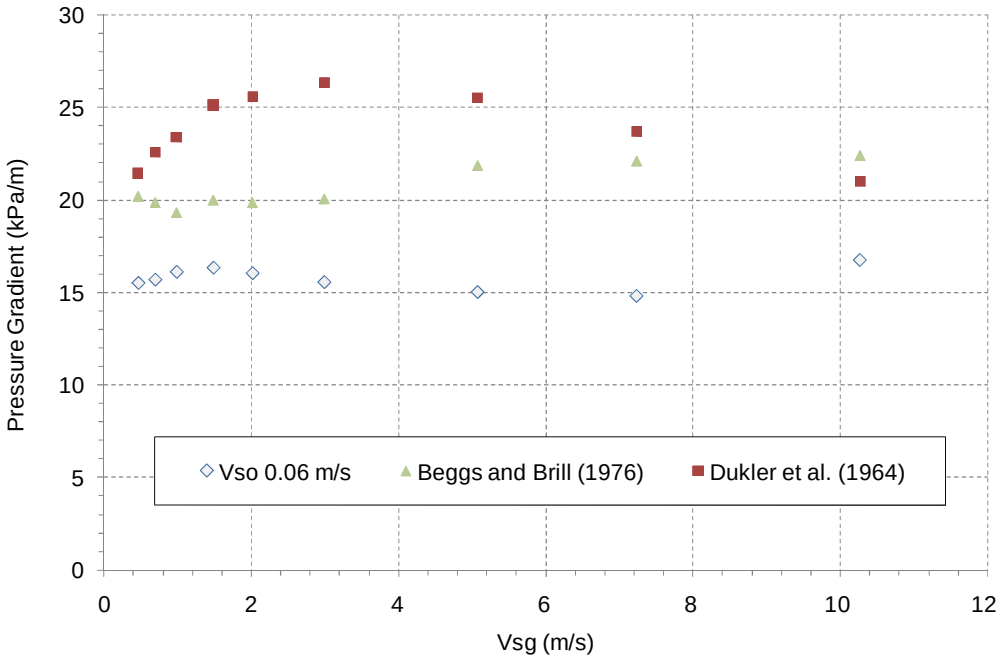

Figure 6-2: Gas injection effect on measured and predicted pressure gradient for averaged V_{so} = 0.06 m/s and μ_o = 4738cP

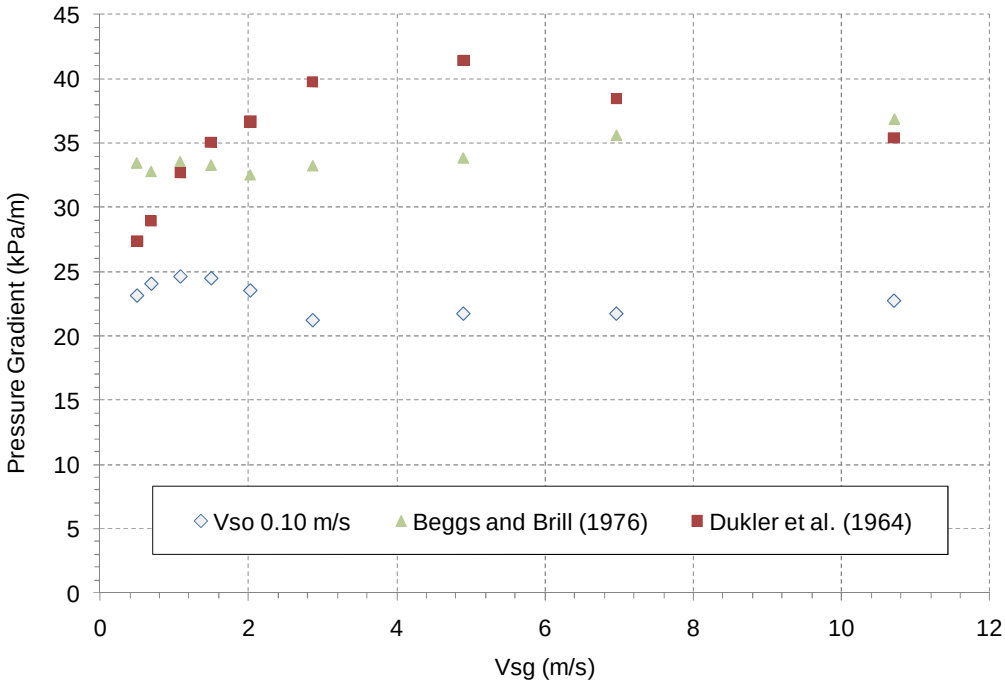

Figure 6-3: Gas injection effect on measured and predicted pressure gradient for averaged V_{so} = 0.10 m/s and μ_o = 4577cP

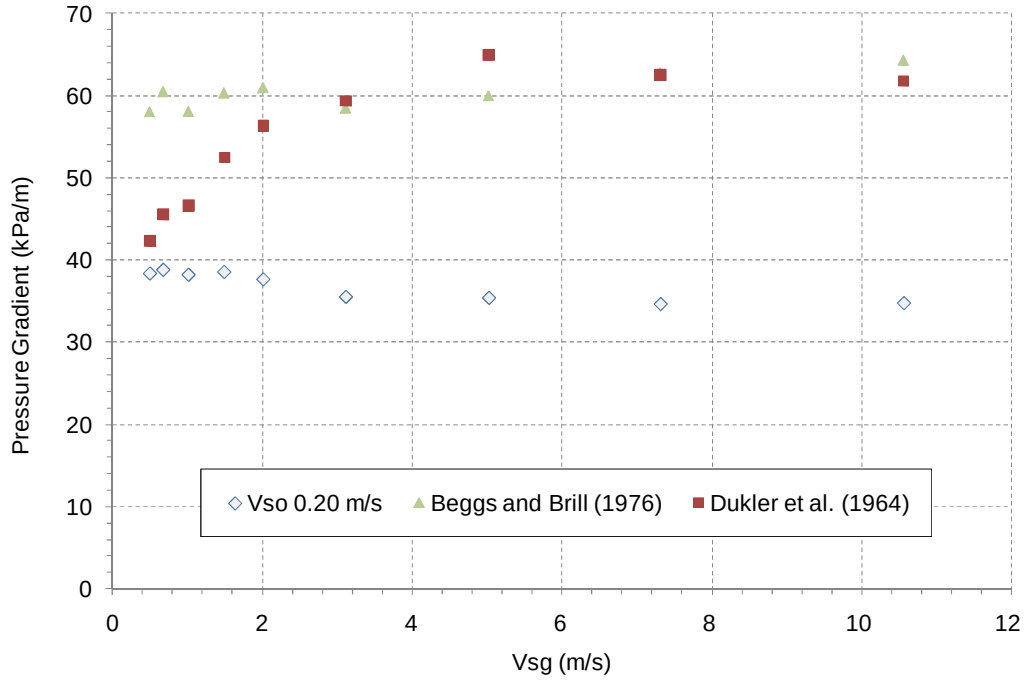

Figure 6-4: Gas injection effect on measured and predicted pressure gradient for averaged V_{so} = 0.20 m/s and μ_o = 4225cP

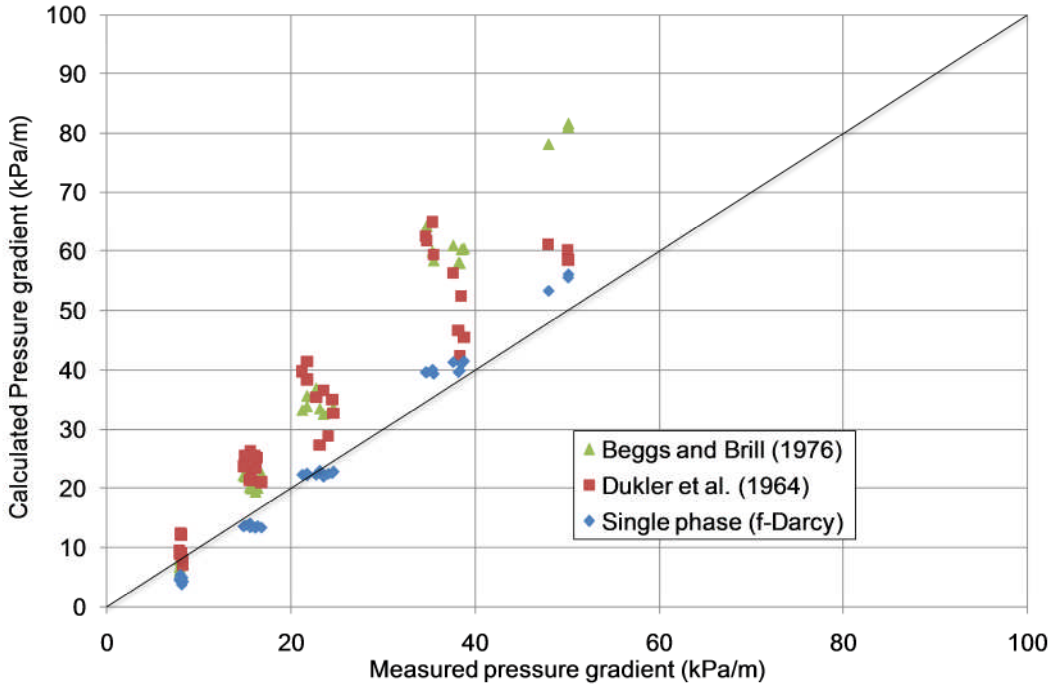

Figure 6-5: Cross plot of models prediction vs. measurement

Finally, the correlations were tested against relatively heavier viscosity oil, averaged around 10605 cP. Darcy's equation for single phase laminar flow was highly under predicting the pressure drop due to the boundary layer thickness effect on higher viscosity as discussed earlier (Chapter 4.2.2.1). Dukler et al. (1964) was found to be under estimating the measured values for most of the presented condition, while Beggs and Brill (1973) had similar trend for V_{sg} lower than 5 m/s and over predicted the pressure gradient for V_{sg} higher than that.

V_{SO}	V_{SG}	μ_o	Measured Pressure Drop	Darcy's equation	P.E.	Beggs and Brill (1973)	P.E.	Dukler et al. (1964)	P.E.
(m/s)	(m/s)	(cP)	(KPa/m)	(KPa/m)	(%)	(KPa/m)	(%)	(KPa/m)	(%)
0.034	0.512	12564	37.64	19.94	-47.01	20.27	-46.15	26.28	-30.18
0.036	0.710	11674	37.09	19.75	-46.76	25.10	-32.34	32.33	-12.85
0.035	0.954	11138	34.77	18.49	-46.82	26.64	-23.40	34.80	0.10
0.037	1.539	10701	34.92	18.67	-46.52	26.89	-22.99	33.22	-4.85
0.040	1.970	10421	33.84	19.50	-42.37	28.25	-16.52	33.82	-0.05
0.039	2.969	10124	32.76	18.87	-42.40	27.61	-15.73	30.22	-7.77
0.041	4.869	9912	31.39	19.17	-38.94	30.78	-1.94	28.33	-9.73
0.044	6.953	9570	29.17	19.94	-31.62	32.79	12.41	28.43	-2.54
0.040	10.072	9341	26.81	17.59	-34.39	29.87	11.42	23.00	-14.20

Table 6-2: Pressure drop predictions vs. measurements for averaged μ_o = 10605 cP.

6.2 Heavy oil-water flow models

6.2.1 CAF prediction validation

In CAF criteria examination, the slip between the two fluids was estimated by examining the video outputs for each individual condition. The slip ratios were obtained by estimating the heavy oil hold up in the pipe for each data point, and calculating the in-situ velocities for the liquids based on their area phase fractions occupying the pipe. The output of this examination can be found in Table 6-3. The resulted figures show a change of slip ratio for different

operational condition. The general trend was observed to be higher slip ratio between the two phases for lower water cuts. Although few differences were obtained for this generalized behaviour, yet these can be linked to the errors of measurements in these estimations as this method does not account for irregularity shapes change of the core nor the amount of oil coating on the pipe wall surface.

V_{so}	V_{sw}	Observed core phase fraction (ε)	Slip ratio	V_o	V_w
m/s	m/s	%		m/s	m/s
0.20	0.07	8%	34.71	2.63	0.08
	0.10	8%	22.50	2.45	0.11
	0.15	6%	19.30	3.09	0.16
	0.20	16%	5.25	1.25	0.24
	0.30	19%	2.89	1.07	0.37
	0.41	9%	5.11	2.28	0.45
0.32	0.05	57%	4.80	0.56	0.12
	0.07	49%	4.81	0.66	0.14
	0.10	40%	4.82	0.80	0.17
0.57	0.05	60%	7.31	0.92	0.13
	0.07	63%	4.58	0.87	0.19
	0.10	50%	5.48	1.10	0.20
	0.15	46%	4.36	1.20	0.28
	0.20	38%	4.50	1.46	0.32
	0.30	33%	3.67	1.64	0.45
	0.40	24%	4.38	2.31	0.53
	0.51	20%	4.43	2.82	0.64
	0.62	19%	3.80	2.89	0.76
	0.70	21%	2.94	2.62	0.89
	0.80	17%	3.26	3.17	0.97
	0.91	15%	3.34	3.58	1.07
	1.00	17%	2.74	3.29	1.20

Table 6-3: Slip ratio outputs for observed CAF

Table 6-3 also show that core phase fraction (ε) can be much less than 50% to achieve CAF, this finding contradicts the very first condition which states that “the core phase must be much thicker than the annulus”.

The volumetric water holdup, H_w, was calculated and compared to the holdup values predicted by Oliemans (1986) and Arney et al. (1993) against obtained water fraction (i.e. water cut), C_w, as shown in Figure 6-6. Since both correlations consisted of determining the water holdup as a function of water cut only, it is believed that the deviation against the experimental values were resulted by the effect of oil coating the wall surface, density difference between the two fluids, and very high viscous oil used in this work.

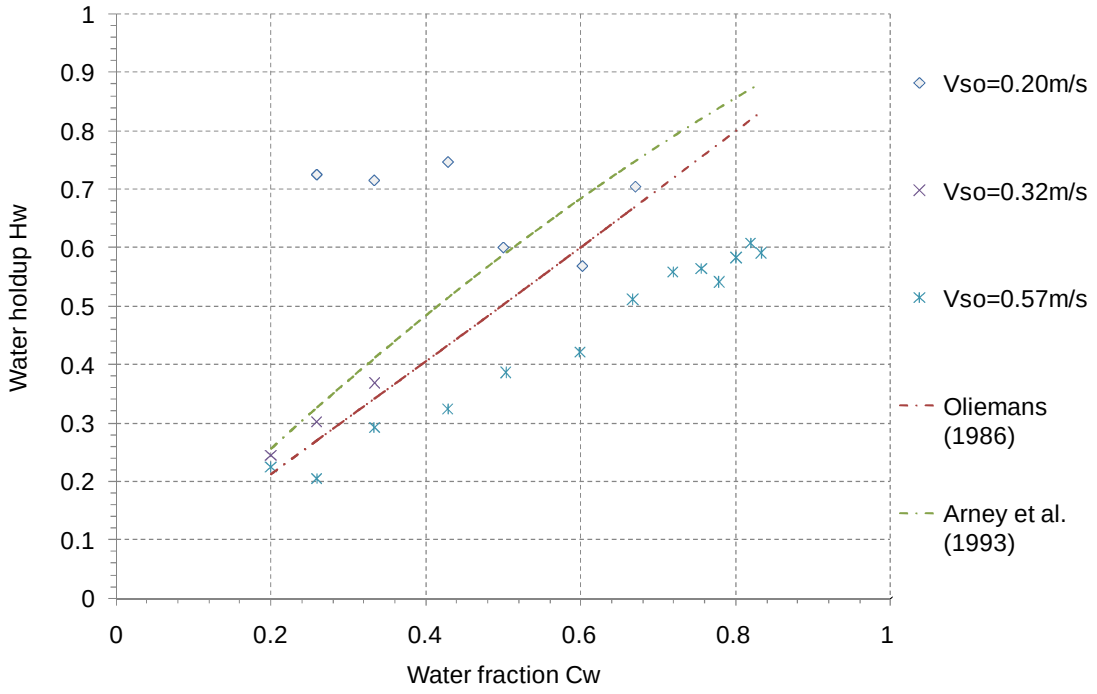

Figure 6-6: Comparison between water fraction and water holdup.

The three criteria refined by Bannwart (2001), which were presented in details previously in Chapter 2.5.3.1, and defined by:

1) $V_{so} > s\, V_{sw}$

2) $\mu_o > \mu_w + 0.0005\rho_w V_{sw} D$, and

3) $8 > \frac{\pi \Delta \rho g D^2 \varepsilon}{4\sigma}$

were implemented and compared against the experimental finding of CAF at this study, shown in Table 6-4, for turbulent annulus flow.

V_{so}	V_{sw}	RHS Value of Criterion			CAF
m/s	m/s	1	2	3	predicted
0.20	0.07	2.49	1.93	0.91	No
	0.10	2.21	2.28	1.02	No
	0.16	3.02	3.04	0.76	No
	0.20	1.05	3.60	1.96	No
	0.30	0.87	4.93	2.27	No
	0.41	2.08	6.28	1.07	No
0.32	0.05	0.25	1.67	6.03	Yes
	0.07	0.34	1.93	5.13	No
	0.10	0.48	2.28	4.23	No
0.57	0.05	0.40	1.7	7.21	Yes
	0.07	0.35	2.0	7.63	Yes
	0.10	0.48	2.3	6.58	Yes
	0.11	0.63	2.4	5.84	No
	0.16	0.72	3.1	5.41	No
	0.15	0.84	2.9	4.90	No
	0.21	0.95	3.7	4.54	No
	0.20	0.95	3.6	3.74	No
	0.30	1.13	4.9	3.27	No
	0.40	1.82	6.2	2.27	No
	0.51	2.35	7.7	1.84	No
	0.62	2.43	9.03	1.81	No
	0.70	2.14	10.14	1.98	No
	0.80	2.71	11.43	1.62	No
	0.91	3.14	12.78	1.43	No
	1.00	2.84	13.96	1.57	No

Table 6-4: Validation of CAF predictions against actual observed CAF

The table shows violations in criterion (1) for most CAF patterns observed in the 1 inch rig, as the Right Hand Side (RHS) values should be lower than corresponding superficial oil velocity; this is related to the stability criterion indicating more viscous fluid (heavy oil) to occupy the cross section area of the pipe than lower viscous phase (water). Though the difference between the core and annulus volume fraction was clearly distinguished by visual observations (Figure 6-7), the oil fouling on the pipe wall surface, dispersed particles of heavy

oil in the annulus phase, and the uncertainties toward the slip calculations are suspected to contribute toward this breach. We should also bear in mind that this criterion was established for two liquids in CAF with the same densities, which is not represented in this study as the densities ratio is around 0.92.

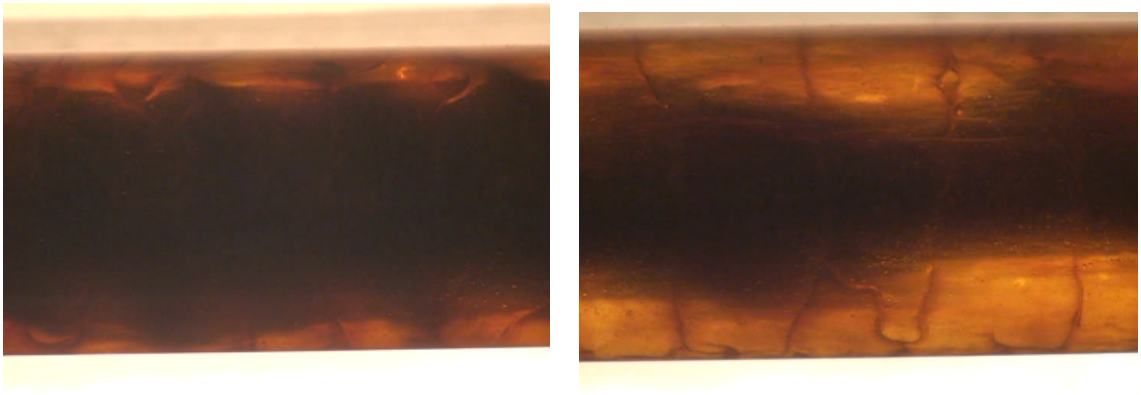

(a) thick core (b) thin core

Figure 6-7: Different observed heavy oil volume fractions in CAF

If criterion (1) was neglected owed to the arguments mentioned above, then all CAF observed in this work would be validated by the other two criteria. Criterion (2) will always be valid for this work as the effective viscosity difference between the two fluids are very high, in favour of heavy viscous oil, which prevent the annulus turbulence from breaking up the core continuity. Finally, criterion (3) relates limit condition of the force associated with the interfacial curvature gradients balances the buoyant force on the core. Stratification was expected to be seen when violating this criterion; however such a flow was never obtained for this range of study.

An exception to the three criteria was given by Bannwart (2001) as “Lubricant input fractions lower than a few percent may cause transition to a dispersion of the lubricant in the viscous phase, which will wet the pipe wall”. This exception was clearly observed, assuming slip ratio to be around 4 based on previous measurement outputs (Table 6-3), in low oil superficial velocities as shown in Table 6-5; however the lubricant input fractions were found to be higher than few percent and obtained at WPO and SWO flow patterns.

V_{so} m/s	water cut	RHS Value of Criterion			CAF predicted	Observed flow pattern
		1	2	3		
0.06	13%	0.04	1.1	7.74	Yes	WPO
	16%	0.05	1.2	6.83	Yes	WPO
0.10	17%	0.08	1.3	6.81	Yes	WPO
0.14	18%	0.12	1.4	6.61	Yes	SWO
0.20	14%	0.13	1.4	7.51	Yes	SWO
	19%	0.19	1.6	6.33	Yes	SWO

Table 6-5: CAF prediction against actual flow patterns

6.2.2 Pressure gradient

Few models have been established to predict the pressure drop associated with CAF pattern. In this section, four models (Arney et al., 1993; Brauner, 2002; Bannwart, 2001; Rodriguez et al., 2009) are presented and applied to the acquired CAF data to examine their validity and helpfulness to understand the mechanism behind the flow behaviour.

The four models were applied for all CAF patterns obtained experimentally. Taking into consideration the measured slip from the video outputs and using the Blasius' friction law values (i.e. b=0.316 and n=0.25) for Bannwart and Rodriguez models. Figure 6-8 shows one set of comparison for the data obtained at V_{so} = 0.57 m/s and different water cuts. Although the graph show a small increase to the pressure gradient as the water cut becomes higher, which is consistent for all the models with the exception of Brauner's model which increases at a higher rate, none of them were in agreement with the measured values due to the oil coating on the wall properties (fouling and wettability) and density difference between the two fluids.

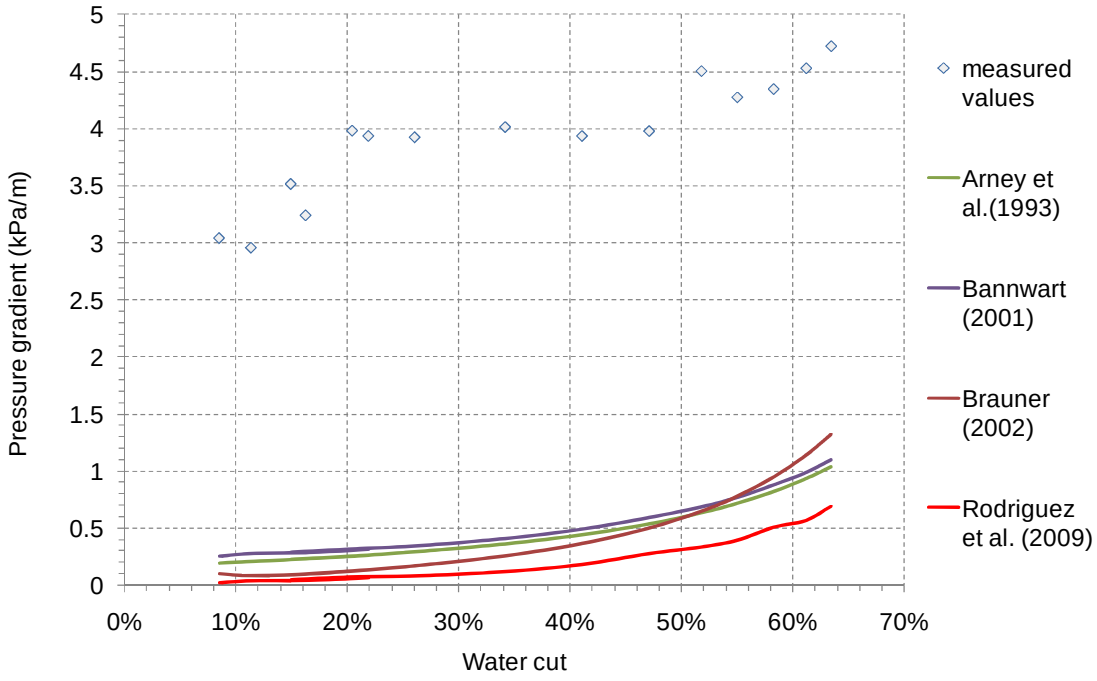

Figure 6-8: Pressure gradient comparison between measured values at V_{so} = 0.57 m/s and calculated using different models (b=0.316 and n=0.25)

More generalised comparison for all the CAF obtained in this study against the different models are shown in Figure 6-9 for the recommended Blasius set (i.e. b=0.316, n=0.25). The performance of all models found to be very poor when compared to the measured pressure gradient for this study. A statistical error analysis was carried out to quantify the performance of each model for the presented CAF data in this study. Three statistical parameters are calculated, namely the Average Percent Error (APE), Absolute Average Percent Error (AAPE), and the Standard Deviation (SD), which are summarized in Table 6-6.

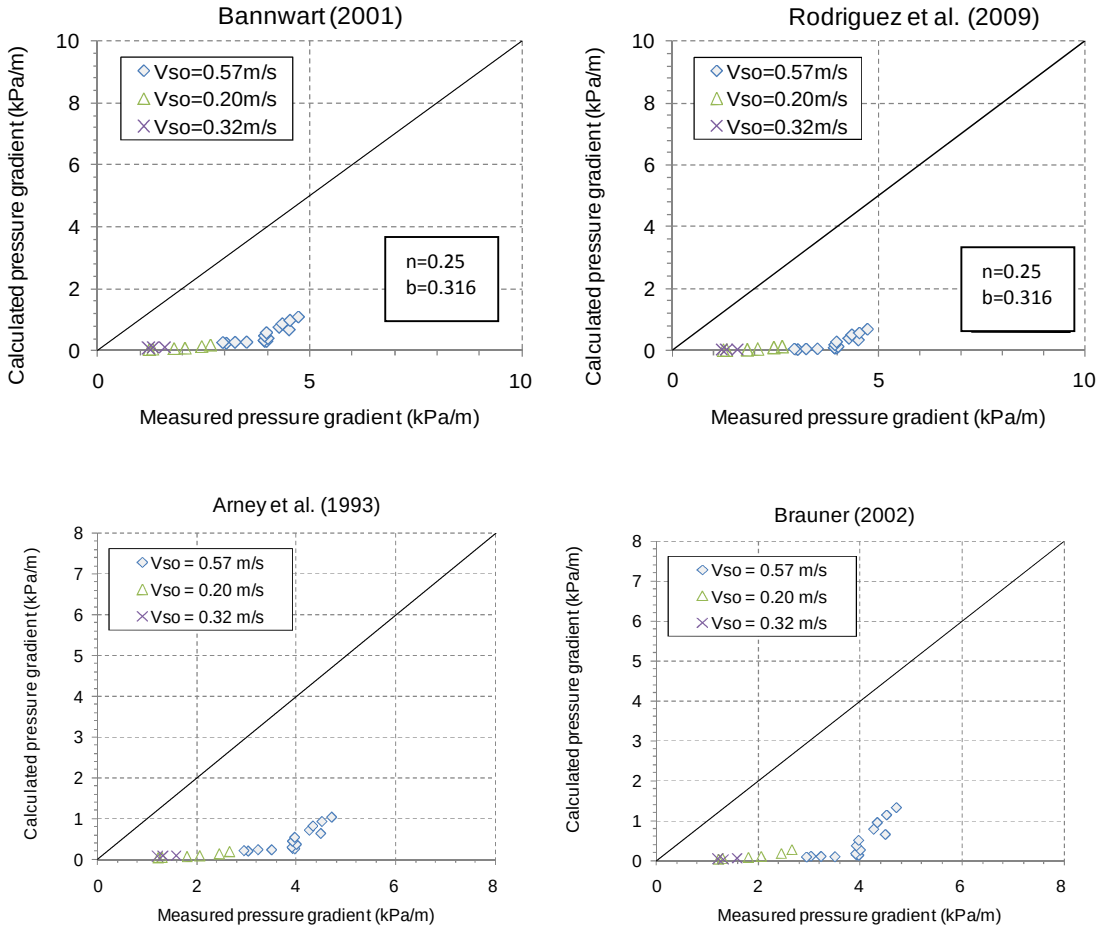

Figure 6-9: Comparison between present pressure gradient data and the four prediction models

Error analysis shows that all the models at their current modes are under predicting experimental data with more than 90% absolute error.

Correlation	APE (%)	AAPE (%)	SD (%)
Arney et al. (1993)	-91.7	91.7	5.67
Bannwart (2001)	-90.9	90.9	5.86
Brauner (2002)	-92.3	92.3	8.11
Rodriguez et al. (2009)	-96.4	96.4	4.33

Table 6-6: Existing correlations comparison

To have a better evaluation of the measured data, the models need to be readjusted. The two-fluid model requires an interactive (numeric) solution of a force balance and the use of suitable closing relations (Ullmann and Brauner, 2004). It requires variables which are not yet well understood, as the structure of the interfacial waves and their effect on the interfacial friction factor. As a consequence of that, the two-fluid model (often) tends to underestimate the frictional pressure gradient at high mixture velocities, this is fairly reported in the literature (for instance in stratified flow, Rodriguez and Oliemans, 2006).

Bannwart (2001) and Rodriguez et al. (2009) correlations were chosen to modify and improved to accommodate the measured experimental values found in this study. As proposed by Bannwart (2001), his model can be tuned by finding the right combination values of b and n to account for pipe wall conditions. The same was proposed by Rodriguez et al. (2009) with the exception of varying one single parameter instead of two. As they showed that by fitting Blasius' friction law coefficient b, it is possible to predict the pressure drop in real fouled pipe with reasonable accuracy.

Overall statistical coefficients of the modified models were obtained to investigate the best approach to modify and choice from the proposed correlations. The Sum of Square of Error (SSE) was used to compute the deviation of the predicted data from the measured pressure drop values; the Mean Square Error (MSE) was obtained to quantify the degree of scatter of the data around the mean difference. By minimizing the SSE through these individual inputs, Investigations were covered for different stages of improvements as illustrated below:

1. Adjusting Blasius' friction law coefficients.

Modified coefficients values were found for both correlations. Figure 6-10 shows the comparison of the between the measured pressure gradient value against the modified obtained Blasius' coefficients for both models, while overall statistical and error analysis is given in Table 6-7.

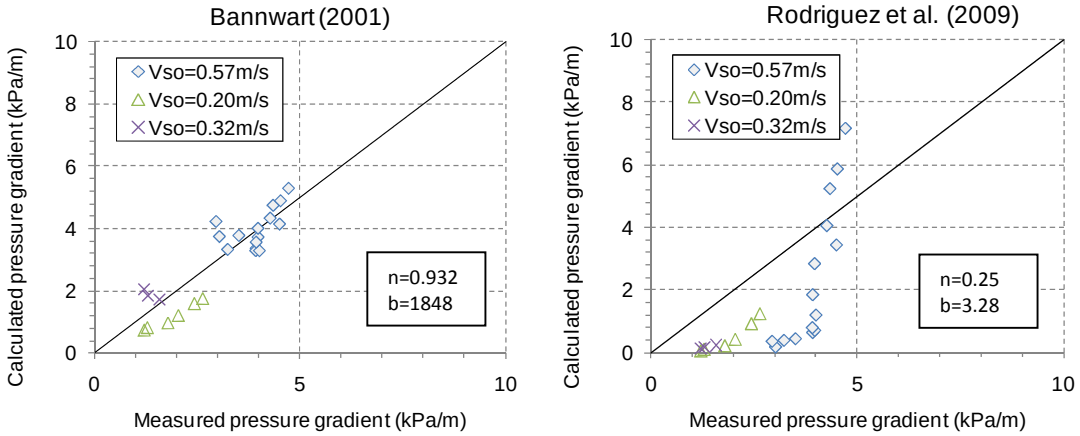

Figure 6-10: Comparison between present pressure gradient data and readjustment coefficients for prediction models

Correlation	n	b	SSE	MSE	APE (%)	AAPE (%)	SD (%)
Bannwart (2001)	0.932	1849	7.9	0.4	-18.6	25.7	23.57
Rodriguez et al. (2009)	0.25	3.279	100.0	4.8	-62.1	68.9	44.98

Table 6-7: Overall statistical and error analysis for stage 1

Rodriguez et al. (2009) model using b = 3.28 and n = 0.25 was still badly predicting the measured values, on the other hand, Bannwart (2001) model had better agreement with b & n equate to 1848 and 0.932 respectively.

2. No slip condition

Though video analysis indicated high slip between heavy oil and water for CAF (Table 6-3 and Figure 6-6), the assumption of no slip condition should be considered as both models, Bannwart (2001) and Rodriguez et al. (2009), assumed relatively much smaller slip ratio between the two phases.

The modified coefficients values were found for both correlations. Figure 6-11 shows the comparison of the between the measured pressure gradient value against the modified n & b coefficients for both models, while overall statistical and error analysis is given in Table 6-8.

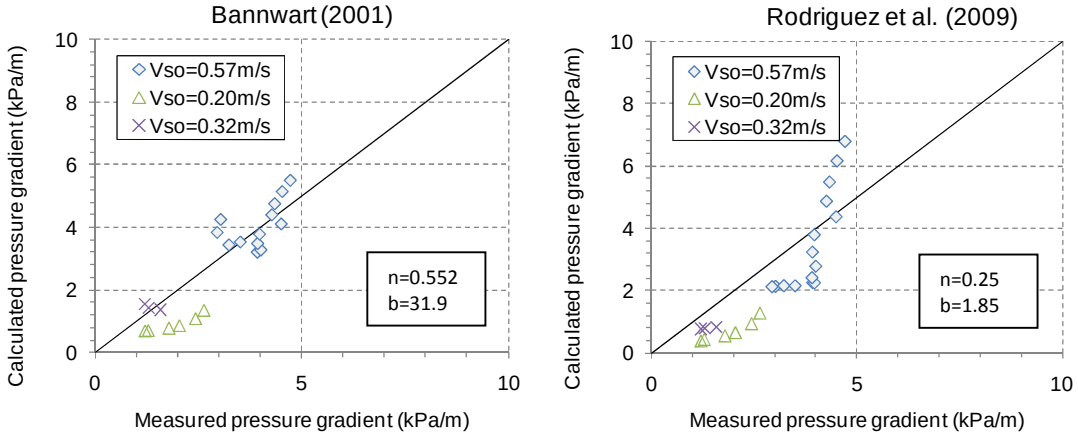

Figure 6-11: Comparison between present pressure gradient data and no slip assumption for prediction models

Correlation	n	b	SSE	MSE	APE (%)	AAPE (%)	SD (%)
Bannwart (2001)	0.552	31.92	12.7	0.6	-25.2	33.1	29.03
Rodriguez et al. (2009)	0.25	1.847	32.4	1.5	-38.9	46.8	34.75

Table 6-8: Overall statistical and error analysis for stage 2

Rodriguez et al. (2009) model using b = 1.85 and n = 0.25 had better prediction when compared with the slip found at stage 1. Bannwart (2001) model had similar estimation with lower b & n values (equating to 31.9 and 0.552 respectively), however it is necessary to point out that it had higher SSE and AAPE than what it was using the slip ratio findings.

3. Proposing fouling/coating parameter.

New coefficient, C, is proposed to account for the fouling observed in the pipe, which can reflects the condition of the pipe. It can contribute toward coating thickness that reduces the effective flowing diameter of the pipe, along with the interface flow roughness between the stationary oil coating layer and the flowing mixture. Bannwart (2001) modified correlation is given as:

$$\frac{dP}{dx} = C + b\left(\frac{\rho_w VD}{\mu_w}\right)^{-n} \frac{\rho_w V^2}{2D}\left[1-\left(1-\frac{\rho_o}{\rho_w}\right)\varepsilon\right]^{1-n}\left[1-\left(1-\frac{\mu_o}{\mu_w}\right)\varepsilon\right]^{-n} \quad (42)$$

While Rodriguez et al. (2009) shall be defined as:

$$\frac{dP}{dx} = C + b\left(\frac{\rho_w VD}{\mu_w}\right)^{-n} \frac{\rho_w V^2}{2D}\left[1-\left(1-\frac{\rho_o}{\rho_w}\right)\varepsilon\right]^{1-n}(1-\varepsilon)^{-n}\left[1+(s-1)\varepsilon\right]^{n-2} \quad (43)$$

By minimizing the SSE with the new parameter, the new modified models were determined for three different cases (Blasius b&n, modified b&n, and no slip condition).

Figure 6-12 shows the comparison of the experimental values against the new modified models with Blasius set values (b=0.316, n=0.25) while considering the new fouling parameter. While both new models have better predictions to the pressure gradients obtained for CAF flow in this study, as C = 2940 & 3175 Pa/m for modified Bannwart (2001) and Rodriguez et al. (2009) respectively, the AAPE associated with both correlations were found to be above 40%. These findings indicate further work is needed to get better performance.

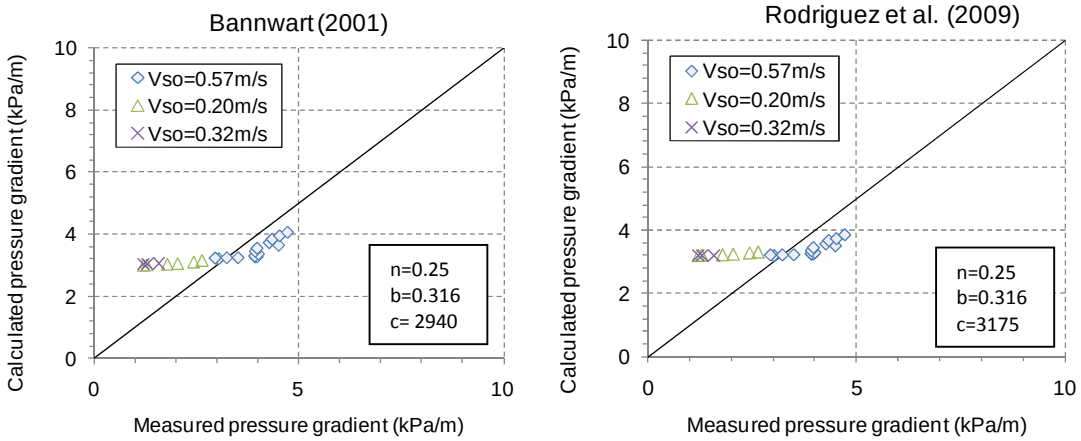

Figure 6-12: Comparison between present pressure gradient data and new fouling parameter for prediction models with Blasius set values.

On these bases, the experimental values against the new modified models were compared while varying the b & n coefficients based on the original authors' recommendations for slip condition (Figure 6-13) and non-slip (Figure 6-14) assumption. Both cases had better performance when put side by side against all previous cases. However by examining the overall statistical and error analysis in Table 6-9, a couple of observations are needed to be highlighted:

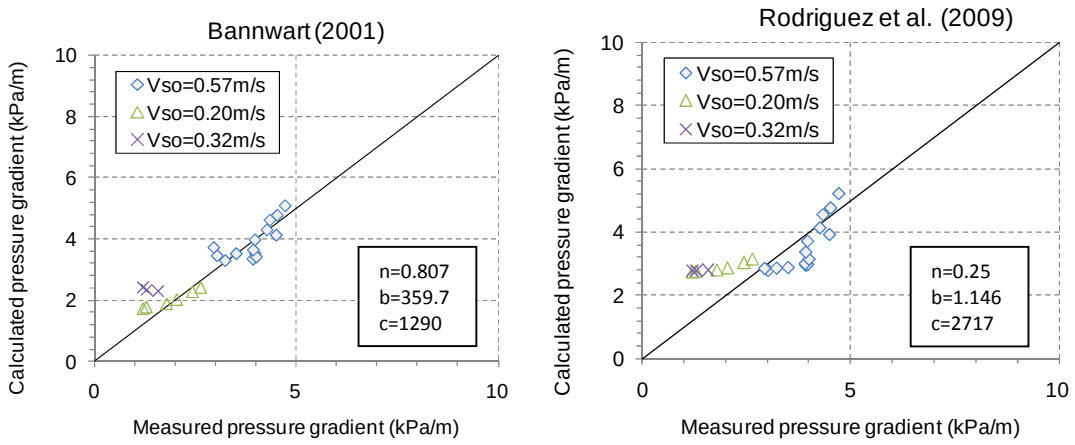

Figure 6-13: Comparison between present pressure gradient data and new fouling parameter for prediction with modified parameter values (with slip)

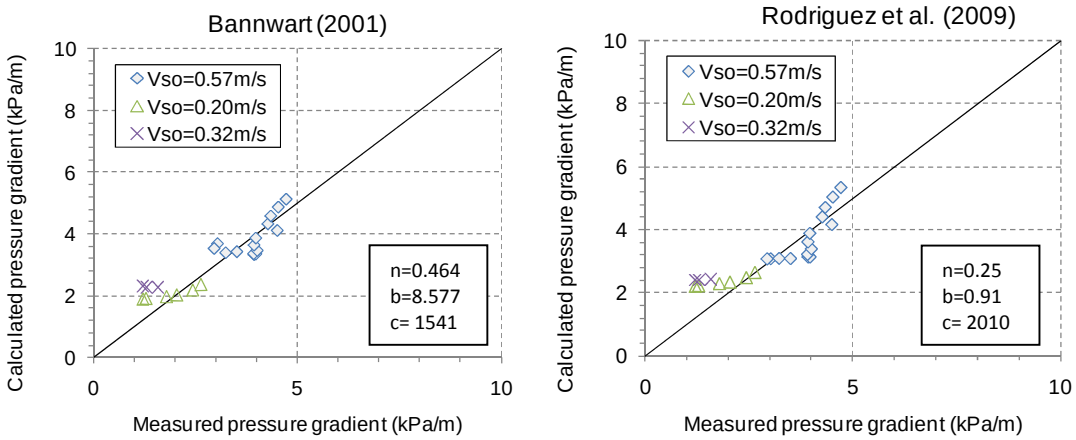

Figure 6-14: Comparison between present pressure gradient data and new fouling parameter for prediction with modified parameter values (no slip)

No slip assumption had the closest Blasius parameters inputs for both correlations with relatively good performance. Modified Rodriguez et al. (2009)

with n = 0.25, b = 0.911, and C = 2010 Pa/m had very good performance when compared with the other cases for the same correlation; while modified Bannwart (2001) performed better with n = 0.464, b = 8.577, and C = 1541 Pa/m. This is believed to be reasonable finding as most of the models validations found in the literature assume no slip condition or relatively smaller slip ratio between the two fluids than the high slip ratio found in this study.

Finally, Modified Bannwart (2001) model had the best performance for the slip case with parameters values of n = 0.807, b = 359.7, and C = 1290 Pa/m with slight over prediction and 9.6% absolute error, and data dispersion around this model represented by standard deviation of 15.49%, which is considered low.

Correlation/condition	n	b	C (Pa/m)	SSE	MSE	APE (%)	AAPE (%)	SD (%)
*** Blasius values**								
Bannwart (2001)	0.25	0.316	2940	13.8	0.7	30.87	42.45	47.26
Rodriguez et al. (2009)	0.25	0.316	3175	17.8	0.8	35.13	48.32	52.92
*** Modified b&n with slip**								
Bannwart (2001)	0.81	359.6	1290	3.0	0.1	4.96	9.60	15.47
Rodriguez et al. (2009)	0.25	1.146	2718	12.0	0.6	25.77	37.56	41.47
*** Modified b&n with no slip**								
Bannwart (2001)	0.464	8.577	1541	3.8	0.2	6.84	12.29	19.17
Rodriguez et al. (2009)	0.250	0.911	2010	5.7	0.3	13.39	20.90	26.14

Table 6-9: Overall statistical and error analysis for stage 3

To summarize the findings, phenomenological models drove from PCAF showed better pressure gradient predictions with the new adjustments for pipe wall condition, modified Bannwart (2001) model gave finer predictions to Rodriguez et al. (2009) as the effect of viscosity difference was emphasized, while Rodriguez model relayed more on the effect of buoyancy between the two "equal densities" fluids.

6.2.3 WAF criterion

As shown from previous graphs, the achievement of water assist flow depends on both mixture velocity and water cut, whereas less relies on the oil viscosity.

Therefore, water cut and mixture velocity are two major factors which is needed to be considered in heavy oil pipeline design.

McKibben et al. (2000a) introduced modified Froude Number to account for the effects from both mixture velocity and water cut in pipeline design (Figure 6-15), which suggest dimensionless group expressing the ratio of inertial to gravitational forces to be considered against water fraction.

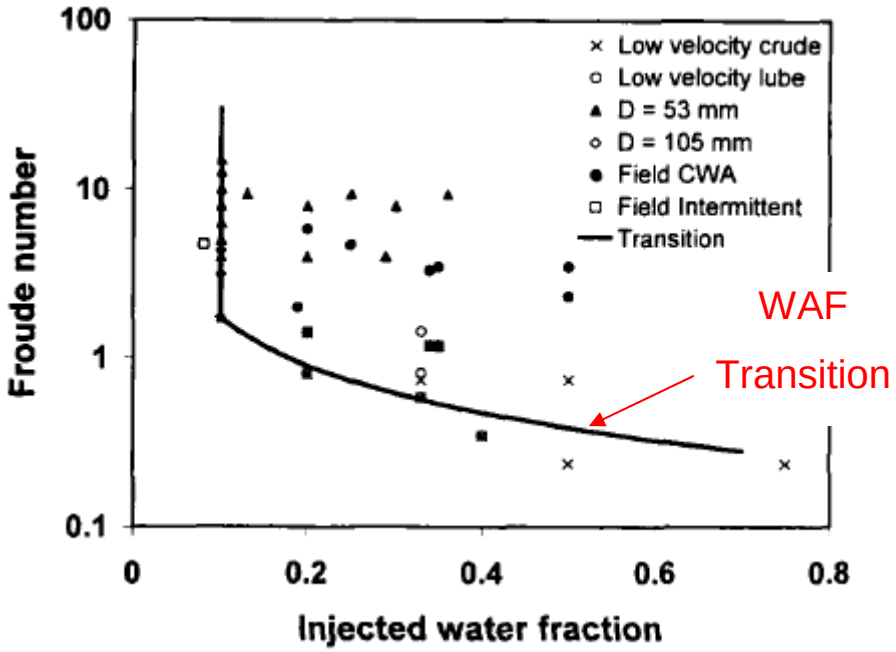

Figure 6-15: WAF criterion from McKibben et al. (2000b)

The area above the transition line represents the condition that WAF can be achieved. Once the operating condition falls below the transition line, the WAF cannot be achieved. The Froude Number used was a densimetric Froude Number, which represents the ratio of inertial to buoyancy forces. It was illustrated as:

$$Fr = \frac{V_m}{\sqrt{gD\left(\frac{\rho_w - \rho_o}{\rho_w}\right)}} \qquad (44)$$

The transition line can be represented mathematically as:

$$\mathrm{Fr} > \frac{0.2038}{(\text{Water cut})^{0.934}} \text{, for water cut} > 0.10 \qquad (45)$$

Based on the definition of WAF given in the previous section, Figure 6-16 shows the WAF conditions plot along with the WAF transition line proposed by McKibben et al. (2000b).

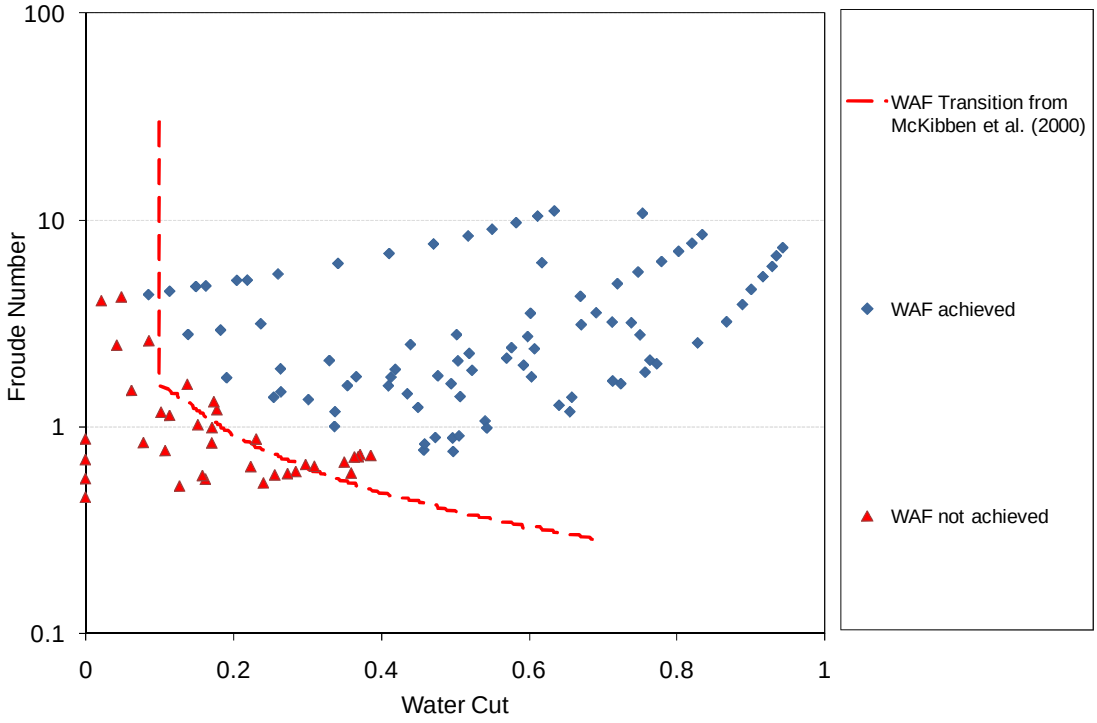

Figure 6-16: Comparison between experimental WAF conditions with McKibben WAF transition boundary (2000b)

It was found that the transition boundary proposed by McKibben et al. (2000b) could predict the experimental WAF conditions fairly well. However some discrepancies were found around the transition line, as WAF condition was achieved with few percent water cut higher than predicted for V_{so} = 0.06 m/s ; while lower water cut was required to achieve WAF at highest V_{so} run (equating to 0.57 m/s). These differences are thought to be caused by the difference of superficial oil velocity used in this study, as it was quite low compared with McKibben's data; also the pipe diameter difference was brought to attention as it might be a factor as McKibben's data were collected for higher pipe diameter.

The transition boundary was plotted against the flow patterns observed in this work as shown in Figure 6-17. The transition boundary mainly covered the change of flow pattern from WPO to SWO; this indicates reasonable prediction as the minimum pressure gradient value was found within the SWO phase as mentioned previously in Chapter 4.2.2.2 Figure 4-32

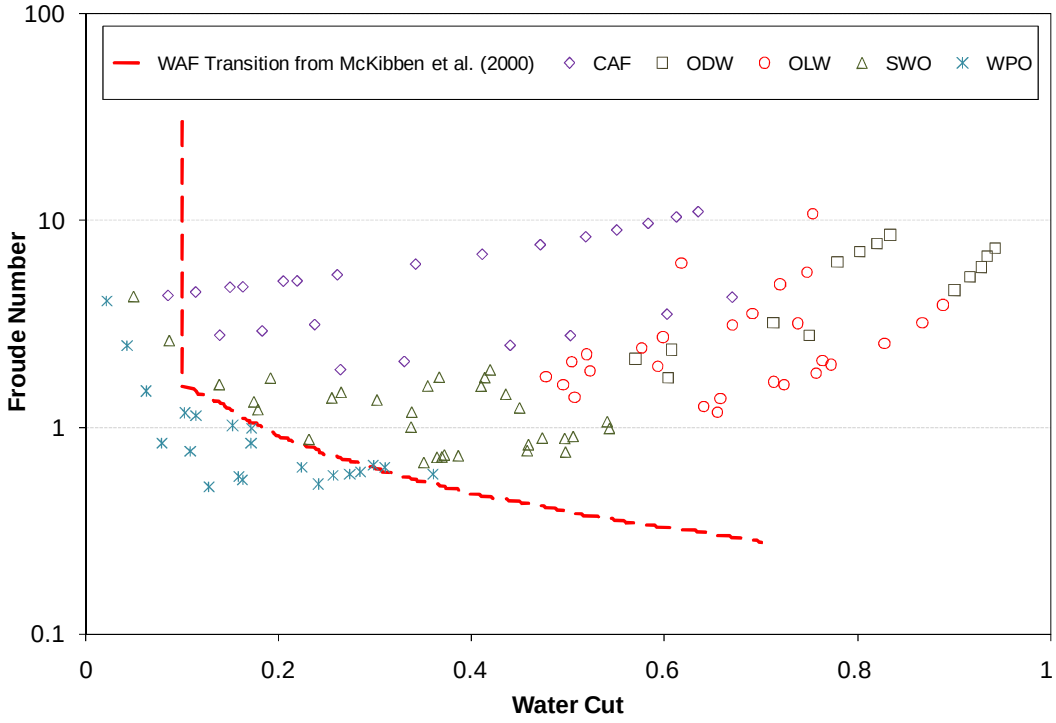

Figure 6-17: Comparison between experimental flow patterns and McKibben WAF transition boundary (2000b)

The three phase (heavy oil/water/gas) experiments were also examined with WAF condition (Figure 6-18). This shows clearly the effect of gas is not detrimental once the WAF criterion is satisfied.

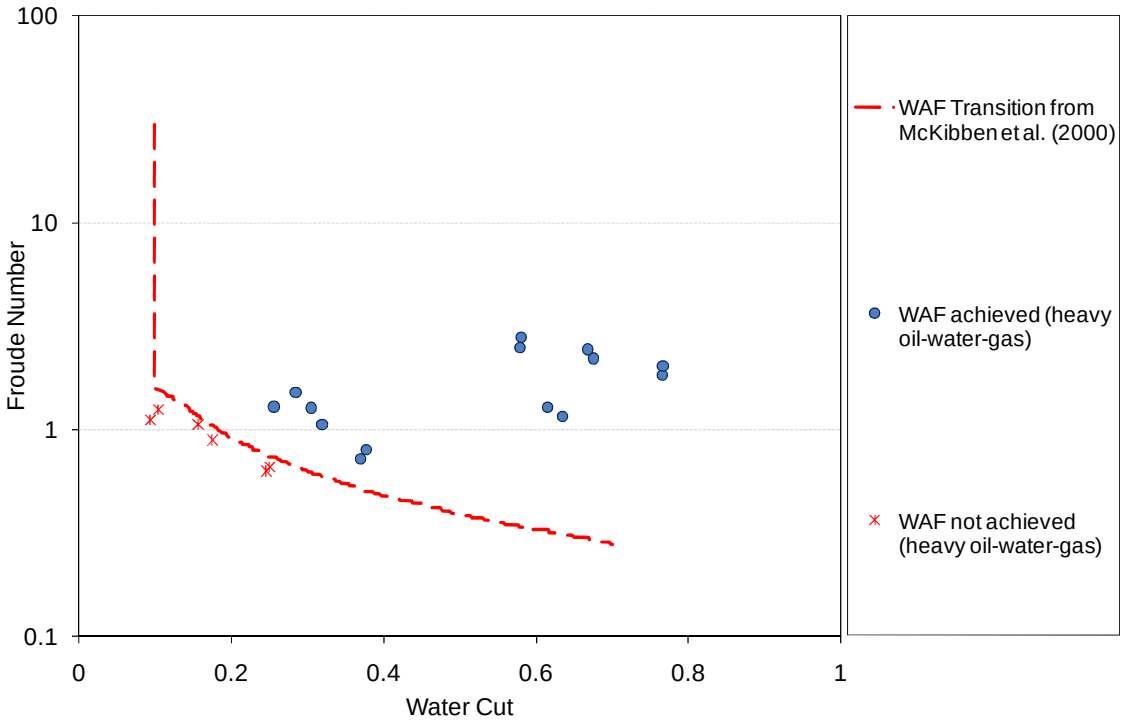

Figure 6-18: Comparison between three phase flow (heavy oil-water-gas) and McKibben WAF transition boundary (2000b)

7 Conclusions and recommendations

The main conclusions drawn from the work described in the thesis are presented in Section 7.1. This is then followed by recommendations for future experimental and analytical work in Section 7.2.

7.1 Conclusions

The main conclusions arising from the present study are as follows:

7.1.1 Conclusions from studies of flow patterns in two phase flows

A major series of experiments on two phase flow (liquid-liquid and liquid-gas) have been conducted over a range of viscosities using the Cranfield University 1 inch multiphase flow facility. The experiments covered horizontal flow and the results were as follow:

- **Observations of flow patterns in heavy oil/air.** These were primarily based on detailed examinations of the video recordings taken for each experiment. Intermittent and segregated flow patterns were distinguished (chapter 4.1.1, Figure 4-1) and classified in this work for different heavy oil viscosities. This combination of flow arise many complexities in analysis, mainly due to the dark colour of the heavy viscous oil and liquid coating associated with the different types of flows. ECT technology showed high potential in giving qualitative information about the flow patterns and phase distribution in the pipe (Appendix B). Used widely in the hydrocarbon industry, Beggs and Brill (1973) flow regime map model was compared with the experiment data but could not predict the transitions of the observed flow; therefore new models should be developed to predict flow patterns more accurately for high viscosity oils.

- **Observations of flow patterns in heavy oil/water.** Three main flow patterns were initially categorized (i.e. oil continuous, water continuous, and transition phase), however five new flow patterns were sub-divided

(namely WPO, SWO, OLW, ODW, and CAF) from conventional definition due to their uniqueness. Retention of water film at the pipe wall was found not essential to obtain CAF “with oil coating” in a pipe, and the variation of viscosity had no significant effect on the observed flow patterns. Flow regime map was generated for these conditions and compared against different data found in the literature; the complexity of the flow patterns found not only depended on the configurations of the pipe properties, length, orientations, and flowing conditions, but also by the actual properties of the examined fluids as well. Since each can contribute toward the rate of exchange of mass, momentum and energy between the different fluid phases in the internal phase distribution.

7.1.2 Conclusions from studies of pressure gradient in single phase, two phase, and three phase flows

The pressure gradient have been experimentally obtained for different phase flows over a wide range of different heavy oil viscosities and operational conditions, to determine the effect of each additional phase on the pressure drop, using the Cranfield University 1 inch multiphase flow facility. The experiments results were:

- **Pressure gradient measurements on heavy oil flow.** General trend of increasing pressure drop with the increase of superficial velocity of the single phase flow was found. Also the rise in heavy oil viscosity led to an increase of pressure gradient and the flow was always in laminar region, over the range of conditions studied.

- **Pressure gradient measurements on heavy oil/air flow.** The pressure gradient increased with increasing liquid velocity and viscosity. The effect of gas in the flow was complex; the pressure gradient was slightly increasing, decreasing, or maintained around the same value with the increase of gas flow, depending on the flow conditions.

- **Pressure gradient measurements on heavy oil/water flow.** Two distinct trends were found depending on the flow conditions. The pressure was mostly decreasing with the increase of water cut in oil continuous flow and increasing with higher heavy oil flowrate; on the other hand the mixture flow pressure gradient would start to increase again after achieving WAF in transition and water continuous flow. Though heavy oil viscosity is very essential to consider at oil continuous phase flow on pressure drop, it had no significant effect beyond WAF condition.

- **Pressure gradient measurements on heavy oil/water/sand flow.** Solid existence in the mixture flow led to minor increase in the pressure gradient when the particles are moving with the flow, higher pressure gradient values were found for more sand concentration in the system.

- **Pressure gradient measurements on heavy oil/water/air flow.** For the later series of tests, the effect of gas flow on liquid mixture flow was complex, pressure gradient either increased or decreased with increasing gas flowrate, depending on the flow conditions; as the addition of gaseous phase was beneficial when introduced to (two liquid mixtures) oil continuous phase, had negative result at the transition phase, and no significant effect on water continuous phase for the pressure gradient. However the addition of both water and air to the heavy oil single phase flow was always beneficial toward reducing the pressure gradient.

7.1.3 Conclusions from modelling studies on two phase flow

The two phase flow (liquid/gas and liquid/liquid) were obtained and compared against different numerical models found in the literature. The main findings were as follow:

- The experimental pressure gradient obtained for heavy oil-air flows were compared with Dukler et al. (1964), Beggs and Brill (1973), and single

phase liquid correlation using Darcy's friction factor. The existing correlations predictions under high viscosity oil condition were discrepant and new high viscosity oil correlation is needed, as the performance of the two phase models were not very good, in fact the measured pressure gradient values were better predicted using Darcy's pressure drop correlation for laminar single phase flow.

- Obtained pressure drop in CAF were compared against four prediction models (Arney et al., 1993; Bannwart, 2001; Brauner, 2002; Rodriguez et al., 2009). All tested models were greatly under predicting the pressure gradients mainly due to the coating (oil fouling) effect associated with this study.

- Furthermore, Bannwart and Rodriguez et al. models were tuned (as suggested by the authors) to account for fouled pipes. By using the optimised coefficients to estimate the pressure gradients, better prediction was obtained between the experimental data and Bannwart model (though the Absolute Average Percentage Error "AAPE" was still large).

- New coating coefficient was introduced to Bannwart (2001) and Rodriguez et al. (2009) work and tested against the obtained experimental data. Model validation showed accurate performance of the suggested correlation.

- The WAF transition line proposed by McKibben et al. (2000b) could predict the experimental WAF conditions fairly well using densimetric Froude Number.

7.2 Recommendations for future work

Obviously, it was not possible to examine every aspect of the generated data in this thesis. However, the work carried out guides the way to priority areas for further development. These works are presented below:

- The present data were obtained for 1-inch horizontal pipeline configuration. Further data accounting for inclination and pipe diameter effect would be valuable in gaining a comprehended understanding of the phase mix in petroleum industry applications.

- By using visual analysis, the coating associated with presented flows in this study was observed to fluctuate with time, along with different local parameters (i.e. phase holdups). It would be valuable to measure the in-situ conditions dynamically to help interpreting the measurements of average quantities.

- Though ECT was used in this study “to see through the pipe” for two phase flow, more effort is needed to achieve satisfactory quality results and overcome the difficulties found to account for the different phases and measure the coating (i.e. higher sample rate to fully capture a single cyclic motion, sensitivity matrix distortion with the presence of water).

- It is clear from the present three phase data (liquid/liquid/gas) that the flows were very complex and enhanced visualisation of the flow patterns would be advantageous. This could be achieved by using high speed video photography and axial viewing techniques (dual modality ECT/ERT combination, Wire mesh sensor).

- Validate the new correlation with full scale data. As it shall be tested against different parameters such as fluid properties, pipe size and orientation, and coating/fouling thickness. With new data, the coating coefficient could be-coupled from Blasius’s friction coefficients, as it’s counting both friction and reduction of the hydraulic diameter within the flow due to the coating.

REFERENCES

Abduvayt, P., Manabe, R., Watanabe, and T., Arihara, N. (2006), “Analysis of oil/water-flow tests in horizontal, hilly terrain, and vertical pipes”, *SPE Production and Operations*, 21 (1), February, 123-133

Aboudwarej, H., Felix, J., and Taylor, S. (2006), "*Oil Field Review - Highlighting Heavy Oil*", available at: http://www.slb.com/~/media/Files/resources/oilfield_review/ors06/sum06/heavy_oil.ashx(accessed 9th September 2011).

Acikgoz, M., Franca, F., and Lahey, R.T. (1992), “An experimental study of three-phase flow regimes”, *Int. J. Multiphase Flow*, 18, 327-336

ACR (2004), "*Alberta Chamber of Resources - Oil Sands Technology Roadmap*", available at: http://www.acr-alberta.com/OSTR_report.pdf (accessed 9th September 2011).

Al-Awadi, H., Zorgani, E., Li, X., Yan, W., Al-lababidi, S., and Yeung, H. (2010), “ECT Tomography Technique for Sand monitoring in Heavy Oil Pipeline”**,** *5th Technology of Oil and Gas Forum (TOG 2010),* 12-14 October, Tripoli-Libya.

Al-Besharah, J. M., Salman, O. A., and Akashah, S. A. (1987), “Viscosity of Crude Blends”, *Ind. Eng. Chem. Res.*, 26 (12), 2445-2449

Al-Safran, E., Gokcal, B., and Sarica, C. (2011), “High viscosity liquid effect on two-phase slug length in horizontal pipes”, *BHRG Multiphase 15*, 15-17 June, Cannes, France, 257-276

Andritsos, N., and Hanratty, T. J. (1987), “Interfacial instabilities for horizontal gas-liquid flows in pipelines”, *Int. J. Multiphase Flow*, 13 (5), 583-603.

Andritsos, N., Williams, L., and Hanratty, T. J. (1989), “Effect of liquid viscosity on the stratified-slug transition in horizontal pipe flow”, *Int. J. Multiphase Flow*, 15 (6), 877-892.

Angeli, P., and Hewitt, G. (2000), “Flow structure in horizontal oil-water flow”, *Int. J. Multiphase Flow*, 26, 1117-1140.

Argiller, J. –F., Henaut, I., Gateau, P., Heraud, J. –P., and Glenat, P. (2005), “Heavy-oil dilution”, *International Thermal Operations and Heavy Oil Symposium*, Calgary, Alberta, Canada, 1-3 November

Arirachakaran, S., Oglesby, K. D., Malinowsky, M. S., Shoham, O., and Brill, J. P. (1989), “An analysis of oil/water flow phenomena in horizontal pipes.”, SPE 18836, *SPE Production Operations Symposium*, Oklahoma City, OK, 13-14 March

Arney, M.S., Bai, R., Guevara, E., Joseph, D.D., and Liu, K. (1993), “Friction factor and holdup studies for lubricated pipelining - I experiments and correlations”, *Int. J. Multiphase Flow*, 19, 1061-1076.

Atmaca, S., Sarica, C., Zhang, H.-Q., and Al-Sarkhi, A.S. (2008), “Characterization of oil water flows in inclined pipes”, *Proceedings - SPE Annual Technical Conference and Exhibition*, 2, 1273-1286

Bai, R., Chen, K., and Joseph, D. D. (1992), “Lubricated pipelining stability of core-annular flow, Part 5. Experiments and comparison with theory”, *J. Fluid Mech.*, 240, 97-142.

Balakhrisna, T., Ghosh, S., Das, G., and Das, P.K. (2010), “Oil-water flows through sudden contraction and expansion in a horizontal pipe – Phase distribution and pressure drop”, *International Journal of Multiphase Flow*, 36, 13-24.

Bannwart, A.C. (1999), “A simple model for pressure drop in horizontal core annular flow”, *Journal of the Brazilian Society of Mechanical Sciences*, 21 (2), 233-244.

Bannwart, A.C. (2001), “Modeling aspects of oil-water core-annular flows”, Journal of Petroleum Science and Engineering, 32, 127-143.

Bannwart, A.C., Rodriguez, O.M.H., de Carvalho, C.H.M., Wang, I.S., and Vara, R.M.O. (2004), “Flow patterns in heavy crude oil-water flow”, *ASME J. Energy Resources Technol.*, 126, 184-189.

Bannwart, A.C., Rodriguez, O.M.H., Trevisan, F.E., Vieira, F.F., and de Carvalho, C.H.M. (2009), “Experimental investigation on liquid-liquid-gas flow: Flow patterns and pressure-gradient”, *Journal of Petroleum Science and Engineering*, 65, 1-13.

Barnea, D. (1991), “On the effect of viscosity on stability of stratified gas-liquid flow-application to flow pattern transition at various pipe inclinations”, *Chem. Eng. Sci.*, 46 (8), 2123-2131

Barnea, D., and Brauner, N. (1985), “Holdup of the liquid slugs in two phase intermittent flow”, *Int. J. Multiphase Flow,* 11, 43-49.

Barnea, D., and Taitel, Y. (1993), “A model for slug length distribution in gas-liquid slug flow”, *Int. J. Multiphase Flow,* 19 (5), 829-838.

Beggs, H.D., and Brill, J.P. (1973), “A Study of Two-Phase Flow in Inclined Pipes”, *J. Pet. Tech.*, 607-617.

Bensakhria, A., Peysson, Y., and Antonini, G. (2004), “Experimental study of the pipeline lubrication of heavy oil transport”, *Oil Gas Sci Technol-Rev IFP*, 59 (5), 523-533;

Bobok, E., Magyari, D., and Udvardi, G. (1996), “Heavy Oil Transport Through Lubricated Pipeline”, SPE 36841, *SPE European Petroleum Conference*, Milan, Italy, 22-24 October, 239-244.

BP (2009), "*BP Frontiers - Getting heavy*", available at: http://www.bp.com/liveassets/bp_internet/globalbp/globalbp_uk_english/reports_and_publications/frontiers/STAGING/local_assets/pdf/bpf24_12-15_chops.pdf. (accessed 9th September 2011).

Brauner, N. (1991), “Two-phase liquid-liquid annular flow”, *Int. J. Multiphase Flow*, 17, 59-76.

Brauner, N. (2002), “Modelling and Control of Two-Phase Phenomena: Liquid-Liquid Two-Phase Flow Systems”, in: Bertola, V. (Ed.), *Liquid-liquid two-phase flow systems*. CISM Center, Udine, Italy.

Brauner, N., and Moalem Maron, D., (1998). “Classification of liquid–liquid two-phase flow systems and the prediction of flow pattern maps”, *2nd International Symposium on Two-Phase Flow Modeling and Experimentation*, 2, Pisa, Italy, 747 – 754.

Brill, J., Schmidt, Z., Coberly, W., Herring, J., and Moore, D. (1980), “Analysis of two phase flow tests in large diameter flow lines in Prudhoe Bay Field”, *SPEJ.*

CEAA (2011), “*Cyclic Steam Stimulation*”, available at: http://www.ceaa.gc.ca/default.asp?lang=En&n=AFF9B551-1&toc=show&offset=8 (accessed 9th September 2011).

Charles, M.E., Govier, G.W., and Hodgson, G.W. (1961), “The horizontal pipeline flow of equal density oil/water mixture”, *Can. J. Chem. Eng.*, 39, 27-36.

Charles, M.E., and Lilleleht, L.U. (1966), “Correlation of pressure gradient for the stratified laminar-turbulent pipeline flow of two immiscible liquids”, *Can. J. Chem. Eng.*, 44 (1), 47-79.

Chen, N.H. (1979), “An explicit equation for friction factor in pipe”, *Ind. Eng. Chem. Fund.*, 18, 296.

Chen, X., and Guo, L. (1999). “Flow patterns and pressure drop in oil–air–water three-phase flow trough helically coiled tubes”, *Int. J. Multiphase Flow* 25, 1053–1072.

Clark, B. (2007), "*The National Petroleum Council (NPC), Global Oil and Gas Study - Heavy Oil, Extra-Heavy Oil and Bitumen*", available at: http://www.npc.org/Study_Topic_Papers/22-TTG-Heavy-Oil.pdf (accessed 9th September 2011).

Clark, A.F. and Shapiro, A. (1949), “*Method of pumping viscous petroleum*”, US Patent No. 2533878.

Colebrook, C.F. (1939). "Turbulent flow in pipes, with particular reference to the transition region between smooth and rough pipe laws". *Journal of the Institution of Civil Engineers*, London, February.

Colmenares, J., Ortega, P., Padrino, J., and Trallero, J. L. (2001), “Slug flow model for the prediction of pressure drop for high viscosity oils in a horizontal pipeline”, SPE 71111, *International Thermal Operations and Heavy Oil Symposium*, Margarita Island, Venezuela, 12-14 March

Cooper, D. (2006), “Floating Heavy Oil Recovery: Current State Analysis”, report number 0704-0188, *US Coast Guard, Research and Development Center*, Groton, CT.

Drebit, G., and Tesciuba, M. (2008), “Worm Hole Predictor Observation with Acoustic Data”, *Schlumberger,* Paper 2008-423

Dukler, A., Moalem-Maron, D., and Brauner, N. (1985), “A physical model for predicting the minimum stable slug length”, *Chem. Eng. Sci.* 40, 1379-1385.

Dukler, A.E., Wicks, M., and Cleveland, R.G. (1964), “Frictional Pressure Drop in Two-Phase Flow: A. A Comparison of Existing Correlations for Pressure Loss and Holdup”, *A.L.Ch.E. Journal*, January, 10 (1), 38-51.

Dusseault, M.B. (2001), “Comparing Venezuelan and Canadian Heavy Oil and Tar Sands”, Calgary, Canada: *Canadian International Petroleum Conference*, available at: http://www.energy.gov.ab.ca/OilSands/pdfs/RPT_Chops_app3.pdf (accessed 9th September 2011).

Dusseault, M.B. (2002), “CHOPS: Cold Heavy Oil Production with Sand in the Canadian Heavy Oil Industry”, *Alberta Department of Energy*, Canada.

Dusseault, M. B. (2007), “CHOPS”, Ch 5 in Warner, H. R., Jr., Ed., *SPE Petroleum Engineers Handbook, Vol 6: Emerging and Peripheral Technologies (EMPT)*, SPE

Escojido, D., Urribarri, O., and Gonzalez, J. (1990), "Part 1: Transportation of Heavy crude oil and Natural Bitumen", *13th World Petroleum Congress*, Buenos Aires, Brazil, 20 – 25 October .

Flores, J.G. (1997), "Characterization of Oil-Water Flow Patterns in Vertical and Deviated Wells", SPE 38810, *SPE Annual Technical Conference and Exhibition*, San Antonio, Texas, 5-8 October

Ghosh, S., Mandal, T.K., Das, G., and Das, P.K. (2009), “Review of oil water core annular flow”, *Renewable and Sustainable Energy Reviews*, 13, 1957-1965.

Gillies, R.G., Hill, K.B., McKibben, M.J., and Shook, C.A. (1999), “Solids transport by laminar Newtonian flows”, *Powder Technology*, 104, 269-277.

Gillies, R.G., Shook, C., Kristoff, B., and Parker, P. (1994), “Sand Transport in Horizontal Wells”, *11th Annual Calgary University Heavy Oils and Oil Sands Technology Symposium*, Canada, 2 March.

Gokcal, B., Wang, Q., Zhang, H.-Q, and Sarica, C. (2006), “Effects of High Viscosity on Oil/Gas Flow Behaviour in Horizontal Pipes”, SPE 102727, *SPE Annual Technical Conference and Exhibition*, San Antonio, Texas, USA, 24-27 September

Govier, G.W., and Aziz, K., (1972), “The Flow of Complex Mixture in Pipes”, *Van Nostrand Reihold Co.*, New York.

Grassi, B., Strazza, D., and Poesio, P. (2008), “Experimental validation of theoretical models in two-phase high-viscosity ratio liquid–liquid flows in horizontal and slightly inclined pipes”, *International Journal of Multiphase Flow*, 34, 950–965

Guevara, E., Gonzalez, J., and Nuíïez, G. (1997), “Highly Viscous Oil Transportation Methods in the Venezuela oil industry”, *15th World Petroleum Congress*, 12 – 17 October, Beijing, China.

Haaland, SE (1983), "Simple and Explicit Formulas for the Friction Factor in Turbulent Flow", *Journal of Fluids Engineering (ASME)*, 103 (5), 89–90.

Halliburton (2011a), “*What Makes Heavy Oil Heavy?"*, available at: http://www.halliburton.com/ps/default.aspx?navid=1995&pageid=4219 (accessed 9th September 2011).

Halliburton (2011b), “*Injecting CO_2 to Enhance Oil Recovery - Cyclic Carbon Dioxide Stimulation: Unlocking Additional Heavy Oil Production*”, available at: http://www.halliburton.com/ps/default.aspx?pageid=4520&navid=2046 (accessed 9th September 2011).

Hasson, D., Mann, U., and Nir, A. (1970), “Annular flow of two immiscible liquids. I. Mechanisms”, *Can J Chem Eng*, 48, 514-520;

IEA (2005), “International Energy Agency, Resources to Reserves - Oil and Gas Technologies for the Energy Markets of the Future", available at: http://www.iea.org/press/pressdetail.asp?PRESS_REL_ID=159

Isaacs, J.D. and Speed, J.B. (1904), “*Method of Piping Fluids.*”, US Patent N° 759374.

James, M., and Wing, R. (2011), “*High Temperature Electric Submersible Pumps Effective in Oil Sands Production*”, available at: http://www.pump-zone.com/pumps/pumps/high-temperature-electric-submersible-pumps-effective-in-oil-sands-production.html (accessed 9th September 2011).

Joseph, D.D., Bannwart, A.C., and Liu, Y.J. (1996), “Stability of annular flow and slugging”, *International Journal of Multiphase Flow*, 22 (6), 1247-1254;

Joseph, D.D., Renardy, Y., and Renardy, M. (1984), “Instability of the flow of immiscible liquids with different viscosities in a pipe”, *Journal of Fluid Mechanics*, 141, 309-317;

Joseph, D.D., Renardy, and Y.Y. (1993), “*Fundamentals of Two-Fluid Dynamics*”. New York: Springer-Verlag

Kasturi, G., and Stepanek, J.B. (1972), “Two phase flow-I. Pressure drop and void fraction measurements in cocurrent gas-liquid flow in a coil”, *Chem. Eng. Sci.,* 27, 1871-1880.

Keskin, C., Zhang, H.-Q., and Sarica, C (2007).,”Identification and classification of new three-phase gas/oil/water flow patterns”, *Proceedings - SPE Annual Technical Conference and Exhibition*, 4, 2363-2375.

Khor, S.H., Mendes-Tatsis, M.A., and Hewitt, G.F. (1997), “One-dimensional modelling of phase holdups in three-phase stratified flow”, *International Journal of Multiphase Flow*, 23 (5), 885-897.

Knoll, R. and Yeung, K.C. (2000), “Drilling Engineering Challenges in Commercial SAGD Well Design in Alberta”, SPE 62862, *SPE/AAPG Western Regional Meeting*, Long Beach, California, 19–23 June 2000.

Lockhart R.W., and Martinelli R.C., (1949), “Proposed Correlation of Data for Isothermal Two-phase Two-component in Pipes”, *Chem. Eng. Process*, 45, 39–48.

Martínez-Palou, R., Mosqueira, M., Rendón, B. Z., Mar-Juárez, E., Bernal-Huicochea, C., Clavel-López, J, and Aburto, J (2011), “Transportation of heavy and extra-heavy crude oil by pipeline: A review”, *Journal of Petroleum Science and Engineering*, January, 75 (3-4), 274-282.

Matsubara, H., and Naito, K. (2011), “Effect of liquid viscosity on flow patterns of gas-liquid two-phase flow in a horizontal pipe”, *IJMF*, December, 37 (10), 1277-1281

Maverickenergy (2011), “*Waterflooding Operations*”, available at: http://www.maverickenergy.com/operations/crawfordCounty.aspx (accessed 9th September 2011).

McAdams, W.H., Woods, W.K., and Heroman Jr., L.C. (1942), “Vaporization inside horizontal tubes – II Benzene-Oil mixtures”, *Trans. ASME* 64, 193-200.

McKibben, M.H., Gillies, R.G., and Shook, C.A. (2000a), “A laboratory investigation of horizontal well heavy oil-water flows”, *The Canadian Journal of Chemical Engineering,* August, 78, 743-751.

McKibben, M.H., Gillies, R.G., and Shook, C.A. (2000b), “Predicting Pressure Gradients in Heavy Oil-Water Pipelines”, *The Canadian Journal of Chemical Engineering,* 78, August, 752-756.

McNeil, D. A., and Stuart, A. D. (2003), “The effects of highly viscous liquid phase on vertically upward two-phase flow in a pipe”, *Inter. J. of Multiphase Flow*, 29, 1523-1549

Miesen, R., Beijnon, G., Duijvestijn, P.E.M., Oliemans, R.V.A., and Verheggen, T. (1992), “Interfacial waves in core-annular flow”, *J. Fluid Mech.,* 238, pp. 97-117.

Mwambela, A.J., and Johansen, G.A. (2001), “Multiphase flow component volume fraction measurement: experimental evaluation of entropic thresholding methods using an electrical capacitance tomography system”, *Institute of Physics Publishing, Meas. Sci. Technol.,* 12, 1092-1101

Nadler, M., and Mewes, D. (1997), “Flow induced emulsification in the flow of two immiscible liquids in horizontal pipes”, *IJMF*, 23 (1), February, 55-68.

Neogi, S., Lee, A., and Jepson, W.P. (1994), “Model for multiphase (gas-water-oil) stratified flow in horizontal pipelines”, *SPE - Asia Pacific Oil & Gas Conference*, 553-562.

Norris, L. (1982), “Correlation of Prudhoe Bay Liquid Slug Lengths and Holdups In cluing 1981 Large Diameter Flowline Tests”, *Internal Report, Exxon Production Research Co.*, Houston, TX.

Oliemans, R.V.A., Ooms, G., Wu, H.L., and Duijvestijn, A. (1987), “Core annular oil/water flow: the turbulent-lubricating-film model and measurements in a 5 cm pipe loop”, *Int. J. Multiphase Flow*, 13, 23-31.

Olimans, R.V.A. (1986), “*The Lubricating-film Model for Core-annular Flow*”, *Ph.D. Thesis, Technische Hogeschool Delft., Delft University Press, The Netherlands.*

Ooms, G., Segal, A., Van Der Wees, A.J., Meerhoff, R., and Rva, O. (1984), “A theoretical model for core-annular flow of a very viscous oil core and a water annulus through a horizontal pipe”, *IJMF*, 10, 41-60;

Pan, L., Jayanti, S., and Hewitt, G.F. (1995), “Flow patterns, phase inversion and pressure gradient in air-oil-water flow in a horizontal pipe”, *2nd Int. Conf. On Multiphase Flow*, Kyoto Japan.

Parda, V.J.W., and Bannwart, A.C. (2001), “Modeling of vertical core-annular flows and application to heavy oil production”, *J Energy Resour Technol ASME*, 123, 194-199;

Pierre, C., Barré, L., Pina, A., and Moan, M. (2004), "Composition and Heavy Oil Rheology", *Oil & Gas Science and Technology,* 59 (5), 489-501

Poesio, P., Sotgia, G., and Strazza, D. (2009), “Very viscous oil/water/air flow through horizontal pipes: Pressure drop measurement and prediction”, *Chem. Eng. Sci.,* 64, 1136-1142.

Rigzone (2011), *“What is Heavy Oil and How is it formed?”*, available at: http://www.rigzone.com/training/heavyoil/insight.asp?i_id=184 (accessed 9th September 2011).

Rodriguez, O.M.H., Bannwart, A.C., and Carvalho, C.H.M. (2009), “Pressure loss in core-annular flow: Modeling, experimental investigation and full-scale experiments”, *Journal of Petroleum Science and Engineering*, 65, 67-75.

Rodriguez, O.M.H., and Oliemans, R.V.A. (2006), “Experimental study on oil-water flow in horizontal and slightly inclined pipes”, *IJMF*, 32, 323-343.

Russell, T.W.F., and Charles, M.E. (1959), “The Effect of the Less Viscous Liquid in the Laminar Flow of Two Immiscible Liquids”, *The Canadian Journal of Chemical Engineering*, 18-24 February.

Saniere, A., Hénaut, I., and Argillier, J. F. (2004), "Pipeline Transportation of Heavy Oils, a Strategic, Economic and Technological Challenge", *Oil & Gas Science and Technology*, 59 (5), 455-466.

Schlumberger (2011), "*Worldwide Heavy Oil Resources by Country*", available at: http://www.slb.com/services/industry_challenges/heavy_oil.aspx (accessed 9th September 2011).

Scott, S., Shoham, O., and Brill, J. (1981), "Prediction of Slug Length in Horizontal Large Diameter Pipes", *SPE J. Prod. Eng.,* 4, 335-340

Shi, H., Jepson, W.P., and Rhyne, L.D. (2003), "Segregated modelling of oil-water flows", SPE 84232, *SPE Annual Technical Conference and Exhibition*, Denver, Colorado, 5-8 October.

Smith, E., Krampa, F.N., Fossen, M., Brekken, C., and Unander, T.E. (2011), "Investigation of horizontal two-phase gas-liquid pipe flow using high viscosity oil: Comparison with experiments using low viscosity oil and simulations", *BHR Group Multiphase*, 15, 293-307.

Sotgia, G., Tartarini, P., and Stalio, E. (2008), "Experimental analysis of flow regimes and pressure drop reduction in oil-water mixtures", *IJMF* 34, 1161-1174

Spedding, P.L., Donnelly, G.F., and Cole, J.S. (2005), "Three phase oil-water-gas horizontal co-current flow: I. Experimental and regime map", *Chemical Engineering Research and Design*, 83 (4 A), 401-411.

Spedding, P.L., Murphy, A., Donnelly, G.F., Benard, E., and Doherty, A.P. (2008), "Pressure drop in three-phase oil-water-gas horizontal co-current flow: Experimental data and development of prediction models", *Asia-Pacific Journal of Chemical Engineering*, 3 (5), 531-543.

Stapelberg, H.H., and Mewes, D. (1994), "Pressure-drop calculation in three-phases lug flow of water, oil, and air", *Int. Chem. Eng.*, 34 (3), 295-314.

Statoil (2011), "*Water-alternating-gas (WAG)*", available at: http://www.statoil.com/en/technologyinnovation/optimizingreservoirrecovery/recoverymethods/wateralternatinggaswag/pages/water-alternating-gas%20(wag).aspx (accessed 9th September 2011).

Stockwell, A., Sit, S. P. and Hardy, W. A. (1988), "Transoil Technology for Heavy Oil Transportation: Results of Field Trials at Wolf Lake Stockwell", SPE 18362, *European Petroleum Conference*, London, United Kingdom, 16-19 October

Strazza, D., Grassi, B., Demori, M., Ferrari, V., and Poesio, P. (2011), "Core-annular flow in horizontal and slightly inclined pipes: Existence, pressure drops, and hold-up", *Chemical Engineering Science*, 66, 2853-2863.

Swamee, P.K., and Jain, A.K. (1976), "Explicit equations for pipe-flow problems", *Journal of the Hydraulics Division, ASCE*, 102 (5), 657–664

Taitel, Y., Barnea, D., and Brill, J.P. (1995), "Stratified three phase flow in pipes", IJMF, 21, 53-60.

Taitel, Y., and Dukler, A.E. (1976), "A Model for Predicting Flow Regime Transitions in Horizontal and Near Horizontal Gas-Liquid Flow", *AlChE Journal,* 22 (1), 47-55.

Taitel, Y., and Dukler, A.E. (1987), "Effect of pipe length on the transition boundaries for high-viscosity liquids", IJMF, 13 (4), 577-581

The oil drum (2007), *"Extracting Heavy Oil: Using Toe to Heel Air Injection (THAI)"*, available at: http://canada.theoildrum.com/node/2907 (accessed 9th September 2011).

The oil drum (2009), *"EROI Update: Preliminary Results using Toe-to-Heel Air Injection"*, available at: http://netenergy.theoildrum.com/node/5183 (accessed 9th September 2011).

Trallero, J.L., (1995), "*Oil-water Flow Patterns in Horizontal Pipes*", Ph.D. thesis. The University of Tulsa;

Ullmann, A., and Brauner, N. (2004), *"Closure relations for the shear stress in two-fluid models for core-annular flow*", Multiph. Sci. Technol., 16, 355–387.

Urquhart, R.D. (1985), "Heavy oil transportation: Present and future", *J. Can. Pet. Technol.,* 25 (2), 68-71.

Valle, A., and Kvandal, H.K. (1995), "Pressure drop and dispersion characteristics of separated oil/water flow: Two-Phase Modeling and Experimentation", 1, 583-591., In: Celata, G.P., Shan, R.K. (Eds), Rome.

Valle, A., and Utvik, O.H. (1997), "Pressure drop, flow pattern and slip for two phase crude oil/water flow: Experiments and model Predictions", *Int Symp on Liquid-Liquid Two-Phase Flow and Transport Phenomena*, Antalya, Turkey, November 3-7

Vedapuri, D., and Jepsen, W.P. (1997), "A Segregated Flow Model to Predict Water Layer Thickness in Oil-Water Flows in Horizontal and Slightly Inclined Pipe Lines", *BHRA*.

Vielma, M., Atmaca, S., Sarica, C., and Zhang, H. (2007), "Characterization of Oil-Water Flows in Horizontal Pipes", SPE 109591, *2007 SPE Annual Technical Conference and Exhibition*, Anaheim, California, USA, 11-14 October.

Vuong, D.H., Zhang, H.-Q., Sarica, C., and Li, M. (2009), "Experimental Study on High Viscosity Oil/Water Flow in Horizontal and Vertical Pipes", SPE 124542, *2009 SPE Annual Technical Conference and Exhibition, New Orleans,* Louisiana, USA, 4-7 October

Wang, W., and Gong, J. (2009), "Experiment research of phase inversion in mineral oil-water two-phase flow in horizontal pipe", *Journal of Energy Resources Technology*, December 2009, 131, 043001, 1-6

Wang, W., Gong, J., Shi, B., and Shuai, H. (2010), "Investigation on heavy crude oil-water two phase flow and related flow characteristics", *7th Int. Conf. on Multiphase Flow*, Tampa, FL USA, May 30- June 4.

Wang, X., Zou, H., Li, G., Nie, C., and Chen, J., (2005), "Integrated Well - Completion Strategies With CHOPS To Enhance Heavy – Oil Production: A Case Study in Fula Oilfield", *SPE International Thermal Operations and Heavy Oil Symposium held in Calgary*, Alberta, Canada, 1– 3 November.

Weisman, J., Duncan, D., Gibson, J., and Crawford, T. (1979), "Effects of fluids properties and pipe diameter on two-phase flow patterns in horizontal lines", IJMF, 5, 437-462.

Wong, T.N., and Yau, U.K. (1997), "Flow patterns in two phase air water flow", *Int. Comm. Heat Mass Transfer*, 24 (1), 111-118

Woods, G.S., Spedding, P.L., Watterson, J.K., and Raghunathan, S. (1998), "Three-phase oil/water/air vertical flow", *Trans. IChemE, Part A. Chem. Eng. Res. Des.*, 76 A, 571-584

World Oil (2011), "*What's new in production - Vapour Extraction*", available at: http://www.worldoil.com/October-2006-Whats-new-in-production.html (accessed 9th September 2011).

Xiao, J.J., Shoham, O., and Brill, J.P. (1990), "A comprehensive mechanistic model for two-phase model", SPE 20631, *Annual Technical Conference and Exhibition*, New Orleans, 23-26 Sept.

Zhang, H.-Q., and Sarica, C. (2005), "Unified modeling of gas/oil/water pipe flow - Basic approaches and preliminary validation", *Proceedings - SPE Annual Technical Conference and Exhibition*, 1375-1383.

Zhang, H.-Q., Wang, Q., Sarica, C., and Brill, J.P. (2003), “Unified model for gas-liquid pipe flow via slug dynamics – Part 1: Model development”, *ASME J. Energy Res. Tech.*, 125, 266

Zorgani, E. (2010), “*Sand particle behaviour in oil pipeline*”, Progress review report, Cranfield University.

Zorgani, E. (2011), “*An experimental study of sand behaviour in multiphase pipeline*”, PhD thesis, Cranfield University. (in preparation)

Appendix A: Heavy viscous oil data for single and multiphase flow

Table 7-1: Single phase data of heavy oil flow at different viscosities

V_{so} (m/s)	ρ_o (kg/m$^{3)}$	T_o (°C)	T_{inlet} (°C)	T_{outlet} (°C)	P_{inlet} (kPa)	P_{outlet} (kPa)	dp/dx (kPa/m)	μ_o by coriolis flow meter (cP)	μ_o using T_o (cP)
0.062	924.1	20.9	20.9	21.8	227.34	192.99	15.83	4600	5441
0.088	924.1	21.0	20.8	21.6	283.08	234.15	22.55	4600	5378
0.147	924.0	21.1	20.9	21.5	386.59	310.33	35.14	4600	5346
0.171	924.0	21.1	21.1	21.5	422.51	336.63	39.57	4600	5319
0.192	924.6	20.7	21.1	21.4	449.79	356.11	43.17	4600	5520
0.222	924.2	21.3	21.3	21.6	507.41	398.76	50.07	4600	5249
0.234	924.5	20.6	20.8	21.7	538.60	420.14	54.59	4600	5550
0.260	924.4	21.4	21.4	21.8	555.73	434.03	56.08	4600	5184
0.254	924.6	20.7	20.9	21.8	571.72	444.50	58.63	4600	5498
0.287	924.7	20.8	21.1	21.9	620.90	480.70	64.61	4600	5447
0.298	925.1	20.9	21.2	21.6	615.92	477.24	63.91	4600	5418
0.340	925.4	21.0	21.3	21.8	686.54	529.10	72.55	4600	5375
0.056	921.8	25.2	23.2	22.0	154.64	122.68	14.72	3306	3738
0.098	921.8	25.2	23.8	22.9	177.95	134.58	19.99	3301	3719
0.145	921.7	25.4	24.3	23.5	203.60	147.50	25.85	3258	3662
0.194	921.6	25.6	24.9	24.1	234.10	162.92	32.81	3191	3594
0.293	921.6	26.0	25.5	24.9	286.18	189.11	44.73	3091	3475
0.393	921.6	26.6	26.0	25.4	328.47	208.31	55.37	2984	3302
0.566	921.9	27.2	26.5	26.0	400.29	239.52	74.09	2933	3143
0.028	938.3	8.7	12.1	14.4	360.67	268.80	42.34	11071	15629

0.070	938.9	8.7	12.0	14.1	417.70	287.24	60.12	11212	15649
0.109	938.9	8.8	12.2	14.4	449.72	282.48	77.07	11152	15515
0.037	934.2	10.0	18.0	15.5	251.28	203.75	21.90	7868	13941
0.105	935.2	10.1	15.7	13.1	466.87	353.88	52.07	8312	13894
0.134	936.3	10.9	14.6	13.0	634.39	472.39	74.65	8500	13000
0.046	934.6	11.3	13.9	14.9	244.95	165.81	36.47	9603	12450
0.059	935.0	11.0	13.7	14.7	272.39	179.91	42.62	9690	12782
0.100	935.8	10.9	13.6	14.5	336.17	197.32	63.99	9923	12923
0.135	936.2	11.1	13.6	14.4	390.74	217.88	79.66	10080	12745
0.178	936.5	11.4	13.7	14.5	459.69	247.72	97.68	10144	12373
0.201	936.7	11.6	13.8	14.5	499.81	268.18	106.74	10115	12230

Table 7-2: Two phase data of Heavy oil-air flow for averaged μ_o = 4326 cP

V_{so} (m/s)	ρ_o (kg/m$^{3)}$	V_{sg} (m/s)	T_g (°C)	T_o (°C)	T_{inlet} (°C)	T_{outlet} (°C)	P_g (bara)	P_{inlet} (kPa)	P_{outlet} (kPa)	dp/dx (kPa/m)	μ_o by coriolis flow meter (cP)	μ_o using T_o (cP)
0.025	918.0	0.484	26.8	24.4	25.0	26.6	2.79	150.50	133.36	7.90	3092	3995
0.024	918.0	0.711	26.8	24.5	25.0	26.6	2.80	151.06	133.62	8.04	3087	3981
0.020	918.0	1.055	26.8	24.5	25.1	26.7	2.81	152.01	134.39	8.12	3081	3969
0.028	917.9	1.516	26.9	24.6	25.1	26.8	2.80	151.69	134.22	8.05	3068	3945
0.029	917.9	2.056	27.3	24.7	25.3	27.0	2.80	150.84	133.53	7.98	3049	3909
0.025	917.8	3.093	27.4	24.7	25.3	26.9	2.80	150.65	133.57	7.87	3040	3895
0.026	917.8	4.962	27.4	24.7	25.3	26.8	2.84	154.40	137.26	7.90	3030	3884
0.024	917.7	7.190	27.5	24.8	25.4	26.7	2.88	158.73	140.80	8.26	3022	3863
0.027	917.7	10.159	27.7	24.8	25.6	27.1	2.86	156.15	138.36	8.20	3007	3849
0.062	920.2	0.465	25.4	22.4	22.9	25.3	3.49	214.07	180.37	15.53	3706	4766
0.061	920.2	0.696	25.4	22.4	22.9	25.2	3.51	215.33	181.24	15.71	3729	4758
0.059	920.2	0.986	25.5	22.4	22.9	25.2	3.55	219.64	184.64	16.13	3726	4748
0.061	920.2	1.486	25.6	22.4	22.9	25.2	3.57	221.07	185.57	16.36	3721	4748
0.060	920.1	2.017	25.8	22.4	23.0	25.3	3.54	219.32	184.46	16.06	3713	4744
0.060	920.0	2.991	25.9	22.5	23.0	25.3	3.50	215.14	181.36	15.57	3704	4733
0.061	920.0	5.073	26.0	22.5	23.0	25.3	3.50	214.00	181.38	15.03	3696	4726
0.061	920.0	7.233	26.1	22.5	23.1	25.2	3.57	220.06	187.90	14.82	3689	4716
0.060	920.1	10.267	26.3	22.5	23.3	25.0	3.80	244.10	207.68	16.78	3684	4702
0.105	920.3	0.496	26.2	22.7	23.5	26.0	4.21	276.40	226.23	23.12	3584	4621

0.102	920.4	0.690	26.1	22.7	23.3	25.7	4.31	285.73	233.55	24.04	3620	4630
0.104	920.4	1.082	26.2	22.7	23.3	25.6	4.37	291.32	237.92	24.61	3620	4618
0.104	920.4	1.498	26.3	22.8	23.3	25.6	4.35	290.44	237.34	24.47	3605	4598
0.101	920.4	2.024	26.3	22.9	23.4	25.5	4.30	285.68	234.64	23.52	3581	4577
0.105	919.8	2.867	26.6	23.0	24.0	26.6	4.03	262.94	216.92	21.21	3453	4508
0.105	920.4	4.899	26.6	22.9	23.6	26.1	4.11	267.79	220.67	21.72	3510	4547
0.103	920.5	6.961	26.6	22.9	23.6	25.8	4.18	273.69	226.57	21.72	3533	4552
0.104	920.5	10.708	26.6	22.9	23.6	25.5	4.48	302.05	252.75	22.72	3534	4547
0.199	920.5	0.501	26.2	23.7	23.9	25.9	5.70	406.18	323.02	38.32	3425	4242
0.200	920.7	0.678	26.1	23.4	23.9	25.9	5.74	409.71	325.59	38.77	3414	4376
0.202	920.3	1.017	26.0	24.0	24.2	25.9	5.72	409.25	326.42	38.17	3350	4158
0.200	920.9	1.492	26.1	23.5	24.0	25.9	5.79	415.86	332.29	38.51	3377	4328
0.204	920.8	2.013	26.2	23.6	24.1	25.9	5.72	410.01	328.42	37.60	3360	4269
0.201	920.2	3.115	26.2	24.0	24.3	26.0	5.51	392.31	315.31	35.48	3277	4127
0.202	920.8	5.023	26.4	23.9	24.1	26.0	5.51	389.39	312.65	35.36	3311	4191
0.201	920.5	7.312	26.4	23.9	24.2	26.1	5.46	384.56	309.48	34.60	3290	4170
0.201	920.6	10.556	26.5	23.9	24.2	26.1	5.56	393.31	317.97	34.72	3281	4165
0.303	920.4	0.753	26.1	24.6	24.7	27.0	6.85	506.65	397.90	50.11	3161	3914
0.302	920.2	1.037	26.1	24.7	24.8	26.9	6.88	510.05	401.37	50.08	3129	3881
0.298	920.0	1.445	26.2	25.1	25.1	26.9	6.71	495.25	391.18	47.96	3035	3773

Table 7-3: Two phase data of Heavy oil-air flow for averaged μ_o = 10605 cP

V_{so} (m/s)	ρ_o (kg/m$^{3)}$	V_{sg} (m/s)	T_g (°C)	T_o (°C)	T_{inlet} (°C)	T_{outlet} (°C)	P_g (bara)	P_{inlet} (kPa)	P_{outlet} (kPa)	dp/dx (kPa/m)	μ_o by coriolis flow meter (cP)	μ_o using T_o (cP)
0.034	933.6	0.512	23.0	11.2	14.3	14.1	5.45	377.74	296.06	37.64	NA	12564
0.036	933.4	0.710	23.1	12.1	14.6	14.8	5.52	384.77	304.28	37.09	NA	11674
0.035	933.1	0.954	23.2	12.6	15.0	15.3	5.27	362.24	286.79	34.77	NA	11138
0.037	932.7	1.539	23.3	13.1	15.3	15.8	5.33	367.82	292.05	34.92	NA	10701
0.040	932.5	1.970	23.3	13.4	15.5	16.1	5.23	358.94	285.51	33.84	NA	10421
0.039	932.1	2.969	23.4	13.7	15.8	16.4	5.13	350.67	279.58	32.76	NA	10124
0.041	931.8	4.869	23.5	14.0	15.9	16.9	4.98	337.34	269.22	31.39	NA	9912
0.044	931.5	6.953	23.6	14.4	16.3	17.3	4.81	322.04	258.74	29.17	NA	9570
0.040	931.2	10.072	23.7	14.6	16.6	17.8	4.74	317.06	258.89	26.81	NA	9341

Table 7-4: Two phase data of Heavy oil-water flow for averaged μ_o = 3840 cP

V_{so} (m/s)	ρ_o (kg/m$^{3)}$	V_{sw} (m/s)	T_o (°C)	T_w (°C)	T_{inlet} (°C)	T_{outlet} (°C)	P_{inlet} (kPa)	P_{outlet} (kPa)	dp/dx (kPa/m)	μ_o by coriolis flow meter (cP)	μ_o using T_o (cP)
0.065	919.9	0.000	25.1	19.1	23.9	22.6	146.89	116.56	13.98	3512	3767
0.064	920.0	0.009	24.1	23.3	23.8	25.7	134.58	106.97	12.73	3456	4094
0.066	920.8	0.013	24.1	22.1	23.2	24.8	183.58	153.36	13.93	3476	4098
0.070	921.1	0.020	24.1	22.2	23.2	25.5	177.14	146.41	14.16	3496	4098
0.062	919.7	0.021	25.0	19.5	22.5	23.2	134.50	108.23	12.10	3575	3789
0.062	919.4	0.025	24.8	22.2	23.9	26.0	158.02	133.70	11.21	3260	3855
0.055	919.5	0.031	24.7	22.5	23.6	25.2	139.72	119.56	9.29	3232	3880
0.064	919.4	0.040	25.2	23.2	22.0	22.1	91.66	87.56	1.89	3544	3738
0.060	919.3	0.050	25.3	25.2	22.0	21.6	92.88	88.78	1.89	3505	3696
0.063	919.2	0.063	25.4	26.1	22.2	21.7	93.14	88.87	1.97	3474	3669
0.054	919.3	0.054	24.2	22.5	23.6	24.7	96.97	92.60	2.01	3347	4080
0.058	919.4	0.110	24.0	22.4	23.0	24.7	90.37	86.72	1.68	3236	4145
0.064	918.2	0.200	24.9	19.4	22.1	26.0	95.96	92.61	1.54	3018	3836
0.063	918.1	0.303	24.9	19.2	21.2	25.1	97.07	92.59	2.06	3024	3826
0.062	918.0	0.402	24.9	18.5	20.0	24.3	96.71	92.20	2.08	3030	3819
0.063	918.0	0.500	24.9	17.7	19.3	23.6	98.03	92.83	2.39	3033	3820
0.066	917.9	0.601	25.1	17.1	18.4	22.9	99.55	93.75	2.67	3022	3775
0.064	918.0	0.704	24.9	16.8	18.1	22.0	101.67	95.47	2.85	3012	3835
0.061	918.2	0.800	24.8	15.6	16.9	21.2	104.03	97.33	3.08	3024	3846
0.064	918.2	0.906	24.8	15.2	16.0	20.4	107.00	99.70	3.36	3030	3850

0.060	918.2	1.000	24.8	14.9	15.7	19.8	109.68	101.93	3.57	3033	3852
0.099	919.3	0.000	25.4	26.2	24.2	24.1	163.37	124.28	18.01	3426	3660
0.098	918.9	0.012	25.6	26.3	24.3	24.5	153.05	116.66	16.77	3357	3595
0.099	918.8	0.020	25.7	27.0	24.5	24.7	146.88	113.27	15.49	3323	3566
0.096	918.7	0.029	25.8	27.4	24.5	24.5	113.50	103.11	4.79	3295	3544
0.095	918.5	0.048	25.9	27.6	24.3	24.5	90.50	86.40	1.89	3267	3522
0.098	918.5	0.080	25.9	27.8	25.1	25.1	93.02	88.93	1.89	3243	3499
0.099	918.5	0.102	26.0	28.0	25.6	25.6	93.44	89.05	2.02	3226	3486
0.099	918.5	0.151	26.0	28.0	26.1	26.0	93.33	89.08	1.96	3210	3481
0.100	918.5	0.300	26.0	28.2	26.5	26.7	94.14	89.35	2.21	3198	3482
0.144	920.0	0.018	24.9	17.1	19.4	21.0	184.65	137.53	21.72	3808	3823
0.143	919.5	0.031	25.2	18.5	18.2	20.4	97.21	92.69	2.08	3789	3716
0.148	919.4	0.050	25.6	20.6	18.7	19.8	96.21	92.33	1.79	3719	3613
0.146	919.3	0.080	25.8	23.3	19.0	19.1	96.47	92.25	1.95	3645	3534
0.146	919.3	0.103	26.0	25.4	19.9	20.0	97.30	92.37	2.27	3584	3480
0.148	919.1	0.150	26.2	26.9	22.1	21.6	98.30	92.83	2.52	3531	3434
0.147	918.9	0.200	26.3	28.0	24.6	24.0	97.57	92.50	2.34	3481	3397
0.148	918.8	0.300	26.4	28.6	26.1	25.8	97.71	92.43	2.44	3440	3372
0.201	919.6	0.013	25.6	26.1	24.9	25.0	203.53	142.11	28.31	3177	3598
0.198	919.6	0.032	25.6	25.9	24.7	24.6	119.36	111.41	3.66	3197	3608
0.199	919.6	0.047	25.5	25.7	24.3	24.3	102.49	99.81	1.23	3220	3631
0.200	919.7	0.072	25.4	25.6	24.0	23.8	96.79	94.13	1.23	3249	3652
0.200	919.8	0.098	25.4	25.2	23.3	23.2	92.51	89.68	1.30	3275	3673
0.200	919.9	0.157	25.3	23.6	23.2	22.6	94.54	90.63	1.80	3320	3707
0.198	919.5	0.200	23.3	16.0	21.9	23.2	100.48	96.02	2.06	3175	4403
0.200	920.5	0.302	23.0	15.7	20.4	22.5	102.57	97.27	2.45	3288	4506

0.201	920.5	0.406	23.1	15.6	18.4	22.0	104.26	98.51	2.65	3335	4484
0.196	920.5	0.504	23.2	15.6	17.7	21.4	106.07	99.94	2.83	3346	4459
0.201	920.4	0.596	23.3	15.5	17.5	20.9	107.76	101.36	2.95	3339	4416
0.198	920.4	0.699	23.4	15.6	17.2	20.4	110.18	103.42	3.12	3315	4367
0.199	920.3	0.805	23.5	15.7	17.5	20.3	113.01	105.67	3.38	3287	4327
0.198	920.2	0.903	23.6	15.1	17.0	20.0	115.90	108.04	3.62	3261	4290
0.201	920.2	1.012	23.7	14.8	16.5	19.4	119.34	110.93	3.87	3242	4251
0.566	921.9	0.012	26.3	21.6	25.4	25.5	352.26	235.71	53.71	2989	3395
0.575	921.3	0.029	26.2	19.9	25.5	24.8	104.24	97.31	3.20	3010	3422
0.569	919.6	0.053	26.6	25.4	26.2	24.9	99.90	93.31	3.04	2926	3294
0.572	919.8	0.074	26.6	25.0	26.1	24.7	99.50	93.09	2.95	2946	3315
0.573	919.8	0.112	26.6	23.9	26.1	24.7	100.93	93.91	3.24	2957	3317
0.571	919.9	0.160	26.6	20.9	25.9	24.7	103.54	95.01	3.93	2984	3303
0.574	921.3	0.101	24.9	27.2	24.9	24.1	104.16	96.54	3.51	-	3832
0.575	921.3	0.148	24.7	26.8	24.4	23.6	106.29	97.66	3.98	-	3903
0.575	920.8	0.203	23.3	15.5	23.8	21.9	114.52	106.01	3.92	3259	4393
0.575	921.3	0.299	23.5	15.1	19.7	21.0	116.23	107.53	4.01	3323	4309
0.575	921.2	0.401	23.9	15.0	18.6	20.2	116.58	108.04	3.93	3293	4167
0.575	921.0	0.512	24.2	15.6	18.3	18.6	118.61	109.98	3.97	3226	4054
0.575	920.4	0.617	23.5	15.7	18.6	21.1	122.47	112.71	4.50	3154	4321
0.575	921.4	0.703	23.6	15.5	17.6	19.2	124.73	115.46	4.27	3278	4295
0.575	921.2	0.802	23.8	15.7	17.5	18.4	128.21	118.79	4.34	3287	4228
0.575	921.1	0.906	23.9	15.8	17.8	18.4	132.25	122.42	4.53	3270	4173
0.575	921.0	0.997	24.1	15.4	17.4	18.1	136.28	126.04	4.72	3251	4120

Table 7-5: Two phase data of Heavy oil-water flow for averaged μ_o = 8325 cP

V_{so} (m/s)	ρ_o (kg/m$^{3)}$	V_{sw} (m/s)	T_o (°C)	T_w (°C)	T_{inlet} (°C)	T_{outlet} (°C)	P_{inlet} (kPa)	P_{outlet} (kPa)	dp/dx (kPa/m)	μ_o by coriolis flow meter (cP)	μ_o using T_o (cP)
0.319	929.9	0.014	16.6	8.5	20.1	18.8	133.08	102.98	13.87	5125	7852
0.319	930.1	0.030	16.4	7.9	19.7	17.9	93.48	90.55	1.35	5182	8005
0.320	930.2	0.052	16.4	7.5	19.8	17.6	92.35	89.74	1.20	5213	7997
0.319	930.4	0.071	16.5	7.3	19.4	17.7	92.68	89.84	1.31	5295	7956
0.318	930.9	0.099	16.5	7.2	19.4	17.9	93.58	90.15	1.58	5459	7926
0.318	929.6	0.514	15.9	8.3	14.2	13.4	107.74	97.20	4.86	5130	8397
0.336	937.2	1.028	13.7	8.7	12.6	11.9	112.16	100.10	5.56	5300	10141

Table 7-6: Two phase data of Heavy oil-water flow for averaged μ_o = 13160 cP

V_{so} (m/s)	ρ_o (kg/m$^{3)}$	V_{sw} (m/s)	T_o (°C)	T_w (°C)	T_{inlet} (°C)	T_{outlet} (°C)	P_{inlet} (kPa)	P_{outlet} (kPa)	dp/dx (kPa/m)	μ_o by coriolis flow meter (cP)	μ_o using T_o (cP)
0.052	933.9	0.017	11.0	9.8	15.3	16.9	180.97	134.41	21.46	9154	12838
0.055	935.1	0.021	10.1	10.4	14.9	16.0	154.52	117.48	17.07	9033	13889
0.059	934.8	0.025	10.0	11.0	15.2	16.7	144.21	116.59	12.73	8893	14016
0.056	935.0	0.030	10.3	9.7	14.6	15.8	121.49	105.08	7.56	9034	13648
0.059	933.6	0.034	11.3	10.1	15.0	16.3	101.60	92.31	4.28	9029	12552
0.059	934.9	0.035	10.6	9.2	14.1	15.8	105.36	94.02	5.23	9004	13342
0.058	933.3	0.049	11.6	10.0	13.9	15.7	93.96	89.40	2.10	8878	12231
0.058	933.2	0.059	11.6	9.8	13.3	15.0	94.86	90.04	2.22	8836	12148
0.059	933.1	0.070	11.7	9.6	13.1	14.6	94.69	89.92	2.19	8751	12099
0.059	934.7	0.104	10.8	8.5	12.6	14.4	93.92	88.09	2.68	8931	13006
0.057	934.5	0.151	11.0	8.0	11.7	13.3	95.58	89.07	3.00	8884	12812
0.059	934.4	0.201	11.2	8.0	11.0	12.3	95.60	89.07	3.01	8816	12642
0.101	933.2	0.009	11.7	12.3	15.6	16.8	248.99	158.74	41.59	8176	12077
0.101	933.9	0.052	11.2	10.3	15.1	17.2	91.35	87.09	1.96	8300	12611
0.105	935.9	0.022	10.0	14.2	14.3	17.8	161.67	114.32	21.82	9665	14051
0.104	935.4	0.080	10.0	11.3	14.5	17.8	94.68	89.60	2.34	9597	14005
0.104	935.5	0.102	10.2	8.9	13.6	15.8	94.54	89.09	2.51	9535	13751
0.103	935.5	0.150	10.4	8.1	12.3	13.8	95.23	89.02	2.86	9466	13544
0.107	935.4	0.301	10.6	7.6	10.7	11.8	97.53	90.02	3.46	9378	13287
0.133	937.5	0.015	10.3	11.3	13.3	15.7	185.87	125.89	27.64	10583	13636

0.138	937.1	0.029	10.4	10.7	13.9	15.5	99.66	92.64	3.24	10325	13495
0.137	937.1	0.049	10.5	10.8	14.1	15.5	96.27	91.67	2.12	10189	13392
0.140	936.9	0.081	10.6	10.7	13.9	15.2	95.50	90.87	2.14	10039	13307
0.139	936.8	0.101	10.6	9.6	13.6	14.4	97.18	92.16	2.31	9899	13233
0.138	936.7	0.149	10.7	8.4	12.8	13.8	98.69	92.60	2.81	9748	13180
0.139	936.7	0.207	10.6	7.5	11.7	12.6	100.33	93.37	3.21	9655	13258
0.139	936.8	0.311	10.6	7.2	10.8	11.3	102.16	94.19	3.67	9676	13280

Table 7-7: Two phase data of Heavy oil-water flow for averaged μ_o = 15979 cP

V_{so} (m/s)	ρ_o (kg/m$^{3)}$	V_{sw} (m/s)	T_o (°C)	T_w (°C)	T_{inlet} (°C)	T_{outlet} (°C)	P_{inlet} (kPa)	P_{outlet} (kPa)	dp/dx (kPa/m)	μ_o by coriolis flow meter (cP)	μ_o using T_o (cP)
0.070	938.9	0.000	8.7	18.2	12.0	14.1	417.70	287.24	60.12	11150	15649
0.062	938.4	0.010	7.9	18.8	13.5	16.4	234.10	145.76	40.71	11850	16805
0.056	937.9	0.025	8.4	18.7	14.3	17.1	163.02	114.43	22.39	11450	16090
0.057	937.4	0.033	8.4	18.5	13.9	17.4	131.86	103.04	13.28	11355	16114
0.059	937.2	0.053	8.6	18.5	14.1	18.1	100.39	92.14	3.80	11265	15869
0.062	937.0	0.073	8.5	18.6	15.1	18.4	97.37	91.20	2.84	11267	15977
0.060	936.2	0.116	8.1	18.6	15.2	18.4	96.28	91.00	2.43	11340	16546
0.061	935.7	0.151	7.8	18.5	15.0	18.5	94.84	90.51	2.00	11250	16942
0.063	935.6	0.205	7.7	18.4	16.8	18.8	96.06	91.28	2.20	10522	17071
0.109	938.9	0.000	8.8	18.2	12.2	14.4	449.72	282.48	77.07	11210	15515
0.108	938.7	0.019	8.2	18.8	11.6	16.7	175.11	117.19	26.69	11180	16398
0.119	936.8	0.052	7.9	18.7	11.6	18.0	97.92	90.77	3.30	11000	16795
0.116	938.1	0.105	9.1	18.4	13.1	18.3	96.66	91.17	2.53	10850	15187
0.116	938.4	0.081	8.8	18.5	12.6	18.3	95.95	90.93	2.31	11023	15557
0.116	938.0	0.153	9.2	18.4	13.8	18.3	96.19	90.66	2.55	10725	14966
0.118	937.8	0.182	9.2	18.3	14.1	18.4	97.11	91.26	2.70	10670	15027
0.116	938.0	0.287	8.9	19.7	16.6	18.9	98.85	93.26	2.58	10150	15392
0.112	938.3	0.123	8.7	19.8	14.5	18.4	94.62	90.11	2.08	10293	15719

Table 7-8: Three phase flow data of heavy oil-water-air for V_{so} = 0.06 m/s and averaged μ_o = 3286 cP

V_{so} (m/s)	ρ_o (kg/m$^{3)}$	V_{sw} (m/s)	V_{sg} (m/s)	T_o (°C)	T_w (°C)	T_g (°C)	T_{inlet} (°C)	T_{outlet} (°C)	P_{inlet} (kPa)	P_{outlet} (kPa)	dp/dx (kPa/m)	μ_o by coriolis flow meter (cP)	μ_o using T_o (cP)
0.069	917.29	0.023	1.027	27.12	26.92	21.12	24.17	23.98	108.77	97.58	5.15	2985	3157
0.066	917.26	0.023	1.528	27.14	27.30	21.14	25.03	24.49	104.82	95.11	4.48	2971	3152
0.069	917.21	0.022	1.939	27.16	27.54	21.16	25.51	24.94	103.43	94.54	4.10	2961	3145
0.067	917.20	0.022	3.136	27.17	27.81	21.24	25.91	25.31	101.56	94.22	3.38	2946	3142
0.065	917.16	0.022	5.173	27.19	27.90	21.32	25.98	25.44	102.25	94.75	3.45	2940	3138
0.067	917.14	0.023	6.995	27.19	27.97	21.36	25.77	25.42	101.46	94.70	3.12	2934	3139
0.065	917.20	0.023	10.270	27.21	28.11	21.56	25.55	25.34	102.67	95.58	3.26	2924	3131
0.066	917.18	0.039	1.105	27.17	28.25	21.65	27.18	26.54	103.94	93.79	4.68	2894	3142
0.062	917.75	0.039	1.530	27.16	28.26	21.62	27.17	26.61	100.71	92.82	3.64	2889	3145
0.059	920.25	0.041	1.963	25.81	24.84	19.85	21.43	21.96	103.74	94.96	4.05	3521	3537
0.063	920.07	0.042	2.968	25.98	25.58	19.85	22.48	22.36	101.88	94.44	3.43	3479	3487
0.062	919.92	0.040	5.191	26.11	25.99	19.89	23.39	23.06	101.16	94.72	2.97	3440	3446
0.060	919.70	0.038	7.017	26.22	26.31	19.97	23.90	23.58	101.00	94.94	2.79	3406	3415
0.062	919.43	0.038	10.028	26.34	26.72	20.14	24.31	24.06	100.66	94.82	2.69	3358	3379
0.062	919.17	0.201	1.039	26.39	27.17	20.20	26.16	25.90	97.56	94.06	1.61	3322	3364
0.060	918.84	0.199	1.485	26.40	27.26	20.30	26.30	26.21	97.41	93.86	1.64	3297	3360
0.061	918.68	0.200	2.015	26.42	27.32	20.39	26.40	26.34	97.38	93.78	1.66	3278	3354
0.062	918.66	0.201	3.203	26.45	27.39	20.41	26.50	26.35	97.30	93.78	1.62	3254	3346
0.065	918.51	0.199	4.966	26.50	26.05	20.46	26.57	26.34	97.60	93.99	1.66	3232	3331
0.063	918.51	0.202	6.915	26.51	22.70	20.52	24.76	24.86	98.31	94.37	1.82	3217	3328
0.062	918.60	0.197	9.844	26.38	22.15	20.60	23.08	23.09	100.01	95.06	2.28	3207	3366

Table 7-9: Three phase flow data of heavy oil-water-air for V_{so} = 0.10 m/s and averaged μ_o = 3411 cP

V_{so} (m/s)	ρ_o (kg/m$^{3)}$	V_{sw} (m/s)	V_{sg} (m/s)	T_o (°C)	T_w (°C)	T_g (°C)	T_{inlet} (°C)	T_{outlet} (°C)	P_{inlet} (kPa)	P_{outlet} (kPa)	dp/dx (kPa/m)	μ_o by coriolis flow meter (cP)	μ_o using T_o (cP)
0.104	920.9	0.022	1.000	24.8	23.5	19.2	21.6	22.4	137.61	109.48	12.96	3620	3860
0.104	920.4	0.023	1.504	25.2	24.5	19.1	23.2	23.2	123.77	103.13	9.52	3572	3735
0.106	920.3	0.023	2.130	25.5	25.2	19.1	24.0	23.7	113.54	98.78	6.80	3514	3640
0.105	920.1	0.023	3.164	25.8	26.1	19.1	24.6	24.0	107.71	96.62	5.11	3439	3535
0.108	919.9	0.023	5.054	26.1	26.9	19.1	24.8	24.2	106.92	96.87	4.63	3348	3445
0.108	919.8	0.024	7.114	26.2	27.3	19.2	24.8	24.3	106.91	97.20	4.47	3301	3405
0.107	919.7	0.024	10.074	26.4	27.8	19.4	24.6	24.4	107.27	97.71	4.41	3261	3370
0.104	919.4	0.048	1.379	26.7	28.7	19.5	26.1	25.9	104.55	93.03	5.31	3164	3265
0.110	919.3	0.049	2.051	26.8	28.8	19.4	26.5	26.3	102.24	92.57	4.46	3141	3241
0.109	919.1	0.052	2.983	26.9	28.9	19.4	26.8	26.5	99.91	92.20	3.55	3117	3227
0.107	919.2	0.051	4.968	26.9	29.0	19.4	26.9	26.6	99.31	92.66	3.06	3102	3230
0.107	919.2	0.050	7.270	26.7	29.0	19.5	26.9	26.7	99.41	92.98	2.96	3097	3264
0.109	919.3	0.050	10.281	26.7	29.1	19.5	26.7	26.6	99.09	92.97	2.82	3097	3286
0.103	919.3	0.214	1.065	25.6	25.9	18.8	21.0	20.2	98.03	94.29	1.72	3521	3596
0.103	919.2	0.214	1.483	25.8	27.9	18.8	25.5	25.0	97.90	94.06	1.77	3500	3544
0.102	919.0	0.216	1.944	26.1	28.5	18.9	26.4	26.3	97.93	93.99	1.81	3447	3435
0.106	918.9	0.205	3.114	26.4	28.7	19.0	26.8	26.7	97.84	94.01	1.77	3392	3355
0.102	919.0	0.208	4.984	26.7	28.9	19.2	27.2	26.8	98.26	94.36	1.80	3328	3284
0.106	918.6	0.207	6.987	26.8	25.9	19.4	27.2	27.0	98.90	94.72	1.93	3294	3256
0.105	918.5	0.206	10.016	26.8	23.9	19.5	25.8	25.7	99.88	95.19	2.16	3263	3242

Table 7-10: Three phase flow data of heavy oil-water-air for V_{so} = 0.14 m/s and averaged μ_o = 3270 cP

V_{so} (m/s)	ρ_o (kg/m$^{3)}$	V_{sw} (m/s)	V_{sg} (m/s)	T_o (°C)	T_w (°C)	T_g (°C)	T_{inlet} (°C)	T_{outlet} (°C)	P_{inlet} (kPa)	P_{outlet} (kPa)	dp/dx (kPa/m)	μ_o by coriolis flow meter (cP)	μ_o using T_o (cP)
0.15	918.7	0.015	0.85	26.0	21.2	19.5	24.7	25.2	155.46	120.36	16.18	3189	3469
0.15	918.6	0.015	1.40	26.0	21.5	19.5	25.1	25.1	138.96	112.45	12.22	3191	3485
0.15	918.6	0.015	2.20	26.0	21.7	19.5	25.5	25.1	123.37	105.49	8.24	3186	3477
0.14	918.7	0.016	3.00	26.0	21.9	19.6	25.5	25.1	126.94	108.53	8.48	3162	3483
0.15	918.9	0.016	5.42	25.8	22.2	19.8	25.3	25.0	163.57	137.18	12.16	3163	3543
0.14	918.8	0.016	7.11	26.7	25.1	20.8	26.7	26.5	163.16	133.96	13.46	2961	3271
0.14	918.7	0.016	9.94	26.6	22.9	21.0	26.6	26.4	179.30	136.76	19.60	2962	3297
0.14	918.6	0.048	1.43	26.6	22.3	21.0	27.3	26.8	112.39	95.45	7.81	2959	3304
0.14	918.7	0.051	2.07	26.5	22.4	21.0	26.5	26.5	105.71	94.33	5.25	2949	3319
0.14	918.8	0.054	3.08	26.5	22.5	21.0	25.7	25.5	102.54	93.89	3.98	2950	3345
0.14	918.9	0.056	5.10	26.3	22.7	21.0	25.2	25.0	102.32	94.37	3.67	2956	3380
0.15	918.3	0.050	6.99	27.0	27.3	21.2	24.8	23.9	104.74	96.41	3.84	2936	3180
0.15	918.2	0.049	10.42	27.1	27.6	21.4	25.2	24.8	104.96	96.90	3.71	2911	3149
0.15	918.1	0.209	1.55	27.3	28.3	21.4	27.0	26.7	98.01	93.82	1.93	2863	3111
0.15	918.0	0.204	1.99	27.4	28.5	21.4	27.3	27.2	97.86	93.70	1.92	2844	3087
0.15	918.0	0.206	2.99	27.4	28.6	21.4	27.5	27.4	98.10	93.79	1.99	2810	3072
0.15	917.9	0.205	5.24	27.5	28.7	21.5	27.5	27.5	99.19	94.39	2.21	2795	3058
0.15	917.9	0.206	7.19	27.5	28.7	21.6	27.6	27.6	99.76	94.75	2.31	2781	3052
0.15	917.9	0.205	10.67	27.5	28.8	21.7	27.7	27.7	100.62	95.35	2.43	2766	3056

Table 7-11: Three phase flow data of heavy oil-water-air for V_{so} = 0.06 m/s and averaged μ_o = 12495 cP

V_{so} (m/s)	ρ_o (kg/m$^{3)}$	V_{sw} (m/s)	V_{sg} (m/s)	T_o (°C)	T_w (°C)	T_g (°C)	T_{inlet} (°C)	T_{outlet} (°C)	P_{inlet} (kPa)	P_{outlet} (kPa)	dp/dx (kPa/m)	μ_o by coriolis flow meter (cP)	μ_o using T_o (cP)
0.064	933.8	0.021	1.136	11.4	14.1	21.1	17.6	17.7	157.66	110.02	21.95	8538	12392
0.065	933.7	0.019	1.430	11.6	12.5	21.1	17.7	17.5	166.13	112.18	24.86	8466	12208
0.063	933.6	0.019	2.163	11.7	11.1	21.1	17.4	17.3	157.68	110.02	21.96	8910	12041
0.062	933.4	0.020	3.046	11.8	10.5	21.1	16.9	16.9	159.02	109.68	22.73	8377	11928
0.064	933.3	0.020	5.271	12.0	10.0	21.2	16.1	16.5	164.80	114.43	23.21	8312	11759
0.064	933.2	0.021	6.875	12.1	9.7	21.2	15.6	16.0	156.28	113.35	19.78	8246	11642
0.066	933.1	0.024	10.303	12.2	9.4	21.3	15.1	15.7	134.89	105.34	13.62	8186	11539
0.065	932.8	0.039	1.473	12.4	9.0	21.3	14.7	15.5	112.10	99.94	5.61	8062	11367
0.065	932.7	0.041	2.002	12.3	8.7	21.4	13.7	14.5	111.93	99.61	5.68	8012	11412
0.068	932.9	0.042	3.122	12.1	8.7	21.4	13.4	14.2	113.07	99.12	6.43	8088	11703
0.063	935.2	0.038	5.186	10.0	10.8	18.2	14.7	15.5	129.54	102.01	12.69	10052	13951
0.062	935.2	0.040	7.533	10.1	9.9	18.4	14.1	15.0	126.42	101.03	11.70	10048	13857
0.062	935.1	0.042	9.700	10.2	9.4	18.5	13.4	14.5	122.68	100.24	10.34	10026	13744
0.061	934.7	0.201	1.494	10.7	7.3	18.5	9.9	11.2	100.52	94.78	2.65	9887	13220
0.061	934.6	0.200	2.114	10.8	7.5	18.5	9.8	11.2	101.57	95.12	2.97	9841	13093
0.063	934.4	0.207	2.931	10.9	8.0	18.5	9.8	11.2	103.05	95.64	3.41	9780	12980
0.065	934.4	0.202	4.943	10.9	8.6	18.5	10.3	11.6	105.10	96.45	3.98	9725	12906
0.064	934.3	0.203	6.900	11.0	10.4	18.6	10.5	11.7	106.73	97.26	4.36	9693	12846
0.061	934.3	0.200	9.967	11.0	11.3	18.7	11.9	12.9	107.43	97.84	4.42	9646	12814

Table 7-12: Three phase flow data of heavy oil-water-air for V_{so} = 0.10 m/s and averaged μ_o = 12739 cP

V_{so} (m/s)	ρ_o (kg/m$^{3)}$	V_{sw} (m/s)	V_{sg} (m/s)	T_o (°C)	T_w (°C)	T_g (°C)	T_{inlet} (°C)	T_{outlet} (°C)	P_{inlet} (kPa)	P_{outlet} (kPa)	dp/dx (kPa/m)	μ_o by coriolis flow meter (cP)	μ_o using T_o (cP)
0.113	936.2	0.021	2.292	11.2	10.0	19.7	16.0	17.3	179.39	112.08	31.02	8726	12641
0.110	936.1	0.022	2.974	11.3	10.2	19.7	15.8	16.8	166.02	111.56	25.10	8629	12466
0.114	935.9	0.023	5.282	11.5	10.2	19.7	15.3	16.0	150.56	113.96	16.87	8552	12269
0.114	935.8	0.026	7.492	11.7	10.2	19.8	14.8	15.7	151.62	114.88	16.93	8436	12036
0.112	935.6	0.025	10.336	11.9	10.2	19.9	14.5	15.4	146.36	114.49	14.69	8327	11862
0.113	935.4	0.050	2.264	12.1	10.0	19.9	14.4	15.0	111.09	99.60	5.30	8178	11696
0.115	935.5	0.051	3.284	11.9	9.8	19.9	14.0	14.7	110.34	98.71	5.36	8217	11827
0.103	936.3	0.050	3.956	10.1	11.0	17.9	14.5	15.2	104.77	93.30	5.28	9939	13860
0.103	936.2	0.052	4.604	10.3	9.3	18.0	13.6	14.5	108.64	95.15	6.22	9893	13651
0.103	936.2	0.055	7.271	10.5	8.8	18.3	12.6	13.7	109.13	95.47	6.30	9869	13458
0.105	936.1	0.052	9.871	10.6	8.6	18.4	12.3	13.2	112.51	96.81	7.23	9835	13284
0.104	935.8	0.209	2.095	10.9	7.7	18.4	10.9	11.9	99.83	92.18	3.52	9710	12992
0.106	935.6	0.206	3.078	10.9	7.8	18.5	10.7	11.5	100.09	92.40	3.54	9652	12912
0.104	935.6	0.203	5.067	10.9	8.0	18.5	10.6	11.4	102.29	93.39	4.10	9638	12910
0.105	935.6	0.201	7.048	10.9	8.3	18.6	10.8	11.4	104.19	94.35	4.53	9611	12949
0.104	935.6	0.204	10.006	10.8	8.5	18.7	10.8	11.4	106.01	95.43	4.88	9642	13004

Table 7-13: Three phase flow data of heavy oil-water-air for V_{so} = 0.14 m/s and averaged μ_o = 12949 cP

V_{so} (m/s)	ρ_o (kg/m$^{3)}$	V_{sw} (m/s)	V_{sg} (m/s)	T_o (°C)	T_w (°C)	T_g (°C)	T_{inlet} (°C)	T_{outlet} (°C)	P_{inlet} (kPa)	P_{outlet} (kPa)	dp/dx (kPa/m)	μ_o by coriolis flow meter (cP)	μ_o using T_o (cP)
0.14	935.9	0.017	1.88	11.0	8.4	18.7	14.5	16.5	255.22	151.57	47.76	9809	12862
0.14	935.9	0.017	2.62	11.0	8.9	18.8	14.5	16.1	252.50	149.97	47.25	9728	12825
0.15	935.8	0.018	4.98	11.0	9.0	18.9	14.2	15.0	189.20	135.86	24.58	9639	12852
0.14	935.9	0.019	6.60	10.9	9.1	19.0	14.0	14.6	218.68	160.86	26.65	9622	12938
0.14	936.3	0.020	8.75	10.8	9.1	19.2	13.7	14.5	243.26	185.82	26.47	9699	13065
0.14	934.9	0.055	1.62	11.8	8.5	16.6	12.8	13.2	104.39	96.99	3.41	8893	11970
0.14	935.0	0.051	2.75	11.8	8.6	16.6	12.7	13.2	109.32	98.94	4.78	8923	11982
0.14	935.2	0.050	4.78	11.8	8.6	16.7	12.5	13.1	114.20	100.81	6.17	8961	12016
0.14	935.2	0.051	6.70	11.8	8.7	16.7	12.4	13.1	118.17	101.87	7.52	8995	12005
0.14	935.2	0.051	9.77	11.8	8.7	16.9	12.3	13.1	121.05	103.16	8.24	9012	12003
0.15	937.4	0.205	1.45	10.1	8.2	13.9	12.9	14.3	99.31	94.27	2.32	10245	13839
0.15	937.4	0.201	2.00	10.2	7.2	13.8	10.6	11.8	101.18	95.20	2.76	10229	13744
0.15	937.5	0.196	3.05	10.2	7.1	13.9	10.5	11.4	104.33	96.48	3.62	10216	13707
0.15	937.6	0.214	5.26	10.2	7.0	14.1	10.3	11.1	109.62	98.78	4.99	10261	13777
0.15	937.8	0.204	7.17	10.2	7.1	14.4	10.2	10.9	111.78	100.08	5.39	10312	13795
0.15	937.9	0.203	10.20	10.2	7.2	14.7	10.2	10.9	113.69	101.45	5.64	10307	13804

Table 7-14: Three phase flow data of heavy oil-water-sand (1% sand concentration)

V_{so} (m/s)	ρ_o (kg/m$^{3)}$	V_{ss} (m/s)	T_o (°C)	T_w (°C)	T_{inlet} (°C)	T_{outlet} (°C)	P_{inlet} (kPa)	P_{outlet} (kPa)	dp/dx (kPa/m)	μ_o by coriolis flow meter (cP)	μ_o using T_o (cP)
0.103	930.3	0.707	16.0	13.9	14.2	14.7	107.53	98.32	4.24	7380	8313
0.098	930.0	0.594	16.0	13.9	14.6	14.6	101.73	95.35	2.94	7340	8319
0.099	929.9	0.503	16.0	13.9	14.7	14.7	99.32	94.13	2.40	7323	8312
0.098	929.8	0.408	16.0	13.9	14.6	14.8	97.32	93.21	1.90	7311	8307
0.095	929.8	0.302	16.0	13.9	14.6	15.0	95.33	92.40	1.35	7299	8289
0.099	929.7	0.205	16.1	13.9	14.8	15.3	94.96	92.16	1.29	7281	8263
0.099	929.7	0.098	16.1	14.0	15.7	15.5	95.82	92.88	1.36	7256	8267
0.095	929.4	0.057	16.1	14.1	15.7	15.8	98.66	93.34	2.45	7144	8247
0.084	929.6	0.000	16.1	14.1	16.2	16.3	190.85	125.54	30.10	7134	8227
0.143	929.0	0.601	16.5	14.8	13.9	13.8	102.89	95.51	3.40	6700	7939
0.143	929.1	0.502	16.5	14.8	14.1	13.9	100.23	94.25	2.76	6700	7941
0.141	929.0	0.397	16.5	14.8	14.0	14.0	97.73	93.16	2.11	6700	7932
0.140	929.0	0.312	16.5	14.8	14.1	14.5	95.93	92.42	1.62	6700	7934
0.140	929.0	0.211	16.5	14.8	14.4	15.0	94.59	91.77	1.30	6700	7949
0.140	929.1	0.146	16.4	14.8	15.2	14.7	100.55	93.66	3.18	6700	8021
0.137	929.2	0.096	16.3	14.9	16.2	15.1	97.61	92.72	2.25	6700	8087
0.139	929.3	0.067	16.3	14.9	16.3	15.2	96.82	92.43	2.02	6700	8112
0.138	929.6	0.048	16.1	14.9	16.5	15.5	98.09	92.73	2.47	6700	8221

Table 7-15: Three phase flow data of heavy oil-water-sand (5% sand concentration)

V_{so} (m/s)	ρ_o (kg/m$^{3)}$	V_{ss} (m/s)	T_o (°C)	T_w (°C)	T_{inlet} (°C)	T_{outlet} (°C)	P_{inlet} (kPa)	P_{outlet} (kPa)	dp/dx (kPa/m)	μ_o by coriolis flow meter (cP)	μ_o using T_o (cP)
0.096	930.2	1.216	16.0	14.1	13.6	14.1	120.33	103.15	7.92	7200	8305
0.102	930.1	0.969	16.0	14.1	14.2	14.2	111.52	99.23	5.67	7200	8273
0.099	930.2	0.850	16.0	14.1	14.5	14.2	108.10	97.92	4.69	7200	8278
0.097	930.1	0.832	16.0	14.0	14.5	14.2	108.56	98.13	4.81	6700	8277
0.093	929.7	0.592	16.0	16.5	14.4	13.1	103.53	95.00	3.93	6700	8300
0.098	929.6	0.501	16.0	16.4	14.6	13.0	99.67	93.12	3.02	6700	8294
0.096	929.6	0.401	16.0	16.4	14.7	13.1	96.60	91.79	2.22	6700	8294
0.093	929.6	0.295	16.0	16.4	13.8	13.9	94.50	91.08	1.58	6700	8298
0.141	930.0	0.518	16.1	14.8	16.0	15.1	101.36	95.63	2.64	7102	8263
0.139	929.9	0.396	16.1	14.8	16.1	15.4	98.82	94.65	1.92	7066	8248
0.140	929.9	0.300	16.1	14.8	16.0	15.7	98.53	94.40	1.90	7049	8253

Table 7-16: Three phase flow data of heavy oil-water-sand (10% sand concentration)

V_{so} (m/s)	ρ_o (kg/m$^{3)}$	V_{ss} (m/s)	T_o (°C)	T_w (°C)	T_{inlet} (°C)	T_{outlet} (°C)	P_{inlet} (kPa)	P_{outlet} (kPa)	dp/dx (kPa/m)	μ_o by coriolis flow meter (cP)	μ_o using T_o (cP)
0.111	929.4	0.680	16.2	16.0	15.9	15.6	100.28	93.37	3.18	6830	8171
0.111	929.4	0.556	16.2	16.0	16.1	15.4	96.68	91.66	2.32	6812	8161
0.110	929.4	0.442	16.2	16.0	16.3	15.6	94.91	90.72	1.93	6795	8160
0.141	929.8	0.678	16.0	16.0	16.5	16.6	102.24	94.31	3.65	6920	8277
0.143	929.8	0.605	16.1	16.0	16.5	16.7	99.41	93.07	2.92	6898	8268
0.141	929.7	0.477	16.1	16.0	16.6	16.8	96.45	91.83	2.13	6879	8260
0.143	929.7	0.380	16.0	16.0	16.6	16.9	96.55	91.66	2.26	6864	8271

Appendix B: ECT in oil/ water and oil/ air (two phase) flows

- ECT in oil/gas flow:

The ECT sensor was tested in the 1 inch pipe line to dynamically monitor the two phase heavy oil/ water flow for both intermittent (i.e., Plug and Slug) and annular flows. The heavy oil was registered as low permittivity reference (blue colour), while air was assigned with the high permittivity reference (coded as red).

In the intermittent flow, ECT gave reasonable representation of both liquid bodies and gas pockets associated with this type of flow, shown in Figure 7-1. The output was sequential and repetitive for different plugs/slugs observed in the pipe. Initial, large gas pocket was detected by the ECT as it passed through the sensor while coated with oil layer in the circumference (Figure 7-1a); then larger amount of oil would accumulate in the bottom of the pipe due to gravity (Figure 7-1b) while the gas pocket raised upward due to the deference in densities between the two fluids (Figure 7-1c). Finally the liquid body of heavy oil passed through the ECT sensor to complete a single cycle of an intermittent flow (Figure 7-1d).

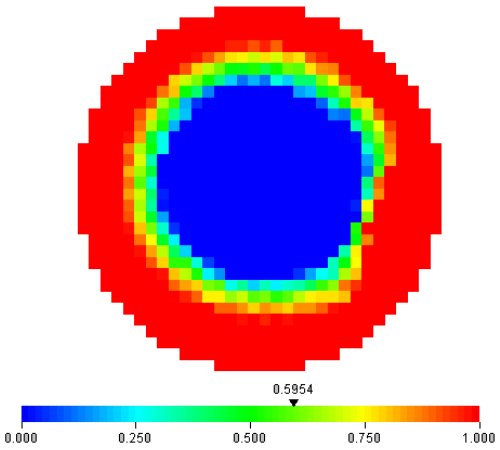

(a) Gas pocket in heavy oil

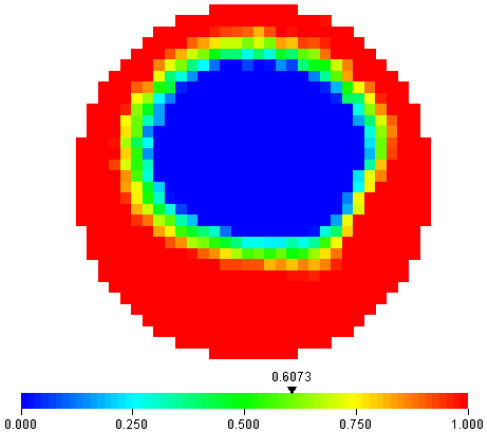

(b) Heavy oil level starts to increase

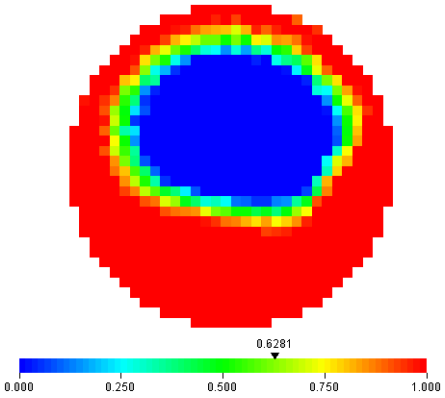

(c) More heavy oil with less gas.

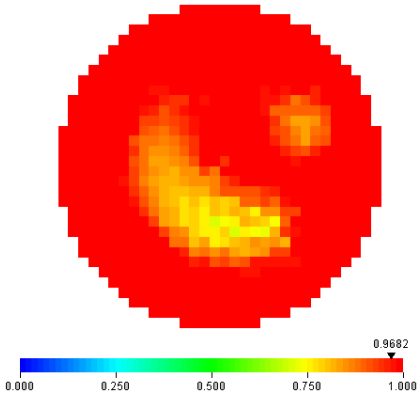

(d) Plug/slug body passing

Figure 7-1: ECT cross sectional area outputs for intermittent flow.

It was noted that lower permittivity values, that should represent gas traces in ECT output, were detected as plug/slug body passed through the sensor. This phenomenon was thought to be caused by: the limitation of the ECT sampling rate being slow to captivate the full motion of a single plug/slug passing through, that leads to capturing a portion of the fully occupied liquid body; another is the dispersed bubbles entrained in the liquid phase in the oil as it was observed previously in the oil coating film (Figure 7-2).

The instrument has the potential to provide qualitative information for the heavy oil/air flow. By examining the 66 output readings from the different pairs of electrodes, the frequency of the heavy oil liquid body can be determined by examining the normalized pixel permittivity's minimum, mean, and maximum values against time. Figure 7-2 represents the signal output for a plug flow at 0.03 m/s V_{so} and 1.0 m/s V_{sg}. The 2d stacked image is presented for comparison with the produced graph.

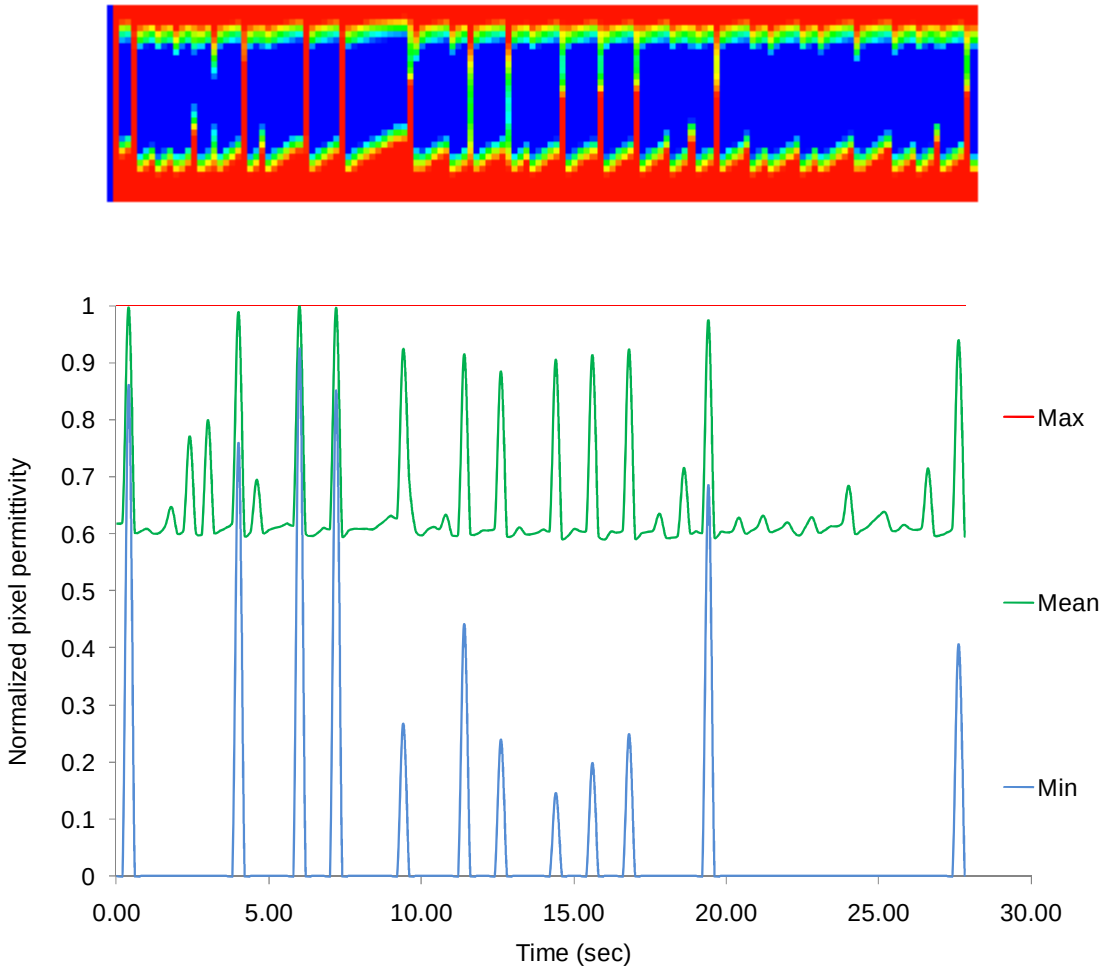

Figure 7-2: Liquid body tracer in intermittent "plug" flow

When examining the Min curve in the graph against the stacked image, the trend of the 'detected' liquid body frequency can be considered when the normalized pixel permittivity values spiked above 0. However, most of the 'actual' liquid bodies could not be captured by the device due to the slow

sampling response of this acquired instrument. The mean signal gives the same outcome above 0.8, yet lower values should be considered to capture the 'actual' frequency of liquid bodies. Finally, the Min value maintained constant at 1.0, indicating that one pixel at least was representing pure oil droplet in the reconstructive image at all time. For the presented data, the 'detected' frequency was found to be 0.46 Hz. However, as mentioned above, the 'actual' frequency corresponding was found to be much higher than the one produced by ECT.

The low sampling rate issue becomes even more significant as V_{sg} was increased in the system. Although the actual flow was confirmed by reviewing the recordings from the HD video camera, the ECT output results started to skip the last output (Figure 7-1d) in the intermittent cycle and less plug/slug bodies were captured by the instruments. A sample of slug flow signal is presented in Figure 7-3 for superficial velocities of 0.03 and 5.0 m/s for heavy oil and gas respectively. Again the 2d stacked image is presented for comparison with the produced graph.

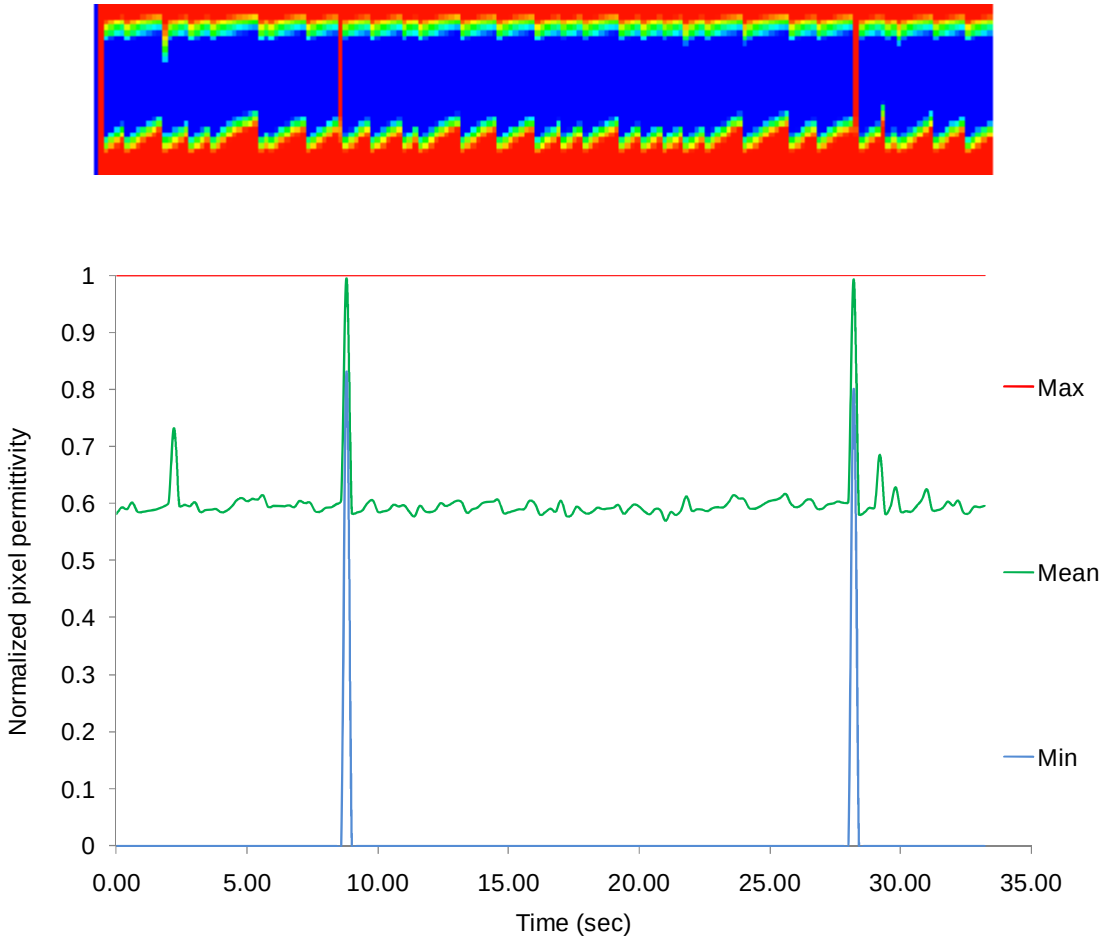

Figure 7-3: Liquid body tracer in intermittent "slug" flow

Annular flow observed by ECT output is best described as continuous eccentric gas stream flowing eccentrically along the centre of the pipe (Figure 7-4). The heavy oil film is much thicker at the bottom of the pipe due to gravity, leaving thinner coated layer of oil in the upper section of the pipe. However, this also can be categorized as stratified flow with continuous oil coating.

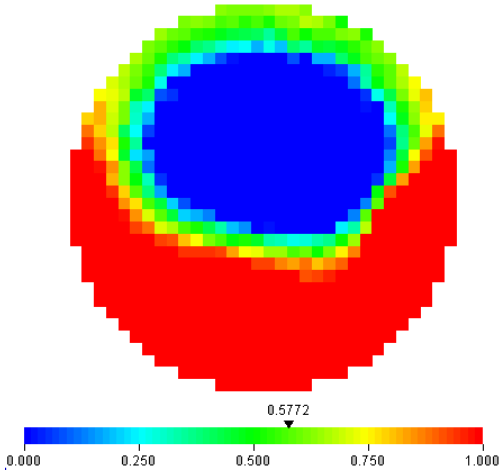

Figure 7-4: ECT cross sectional area output for annular flow.

Images can be stacked together to form a time or spatial series. The visual stacked 3d output for annular flow is given in Figure 7-5. It is shown that the flow of each fluid is persistent and continuous in their separate zone layers.

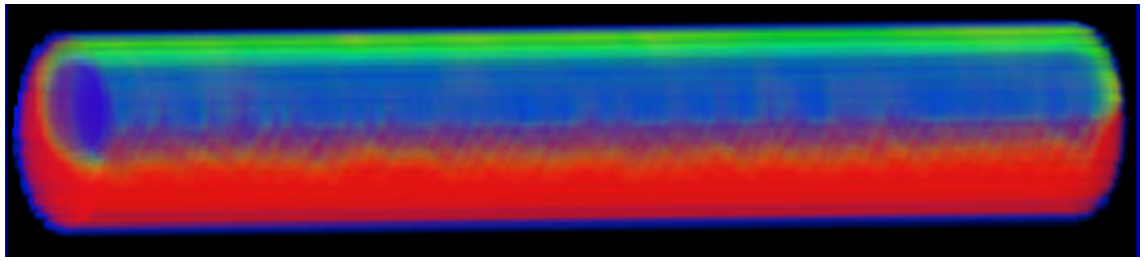

Figure 7-5: Stacked 3d output for annular flow

Finally, the normalized pixel permittivity output is shown in Figure 7-6 with the 2d stacked image. As expected, no significant changes in the measured values were found by the instrument as traces of liquid bodies were never found in this type of flow.

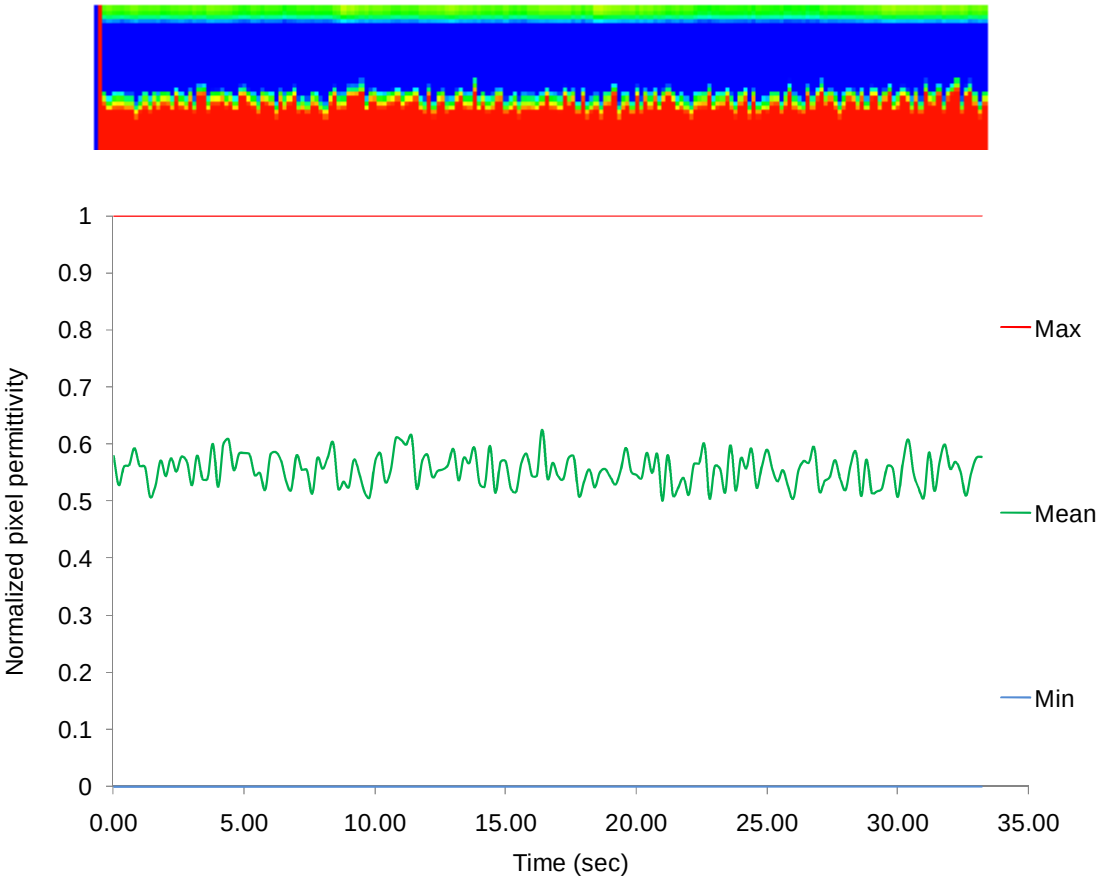

Figure 7-6: Liquid body tracer in annular flow

- ECT in oil/water flow:

The ECT sensor was tested in the 1 inch pipe line to dynamically monitor the two phase heavy oil/ water flow for the 3 main flow patterns (i.e., water continuous, oil continuous, and transition phase). The heavy oil was registered as low permittivity reference (blue colour), while water was assigned the high permittivity reference (coded as red).

In the oil continuous phase, the periodic lumps of water travelling through heavy oil, found in WPO, were distinguished using the ECT as two unique outputs. The motion was cyclic shift between pure heavy oil (Figure 7-7a) and the lumps of water in heavy oil (Figure 7-7b); though the output was indicating water is travelling in the core and the annulus at the same time (presented in green),

which is believed artificial yet unconfirmed through the presented study due to the dimness colour of heavy oil, It is thought that the effect of low water concentration over the sensitivity matrix distortion may cause the false reading in the core, as it has been reported in the literature for low sand concentrations (Al-Awadi et al., 2010). Also the annulus representation of water thickness ratio is inadequate; this is believed to be resulted by having the sensitivity field of the ECT (in principle) stronger at the perimeter than the core, and the very high permittivity nature of water which will disturb the sensitivity matrix of the system (Mwambela and Johansen, 2001),

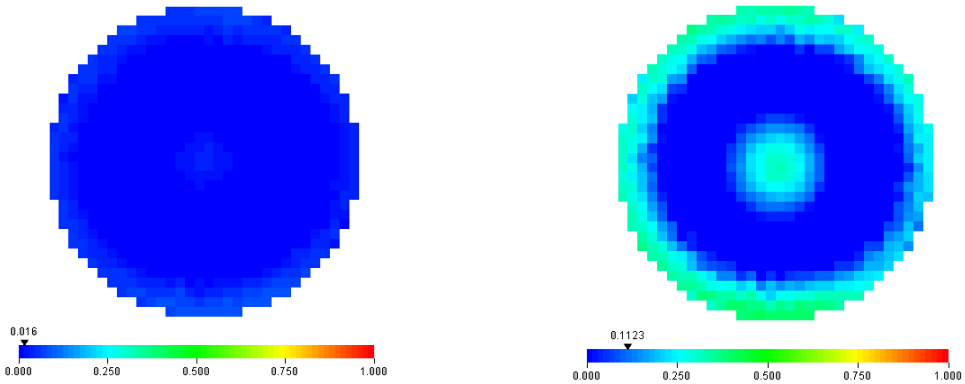

(a) Pure heavy oil phase **(b) Water lump in heavy oil**

Figure 7-7: WPO ECT cross sectional area outputs

Images can be stacked together to form a time series or spatial series. The visual stacked 3d output for the oil continuous phase is shown in Figure 7-8. It is shown that the existence of water portions would occur periodically in the pipe.

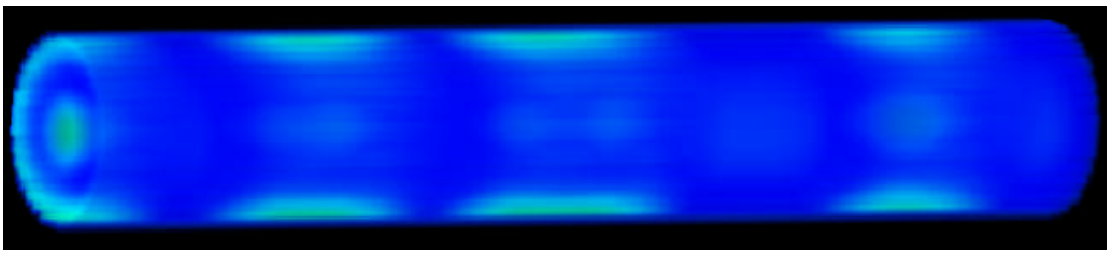

Figure 7-8: Stacked 3d output for oil continuous flow

Although the reconstructive image technique used in ECT for online measurement, Linear Back Projection (LBP), produces poor-quality images and difficult to provide quantitative information in this region (oil continuous phase), the instrument can provide qualitative information for the water/heavy oil flow in this regime; as the frequency of water pulse appearance in the heavy oil pipe can be determined by examining the normalized pixel permittivity's minimum, mean, and maximum values against time as shown in Figure 7-9. The 2d stacked image is presented for comparison with the produced graph.

When examining the max curve in the graph against the stacked image, the trend of the 'water pulse' can be considered when the normalized pixel permittivity values exceed 0.3. Although the mean curve gives the same outcome above 0.1, yet it is uncared for since the effect of core 'noise' signal was considered in its calculations. Finally, the minimum value maintained constant at 0.0, indicating that one pixel was at least representing pure oil droplet in the reconstructive image. For the presented data, the frequency of the 'water plug' was found to be 0.114 Hz. However, the frequency corresponding to the video output was found to be much higher than the one produced by ECT; this was thought to be due to the followings:

1. The single water plug represented by ECT output may consider more than one plug observed by the camera. As each individual plug took more than 5 seconds to pass through the ECT sensor, the ECT length is around 4D ≈ 0.11 m; and most of the plugs had a visible length of 2D.
2. Some of the ECT outputs were discarded from the frequency calculations since their maximum normalized permittivity values were very low (<0.2).

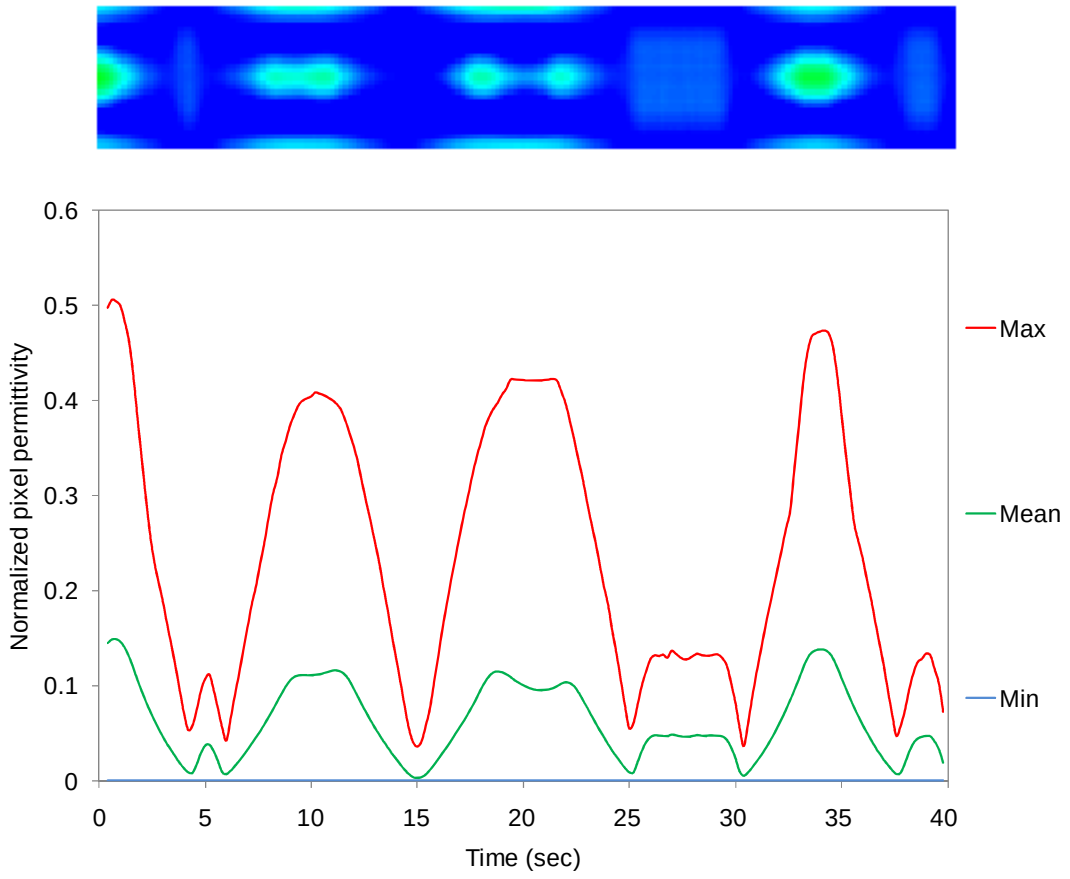

Figure 7-9: water tracer in heavy oil phase

Unfortunately for both water continuous and transient phase flow, none of the associated flow patterns were distinguished using the instrument. The higher water cut introduced to the fluid mixture, for the desired flow pattern, led to more distortion to the reconstructed ECT image, and even made the ECT out of work. The fluid occupying the core in CAF should be heavy oil surround by water phase with oil fouling on the annulus of the pipe; however the visual stacked 3d results showed conflicting output as high permittivity signal (water) was travelling in the centre and coating the wall (Figure 7-10) in lower permittivity phase (heavy oil) .

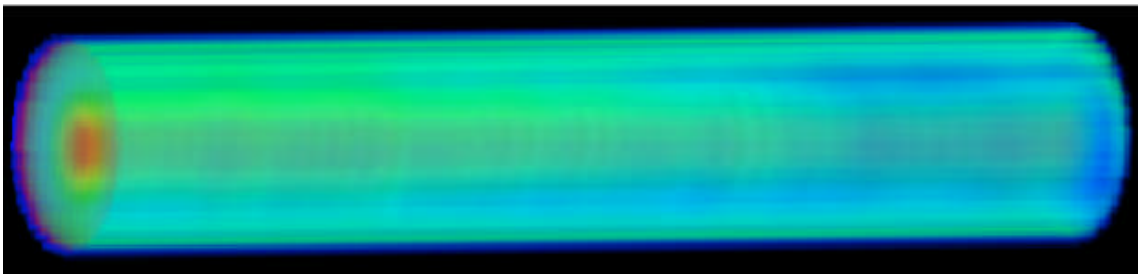

Figure 7-10: Stacked 3d output for CAF

Also at the transition phase (SWO), the ECT image output was incapable of reconstruct the flow pattern due to the same reasons mentioned above. The stacked 3d output for this phase is shown in Figure 7-11

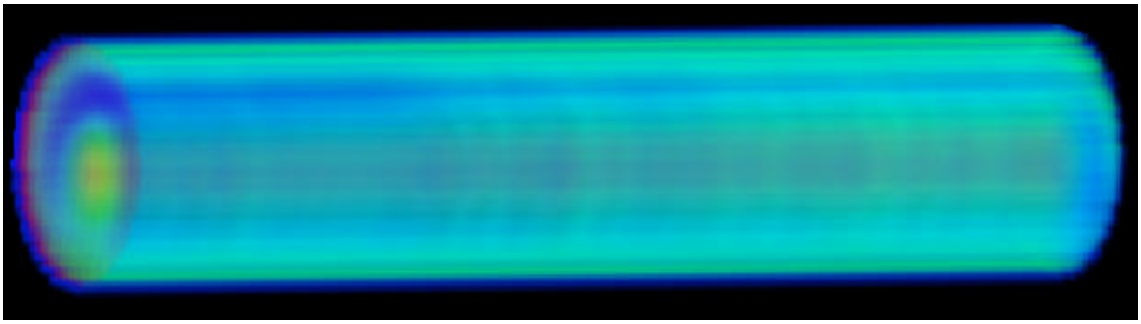

Figure 7-11: Stacked 3d output for SWO